FINITE DIFFERENCE TIME DOMAIN ANALYSIS OF MICROSTRIP ANTENNA-CIRCUIT MODULES

by

CHRISTOS KALIALAKIS

A thesis submitted to the Faculty of Engineering
of The University of Birmingham
for the degree of
DOCTOR OF PHILOSOPHY (Ph.D.)

School of Electronic and Electrical Engineering
The University of Birmingham
July 1999

SYNOPSIS

Compact microstrip antenna-circuit modules, which could be used as front-ends for future wireless systems applications, require electromagnetic modelling due to the close interaction of the circuit with the antenna. Spectrum crowding and EMC/EMI issues call for modelling of the radiation of such modules. *Coupling* through fringing fields and the *nonlinearities* of active devices must be addressed.

In this work, the FDTD method was used because it can provide the framework for inclusion of circuit elements in a full wave calculation. A software tool was developed and validated based on this method.

The modules studied were chosen due to their compactness and their merit as system components. A module with simultaneous transmit-receive operation integrating an active circulator (using *amplifiers* in a ring-like arrangement) and a quarter wavelength antenna was analysed. Coupling effects were identified and their impact on the radiation patterns were shown. Electronically tuneable microstrip patch antennas using varactor diodes were also studied. Tuning range and harmonic radiation were demonstrated. Single and dual device Gunn oscillator antennas were analysed and their radiation patterns were calculated for the first time. All of the results were in agreement with experimental findings.

ACKNOWLEDGMENTS

I would like to express my gratitude to my supervisors Professor Peter S. Hall and Dr. Peter Gardner for their guidance and patience.

Many thanks go to my colleagues at the Communications Engineering Group. Especially I would like to mention Mr. Dilbagh Singh, now with Roke Manor, for fruitful discussions on H shaped antennas and Dr. Martin J. Cryan, who joined University of Perugia, for discussions on integrated active circulators.

My thanks extend to Dr. David Checketts, computer officer of the School who ensured a reliable operation of the Sun workstation network where all of the calculations in this thesis were performed.

I would also like to acknowledge the financial support received through a studentship award by the School of Electronic and Electrical Engineering for three years that enabled me to undertake this research project.

TABLE OF CONTENTS

APPENDICES

CHAPTER 1

INTRODUCTION

1.1 Motivation

Wireless communication systems have been attracting a constantly increasing interest for the last few years. The amazing expansion of cellular mobile communications in the late ‘80s and early ‘90s is a typical example of large scale market development (Darnbrough 1998). New markets are ahead for wireless systems utilising every part of the microwave spectrum with the millimeter wave region to follow; automotive communications, smart antennas, indoor communications, sensors, multimedia, tagging are some of the prospective applications. The commercial requirements for compact, light-weight, low cost and mass production solutions have dictated the increased use of monolithic technology. The circuit parts have already utilised developments in semiconductor devices to exploit planar technology. Antennas, traditionally the last part of a conventional front end and completely separated from the circuit part, have been transformed to a variety of low profile and low weight structures following developments in planar microstrip antennas (James and Hall 1989). Demands for ever more compactness has initiated the integration of circuits and antennas on the same substrate resulting in *antenna-circuit modules* (IEEE Workshop 1995) which can also be met under the term *active integrated antennas* (Lin and Itoh 1994). In addition to the compactness, the use of planar (monolithic) technology provides the capability of low-cost mass production. Another important reason for their consideration is power generation in the millimetre wave band. Power produced by semiconductor devices decreases as frequency increases. Power combining is the only way to achieve the required

power levels. Circuit combining is inefficient due to losses in the interconnections. Arrays of compact antenna-circuit modules utilising quasi-optical (i.e. spatial) power combining techniques avoid these losses and offer an attractive solution for millimetre wave band power generation as suggested by Mink(1986). For these reasons, antenna-circuit modules seem to be a very likely candidate for future generations of commercial wireless systems.

The main drawback of planar technologies used is that tuning modifications are difficult to do after the prototype has been fabricated. Therefore accurate design is an integral part of the engineering process and necessary to avoid costly trial and error approaches. In order to facilitate that task CAD (Computer Aided Design) and CAE (Computer Aided Engineering) tools are in great demand. Traditionally in microwave frequencies two distinct families of components were developed; circuits and antennas, each using a different set of design methods. The design approach to build a front end was to separate the two and try to combine the solutions at a later stage. However the advent of MMIC (Monolithic Microwave Integrated Circuit) technology and of compact antenna-circuit modules has shown the need for a different approach to the design (IEEE Workshop 1995). The issues that need to be addressed for the successful analysis and design of compact antenna-circuit modules include nonlinearities from active devices, broadband operation and parasitic coupling. Circuit methods can handle the nonlinearity aspect and certain cases of coupling. However they are not flexible enough to account for dynamic parasitic coupling. On the other hand, full wave methods (direct solution of Maxwell equations) do not introduce any simplifying assumption and therefore are more general. Broadband operation favours time domain approaches that can offer wideband information with a single run. Consequently a

general solution to the problem of analysis of compact antenna-circuit modules can be provided by a full wave method that can handle circuit structures in time domain.

The Finite Difference Time Domain (FDTD) method is a popular full wave approach for antenna problems (Chebolu et al. 1996) and the theoretical formulation to include circuit elements in the three dimensional FDTD method was laid in the mid 90s (Piket-May et al. 1994). The method as applied to circuit elements is usually referred to as *extended FDTD* or *lumped element FDTD*. Although the merits of the method were recognised not much work had been done towards characterisation of complex structures and systems. This thesis is mainly concerned with applications of this method to complex structures, specifically to the problem of radiation of compact antenna-circuit modules.

1.2 Project aims

This project is concerned with the analysis and design aspects of compact microstrip antenna-circuit modules. Certain aims were set up in the beginning of the project.

First a software tool would be developed based on the extended FDTD method. The program would be based on ongoing research literature and adjustments would be made for the needs of the project.

For validation purposes, the developed software would then be used to analyse certain test structures. Other methods(e.g. Method of Moments) and established CAD software (like HP-MDS) along with measurements would be used for comparison.

The last part would be concerned with the characterisation of complex modules. The choice of the structures would reflect the range of circuit functions that can be integrated with an antenna. FDTD would be used for the analysis part and would eventually provide design implications. Prototype configurations were being developed at the same time in the Communications Engineering Group, thus providing valuable opportunities for comparisons and feedback.

1.3 Organisation of the thesis

Chapter 2 provides an overview of the literature on the analysis of antenna-circuit modules. It is also attempted to classify published configurations in order to highlight the choice of structures that were studied in this thesis.

Chapters 3 and 4 give the background material that was needed to develop the FDTD software tool. Chapter 3 serves as a mathematical introduction to the FDTD method as it could be applied to microwave passive structures and circuit elements. In Chapter 4 important issues for the successful implementation of the FDTD algorithm including excitation schemes and boundary conditions are presented.

Chapter 5 is concerned with the validation of the three dimensional FDTD code. Antennas are presented to validate the passive part of the code. Test circuits, including linear and nonlinear devices, are analysed and compared with other methods and the open literature where possible.

Chapter 6,7,8 are devoted to the specific structures that were studied.

In chapter 6 modules based on integration of microstrip antennas with active circulators are analysed. These structures exhibit transmit-receive operation at the same frequency. The importance of coupling on their performance (isolation, radiation patterns) is investigated and design guidelines are drawn.

In chapter 7 varactor-loaded microstrip patch antennas that can be electronically tuned are examined. Tuneable elements are of interest as components in frequency agile systems. However varactors are not without problems; they are nonlinear elements and the issue of the harmonic radiation is addressed.

In chapter 8 microstrip patch oscillators are studied. The coupling mechanism and the nonlinearity add to the complexity of the problem. A microstrip line Gunn diode oscillator is used as a circuit structure that validates the model. The onset of the oscillations is simulated and the generated harmonic spectrum is extracted. Single and dual Gunn device microstrip patch antenna oscillators are modelled and compared with experimental results from the open literature.

In chapter 9 the conclusions arising from this research are drawn. A discussion on possible future research towards improved full wave analysis and directions for module configurations is also included.

CHAPTER *2*

ANTENNA-CIRCUIT MODULES

A review on antenna-circuit modules terminology is presented. A clarification and a classification of configurations is deemed necessary to set up the context for the next chapters. In addition to that a literature review on the problem of their electromagnetic characterisation is included.

2.1 Levels of integration

Many configurations exist for antenna-circuit modules. It is possible to distinguish certain levels of integration depending on the degree of interaction of the circuits with the antenna (Hall and Fusco 1995).

In the conventional (non-integrated) modules, the antenna is completely separated from the active circuitry. The impedance seen from each part is set to a predetermined value, usually 50 Ω. Hence every subsystem is considered matched and each part can be analysed and optimised separately. For example a microstrip antenna is fed by a 50 Ω line that is connected to the 50 Ω output line of a circuit board (Figure 2.1.a).

In partially integrated configurations, antenna and circuit interaction is through a transmission line. For example an amplifier may be used to match the antenna and improve its bandwidth. The antenna is in proximity with the circuit but coupling is prevented by the common ground plane (Figure 2.1.b). The performance analysis can still be done separately

because of the negligible coupling. Combination of the solutions usually in terms of S-parameters is possible.

In full integration (Figure 2.1.c), the antenna and circuit interact through transmission line *and* fringing field coupling. The analysis of the performance must include now the parasitic coupling effects. In the example given, a Gunn diode is located on the patch forming an oscillator-antenna module where the interface between circuit and antenna cannot be defined.

The term active integrated antenna is kept for all configurations where a circuit is integrated with the antenna *on the same substrate* (Lin and Itoh 1994). This means that the term does not apply to combinations of active circuits with wire antennas that were implemented in the 60's and 70's following the invention of semiconductor transistors.

In terms of geometries there seem to be the following possibilities (Gupta 1994) for integrating circuit functions with microstrip patch antennas.

- Circuit and radiating patches laid out side-by-side on the same substrate.
- Active devices located on the patch.
- Multilayer configurations. Circuits are located on a lower layer below the one where the radiating patch is deposited.
- Circuit on the back side of the ground plane.

The first two geometries lead to configurations which are easy to fabricate, especially in hybrid form. However the selection of substrate must be compromised since circuits perform better on thin substrates of high dielectric constant and antennas require thick substrates of

low dielectric constant. The third and fourth geometries combat the problem of substrate selection but are more cumbersome to fabricate and occupy additional space.

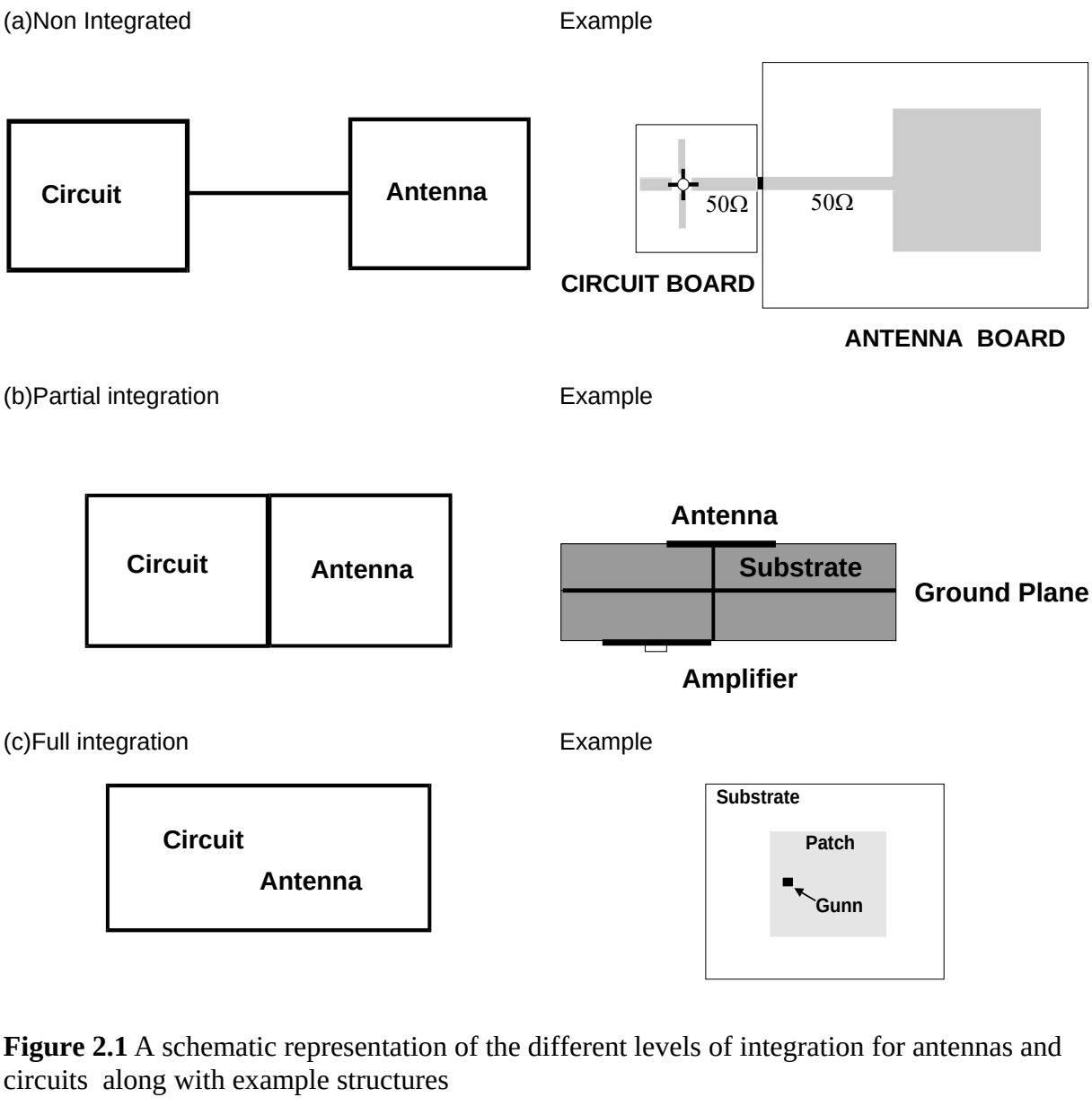

Figure 2.1 A schematic representation of the different levels of integration for antennas and circuits along with example structures

In this work single elements that follow the first two geometries are examined. They are realised on microstrip technology and could be characterised as fully or partially integrated structures.

2.2 Generic types

The basic functions for microwave antennas and active circuits (Navarro and Chang 1995) are radiation, amplification, oscillation, mixing, multiplication, tuning and switching. Antenna-circuit modules combine at least two of the above functions. A possible way of classification and the one that is followed here is at circuit level, according to the function of the active device as suggested by Lin and Itoh(1994). An alternative way is a classification at system level. Wireless systems can then be characterised either as transmitters or receivers. Systems combining transmit-receive operation can act as transceivers, transponders or repeaters.

2.2.1 Oscillator type

These structures employ a negative resistance circuit element. This is realised through a diode or a transistor in a feedback configuration. Diodes were the first circuit elements to be combined with antennas (Thomas et al 1984) because of their high power capabilities. However they suffer from heat dissipation problems and low DC to RF efficiency. Transistors offer improved DC to RF efficiency (Birkeland and Itoh 1989). The radiator serves not only as the load but as the resonant circuit that determines the frequency of oscillation. Injection locking techniques have also been used (Chang et al 1989) in order to reduce the frequency drift.

2.2.2 Amplifier type

In the case of a transmitter the antenna is put in the output port of an amplifier and in the case of a receiver in the input port of the amplifier (Robert et al 1992). They are used to increase the gain of the antenna or to detect and amplify the receiving signals using low noise amplifiers. They could be used in repeaters.

2.2.3 Signal control type

In the modules of these type, tuning and switching is combined with the radiation function. The frequency of the incoming RF signal is not affected. The response of such modules can be dynamically adjusted in order to select the kind of signals they respond to.

Tuneable antennas for example can have their resonance changed electronically. Their resonance can change by using varactor diodes. In this case the frequency of the RF signal does not change. The first tuneable microstrip antenna was reported by Bartia and Bahl (1982). Switching type antennas are also included in the signal control category. Few attempts have been reported in the open literature. Sabatier(1995) used diode switches on a handset antenna in order to choose between bands. Antennas with switching polarisation capabilities achieved with four integrated diodes have been reported by Haskins and Dahele(1994).

2.2.4 Frequency conversion type

Frequency conversion modules act on the incoming signal and their output is a new signal of different frequency. Mixers and multiplier antennas belong in this class of configurations. Mixer antennas employ diodes that are combined with radiators (Kerr et al 1977). Multipliers exploit the fact of harmonic generation to give power at very high frequencies (Nam et al 1987). Frequency conversion type antennas find application in transponders. Transponders receive a signal at a given frequency and employ either a mixer (Pobanz and Itoh 1994) or a multiplier (Singh et al. 1997) to retransmit a signal at a different frequency.

In overall the above categories can be considered as the generic elements that offer enhanced functionality to conventional antennas. The tendency though is to incorporate as many functions as possible in one module. Tuneable antennas can be combined with oscillator antennas to provide a dynamic signal range (Haskins et al. 1991). Of particular interest are combinations that yield transmit-receive operation. For instance, a self-oscillating mixer can function as a transceiver antenna element. In transmit mode the FET works as a part of the oscillator. In receive mode the nonlinearities of the FET are exploited to downconvert the receiving signal (Birkeland and Itoh 1989). Cryan et al. (1997) have combined an oscillator and an amplifier in a two element array to provide full duplex operation.

2.3 Electromagnetic characterisation

Although there is now a significant number of antenna-circuit modules, their characterisation has not yet attracted a lot of efforts (Lin and Itoh 1994). Antenna-circuit modules are complex systems that require an interdisciplinary knowledge (Chang and Navarro 1995) of solid-state device modelling, microwave circuit modelling and antenna analysis. The basic issues that need to be addressed for the accurate analysis of microstrip antenna-circuit modules are

- parasitic coupling through fringing fields
- nonlinearities of active devices. Accurate characterisations in order to find the large-signal equivalent circuit models of active devices is essential. However the characterisation requires specialised equipment and measurement techniques are still under development (Leckey et al 1995).

Given an antenna-circuit module, two different approaches to the analysis can be distinguished. According to the first approach, the antenna is treated as an n-port circuit. Circuit-based methods obviously follow that route. Safavi-Naeini et al.(1996) have given results for an amplifier integrated with an antenna. The amplifier was located on the bottom side of the ground plane. They treated the antenna as an equivalent two-port circuit that was connected with the amplifier. Similar approach was followed by Parfitt(1996) for a module which had the oscillator on one substrate and was coupled to the antennas on another substrate. For microstrip antennas, the transmission line model is used and it is combined with the circuit in commercial simulators (Cryan et al 1997). However transmission line models are limited to rectangular geometries and cannot predict cross polarisation radiation and surface wave effects. Multiport network methods (Gupta 1995) have been employed to provide a better circuit representation of microstrip antennas. Green's function is used for the derivation of a network which can account for surface waves and can then be combined with a circuit model. Gupta(1995) reported results on the tuning of a varactor-loaded antenna using this approach. McDowall and Fusco (1995) combined multiport network methods with the harmonic balance method in order to address the nonlinearity problem. Zhang et al.(1996) also applied a harmonic balance approach for the nonlinear circuit part of an oscillator antenna. A conceptually different, but still circuit based approach was suggested by Hall and Morrow (1994) who analysed radiation from an antenna integrated with a matched amplifier in the feed line. They used the S-parameters from the transistor and treated the problem of the device radiation as a radiation from a loaded discontinuity. For the antenna part, a cavity model was used and combined with the radiation from the device. A more accurate approach for the determination of the antenna representation was followed by Erturk et al.(1996) and Chen and Fusco(1996). Erturk et al. (1996) reported the analysis of a partially integrated

antenna oscillator. They used FDTD to obtain the 4×4 S-parameter matrix of the passive structure which was connected with a transistor model in a circuit simulator. Chen and Fusco(1996) demonstrated an FDTD-diakoptiks analysis for an active slot ring antenna by splitting the structure into a passive part and a part that contained the active device. The solutions were then combined via diakoptiks.

The second approach could be characterised as global or concurrent modelling. Here full wave methods are used to provide accurate field modelling of the antenna simultaneously incorporating circuit device models. A frequency domain approach has been reported by Gillard et al. (1991) who applied an integral equation technique for a partially integrated two layer structure with the amplifying element on the lower layer. However treatment of nonlinearities cannot be analysed easily in the frequency domain. The extended FDTD method was applied by Toland et al. (1993) to the analysis of a Gunn oscillator fed microstrip antenna. Toland et al.(1994) in a subsequent paper have also analysed the even-odd modes arising from a two element array. A complex transceiver antenna structure with significant coupling was analysed by Kalialakis et al.(1997).

The structures that were analysed using equivalent circuits for the antenna were partially integrated structures where the coupling was insignificant. Therefore their success depends on the degree and extent of coupling. However they are very fast and could be used for initial assessment of designs. It must be observed that these circuit-based approaches are structure and geometry specific and would not be flexible in changes of materials or shapes, especially when novel combinations are sought. In addition to that, with the frequency of operation going higher and higher even interconnections require accurate field modelling. As the

modules are integrating more functions, full wave based methods are going to become more and more significant and will be the core of future CAD and CAE software.

2.4 Figures of merit

Antenna-circuit modules need to be characterised by both circuit and antenna parameters (Hall and Fusco 1995). Signal power levels, harmonics and stability (phase noise) must be given along with traditional antenna figures e.g. polarisation, radiation patterns. Due to the non-reciprocity introduced by the active devices it is required to provide figures of merit for both transmit and receive operation. For example the radiation patterns can be different.

Due to the close integration some of these parameters must be re-examined or new parameters need to be introduced (Hall 1996). The main difficulty in antenna-circuit modules arises from the fact that it is not often possible to locate an antenna-circuit path and therefore to define unambiguously a port where the measurement will be done. Gain, for example could require a modified definition for amplifier antennas which includes the gains of the antenna and the amplifier (An et al 1993). In antenna-mixer modules the conversion loss, usually measured at the mixer input port, requires use of a modified parameter called isotropic conversion loss. This modified loss is the ratio of the conventional conversion loss to antenna gain. However, neither conventional loss nor gain can be determined independently unlike their ratio (Stephan and Itoh 1984). Additional figures of merit will be required as more and more circuit functions will be integrated in the modules. In the case of receiving modules mixer there might be a need to address image frequency and LO (Local Oscillator) signal rejection to prevent reradiation from the antenna. PM and FM added noise must be included for proper consideration of the module noise figure.

The antenna-circuit combination has resulted in improved performance. Increased bandwidth, size reduction, improvement of noise figure, reduction of mutual coupling in arrays have been reported (Navarro et al 1991). Arrays of antenna-circuit modules offer reliable and more robust performance (Lin and Itoh 1993) than their passive counterparts when some of the array elements fail (graceful degradation).

2.5 Design approaches

The design process starts by defining the application and its specifications. Then a configuration is chosen and several parameters that could be optimised and dictate the performance are decided. A two stage process (Hall and Fusco 1995, Navarro and Chang 1995) is then applied.

- First order design is employed to confirm configuration. Fast methods are required in order to get a rapid first prototype. Circuit based methods may be the first choice due to speed advantage.
- Second order design aims to optimise the structure. An accurate method is required. Most probably a full wave solver will be used for accuracy and optimisation.

The design efforts reported in the literature are based on first order design using circuit-based methods. Fusco(1992) proposed a synthesis procedure for oscillator antennas. An et al. (1993) proposed the real frequency technique for the design of multistage amplifier antennas. Zhang et al. (1996) used neural networks to optimize the feed position of a microstrip line

Gunn oscillator which served as the excitation of a microstrip line-fed rectangular microstrip antenna.

2.6 Summary

Fundamental terminology for antenna-circuit modules has been reviewed based on material drawn from the open literature. Several examples of configurations were given in order to highlight the structures chosen for this study. The analysis problem is a challenging one since it requires a combined knowledge of circuits and antenna methods. The majority of the structures analysed in the literature were partially integrated using circuit-based methods.

CHAPTER 3

THE FDTD METHOD

In this chapter, the fundamentals of the FDTD method are presented as applied to three dimensional passive structures and circuit elements. The development of the method mainly draws on material already published in the open literature; however it was necessary to complete the gaps in the derivations and to provide additional background material from computational mathematics. Since a main requirement of this project was to write a computer program based on the FDTD method, all the necessary details for proper implementation of the FDTD expressions in a computer program are given.

3.1 Full wave methods

Full wave methods in electromagnetics can be classified in many ways. The main objective is to solve the Maxwell equations with certain boundary and initial conditions. One possible classification uses the form in which Maxwell equations are expressed (Becker et al. 1995). According to this criterion three broad classes can be identified,

- partial differential equations techniques
- variational approaches
- integral equations techniques.

Another classification takes into account the domain in which the equations are expressed,

- time or frequency domain
- spatial or spectral (reciprocal space) domain

According to the above schemes, the Method of Moments is an integral equation method and the FEM (Finite Element Method) is a variational approach. Both methods are usually implemented in the frequency domain.

The FDTD method is a full wave time domain differential equation based technique. It is a versatile method that was proposed by Yee(1966) originally for two dimensional problems with metal boundaries. However it did not gain immediate attention for more than a decade mainly due to considerable computer resources requirements and the lack of boundary conditions for open region problems. Initially the FDTD method was applied to scattering problems and subsequently has become one of the most popular methods for solving problems in electromagnetics (Taflove 1995).

3.2 Maxwell's equations-Differential form

The Maxwell equations in charge free regions containing materials without magnetic losses read,

$$\nabla \times \overline{E} = -\frac{\partial \overline{B}}{\partial t} \quad (3\text{-}1) \qquad \nabla \cdot \overline{D} = 0 \quad (3\text{-}2)$$

$$\nabla \cdot \overline{B} = -\frac{\partial \overline{B}}{\partial t} \quad (3\text{-}3) \qquad \nabla \times \overline{H} = \frac{\partial \overline{D}}{\partial t} + \overline{J}_C \quad (3\text{-}4)$$

where $\overline{\mathrm{E}}, \overline{\mathrm{H}}$ are the electric and magnetic field respectively and $\overline{\mathrm{D}}, \overline{\mathrm{B}}$ are the electric and magnetic flux density, $\overline{\mathrm{J}}_c$ the conduction current. The constitutive relations in a linear isotropic material characterised by a permittivity ε, conductivity σ, permeability μ are;

$$\overline{B} = \mu \overline{H} \quad (3\text{-}5)$$

$$\overline{J_c} = \sigma \overline{E} \tag{3-6}$$

$$\overline{D} = \varepsilon \overline{E} \tag{3-7}$$

Solving for the time derivatives of the Maxwell curl equations, (3-3) and (3-4), and using relationships (3-5) to (3-7) leads to:

$$\nabla \times \overline{E} = -\mu \frac{\partial \overline{H}}{\partial t} \Leftrightarrow \frac{\partial \overline{H}}{\partial t} = -\frac{1}{\mu} \nabla \times \overline{E} \tag{3-8}$$

$$\nabla \times \overline{H} = \varepsilon \frac{\partial \overline{E}}{\partial t} + \sigma \overline{E} \Leftrightarrow \frac{\partial \overline{E}}{\partial t} = \frac{1}{\varepsilon} \nabla \times \overline{H} - \frac{\sigma}{\varepsilon} \overline{E} \tag{3-9}$$

Expressions (3-8), (3-9) involve vectors. Taking each component[1] a set of six equations is produced

$$\frac{\partial H_x}{\partial t} = -\frac{1}{\mu}\left(\frac{\partial E_z}{\partial y} - \frac{\partial E_y}{\partial z}\right) \tag{3-10}$$

$$\frac{\partial H_y}{\partial t} = -\frac{1}{\mu}\left(\frac{\partial E_x}{\partial z} - \frac{\partial E_z}{\partial x}\right) \tag{3-11}$$

$$\frac{\partial H_z}{\partial t} = -\frac{1}{\mu}\left(\frac{\partial E_y}{\partial x} - \frac{\partial E_x}{\partial y}\right) \tag{3-12}$$

$$\frac{\partial E_x}{\partial t} = \frac{1}{\varepsilon}\left(\frac{\partial H_z}{\partial y} - \frac{\partial H_y}{\partial z}\right) - \frac{\sigma}{\varepsilon} E_x \tag{3-13}$$

$$\frac{\partial E_y}{\partial t} = \frac{1}{\varepsilon}\left(\frac{\partial H_x}{\partial z} - \frac{\partial H_z}{\partial x}\right) - \frac{\sigma}{\varepsilon} E_y \tag{3-14}$$

[1] The vector identity $\nabla x \overline{F} = \left(\frac{\partial F_z}{\partial y} - \frac{\partial F_y}{\partial z}\right) \cdot \hat{x} + \left(\frac{\partial F_x}{\partial z} - \frac{\partial F_z}{\partial x}\right) \cdot \hat{y} + \left(\frac{\partial F_y}{\partial x} - \frac{\partial F_x}{\partial y}\right) \cdot \hat{z}$ is used.

$$\frac{\partial E_z}{\partial t} = \frac{1}{\varepsilon}\left(\frac{\partial H_y}{\partial x} - \frac{\partial H_x}{\partial y}\right) - \frac{\sigma}{\varepsilon} E_z \qquad (3\text{-}15)$$

3.3 FDTD solution of Maxwell's equations

The FDTD method is concerned with the numerical solution of expressions (3-10) to (3-15). Yee(1966) introduced finite differences for these expressions by dividing the space in cartesian cells. In three dimensions, the nodes have discrete coordinates (iΔx, jΔy, kΔz) and the time is measured in discrete intervals $t = n \cdot \Delta t$, where i, j, k, n are integers. In this scheme any arbitrary vector function $\overline{F}(\bar{r},t)$ can be approximated by a discrete valued function $\overline{F}^n(i,j,k)$. For each node, there is a corresponding cell where the $\overline{H}$ and $\overline{E}$ components reside (Figure 3.1). Observe that the electric field components are placed in the middle of the edges and the magnetic field components reside in the centres of the faces. It is worth noticing that the spatial offset gives readily a geometric representation of the integral form of Maxwell's equations (Taflove 1995). The computational domain is divided in $N_x \times N_y \times N_z$ cells. Due to the spatial offset, the magnetic field components $H_x(i,j+0.5,N_z+0.5)$, $H_x(i,N_y+0.5,k+0.5)$, $H_y(i+0.5,j,N_z+0.5)$, $H_y(N_x+0.5,j,k+0.5)$, $H_z(N_x+0.5,j+0.5,k)$, $H_z(i+0.5,N_y+0.5,k)$ and the electric field components $E_x(N_x+0.5,j,k)$, $E_y(i,N_y+0.5,k)$, $E_z(i,j,N_z+0.5)$ are not defined.

Let us derive the FDTD equation for the H_x component. First (3-10) is written using the finite difference operator Δ to express the derivatives:

$$\frac{\Delta H_x}{\Delta t} = \frac{1}{\mu}\left(\frac{\Delta E_y}{\Delta z} - \frac{\Delta E_z}{\Delta y}\right) \qquad (3\text{-}16)$$

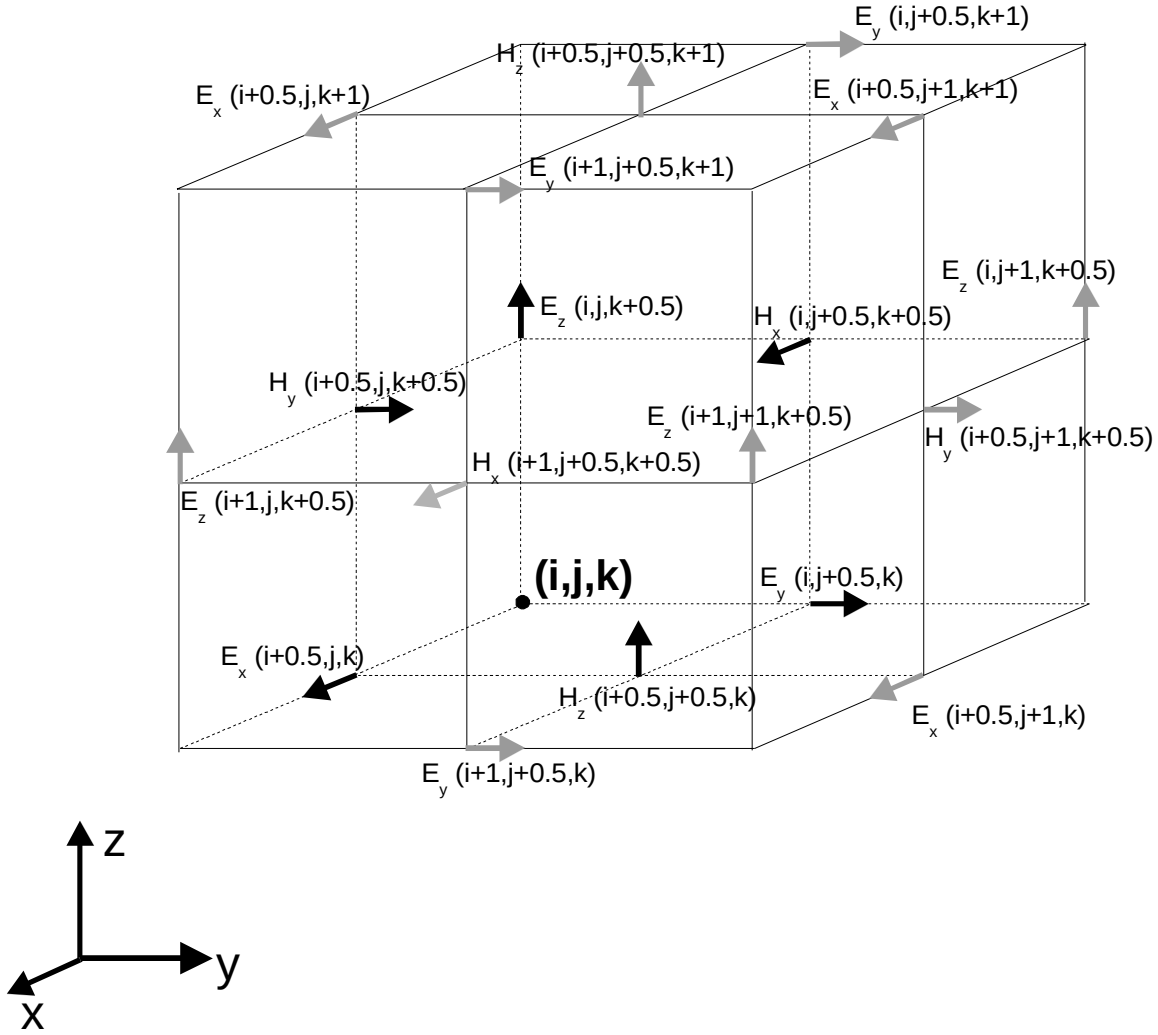

Figure 3.1 The position of the electric and magnetic field components in an FDTD or Yee cell. Black arrows indicate components that are associated with the (i, j, k) node where the grey ones indicate components that belong to other nodes.

The time derivatives for the magnetic field are calculated at the time point n and the space derivatives around the point (i, j, k). Therefore with reference to Figure 3.1, expression(3-16) can be written

$$\frac{H_x^{n+1/2}(i,j+0.5,k+0.5)-H_x^{n-1/2}(i,j+0.5,k+0.5)}{\Delta t}= \frac{1}{\mu}\frac{E_y^n(i,j+0.5,k+1)-E_y^n(i,j+0.5,k)}{\Delta z}-\frac{1}{\mu}\frac{E_z^n(i,j+1,k+0.5)-E_z^n(i,j,k+0.5)}{\Delta y} \quad (3\text{-}17)$$

Rearranging (3-17) and solving for $H_x^{n+1/2}(i, j+0.5, k+0.5)$:

$$H_x^{n+1/2}(i, j+0.5, k+0.5) = H_x^{n-1/2}(i, j+0.5, k+0.5) + \\ + \frac{\Delta t}{\mu \cdot \Delta z}\left[E_y^n(i, j+0.5, k+1) - E_y^n(i, j+0.5, k)\right] \\ - \frac{\Delta t}{\mu \cdot \Delta y}\left[E_z^n(i, j+1, k+0.5) - E_z^n(i, j, k+0.5)\right] \qquad (3\text{-}18)$$

The same can be done for the other components expressed by (3-11) and (3-12) :

$$H_y^{n+1/2}(i+0.5, j, k+0.5) = H_y^{n-1/2}(i+0.5, j, k+0.5) + \\ + \frac{\Delta t}{\mu \cdot \Delta x}\left[E_z^n(i+1, j, k+0.5) - E_z^n(i, j, k+0.5)\right] \\ - \frac{\Delta t}{\mu \cdot \Delta z}\left[E_x^n(i+0.5, j, k+1) - E_x^n(i+0.5, j, k)\right] \qquad (3\text{-}19)$$

$$H_z^{n+1/2}(i+0.5, j+0.5, k) = H_z^{n-1/2}(i+0.5, j+0.5, k) + \\ + \frac{\Delta t}{\mu \cdot \Delta y}\left[E_x^n(i+0.5, j+1, k) - E_x^n(i+0.5, j, k)\right] \\ - \frac{\Delta t}{\mu \cdot \Delta x}\left[E_y^n(i+1, j+0.5, k) - E_y^n(i, j+0.5, k)\right] \qquad (3\text{-}20)$$

Equations (3-18) to (3-20) allows one to calculate values of the magnetic field for every position, based on earlier (by Δt) values of magnetic field at the same position and earlier (by Δt/2) values of electric field at nearest neighbour positions.

The same procedure can be applied to equations (3-13) to (3-14). The FDTD equations will be derived for the E_x component as expressed by (3-13) and for small σ values.

$$\frac{\Delta E_x}{\Delta t} = \frac{1}{\varepsilon}\left(\frac{\Delta H_z}{\Delta y} - \frac{\Delta H_y}{\Delta z}\right) - \frac{\sigma}{\varepsilon}E_x \qquad (3\text{-}21)$$

The time derivatives for the magnetic field are calculated at the time point $n+\frac{1}{2}$ and the space derivatives around the node (i, j, k). With reference to Figure 3.1, expression (3-21) can be written:

$$\frac{E_x^{n+1}(i+0.5,j,k)-E_x^{n}(i+0.5,j,k)}{\Delta t}=\frac{H_z^{n+1/2}(i+0.5,j+\frac{1}{2},k)-H_z^{n+1/2}(i+0.5,j-\frac{1}{2},k)}{\varepsilon\cdot\Delta y}$$
$$-\frac{H_y^{n+1/2}(i+0.5,j,k+0.5)-H_y^{n+1/2}(i+0.5,j,k-0.5)}{\varepsilon\cdot\Delta z})-\frac{\sigma}{\varepsilon}E_x^{n+\frac{1}{2}}(i+0.5,j,k) \qquad (3\text{-}22)$$

In order to be consistent, any electric field component must be computed in integer time steps and any magnetic field component at half steps. Thus a problem of defining the electric field at a time step $n+\frac{1}{2}$ appears in (3-22) making the expression implicit. Kunz and Luebbers(1993) have suggested to use E_x^n as an approximation. However the practice has shown that averaging has been shown to produce more accurate results (Taflove 1995):

$$E_x^{n+\frac{1}{2}}=\frac{E_x^{n}+E_x^{n+1}}{2} \qquad (3\text{-}23)$$

Expression (3-23) is the simplest interpolation which works under the inherent assumption that the variation of the electric field is not rapid over the time interval Δt. In other words, this expression is not valid for phenomena which involve time scales much less than Δt. This observation is consistent with the finite differencing scheme which cannot resolve phenomena in wavelengths less than δ (corresponding to a mesh cut off frequency c/δ) and time scales less than Δt (Potter 1973).

Using (3-23) leads to an expression that is a semi-explicit formulation

$$\frac{E_x^{n+1}(i+0.5,j,k)-E_x^{n}(i+0.5,j,k)}{\Delta t}=\frac{H_z^{n+1/2}(i+0.5,j+0.5,k)-H_z^{n+1/2}(i+0.5,j-0.5,k)}{\varepsilon\cdot\Delta y}-$$
$$-\frac{H_y^{n+1/2}(i+0.5,j,k+\frac{1}{2})-H_y^{n+1/2}(i+0.5,j,k-\frac{1}{2})}{\varepsilon\cdot\Delta z}-\frac{\sigma}{2\varepsilon}E_x^{n}(i+0.5,j,k)-\frac{\sigma}{2\varepsilon}E_x^{n+1}(i+0.5,j,k) \quad (3\text{-}24)$$

Solving (3-24) for $E_x^{n+1}(i+0.5,j,k)$ and rearranging yields,

$$E_x^{n+1}(i+0.5,j,k)=\frac{1-\frac{\sigma\cdot\Delta t}{2\varepsilon}}{1+\frac{\sigma\cdot\Delta t}{2\varepsilon}}E_x^{n}(i+0.5,j,k)+$$
$$+\frac{\Delta t}{\varepsilon(1+\frac{\sigma\cdot\Delta t}{2\varepsilon})\Delta y}\left[H_z^{n+1/2}(i+0.5,j+0.5,k)-H_z^{n+1/2}(i+0.5,j-0.5,k)\right]$$
$$-\frac{\Delta t}{\varepsilon(1+\frac{\sigma\cdot\Delta t}{2\varepsilon})\Delta z}\left[H_y^{n+1/2}(i+0.5,j,k+0.5)-H_y^{n+1/2}(i+0.5,j,k-0.5)\right] \quad (3\text{-}25)$$

Analogous equations are derived for the E_y and E_z components

$$E_y^{n+1}(i,j+0.5,k)=\frac{1-\frac{\sigma\cdot\Delta t}{2\varepsilon}}{1+\frac{\sigma\cdot\Delta t}{2\varepsilon}}E_y^{n}(i,j+0.5,k)+$$
$$+\frac{\Delta t}{\varepsilon(1+\frac{\sigma\cdot\Delta t}{2\varepsilon})\Delta z}\left[H_x^{n+1/2}(i,j,k+0.5)-H_x^{n+1/2}(i,j,k-0.5)\right] \quad (3\text{-}26)$$
$$-\frac{\Delta t}{\varepsilon(1+\frac{\sigma\cdot\Delta t}{2\varepsilon})\Delta x}\left[H_z^{n+1/2}(i+0.5,j,k)-H_z^{n+1/2}(i-0.5,j,k)\right]$$

$$E_z^{n+1}(i,j,k+0.5)=\frac{1-\frac{\sigma\cdot\Delta t}{2\varepsilon}}{1+\frac{\sigma\cdot\Delta t}{2\varepsilon}}E_z^{n}(i,j,k+0.5)+$$
$$+\frac{\Delta t}{\varepsilon(1+\frac{\sigma\cdot\Delta t}{2\varepsilon})\Delta x}\left[H_y^{n+1/2}(i+0.5,j,k)-H_y^{n+1/2}(i-0.5,j,k)\right] \quad (3\text{-}27)$$
$$-\frac{\Delta t}{\varepsilon(1+\frac{\sigma\cdot\Delta t}{2\varepsilon})\Delta y}\left[H_x^{n+1/2}(i,j+0.5,k)-H_x^{n+1/2}(i,j-0.5,k)\right]$$

where the constitutive parameters are functions of position,

$$\sigma = \sigma(i, j, k) \tag{3-28}$$

$$\varepsilon = \varepsilon(i, j, k) \tag{3-29}$$

$$\mu = \mu(i, j, k) \tag{3-30}$$

It must be noted that having the possibility to change the constitutive parameters for every position, it is straightforward to model inhomogeneous materials in the FDTD context since the fundamental equations do not change. This is in contrast with other full wave methods in use e.g. the Method of Moments which requires a new Green's function when inhomogeneities are introduced in the material.

3.4 Implementation of Circuit Elements into FDTD

The conventional FDTD is unable to incorporate circuit elements. The method was extended recently, in two dimensions by Sui et al.(1992) and in three dimensions by Piket-May et al.(1994). The idea draws on the interpretation of Ampere's Current Law. Expression (3-4) gives the total current density in terms of the displacement and the conduction current. A lumped current density $\bar{J}_L$ can be added to accommodate any circuit element,

$$\nabla \times \overline{H} = \frac{\partial \overline{D}}{\partial t} + \overline{J_c} + \overline{J_L} \tag{3-31}$$

If I_L is the current through a surface characterised by a vector $\bar{S} = S \cdot \hat{n}$ where $\hat{n}$ is the unit vector normal to the surface then :

$$\bar{J}_L = \frac{I_L}{S} \hat{n} \tag{3-32}$$

and (3-31) yields

$$\nabla \times \overline{H} = \varepsilon \frac{\partial \overline{E}}{\partial t} + \sigma \overline{E} + \frac{I_L}{\overline{S}} \Leftrightarrow \frac{\partial \overline{E}}{\partial t} = \frac{1}{\varepsilon} \nabla \times \overline{H} - \frac{\sigma}{\varepsilon} \overline{E} - \frac{1}{\varepsilon} \frac{I_L}{S} \hat{n} \qquad (3\text{-}33)$$

Let us consider a circuit element located in a cell with z-directed current flow. Therefore only one component, the E_z component, is important. Taking into account that $\overline{S} = \Delta x \cdot \Delta y \cdot \hat{z}$, then (3-33) reads

$$\frac{\partial E_z}{\partial t} = \frac{1}{\varepsilon} (\nabla \times \overline{H})_z - \frac{\sigma}{\varepsilon} E_z - \frac{1}{\varepsilon} \frac{I_L}{\Delta x \cdot \Delta y} \qquad (3\text{-}34)$$

The FDTD expression for (3-33) is discretised as in the previous paragraph, using (3-23).

$$\frac{E_z^{n+1} - E_z^n}{\Delta t} = \frac{\sigma}{2\varepsilon} \left(E_z^n + E_z^{n+1} \right) - \frac{1}{\varepsilon} \frac{I_L^{n+1/2}}{\Delta x \cdot \Delta y} + \frac{1}{\varepsilon} (\nabla \times \overline{H})_z^{n+\frac{1}{2}} \qquad (3\text{-}35)$$

The $(\nabla \times \overline{H})_z^{n+1/2}$ notation was used for the discrete form of $(\nabla \times \overline{H})_z$ and the position coordinates of the circuit element were dropped for brevity. Solving expression (3-35) for E_Z^{n+1} leads to:

$$E_z^{n+1} = \frac{1 - \frac{\sigma \cdot \Delta t}{2\varepsilon}}{1 + \frac{\sigma \cdot \Delta t}{2\varepsilon}} E_z^n + \frac{\Delta t}{\varepsilon(1 + \frac{\sigma \cdot \Delta t}{2\varepsilon})} (\nabla \times \overline{H})_z^{n+1/2} - \frac{\Delta t}{\varepsilon(1 + \frac{\sigma \cdot \Delta t}{2\varepsilon})} \frac{I_L^{n+1/2}}{\Delta x \cdot \Delta y} \qquad (3\text{-}36).$$

3.4.1 Approaches to calculate the current density of circuit elements

The main problem in incorporating a circuit element into FDTD is to calculate the current density contribution in a discrete form. There are certain ways to represent devices :

- *physical modelling*: this requires the knowledge of the actual materials that constitute the device. For example if there is a diode in the FDTD region then the $\overline{J}_L$ term is calculated using charge transport equations originating from solid state physics (Ciampolini et al. 1997). The main advantage of that technique is that such a global simulation links

directly electromagnetic fields and technology related parameters like doping profiles of semiconductor devices.

- *equivalent circuits*: The other approach which is common in the commercial simulators is to represent devices by series and parallel combinations of lumped elements (resistors, capacitors, inductors, diodes) and controlled sources (voltage or current sources).

In this work the equivalent circuit approach is used which is the approach favoured in the open literature [Sui et al.(1992), Piket-May et al.(1994)]. Expression (3-37) serves as the framework for development of equations for specific circuit elements. In Chapter 5 expressions are shown for lumped elements (linear and nonlinear) and independent sources. Controlled voltage sources appear in Chapter 6.

3.5 Computer implementation of FDTD expressions

Expressions (3-18) to (3-20) and (3-25) to (3-27) are programmable in a computer. Each field component can be represented by an array with the coordinates as the indices. However array indexing of the above expressions must be adjusted in an appropriate way since half integer indices are not possible. The position indexing can be interpreted as the node coordinate rather than the exact position. By carefully examining these expressions unnecessary calculations can be avoided by having the constants absorbed in precalculated coefficients. Below the expressions for the field calculations are given, presented in pseudocode form. These correspond to equations (3-18), (3-19), (3-20) for the magnetic field and (3-25), (3-26) (3-27) for the electric field.

$$E_X(i,j,k) = C_{E1} \cdot E_X(i,j,k) + C_{E2Y} \cdot [H_Z(i,j,k) - H_Z(i,j-1,k) + C_{E2Z} \cdot [H_Y(i,j,k-1) - H_Y(i,j,k)] \quad (3\text{-}37)$$

$$E_Y(i,j,k) = C_{E1} \cdot E_Y(i,j,k) + C_{E2Z} \cdot [H_X(i,j,k) - H_X(i,j,k-1)] + C_{E2X} \cdot [H_Z(i-1,j,k) - H_Z(i,j,k)] \quad (3\text{-}38)$$

$$E_Z(i,j,k) = C_{E1} \cdot E_Z(i,j,k) + C_{E2X} \cdot [H_Y(i,j,k) - H_Y(i-1,j,k)] + C_{E2Y} \cdot [H_X(i,j-1,k) - H_X(i,j,k)] \quad (3\text{-}39)$$

$$H_X(i,j,k) = H_X(i,j,k) + C_{H2Z} \cdot [E_Y(i,j,k+1) - E_Y(i,j,k)] + C_{H2Y} \cdot [E_Z(i,j,k) - E_Z(i,j+1,k)] \quad (3\text{-}40)$$

$$H_Y(i,j,k) = H_Y(i,j,k) + C_{H2X} \cdot [E_Z(i+1,j,k) - E_Z(i,j,k)] + C_{H2Z} \cdot [E_X(i,j,k) - E_X(i,j,k+1)] \quad (3\text{-}41)$$

$$H_Z(i,j,k) = HZ(i,j,k) + C_{H2Y} \cdot [E_X(i,j+1,k) - E_X(i,j,k)] + C_{H2X} \cdot [E_Y(i,j,k) - E_Y(i+1,j,k)] \quad (3\text{-}42)$$

The coefficients related with the electric field are,

$$C_{E1} = \frac{1 - \frac{\sigma(i,j,k) \cdot \Delta t}{2\varepsilon(i,j,k)}}{1 + \frac{\sigma(i,j,k) \cdot \Delta t}{2\varepsilon(i,j,k)}} \quad (3\text{-}43)$$

$$C_{E2X} = C_{E2} \cdot \Delta x \quad (3\text{-}44)$$

$$C_{E2y} = C_{E2} \cdot \Delta y \quad (3\text{-}45)$$

$$C_{E2z} = C_{E2} \cdot \Delta z \quad (3\text{-}46)$$

where:

$$C_{E2} = \frac{\Delta t}{\varepsilon(i,j,k) \cdot (1 + \frac{\sigma(i,j,k) \cdot \Delta t}{2 \cdot \varepsilon(i,j,k)})} \quad (3\text{-}47)$$

For the magnetic field the coefficients are,

$$C_{H2X} = C_{H2} \cdot \Delta x \tag{3-48}$$

$$C_{H2Y} = C_{H2} \cdot \Delta y \tag{3-49}$$

$$C_{H2z} = C_{H2} \cdot \Delta z \tag{3-50}$$

where

$$C_{H2} = \frac{\Delta t}{\mu_o} \tag{3-51}$$

in the case of non-magnetic materials where it is assumed $\mu=\mu_o$.

Expressions (3-37) to (3-42) require six real arrays for the six field components. Three real arrays are needed for the materials and three real arrays for the electric field coefficients (3-43) to (3-47). This would lead to a number of coefficients equal to the number of cells. However the coefficients correspond to *different types of material* rather than to each cell. Therefore the number of different possible coefficients is reduced to the number of materials present which in most problems is usually less than ten. An integer indexing system is adopted that maps a given position (i, j, k) in the computational domain with a type of material and its corresponding coefficient. Thus for a distinct number of media in a specific problem, the storage requirements (see Appendix B) can be reduced by introducing three integer arrays instead of real arrays to map each component of the electric field with the corresponding coefficient [Kunz and Luebbers 1993, Taflove 1995]. No mapping is required for the magnetic field coefficients (3-48) to (3-51) since they are independent of position and constant.

The above implementation scheme for the layout of FDTD equations has been utilised for modelling of passive structures and it is used in this work. Circuit elements can be treated as

effective materials and treated in equations as another type of material with their own coefficients (see Chapter 5).

3.6 Stability and error considerations

For a numerical method such as the FDTD, one must be concerned with the accuracy and stability of the algorithm. Errors have a twofold origin; some are introduced by the approximations of a specific method and others by the discrete and the finite arithmetic of computers. The latter are round off (truncation) errors and are machine specific. Methods requiring intensive matrix inversions are especially vulnerable to such errors. The FDTD method is an iterative method which avoids matrix inversions. The former errors can be usually characterised in terms of the accuracy of approximation in relation with the resolution of the method. FDTD is classified as a second order accurate method. Given a spatial resolution δ the error in the magnitude is of the order of the δ^2. Thus the smaller the resolution, the closer the numerical expression gets to the continuous case. Another way to understand the meaning of second order error is to consider solution of the same problem corresponding to two resolutions δ_1,δ_2 with corresponding errors $\varepsilon_1,\varepsilon_2$. Then if $\delta_2=\delta_1/2$ is chosen then the error is reduced four times $\varepsilon_2=\varepsilon_1/4$. The errors introduced in finite difference schemes for solving time dependent wave equations like Maxwell's equations are (Liu 1995) dispersion, anisotropy and dissipation. Dissipation causes the attenuation of the wave amplitude. Dispersion results to incorrect wave propagation velocity which translate to phase errors. Error anisotropy means that errors depend on the direction of the wave propagation with respect to the grid. The FDTD scheme is prone only to numerical dispersion errors.

Maxwell's equations are hyperbolic Partial Differential Equations (PDE). Any numerical solution of PDEs may lead to unbounded solutions due to poor resolution. For PDEs it is necessary to have a stability criterion. A well known criterion is the CFL (Courant-Friedrichs-Lewy) condition, or just Courant condition, that relates the time and space resolution. For FDTD it has been proved (Taflove 1995) that the Courant condition is expressed by the inequality:

$$\Delta t \le \frac{1}{c\sqrt{\left(\frac{1}{\Delta x}\right)^2+\left(\frac{1}{\Delta y}\right)^2+\left(\frac{1}{\Delta z}\right)^2}} \qquad (3\text{-}52)$$

where c is the highest speed of the electromagnetic waves in the medium. Some concerns about this criterion have been raised by Sadiku et al. (1990) when the upper limit is used. It must be noted that the above Courant condition is *necessary* but *not always sufficient* for stability when modifications like absorbing boundary conditions are added to the finite differencing scheme (Abarbanel and Gottlieb 1997).

In order to provide a physical explanation of the stability condition (3-54), cubic cells are considered ($\delta=\Delta x=\Delta y=\Delta y$). Then the CFL criterion is expressed as

$$\Delta t \le \frac{\delta}{c\sqrt{3}} \qquad (3\text{-}53)$$

It can be proved (Potter 1973) that for any dimension d the CFL criterion can be rewritten as

$$\Delta t \le \frac{\delta}{c\sqrt{d}} \qquad (3\text{-}54)$$

For one dimension (d=1), $$\Delta t \le \frac{\delta}{c} \qquad (3\text{-}55)$$

A geometrical interpretation of the stability criterion is possible when the concept of domain of dependence for differential equations is introduced. This concept is inherently connected with the convergence of the solution of the difference equation to the solution of the corresponding differential equation (Mitchell and Griffiths 1980). For one dimension n=1, the differential wave equation defines for every point in the time-space lattice a domain of dependence which is bounded by characteristic lines. In the case of electromagnetic waves (Figure **3.2**) the slope of these lines is equal to inverse of the wave velocity, 1/c (Kim and Hoefer 1991). All the points inside this continuous domain contribute to the value of the point P that is at the apex.

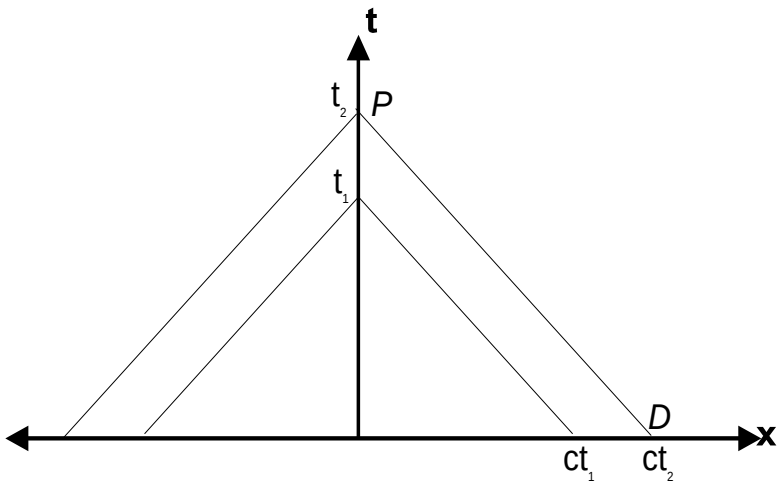

Figure 3.2 Domain of dependence for the wave equation in one dimension

The partial differential equation is approximated with the FDTD scheme in a time-space grid that replaces the continuum (Figure 3.3). According to this scheme the value at a point is calculated by accounting the contribution from the same spatial point one time step before and the two neighbouring magnetic field components half a time step before.

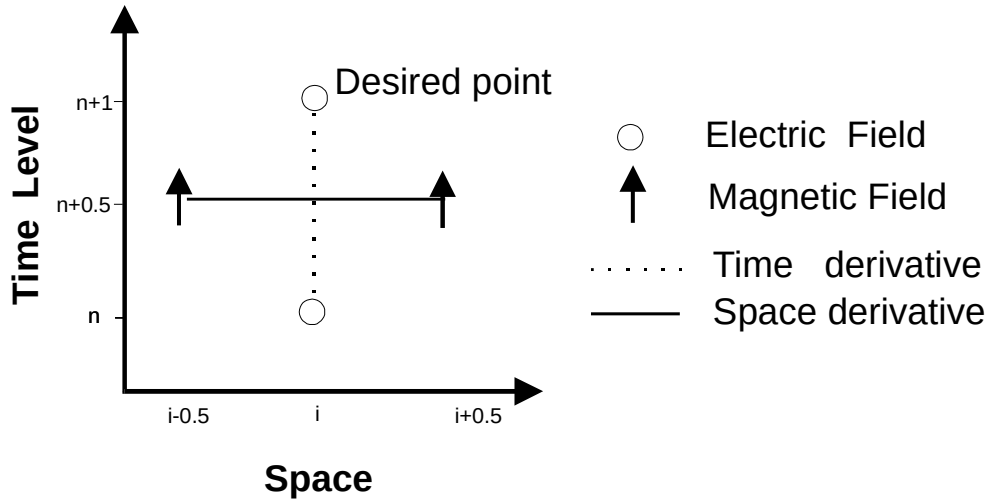

Figure 3.3 Schematic representation of the staggered leapfrog differencing in one dimension FDTD using a time-space diagram.

A *domain of dependence* contains all discrete points in the grid which contribute to the value of the point under consideration (Figure 3.4). In the limit $\delta \to 0$ the solution of the numerical equation should always converge to the solution of the analytical equation. Any slight changes in initial field values that affect the numerical solution at point P (Figure 3.4) should also affect the analytical solution. The domain of dependence of the differential equation must be included in the domain of dependence of the difference equation (Smith 1978) . Thus the slope of numerical domain of dependence (lines PQ, PQ') should be smaller than the slope of the continuous domain of dependence (lines PD, PD') or $\frac{\Delta t}{\delta} \le \frac{1}{c}$ which leads to the CFL criterion (3-55).

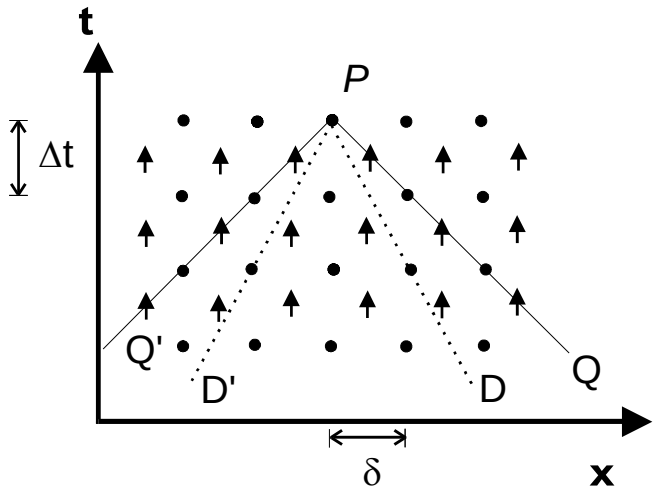

Figure 3.4 Domain of dependence for the FDTD difference equations equation in one dimension

Since FDTD is a sampling technique, the chosen spatial resolution must at least obey the Nyquist criterion. The space resolution ($\Delta x, \Delta y, \Delta z$) therefore must be at least $\lambda/2$. In the FDTD community the conventional working assumption of a resolution between $\lambda/10$ and $\lambda/20$ has prevailed as a guide for good results. Petropoulos(1994) has shown how the space resolution is related to the phase error and the number of periods (duration of the simulation) and how the conventional choice gives an acceptable but suboptimal phase error.

3.7 Summary

The solution of the Maxwell equations was presented using the FDTD method for passive structures and antennas including the incorporation of active devices. This is general background material complemented with comments and additions which can serve as a standalone introduction to the method. Expressions that are directly transferable to computer programs have been given. A discussion of the CFL stability criterion based on a geometrical interpretation was also included.

CHAPTER 4

IMPLEMENTATION ASPECTS OF FDTD ALGORITHMS

The expressions derived in chapter 3 serve as the backbone of the FDTD algorithm. However there are issues that need to be addressed before any useful working code is realised. Source modelling and termination of the computational domain are expansions that are required. Extraction of results necessary for this work e.g. radiation patterns is also examined. The flowcharts in appendix B should also be taken under consideration towards the realisation of code for this work.

4.1 Source modelling

In real problems an excitation source or other sources are present. FDTD equations were derived in a source free region so it is clear that these equations must change in the source position. The source also provides the initial condition which is necessary for a time marching solution problem. The source approach falls either in the *added* or *replaced* source category (Buechler et al. 1995). In the replaced source scheme, the calculated electric field is replaced at every time step by the source which is not affected by its environment This scheme is also known as the hard source approach (Taflove 1995) and it is the simplest to implement. If the source is at a position $\overline{r_o}$ then

$$\overline{E}(\overline{r_o},t) = \overline{E}_{source}(t) \qquad (4\text{-}1)$$

In an added source, the source is superimposed on the calculated field at that position. In mathematical terms this is expressed as

$$\overline{E}(\overline{r_o}, t_{n+1}) = \overline{E}(\overline{r_o}, t_n) + \overline{E}_{source} \qquad (4\text{-}2)$$

The replaced source is forcing the field to take specific values thus unphysical reflections occur that will contaminate the correct solution. On the other hand, the added source scheme allows incident local fields to interact and can be transparent to incoming waves.

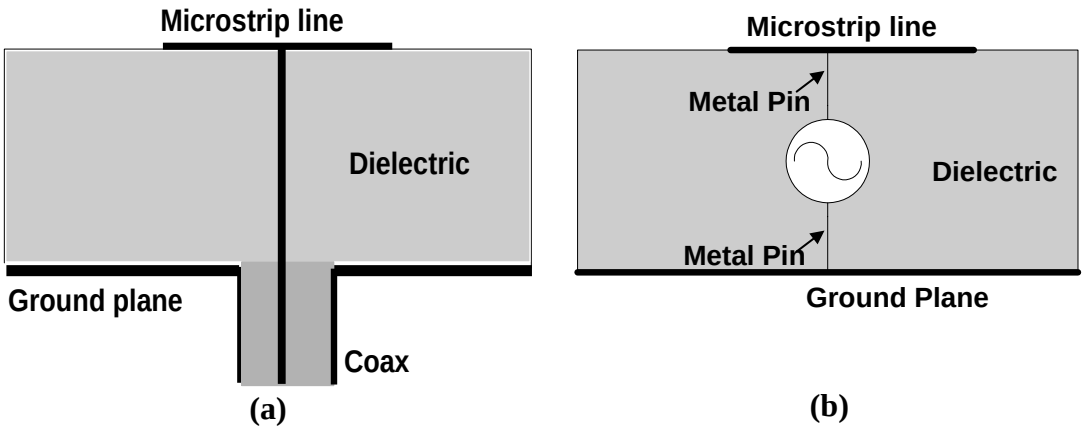

Figure 4.1 In microstrips a coaxial probe feed(a) is equivalent to a voltage source feed(b)

A solution particularly suited for microstrip circuits is to model an added source like a matched circuit source. Sui et al.(1992) introduced a voltage source for two dimensional FDTD methods and Piket-May et al.(1994) extended the validity of the model to three dimensions. This source is particularly attractive in the computation of S parameters because no splitting of the reflected and incoming wave is required (Pekonen et al. 1996). In addition to that, Luebbers and Langdon(1996) have shown that the resistive voltage source formulation is advantageous in terms of calculation time when modelling microstrip structures. An issue that remains is the connection of the source to the structure. In this work, it was chosen to embed the source cell in the substrate and connect it with one cell sized metal pins to the microstrip signal line and the ground plane. This realisation draws

from the equivalence of a voltage source with a coaxial feed (Figure 4.1) which has been proven advantageous in problems modelled by the Method of Moments (Itoh 1989).

4.2 Matched Circuit Sources

A circuit source is formed by connecting a voltage source in series with a resistor or a current source in parallel with a resistor (Figure 4.2). Applying Kirchoff's voltage law to the circuit of Figure 4.2.a, the current will be:

$$I_L = \frac{V_s + V_Z}{R_S} = \frac{V_S}{R_S} + \frac{V_Z}{R_S} \qquad (4\text{-}3)$$

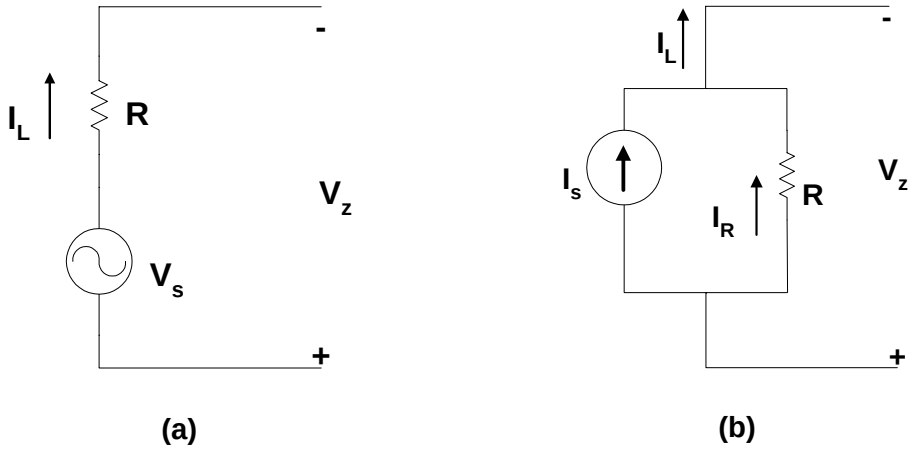

Figure 4.2 Circuit sources to be embedded in a cell of the FDTD region (a) voltage source (b) current source

In the same way one can describe a current source. Applying Kirchoff's current law to the circuit of Figure 4.2.b:

$$I_S = I_L + I_R \Rightarrow I_L = I_S + \frac{V_Z}{R_S} \qquad (4\text{-}4)$$

Obviously (4-3) and (4-4) are equivalent when $V_S = I_S \cdot R_S$ (Thevenin theorem) so the equation needs to be derived for only one of them. Discretising (4-4):

$$I_L^{n+\frac{1}{2}} = \frac{V_S}{R_S} + \frac{(E_z^{n+1} + E_z^n)\cdot \Delta z}{2R_S} \tag{4-5}$$

Substitution into (3-36) gives the update equation for the electric field in the source cell.

$$E_z^{n+1} = \frac{1 - \dfrac{\sigma\cdot\Delta t}{2\varepsilon} - \dfrac{\Delta t\cdot\Delta z}{2R_S\cdot\varepsilon\cdot\Delta x\cdot\Delta y}}{1 + \dfrac{\sigma\cdot\Delta t}{2\varepsilon} + \dfrac{\Delta t\cdot\Delta z}{2R_S\cdot\varepsilon\cdot\Delta x\cdot\Delta y}} E_z^n + \frac{\Delta t}{\varepsilon + \dfrac{\sigma\cdot\Delta t}{2} + \dfrac{\Delta t\cdot\Delta z}{2R_S\cdot\Delta x\cdot\Delta y}} (\nabla\times\overline{H})_z^{n+1/2} - \frac{\Delta t}{\varepsilon + \dfrac{\sigma\cdot\Delta t}{2} + \dfrac{\Delta t\cdot\Delta z}{2R_S\cdot\Delta x\cdot\Delta y}} \frac{V_S^{n+1/2}}{R_S\cdot\Delta x\cdot\Delta y} \tag{4-6}$$

The equations for the other field components are unaffected.

In order to transform these expressions in a computer program one has to observe that the expression (4-6) have, apart from the extra term coming from the source, similar form with (3-27) and its corresponding computer expression (3-39) but with different coefficients. Thus for the source position, the usual FDTD expression can be calculated with different coefficients and then the correction term for the source can be applied. In pseudocode form this is a two step procedure. First use,

$$\begin{aligned} E_Z(i_s,j_s,k_s) = {} & C_{E1}(source)\cdot E_Z(i_s,j_s,k_s) + \\ & C_{E2X}(source)\cdot[H_Y(i_s,j_s,k_s) - H_Y(i_s-1,j_s,k_s)] + \\ & C_{E2Y}(source)\cdot[H_X(i_s,j_s-1,k_s) - H_X(i_s,j_s,k_s)] \end{aligned} \tag{4-7}$$

where the coefficients related with the electric field are

$$C_{E1}(source) = \frac{1 - \dfrac{\sigma\cdot\Delta t}{2\varepsilon} - \dfrac{\Delta t\cdot\Delta z}{2R_S\cdot\varepsilon\cdot\Delta x\cdot\Delta y}}{1 + \dfrac{\sigma\cdot\Delta t}{2\varepsilon} + \dfrac{\Delta t\cdot\Delta z}{2R_S\cdot\varepsilon\cdot\Delta x\cdot\Delta y}} \tag{4-8}$$

$$C_{E2X} = C_{E2} \cdot \Delta x \tag{4-9}$$

$$C_{E2y} = C_{E2} \cdot \Delta y \tag{4-10}$$

$$C_{E2}(source) = \frac{\Delta t}{\varepsilon + \frac{\sigma \cdot \Delta t}{2} + \frac{\Delta t \cdot \Delta z}{2R_S \cdot \Delta x \cdot \Delta y}} \tag{4-11}$$

Then at the same time step, a correction is applied to the calculated value to account for the presence of the generator

$$E_Z(i_S, j_S, k_S) \leftarrow E_Z(i_S, j_S, k_S) - C_S \cdot V_g(n) \tag{4-12}$$

where $\leftarrow$ denotes substitution , V_g is the generator function value at time step n, C_s the source correction coefficient equal to

$$C_S = \frac{\Delta t}{\varepsilon + \frac{\sigma \cdot \Delta t}{2} + \frac{\Delta t \cdot \Delta z}{2R_S \cdot \Delta x \cdot \Delta y}} \frac{1}{(R_S \cdot \Delta x \cdot \Delta y)} \tag{4-13}$$

Thus a source cell is treated as a cell filled with an effective material characterised by its own coefficients (4-8) to (4-11) and (4-13).

4.3 Excitation functions for sources

Since FDTD is a time domain method, wideband results can be produced in one run by using a pulse excitation. Thus any required quantities can be calculated through Fourier transform of the transient system response. Also monochromatic simulations are sometimes useful, especially for applications to frequency dependent materials or overmoded problems (Roper and Baird 1992).

The initial turn-on of the source is an important consideration. If the fields start with a high value then effectively they are multiplied by a step function. This causes higher harmonics to be excited that tend to die out slowly due to the dispersive nature of the rectangular mesh, prolonging the simulation time. Therefore a first obvious requirement is to use sources that have a slow build-up from zero. For example, in a single frequency source it is better to use a sinusoid rather than a cosine. However, a sinusoid has a step in its derivative so the normally directed fields which are not sourced are discontinuous. One solution is to have the smoothest possible transition, using an envelope function. The generator function for a monochromatic excitation should be

$$V_g(t) = e(t)\sin(2\pi ft) \qquad (4\text{-}14)$$

with e(t) being an envelope function. The raised cosine has given the best results (Roper and Baird 1992) and it is the preferred choice compared with linear and exponential ramps.

$$e(t) = 0.5 \cdot \left[1 - cos\left(\frac{2\pi ft}{2a}\right)\right] \qquad (4\text{-}15)$$

α being the number of periods of the source frequency that is required for the function to reach the maximum envelope value.

In a wideband problem, what is usually needed is information from DC to a maximum frequency or from a frequency band f_1 to f_2. In order to produce such wideband results, an excitation with sufficient content over these frequencies is needed. Ideally there should be constant spectral content over the frequency range which translates to a delta function in time domain. However it is not practical to use step sources from a numerical point of view as discussed above. More practical excitations are needed.

Kunz and Luebbers(1993) suggest that reasonable results are expected by FDTD up to a frequency f_u which corresponds to an $\lambda_o/10$ sampling. At a frequency that corresponds to $\lambda_o/4$ sampling, there must not be appreciable content in order to avoid aliasing effects.

In a problem involving structures with dielectric constant $\varepsilon_r>1$, the upper useful frequency limit f_u is different because in dielectrics the guided wavelength λ_g is smaller than λ_o. Let us a consider a situation where a resolution δ corresponding to $\lambda_o/10$ has been chosen. If a a dielectric $\varepsilon_r=4$ is used then the resolution is $\lambda_g/5$. Therefore for the same accuracy, the upper useful frequency limit $f_u = \frac{c}{10 \cdot \delta}$ is reduced to $f_u^{'} = \frac{f_u}{\sqrt{\varepsilon_r}}$. It must be noted again that because of its lattice structure there is another maximum cut off frequency for the FDTD grid equal to $f_{cutoff} = \frac{c}{\delta}$.

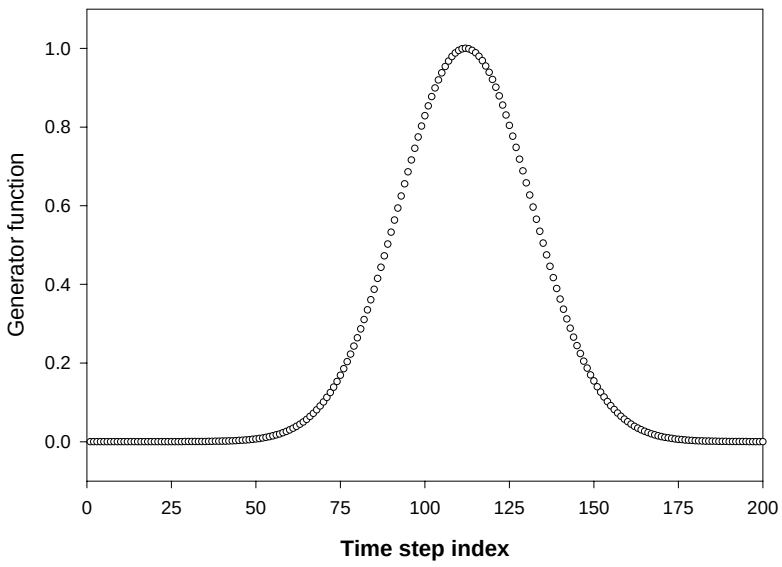

Figure 4.3 A truncated discrete Gaussian pulse used as wideband excitation in FDTD problems ($\beta=132$, $\Delta t=1.45 \cdot 10^{-12}$).

The Gaussian waveform is the excitation of choice. Kunz and Luebbers(1993) suggest a truncated Gaussian pulse of the form

$$V_g(t) = exp\left[-\alpha(t-\beta\Delta t)^2\right] \qquad (4\text{-}16)$$

The truncation value is

$$\alpha = \left(\frac{4}{\beta\Delta t}\right)^2 \qquad (4\text{-}17)$$

which gives a truncation value exp(-16)=140dB down (using 20logα) at the trailing edges.

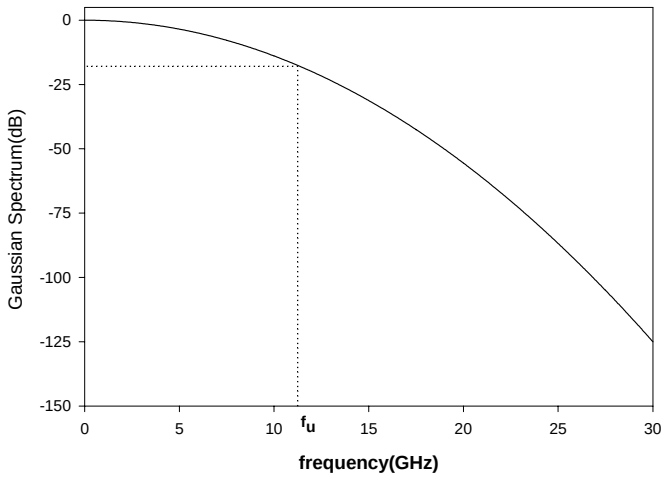

Figure 4.4 Spectrum of the truncated discrete Gaussian pulse of Figure 4.3 used as wideband excitation in FDTD problems (β=132, $\Delta t=1.45\cdot10^{-12}$ sec).

The frequency spectrum of a Gaussian pulse has the same functional dependence. Specifically,

$$V_g(f) = exp\left(-\frac{\pi^2}{\alpha}f^2\right) \qquad (4\text{-}18)$$

At the frequency f_u, magnitude of -20dB is favoured and for the frequency that corresponds to $\lambda/4$ sampling, less than -100dB. The truncation value α can be determined using (4-18)

and then β can be calculated using (4-17). Thus using excitation of the form of the spectrum (4-16) can be controlled with parameters α,β. For example in Figure 4.4 the synthesised pulse spectrum is shown for f_u=12 GHz in the case of free space. Its time domain form is shown in Figure 4.3. If there is dielectric material present in a problem, it is desired to have the same accuracy and maintain the frequency limit f_u and not the smaller limit $f_u^{'}$, then one has to use a smaller resolution $\delta = \frac{\delta}{\sqrt{\varepsilon_r}}$. At the same time β should be increased to $\beta = \beta\sqrt{\varepsilon_r}$ in order to avoid narrowing of the pulse.

4.4 Computational Domain Truncation

In situations where the boundary conditions are not imposed by the nature of the problem, like in the case of metal enclosures, it is necessary to simulate propagation in free infinite space in a finite region. For this reason, a proper truncation of the computational domain was a major concern in the development of FDTD. Because of the FDTD expressions and the positioning of the field components, some field values at extreme positions of the grid cannot be calculated (TABLE 4-1). For example $E_x(i,j,1)$ cannot be calculated because the magnetic field $H_y(i,j,0)$ cannot be defined. All these field components reside on faces, edges and corners.

TABLE 4-1

Restriction of indices for FDTD field components

Component			
$E_x(i,j,k)$	i=1,2,… N_x-1	j=2,3,…N_y-1	k=2,3,…N_z-1
$E_y(i,j,k)$	i=2,3,…. N_x-1	j=1,2,…N_y-1	k=2,3,…N_z-1

$E_z(i,j,k)$	i=2,3,…. N_x-1	j=2,3,…N_y-1	k=1,2,…N_z-1

The values of the components should be provided by the boundary conditions. These can be classified into two distinct classes. The first class could be characterised as radiation boundary conditions and the second as absorbing boundary conditions.

4.4.1 Radiation Boundary Conditions

The radiation boundary conditions are based on the assertion that solution of the curl equations is equivalent to solving the wave equation (Potter 1973). If the fields in the boundary satisfy a radiating condition then they are not reflected back to the computational domain . The general three dimensional wave equation for the electric field is:

$$\frac{\partial^2 \overline{E}}{\partial x^2} + \frac{\partial^2 \overline{E}}{\partial y^2} + \frac{\partial^2 \overline{E}}{\partial z^2} - \frac{1}{c^2}\frac{\partial^2 \overline{E}}{\partial t^2} = 0 \qquad (4\text{-}19)$$

It can also be written using operators as:

$$L\overline{E} = 0 \qquad (4\text{-}20)$$

where the operator L is by definition,

$$L = \frac{\partial^2}{\partial x^2} + \frac{\partial^2}{\partial y^2} + \frac{\partial^2}{\partial z^2} - \frac{1}{c^2}\frac{\partial^2}{\partial t^2} \equiv D_x^2 + D_y^2 + D_z^2 - \frac{1}{c^2}D_t^2 \qquad (4\text{-}21)$$

Let us consider the case of propagation along one arbitrary direction. The wave equation allows propagation along both ways. In the case of radiation boundary conditions, the focus is on a wave that propagates away (radiates) from the computational space. It is therefore useful to write the operator equation as a split operator equation,

$$L^+ L^- \overline{E} = 0 \qquad (4\text{-}22)$$

where the $L^{\pm}$ operators denote propagation to left and right directions. Considering the case of propagation along the x axis to the right for example, the operator L^+ is written as

$$L^{+} = D_x - \frac{D_t}{c}\sqrt{1 - S^2} \tag{4-23}$$

with the S operator given by

$$S^2 = \left(\frac{D_y}{D_t / c}\right)^2 + \left(\frac{D_z}{D_t / c}\right)^2 \equiv S_y^2 + S_z^2 \tag{4-24}$$

All the radiation boundary conditions that have been developed, depend on the various approximations of the $\sqrt{1 - S^2}$ operator (Kunz and Luebbers 1993). The most popular boundary condition of this type is due to Mur(1981). Mur(1981) has used the simplest possible approximations. The first order approximation yields

$$\sqrt{1 - S^2} \approx 1 \tag{4-25}$$

which leads to the following approximation for the operator L^{+},

$$L^{+} = D_x + \frac{D_t}{c} \tag{4-26}$$

Second order conditions result from the first order binomial expansion,

$$\sqrt{1 - S^2} \approx 1 - \frac{1}{2} S_y^{\,2} - \frac{1}{2} S_z^{\,2} \tag{4-27}$$

The operator corresponding to that approximation is

$$L^{+} = D_x - \frac{D_t}{c} + \frac{cD_y^{\,2}}{2D_t} + \frac{cD_z^{\,2}}{2D_t} \tag{4-28}$$

Finite difference approximations to these operators lead to the first and second order Mur conditions suitable for FDTD algorithms. Complete derivation along with the finite difference realisation is given on Appendix C. First order conditions are used for the edges and the corners and second order for the faces of the computational domain.

4.4.2 Absorbing Boundary Conditions

The other class of truncation conditions is based on the introduction of artificial materials that can readily absorb the waves reaching the boundary. This in effect is an attempt to reproduce the situation of an anechoic chamber. Berenger(1994) introduced the PML (Perfectly Matched Layer) concept for two dimensions which was found to give very small reflection coefficients. This was verified by Katz et al.(1994) which extended it to three dimensions. The PML concept is based on the introduction of an artificial layer of n cells thickness having both electric losses σ and magnetic losses σ^* (dual quantity). These layers have wave impedance completely matched with the vacuum impedance and the same phase velocity.

4.4.3 Choice of Boundary Conditions

Because the absorbing conditions are not perfect, some non-physical reflections occur. The absorption depends on the choice of offset(white space) from the structure and the angle of incidence. PML conditions are known to give better reflection coefficient with less white space. They seem to be the main candidate for use in accurate calculations of radar cross sections of complicated structures. Their disadvantage is the increased computational overhead compared to the Mur conditions. In the case of Mur conditions a working assumption is about 20 cells away from the structure under study (Trueman et al. 1991). Rayner et al. (1996) have shown that white space of half a wavelength away from the structure would give excellent results for radiation patterns regardless of the type of conditions. Mur conditions are known to provide good accuracy for engineering applications

(Taflove 1995), especially when there is white space between the structure under simulation. In this work, Mur conditions of the first and second order are used.

4.5 Modelling of conducting materials

One of the most essential parts in the setup of the problem is the description of the geometry of the structure under study. There are two separate steps in that procedure:

i. Passing the coordinates of the object into the FDTD program.
ii. Making the proper media array assignments. For example the user can determine the position of a wire directed along the z-axis. The code should then change the medium value in that position.

It must be stated that when one desires to assign material to a cell, what is done is assignment of the material to a specific field component rather than just filling Yee cells. To model a metal the static boundary condition is used which requires the tangential component of the electric field to be set to zero. The assignment of parts of the computational domain as metals can be achieved before the algorithm starts by zeroing the coefficients in the field expressions (3.45)-(3.49).

In order to model an infinitely thin wire, the electric field along the direction of the wire is set to zero across the relevant nodes. Modelling of metal sheets is essential in many cases and especially in microstrip antennas. Special care must be exercised to produce a sheet since there is an offset between the E components (Kunz and Luebbers 1993). If it is desired to have a sheet of dimensions $L_x \times L_y$ in the xy-plane then one has to specify the coordinates i_{start}

and $i_{max}=i_{start}+L_x$ and mark the relevant nodes(see Figure 4.5.a) by setting the E_x and E_y coefficients to zero. Same procedure is followed for j_{start} and $j_{max}=i_{start}+L_y$. This is described in pseudocode as shown in Figure 4.5.b

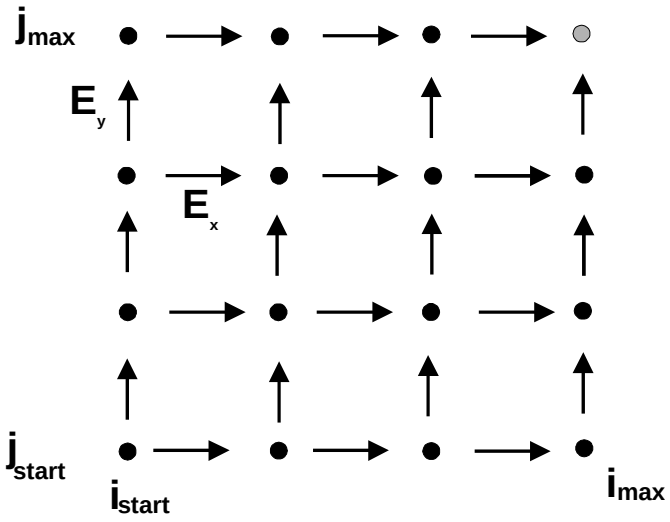


```
for i=istart to imax
  for j=jstart to jmax
    if i ≠ imax set Ex coefficients 0
    if j ≠ jmax set Ey coefficients 0
  end of loop over x
end of loop over y
```

(b)

Figure 4.5 Definition of a thin sheet in the FDTD context. The node in grey does not participate in the building of the metal plate. (b) Pseudocode realisation

4.6 Near to far field transformation

In antenna problems it is imperative to obtain the radiation pattern. Since FDTD can only calculate near fields, a near-to-far field transformation is needed. A transformation surface is chosen and the fields in this surface are calculated. The transform surface is a cuboid enclosing the antenna. Spatial field averaging is required to find the proper values on the transform surface (Kunz and Luebbers1993). For this work, the points of field evaluation are chosen on the centre of the face of the Yee cell that lies on the transform surface.

For faces parallel to xy plane, the surface point coordinates are $(i_s, j_s, k_s)=(i+0.5, j+0.5, k)$

$$E_x^{n+1}(i_s, j_s, k_s) = \frac{E_x^{n+1}(i, j, k) + E_x^{n+1}(i, j+1, k)}{2} \quad (4\text{-}29)$$

$$E_y^{n+1}(i_s, j_s, k_s) = \frac{E_y^{n+1}(i, j, k) + E_y^{n+1}(i+1, j, k)}{2} \quad (4\text{-}30)$$

$$H_x^{n+1/2}(i_s, j_s, k_s) = \frac{H_x^{n+1/2}(i,j,k) + H_x^{n+1/2}(i+1,j,k) + H_x^{n+1/2}(i,j,k-1) + H_x^{n+1/2}(i+1,j,k-1)}{4} \quad (4\text{-}31)$$

$$H_y^{n+1/2}(i_s, j_s, k_s) = \frac{H_y^{n+1/2}(i, j, k) + H_y^{n+1/2}(i, j+1, k) + H_y^{n+1/2}(i, j, k-1) + H_y^{n+1/2}(i, j+1, k-1)}{4} \quad (4\text{-}32)$$

For faces parallel to xz plane, the surface point coordinates is $(i_s, j_s, k_s)=(i, j+0.5, k+0.5)$

$$E_x^{n+1}(i_s, j_s, k_s) = \frac{E_x^{n+1}(i, j, k) + E_x^{n+1}(i, j, k+1)}{2} \quad (4\text{-}33)$$

$$E_z^{n+1}(i_S, j_S, k_S) = \frac{E_z^{n+1}(i, j, k) + E_z^{n+1}(i+1, j, k)}{2} \quad (4\text{-}34)$$

$$H_x^{n+1/2}(i_S, j_S, k_S) = \frac{H_x^{n+1/2}(i, j, k) + H_x^{n+1/2}(i, j-1, k) + H_x^{n+1/2}(i+1, j, k) + H_x^{n+1/2}(i+1, j-1, k)}{4} \quad (4\text{-}35)$$

$$H_z^{n+1/2}(i_S, j_S, k_S) = \frac{H_z^{n+1/2}(i, j, k) + H_z^{n+1/2}(i, j, k+1) + H_z^{n+1/2}(i, j-1, k) + H_z^{n+1/2}(i, j-1, k+1)}{4} \quad (4\text{-}36)$$

For faces parallel to yz plane, the surface point coordinates is $(i_s, j_s, k_s)=(i+0.5, j, k+0.5)$

$$E_y^{n+1}(i_S, j_S, k_S) = \frac{E_y^{n+1}(i, j, k) + E_y^{n+1}(i, j, k+1)}{2} \quad (4\text{-}37)$$

$$E_z^{n+1}(i_S, j_S, k_S) = \frac{E_z^{n+1}(i, j, k) + E_z^{n+1}(i, j+1, k)}{2} \quad (4\text{-}38)$$

$$H_y^{n+1/2}(i_S, j_S, k_S) = \frac{H_y^{n+1/2}(i, j, k) + H_y^{n+1/2}(i, j+1, k) + H_y^{n+1/2}(i-1, j, k) + H_y^{n+1/2}(i-1, j+1, k)}{4} \quad (4\text{-}39)$$

$$H_z^{n+1/2}(i_S, j_S, k_S) = \frac{H_z^{n+1/2}(i, j, k) + H_z^{n+1/2}(i, j, k+1) + H_z^{n+1/2}(i-1, j, k) + H_z^{n+1/2}(i-1, j, k+1)}{4} \quad (4\text{-}40)$$

The coordinates for the fields in (4-29) to (4-40) correspond to the nodes of the cells they belong rather than the actual positions.

Having the field values on the transform surface, the equivalent electric current $\overline{J}_S$ and magnetic current $\overline{M}_S$ densities can be calculated for every point on the surface :

$$\overline{M}_S = \hat{n} \times \overline{E} \quad (4\text{-}41) \qquad \overline{J}_S = -\hat{n} \times \overline{H} \quad (4\text{-}42)$$

where $\hat{n}$ is the unit vector normal to the surface. By virtue of the equivalence theorem the far field can be calculated (see Appendix D). Since a frequency domain transform is used, the field phasors at the desired frequency must be calculated. This could be done by exciting the structure with a sinusoid at that frequency and after steady state is reached, phase and magnitude information is extracted for the fields on the transform surface. The magnitude extraction is based on maximum detection and the phase of the corresponding point relies on monitoring positive zero crossing points. This technique relies on the assumption that a steady state is achieved relatively quickly. If radiation patterns are needed for more than one frequency the code must be run again. By using a wideband Gaussian pulse and Fourier transforming the results on the desired frequencies, radiation patterns can be calculated with one run. In the majority of situations, radiation patterns are sought for a finite set of frequencies. It has been shown (Furse and Gandhi 1994) that for a small number of frequencies it is advantageous in memory savings to use the DFT which is performed during the simulation rather than using FFT in the postprocessing stages.

4.7 Circuit quantities calculation

4.7.1 Current and Voltage Calculation

In FDTD, the normal physical space is approximated with a discrete collection of points. Discrete equivalents of the other laws and definitions of electromagnetics can be derived. In electromagnetics, voltage can be calculated through:

$$V = \int \overline{E} \cdot d\overline{r} \tag{4-43}$$

In discrete form, the preceding expression yields:

$$V(i, j, k+0.5) = E_z(i, j, k+0.5) \cdot \Delta z \tag{4-44}$$

The current is defined as the contour integral of the magnetic field:

$$I = \oint \overline{H} \cdot \overline{dl} \tag{4-45}$$

A discrete form of (4-45) is required for the FDTD calculations. In Figure 4.6 an Ampere loop around the (i, j, k) node is depicted. The current in that case will be z-directed. Similar loops can be drawn for currents flowing in x and y directions. Integral (4-45) is transformed to the following discrete form,

$$\begin{aligned} I_z^{n+\frac{1}{2}}(i, j, k) = & \left[H_y^{n+\frac{1}{2}}(i+0.5, j, k+0.5) - H_y^{n+\frac{1}{2}}(i-0.5, j, k+0.5) \right] \cdot \Delta y + \\ & \left[H_x^{n+\frac{1}{2}}(i, j-0.5, k+0.5) - H_x^{n+\frac{1}{2}}(i, j+0.5, k+0.5) \right] \cdot \Delta x \end{aligned} \tag{4-46}$$

The current calculated by (4-47) is the total current flowing through the cell, including both displacement current and any circuit currents.

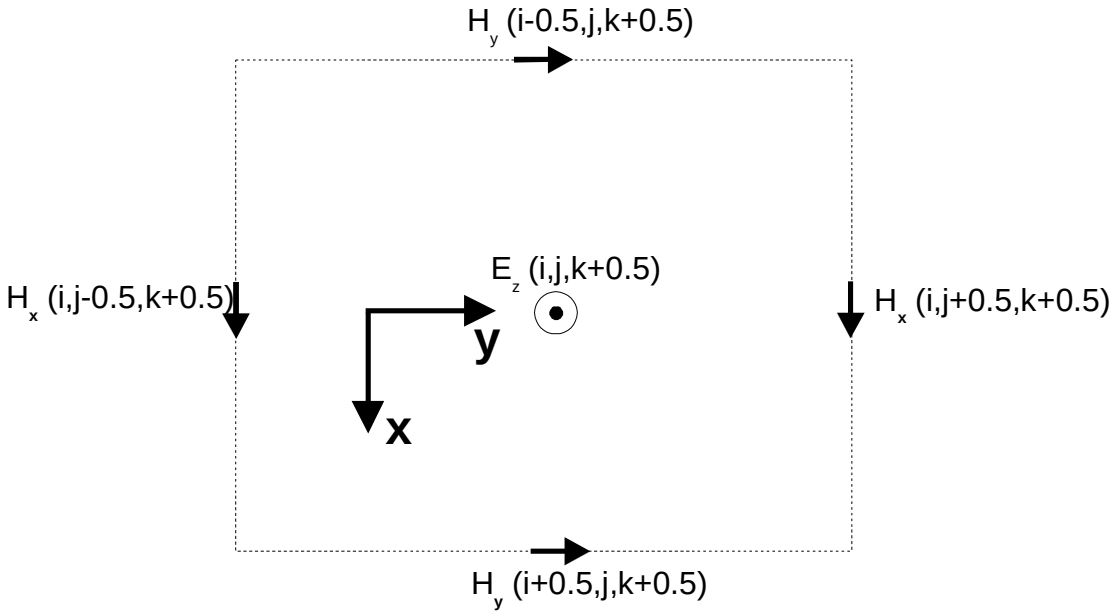

Figure 4.6 Ampere Loop in an FDTD Cell for z-directed current calculation

4.7.2 S-parameters calculation

The scattering parameters S_{mn} of a multiport network terminated by arbitrary impedances is given as

$$S_{mn}(f) = \frac{V_m(f) - Z_m(f) I_m(f)}{V_n(f) - Z_n(f) I_n(f)} \sqrt{\frac{Z_n(f)}{Z_m(f)}} \tag{4-47}$$

where Z_m, Z_n are the impedances $V_m(f)$, $V_n(f)$ are the frequency domain voltages and $I_m(f)$, $I_n(f)$ are the frequency domain currents at ports m and n respectively. Therefore the frequency domain voltages and currents must be extracted by FDTD. The time domain voltages at the ports are monitored during the simulation. Then the frequency domain quantities are given by a DFT (Discrete Fourier Transform) as

$$V(f) = \frac{1}{\Delta t} \sum_{k=0}^{N} V_t(k) e^{j 2\pi \cdot f \cdot k \cdot \Delta t} \tag{4-48}$$

$$I(f) = \frac{1}{\Delta t} \sum_{k=0}^{N} I_t(k) e^{j2\pi \cdot f \cdot k \cdot \Delta t} \tag{4-49}$$

where $V_t(k)$ and $I_t(k)$ are the discrete time voltages and currents. In the FDTD expressions, voltage is calculated from the electric field therefore it corresponds at time step n, whereas current is calculated at $n + \frac{1}{2}$ due to the time offset of the magnetic fields relative to the electric field. Consequently the current must be corrected for this offset (Fang and Xeu 1995) as

$$I'(f) = \frac{1}{\Delta t} \sum_{k=0}^{N} I_t(k) e^{j2\pi \cdot f(k+1/2) \cdot \Delta t} = I(f) \cdot e^{j2\pi \cdot f \cdot \frac{\Delta t}{2}} \tag{4-50}$$

The expressions (4-48) and (4-50) are the ones that should be inserted into (4-47). The input impedance should be calculated as

$$Z_{in}(f) = \frac{V(f)}{I'(f)} = \frac{V(f)}{I(f)} e^{-j\pi \cdot f \cdot \Delta t} \tag{4-51}$$

The Fourier Transform of voltages and currents is performed using an FFT algorithm (Press et al. 1986) which is applied after the end of simulation when all the samples are available. Zero padding up to 32000 samples is used to improve the resolution of the FFT.

Antennas in some come cases can be considered one-port networks fed by a transmission line of characteristic impedance Z_s. Then there is a specific interest in the S_{11} parameter that has a minimum at the resonant frequency. This can be calculated from FDTD based on the corrected input impedance (4-51),

$$S_{11}(f) = \frac{Z_{in}(f) - Z_s}{Z_{in}(f) + Z_s} \tag{4-52}$$

4.8 Summary

In this chapter, the general details have been presented, drawn from the published literature, that need to be taken into account in order to build a working code based on FDTD methods for systems that include antennas and circuit elements. The circuit source and its adaptation in this work has been described. Mur conditions have been selected to provide the truncation conditions. Methods of extracting antenna figures of merit (radiation patterns) along with circuit quantities (voltages, currents and S-parameters) have been reviewed. A flowchart of the code is given in Appendix B.1. An estimation of the overall computer requirements for a typical size problem including termination conditions is given in Appendix B.2 .

CHAPTER 5

PASSIVE ANTENNAS AND SIMPLE CIRCUITS

This chapter is concerned with the validation of three dimensional FDTD code used in this work. This code, based on the theory and developments described in chapters 3 and 4, can be applied to antennas, circuits and combinations of antennas and circuits. A wire dipole is studied as an antenna validation example. Furthermore the method is applied to the analysis of a new small microstrip antenna suitable for MMIC applications. Simple circuits are also presented to validate the modelling of lumped components, both linear (resistors, capacitors, inductors) and nonlinear (Schottky diodes).

5.1 A Wire Dipole Antenna

The first structure chosen for validation is a wire dipole. The structure is geometrically simple and it is still used as the radiator in numerical simulations when the important issue of interaction between electromagnetic fields and human tissues is addressed (Martens et al. 1995). Also it is used in EMC problems to investigate coupling from shielded enclosures (Hockanson et al. 1995). An additional practical reason is to test the code for the modelling of metal pins. These are essential to the code because they provide the connections for the source and the circuit elements. For comparison measurements and the Method of Moments (MoM) were used. MoM was selected as this is the traditional method for analysis of wire antennas. The MoM calculations were performed with a computer program based on a program found in Balanis(1997). This program was extended to calculate scattering

parameters and directivity. The formulation used is the Pocklington's magnetic potential integral equation.

The FDTD modelling of the wire as described in chapter 3 requires that the tangential component of the relevant electric field nodes to be set to zero (Figure 5.1). This implies that the wire is of infinitely thin radius. However due to the nature of the method, the wire radius is not zero. Hockanson et al (1995) demonstrated that good practical results are feasible with a wire of effective radius α_{eff}=0.2 Δx which has been followed in this work. Similar effective radii were suggested by Luebbers and Begs(1992) who argued that the transverse cells must have dimensions such that the cross section is equal to the cylindrical wire cross section.

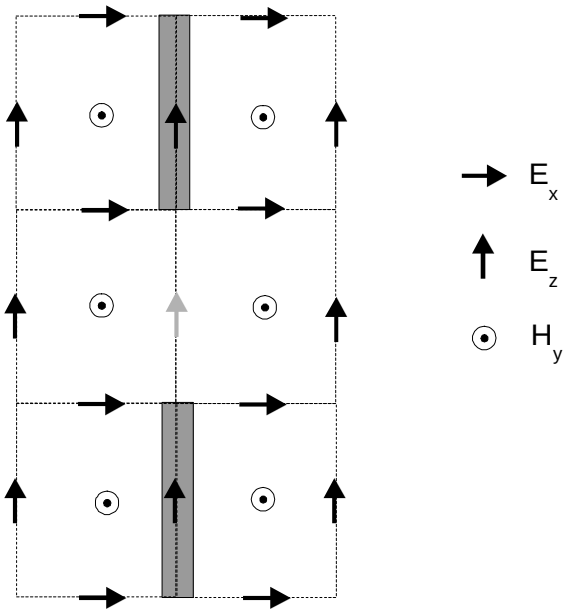

Figure 5.1 Part of the FDTD domain for a dipole along the z direction (xz plane cross-section). The grey arrow in the middle of the dipole indicates the excitation position.

A dipole was made in the laboratory to resonate close to the 900 MHz region using a 50Ω coaxial cable and a wire of length L=154.5mm and diameter of d=1.25mm. For the FDTD modelling, 61 cells were used for the length thus leading to Δz=2.53mm. For the radius,

choice of spatial resolution of $\Delta x=\Delta y=3.125$ mm leads to an effective radius equal to the experimental one according to Hockanson et al (1995). The excitation was a Gaussian pulse with parameters chosen as described in chapter 4. The simulation was stopped when the transients dissipated. This happened after approximately 3000 steps. For the MoM, 61 pulses were used which correspond to using 61 segments for the dipole.

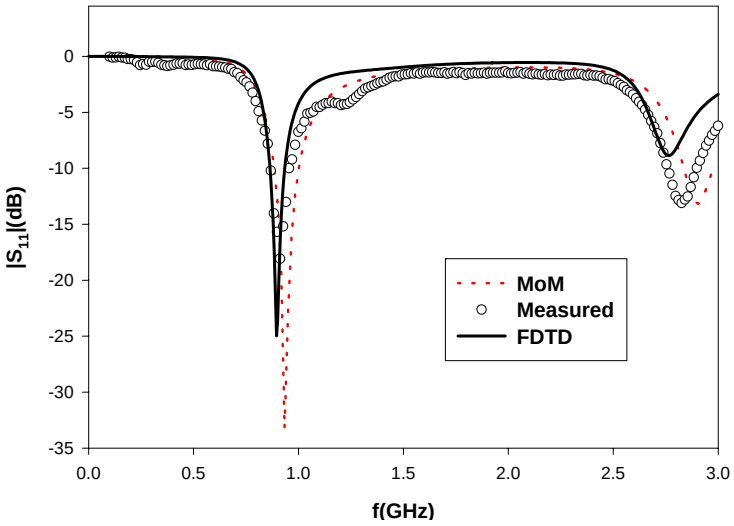

Figure 5.2 S_{11} magnitude for a dipole of length L=154.5 mm and radius α=0.625mm

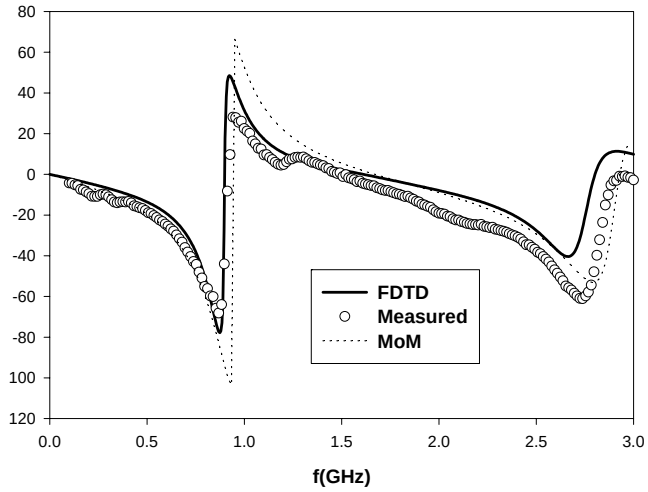

Figure 5.3 S_{11} phase for a wire dipole (length L=154.5 mm, radius α=0.625mm)

The magnitude and phase of the return loss S_{11} is shown in Figure 5.2 and Figure 5.3 respectively. At 0.9 GHz, the dipole is half wavelength long. At 2.8 GHz, close the second resonance the dipole is approximately 1.5 wavelengths. The radiation patterns for the plane that contains the dipole are shown in Figure 5.4.

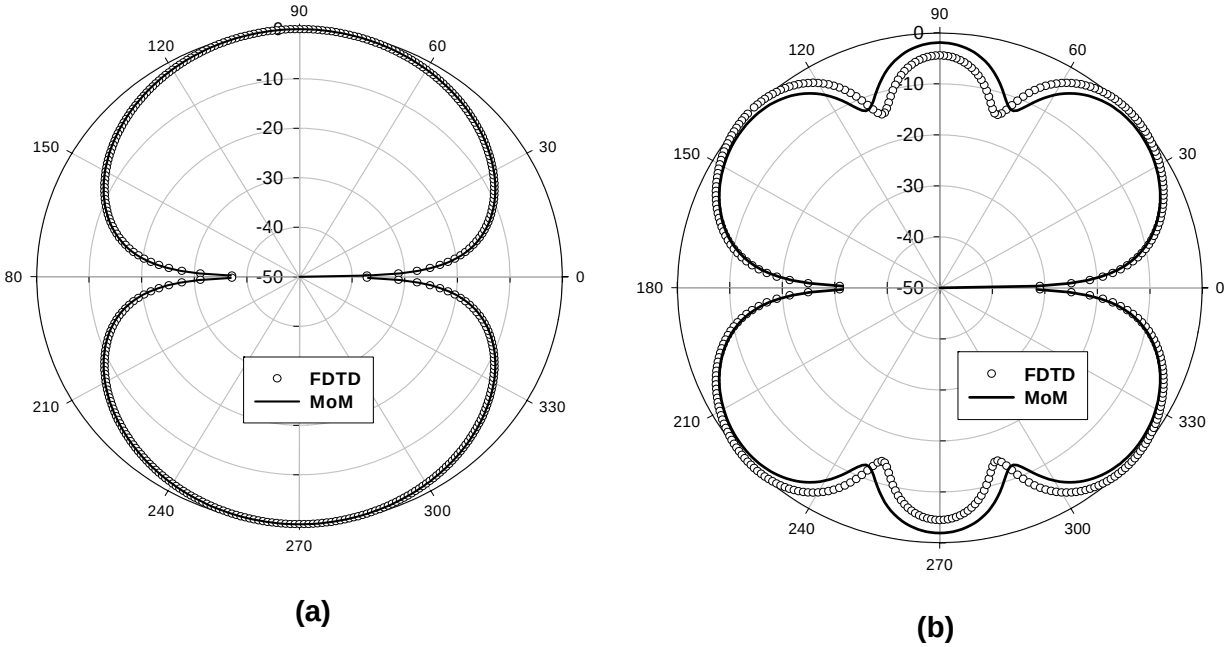

Figure 5.4 Radiation pattern for a dipole of length 154.5 mm and radius α=0.625mm at (a) 0.9 GHz and at (b) 2.8 GHz

The agreement between FDTD and Method of Moments (MoM) is very good for the first resonance. There is a difference between the two methods for the second resonance. These can be attributed to the modelling of the source. Both employ a gap source model but the MoM uses a delta (infinitesimal) gap model whereas in FDTD a finite gap is used. At the second resonance the finite gap becomes electrically larger whereas in MoM the source gap still is infinitesimal.

The directivities were calculated with both methods (TABLE 5-1) for the same two frequencies where the radiation patterns are calculated. There is excellent agreement for 0.9GHz. There is a difference of 0.7dB at 2.8GHz which is due to the small differences in the radiation patterns (Figure 5.4.b)

TABLE 5-1

Calculated Directivities for a wire dipole

f(GHz)	FDTD	Method of Moments
0.9	2.13dB	2.10dB
2.8	3.40dB	2.74dB

5.2 Small H-Shaped Microstrip Antennas

For this work, it is essential to model accurately microstrip antennas that form the radiating part of the antenna-circuit configurations under study. In general, antennas are physically larger than the circuits. In millimeter wave frequencies their size is quite small but in frequencies of a few GHz they tend to occupy a lot of space. The cost of monolithic circuits is directly related to the semiconductor substrate area. Therefore integration of microwave active devices and antennas on GaAs require small antennas.

A small H-shaped short-circuited microstrip antenna (Figure 5.5) has been proposed by Singh et al.(1997) that exhibits significant reduction in the resonant frequency. The antenna combines size reduction of a quarter wavelength short-circuited antenna (James and Hall 1989) with an H shaped antenna (Palanisamy and Garg 1985).

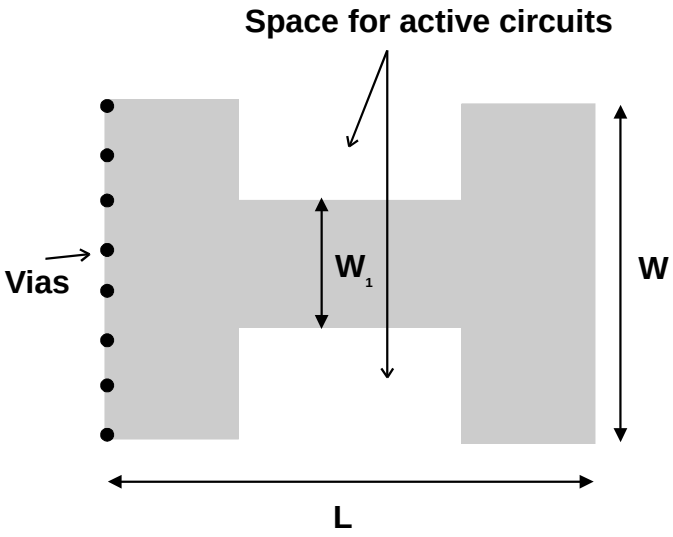

Figure 5.5 A small H-shaped short-circuited antenna layout suitable for MMIC applications.

Control of the resonant frequency is achieved by changing the width W_1 of the middle section. Five antennas with widths 1, 3, 5, 7mm were modelled. The value 11mm corresponds to a quarter wavelength antenna and is used as the normalising value in Figure 5.6. The resonant frequency is determined by the frequency where minimum magnitude of S_{11} occurs. The substrate is a duroid material of dielectric constant ε_r=2.2 and thickness h=0.51mm. The H-antenna was modelled using a grid of 161×151×51 cells with spatial resolution Δx=0.46mm, Δy=0.5mm, Δz=0.17mm. The corresponding time step is Δt=0.5ps. Very good agreement can be seen between calculated and measured resonant frequency as a function of the width (Figure 5.6).

The radiation patterns for microstrip antennas are given for two planes called E and H plane. In the position of the planes relative to the antenna is shown. Throughout the thesis, the microstrip antennas always lie on the xy plane and the length is along the x-axis.

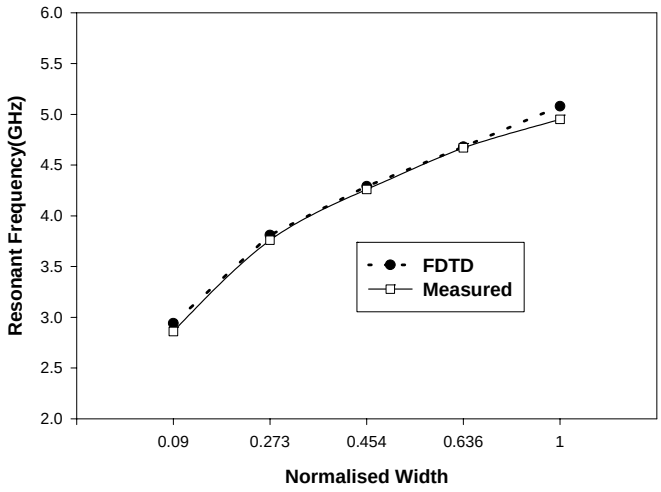

Figure 5.6 Resonance frequency of H-shaped short circuited antennas (Normalisation Width=11mm corresponds to a quarter wavelength antenna)

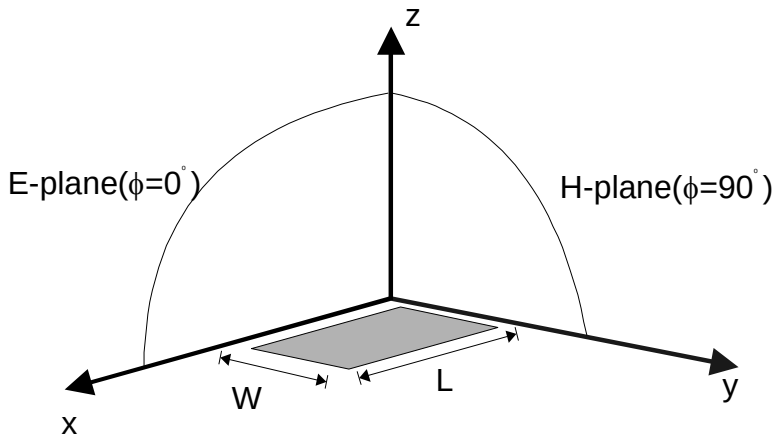

Figure 5.7 Definition of planes for microstrip antennas

Excellent agreement between experimental and FDTD radiation patterns (Figure 5.8, Figure 5.9) is shown for the upper half plane and good agreement is also obtained for the back lobes which are dependent on the finite ground plane. Very good agreement was obtained between FDTD and experimental results for antennas with different values of width W_1. The results show that the back lobe of E and H of the antenna increases as the resonance frequency decreases. Since the physical size of the ground plane remained constant for all tested

antennas, its electrical length at resonance was reduced as the resonance frequency reduced. In the case when W_1 = 1mm, the resonant frequency is close to 3GHz and the ground plane length is approximately half the size it is at 5GHz and the diffraction is less prominent at the back plane (Figure 5.8.b, Figure 5.9.b).

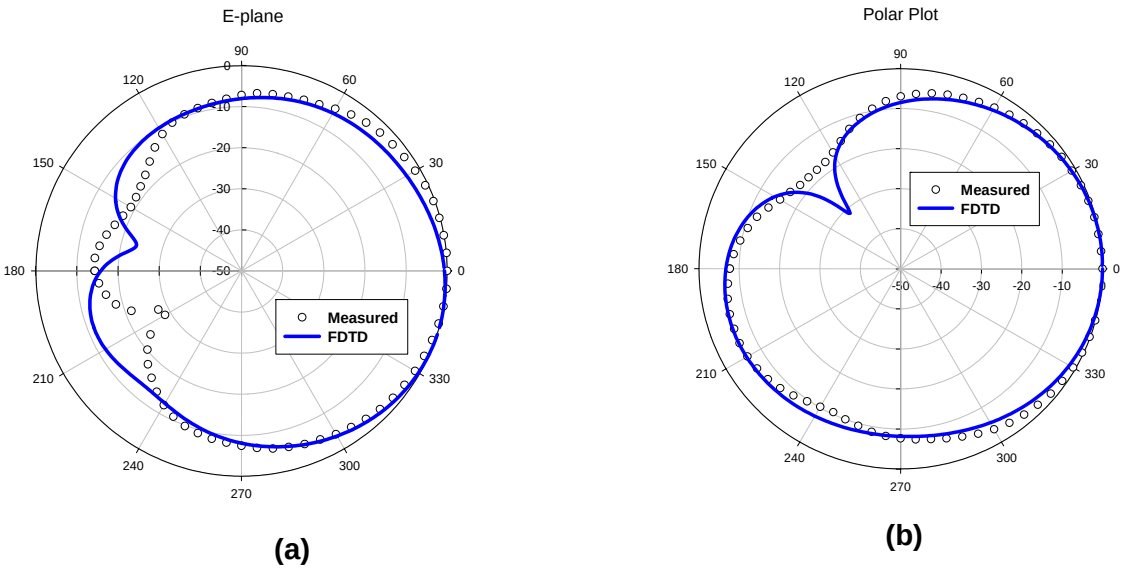

Figure 5.8 E-plane copolar radiation patterns (a)for a quarter wavelength antenna(b) H antenna of width W_1=1 mm

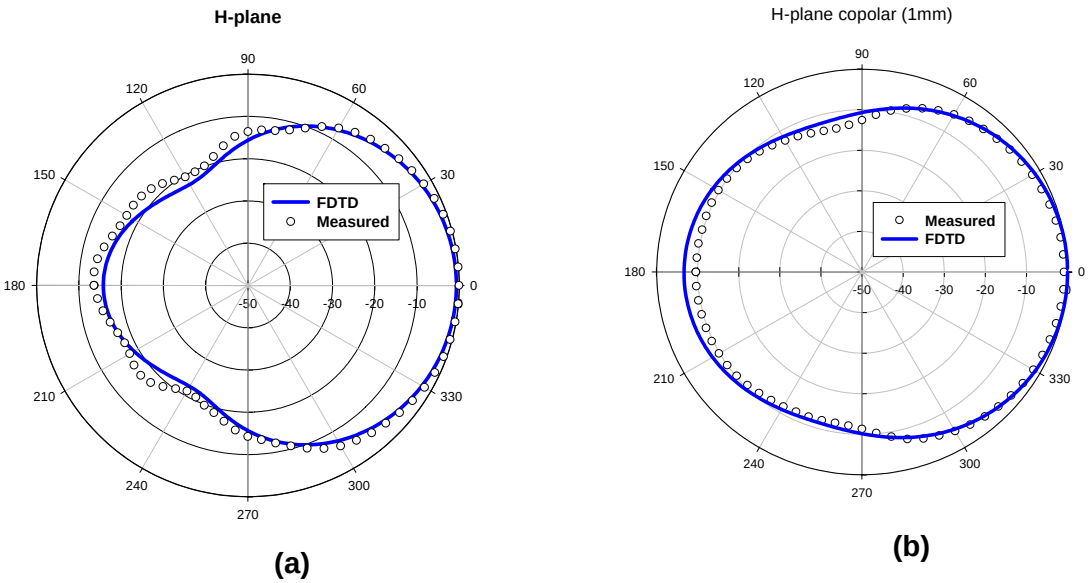

Figure 5.9 H-plane copolar radiation patterns (a)for a quarter wavelength antenna (b) H antenna of width W_1=1 mm

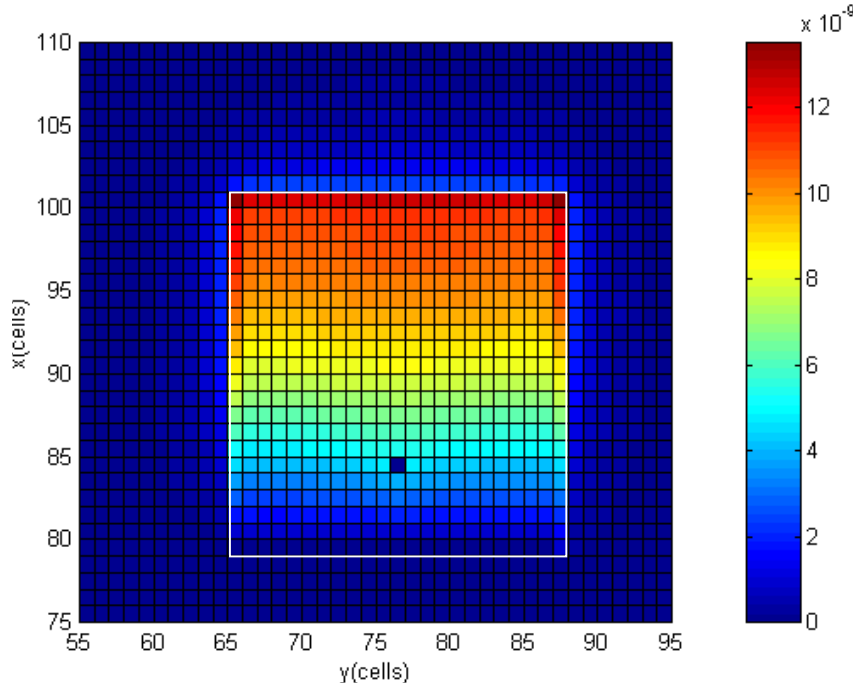

(a)

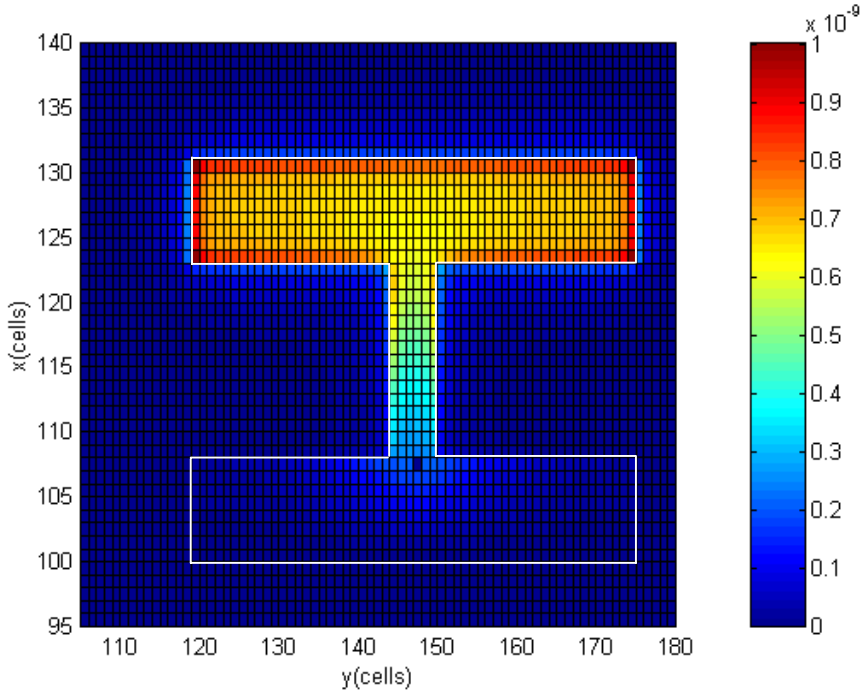

(b)

Figure 5.10 Calculated electric field distribution on the antenna at the first resonant frequency

(a) Quarter Wavelength W_1=11mm (5GHz) (b) H antenna W_1=1mm (2.87GHz)

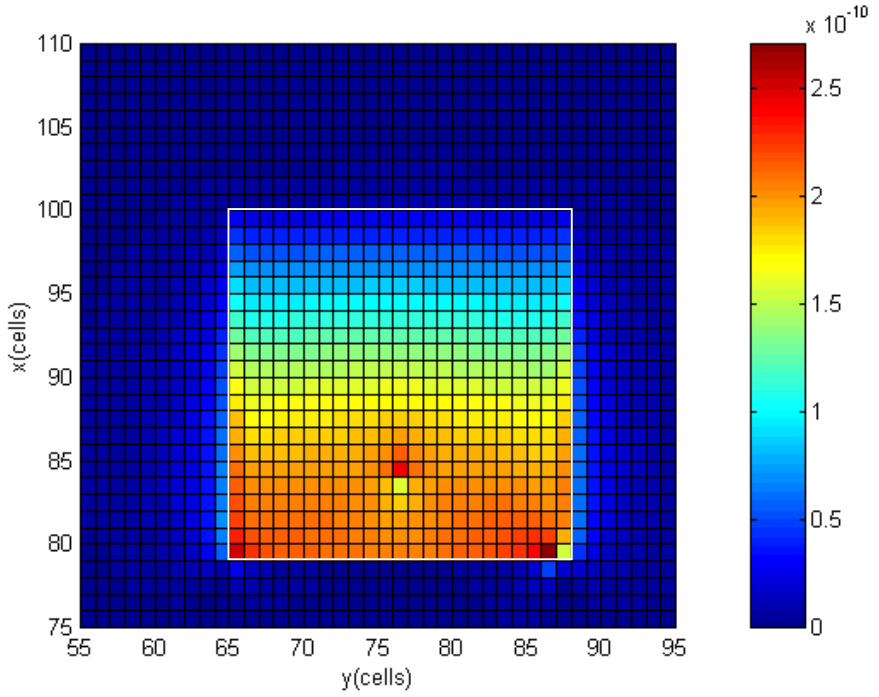

(a)

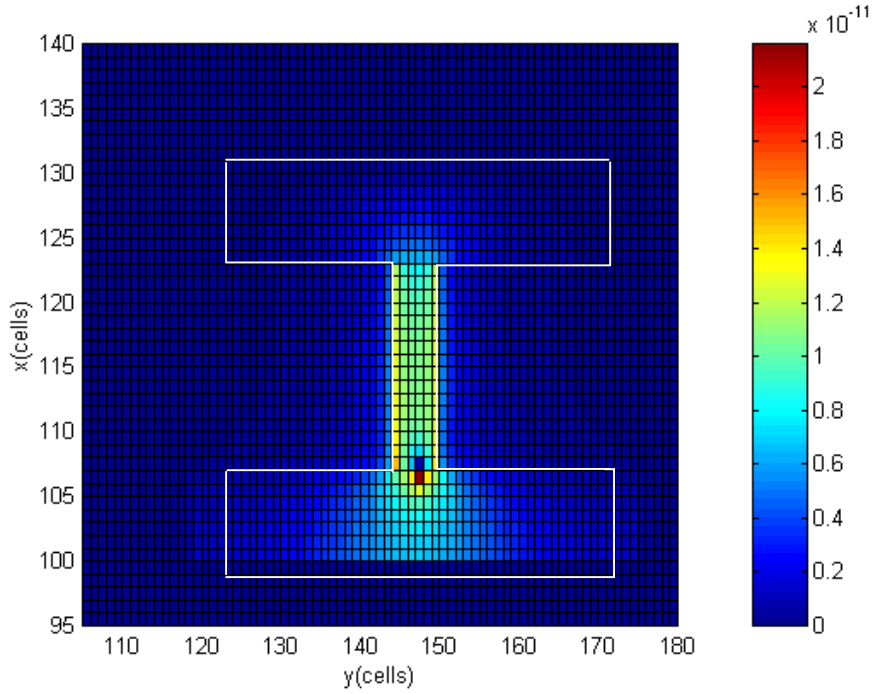

(b)

Figure 5.11 Calculated current density distribution on the antenna at the first resonant frequency(a) Quarter Wavelength W_1=11mm (5GHz) (b) H antenna W_1=1mm (2.87GHz)

The simulations were performed with a pulse excitation. Therefore a Fourier transform of the fields at the resonant frequency can provide the field distribution on the antenna surface . For a quarter wavelength antenna, the electric field E_z (component normal to the surface) at the resonant frequency is minimum at the short-circuits and maximum at the radiating edge (Figure 5.10.a). The introduction of a narrow middle section that forms the H antenna, forces the field to conform to the metal layout. The fringing fields are clearly seen and these should be taken into account when integration with active devices will be considered (Figure 5.10.b). The longitudinal current density for the quarter wavelength antenna (Figure 5.11.a) is maximum at the short-circuited side. Observe the shift of the maximum current density towards the narrow middle section (Figure 5.11.b) which reveals the distributed inductive behaviour that causes the reduction in resonant frequency.

The above results were for an antenna on a soft duroid substrate. An H shaped quarter wavelength antenna was designed for operation at 5.8 GHz and fabricated using the GEC Marconi F20 MESFET MMIC process (Singh 1999). The thickness of the GaAs (ε_r=12.9) substrate used was 0.2 mm. The overall size of the designed chip was 4.1 mm × 2.1 mm. The experimental resonant frequency of the antenna was 5.98 GHz, 3% different from that computed using the HP Momentum software which is based on method of moments (Singh 1999). This discrepancy in the resonance frequency is conjectured to be caused by the finite substrate and ground plane of the test fixture (25mm×25mm) that is necessary for the measurement set up of MMICs. HP Momentum models only infinite ground planes. In order to understand these effects further, an FDTD simulation was performed for grid with 251×131× 51 cells (spatial resolution Δx = 0.1 mm, Δy = 0.22 mm, Δz = 0.067 mm). The

larger number of cells was used to accommodate the electrically large ground plane. The resonance frequency of the MMIC antenna was found to be 6.03 GHz, giving 0.8 % difference from experiment, leading to the conclusion that it is very important to include the test fixture effects when comparing with measurements from MMIC antennas. Such small low cost GaAs MMICs could find applications in short range communications (Camiade et al 1996).

5.3 Analysis of a loaded microstrip line

Equivalent circuits of semiconductor devices are composed of lumped components and circuit sources. In order to validate the modelling of lumped components in the FDTD code, a 50Ω microstrip transmission line on a substrate of dielectric constant ε_r=2.2, thickness h=1.1mm, terminated by various types of loads, was chosen as the test structure (Figure 5.12).

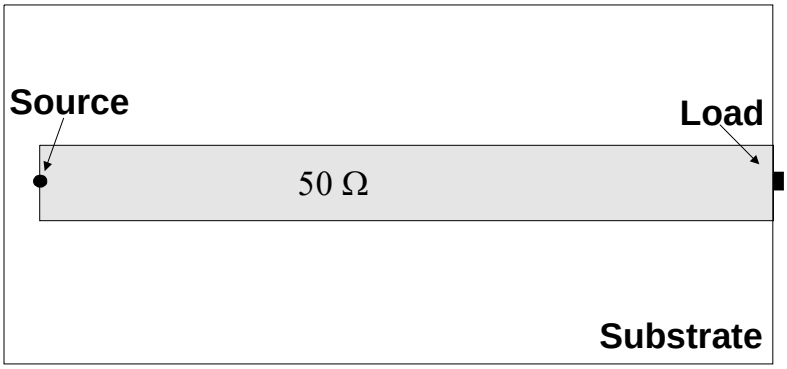

Figure 5.12 A loaded microstrip transmission line excited by a circuit voltage source(top view)

There is an incentive for investigations of digital signal propagation in microstrip lines. Microstrip lines form the signal tracks in computer processor boards where the signal integrity depends on the circuit topology and the loads terminating the lines (Yoguchi et al. 1998). The frequency of operation (corresponding to clock cycles) goes higher and higher

and has already reached frequencies in the microwave region. Consequently signals become susceptible to wave effects, mainly propagation and dispersion but also to coupling through fringing fields. Full wave methods like the lumped element FDTD gain in significance (Piket-May et al. 1994) for such problems.

The computational volume in FDTD was 101x71x61 cells with each cell having dimensions(in mm) 0.75×0.75×0.37. The line was 60×5 cells long and the substrate was 3 cells high.

5.3.1 Resistive termination

Let us consider a resistor placed along z-axis. From circuit theory:

$$R = \frac{V_Z}{I_L} \tag{5-1}$$

where V_z is also the voltage across the FDTD cell. Discretising (5-1) yields:

$$I_L^{n+\frac{1}{2}} = \frac{(E_z^{n+1} + E_z^n)\Delta z}{2R} \tag{5-2}$$

Substitution into (3-36) will give the update equation for the field at the cell where the resistor lies:

$$E_z^{n+1} = \frac{1 - \dfrac{\Delta t \cdot \Delta z}{2R \cdot \varepsilon \cdot \Delta x \cdot \Delta y}}{1 + \dfrac{\Delta t \cdot \Delta z}{2R \cdot \varepsilon \cdot \Delta x \cdot \Delta y}} E_z^n + \frac{\Delta t}{\varepsilon + \dfrac{\Delta t \cdot \Delta z}{2R \cdot \Delta x \cdot \Delta y}} (\nabla \times \overline{H})_z^{n+1/2} \tag{5-3}$$

The rest of the equations will be the same. Observe that the equation (5-3) results from the voltage source equation (4-6), when V_S is set to zero. The term introduced due to the presence of the resistance has the form of a conductivity term. An effective conductivity can be defined as

$$\sigma_{eq} = \frac{\Delta z}{R \cdot \Delta x \cdot \Delta y} \tag{5-4}$$

Thus (5-3) can be rewritten as

$$E_z^{n+1} = \frac{1 - \frac{\sigma_{eq} \cdot \Delta t}{2\varepsilon}}{1 + \frac{\sigma_{eq} \cdot \Delta t}{2\varepsilon}} E_z^n + \frac{\Delta t}{\varepsilon + \frac{\sigma_{eq} \cdot \Delta t}{2\varepsilon}} (\nabla \times \overline{H})_z^{n+1/2} \tag{5-5}$$

The line was terminated with 50Ω and 75Ω resistors excited by a resistive voltage source which was described in chapter 4. Although these are microstrip lines exhibiting dispersion, estimates of the magnitude of the pulses travelling in the line can be done using TEM transmission line theory.

The line was excited with a square pulse of subnanosecond duration, 0.245ns and amplitude 0.1V. This would be of interest in the case of digital modulation schemes. When the 50Ω source excites the line which is terminated with a matched load 50Ω, half the voltage (0.05V) is launched with the peak current being 1mA(=0.05/50) (Figure 5.13). When the line is terminated with 75Ω, the load presents a reflection coefficient ρ_L=0.2. Subsequently at the source position, a reflected voltage pulse of 0.01V (=0.2×0.5) and a negative current pulse of -0.2mA are detected (=0.2×1) (Figure 5.14). Then because the source is matched the pulse is not retransmitted.

Let us examine what is happening at the load position. When the load is matched to the line, no pulse is reflected and the amplitude of the load voltage and current (Figure 5.15) are equal to the source response (Figure 5.12). When the line is mismatched, the load voltage is equal to the incident plus the reflected pulse i.e. 0.06V (Figure 5.16).

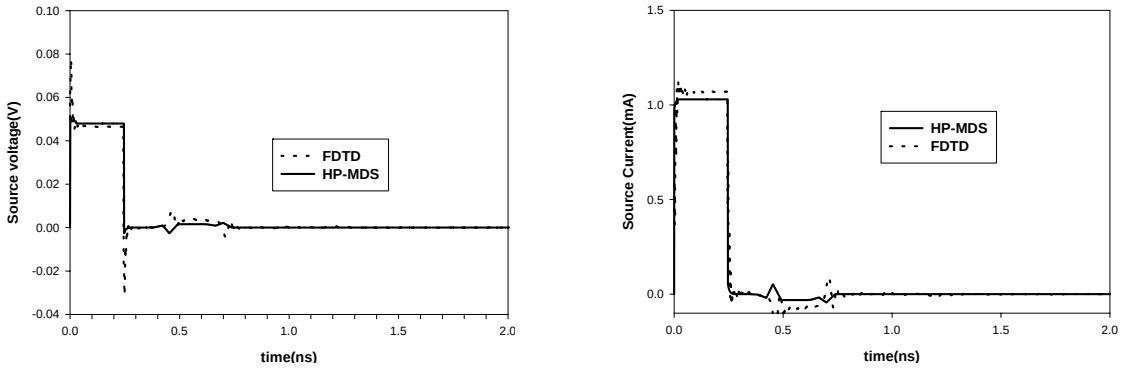

Figure 5.13 Calculated transient response at the source position for 50Ω termination (a) voltage (b) current

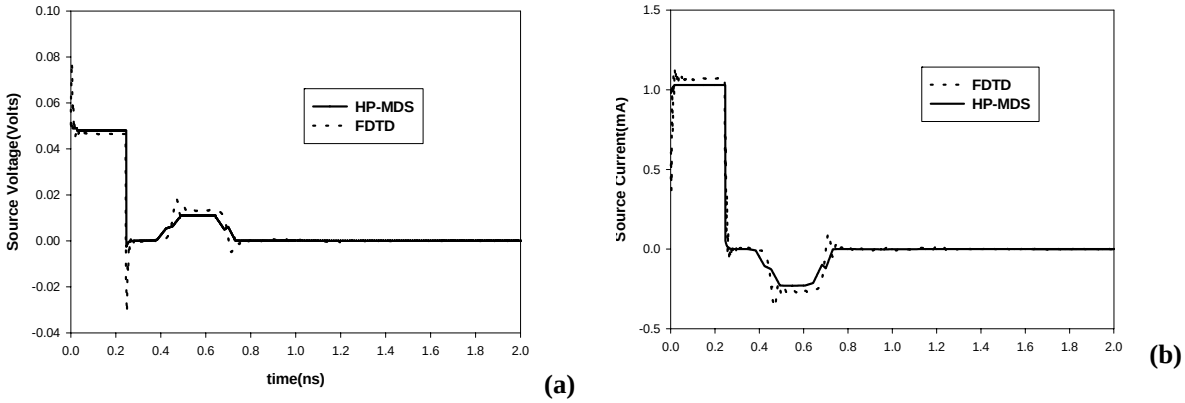

Figure 5.14 Calculated transient response at the source position for 75Ω termination (a) voltage (b) current

Having established the levels of the pulses, HP-MDS was used to investigate propagation effects on the line. The HP-MDS schematic which was used for the validation is shown in Figure E.1, Appendix E. The finite length of the length of the line is shown through the time delay of the load response (Figure 5.15, Figure 5.16). There is excellent agreement with HP-MDS. The second important effect of this very short pulse is the dispersion which is easily seen as the spread of the pulse at the load position. Observe that the dispersion is predicted from the FDTD modelling although the dielectric constant is frequency independent. This

would not be possible if the line was supporting pure TEM modes. However the fact that the microstrip line does support quasi TEM modes allows dispersion effects to be present with a frequency independent dielectric constant.

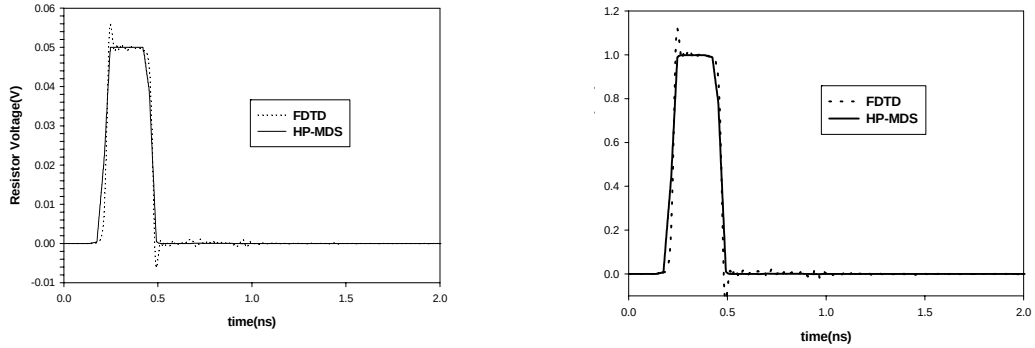

(a) **(b)**

Figure 5.15 Calculated transient voltage response at the load position for 50 Ω termination (a) voltage (b) current

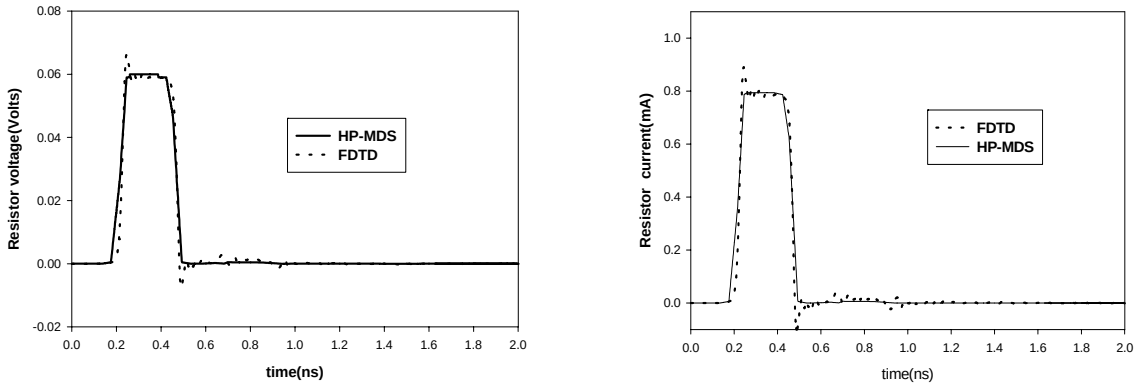

(a) **(b)**

Figure 5.16 Calculated transient voltage response at the source position for 75Ω termination (a) voltage (b) current

5.3.2. Capacitive termination

The current I_L flowing through a capacitance C obeys the equation:

$$I_L = C\frac{dV_Z}{dt} \qquad (5\text{-}6)$$

In discrete form expression (5-6) can be written as:

$$I_L^{n+\frac{1}{2}} = C\frac{\Delta V_Z^{n+\frac{1}{2}}}{\Delta t} = C\frac{(E_z^{n+1} - E_z^n)\cdot \Delta z}{\Delta t} \qquad (5\text{-}7)$$

Substitution of (5-7) to (3-36) gives the update equation for the electric field in the capacitor cell (σ=0 for a lossless substrate) :

$$E_z^{n+1} = E_z^n + \frac{\Delta t}{\varepsilon + \frac{C\cdot \Delta z}{\Delta x\cdot \Delta y}}(\nabla \times \overline{H})_z^{n+1/2} \qquad (5\text{-}8)$$

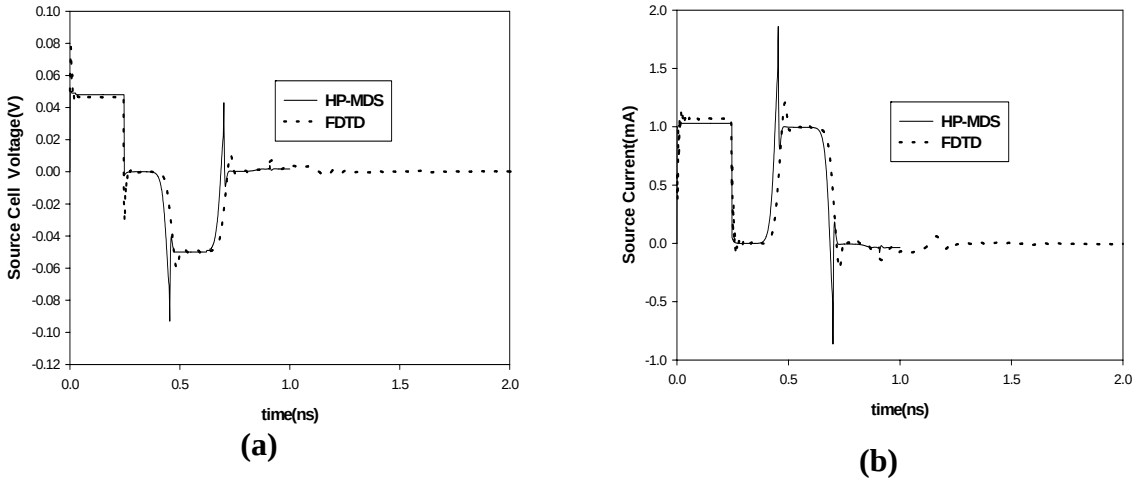

(a) **(b)**

Figure 5.17 Transient response of the matched source when exciting a line terminated with a capacitor C=2nF with a step pulse of duration 0.245ns. (a) voltage (b) current

An equivalent local permittivity can be defined for the additional circuit capacitance.

$$\varepsilon_{eq} = C\frac{\Delta z}{\Delta x\cdot \Delta y} \qquad (5\text{-}9)$$

Then (5-8) can be written as

$$E_z^{n+1} = \frac{1 - \frac{\sigma\cdot\Delta t}{2\varepsilon} + \frac{\varepsilon_{eq}}{\varepsilon}}{1 + \frac{\sigma\cdot\Delta t}{2\varepsilon} + \frac{\varepsilon_{eq}}{\varepsilon}} E_z^n + \frac{\Delta t}{\varepsilon + \frac{\sigma\cdot\Delta t}{2} + \varepsilon_{eq}}(\nabla \times \overline{H})_z^{n+1/2} \qquad (5\text{-}10)$$

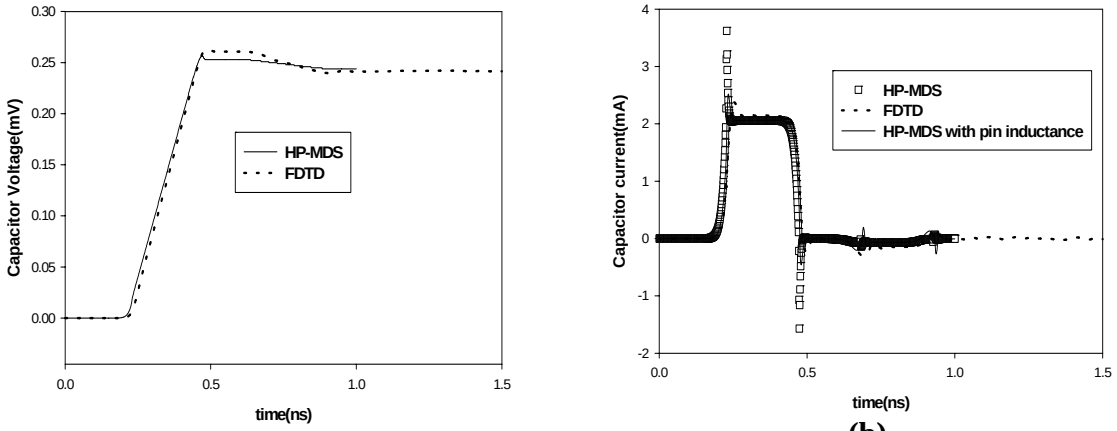

Figure 5.18 Transient response at the capacitor cell of a capacitor C=2nF terminated line to a step pulse of duration 0.245ns (a) voltage (b) current

A step pulse of duration 0.245ns and amplitude of 0.1V was used as the excitation and the transient response was monitored in the source and capacitor position. The HP-MDS schematic which was used for the validation is shown in Figure E.2, Appendix E. Due to finite propagation velocity there is a time delay t_d=0.21ns. At the source position a reflected pulse due to the reactive load is detected (Figure 5.17). The capacitor is charged by the current but due to the time constant of the circuit (100ns), the voltage across the capacitor is practically constant. The agreement between HP-MDS and FDTD is very good. The presence of the spike in the HP-MDS results can be explained by the fact that the circuit simulator assumes ideal wire connections between the circuit element and the line. In the FDTD case the connections are metal pins (Figure 4.1.b) which present inductance that becomes more noticeable as the frequency goes higher. In order to justify that, an additional simulation was performed with HP-MDS with a pin inductance correction. An approximate estimate of the inductance for the simulation can be based on the internal inductance of a piece of wire, small enough to assume uniform current along its length. This inductance per unit length is

L=$\frac{\mu_o}{8\pi}$ (Ramo et al. 1994) so the inductance for a small wire of length 0.4mm will be of the order of 0.1nH . It must be noted that an accurate determination of that inductance is not easy and it is related with the problem of via inductance in MMICs. It can be seen that the spike has now disappeared and the agreement is now excellent (Figure 5.18.b) .

5.3.3 Inductive termination

The voltage across an inductance L obeys the equation

$$V_z = L\frac{dI_L}{dt} \Rightarrow I_L = \frac{1}{L}\int_0^t V_z dt \qquad (5\text{-}12)$$

Discretising (5-12) :

$$I_L^{n+\frac{1}{2}} = \frac{\Delta t \cdot \Delta z}{L}\sum_{m=1}^{n} E_z^m \qquad (5\text{-}13)$$

Substitution of (5-13) to (3-36) gives the update equation for the electric field in the inductor cell:

$$E_z^{n+1} = \frac{1-\frac{\sigma\cdot\Delta t}{2\varepsilon}}{1+\frac{\sigma\cdot\Delta t}{2\varepsilon}} E_z^n + \frac{\Delta t}{\varepsilon(1+\frac{\sigma\cdot\Delta t}{2\varepsilon})}(\nabla\times\overline{H})_z^{n+1/2} - \frac{(\Delta t)^2\cdot\Delta z}{L\cdot\varepsilon\cdot\Delta x\cdot\Delta y(1+\frac{\sigma\cdot\Delta t}{2\varepsilon})}\sum_{m=1}^{n} E_z^m \qquad (5\text{-}14)$$

The transient response was monitored for an inductor L=1μH. The HP-MDS schematic which was used for the validation is shown in Figure E.3, Appendix E. Satisfactory agreement is observed between HP-MDS and FDTD.

At the source position (Figure 5.19), the behaviour is similar to the case of capacitive termination (Figure 5.17). The calculated FDTD inductor current (Figure 5.20.b) can be split in two parts; one due to the parallel equivalent capacitance due to the displacement

current from the FDTD calculation and one due to actual inductance as calculated by (5-14). Circuit software does not account automatically for the presence of this small capacitance which for short pulses could affect the total current transients.

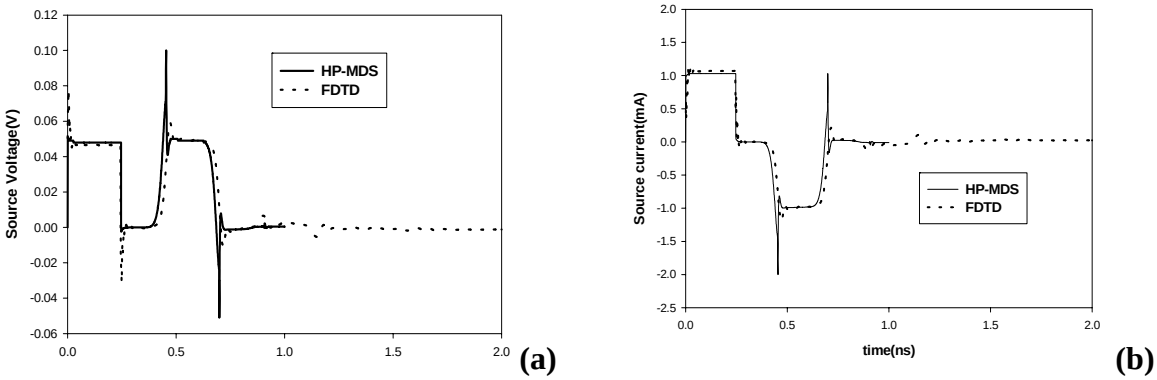

Figure 5.19 Transient response of the matched source when exciting a line terminated with an inductance L=1μH with a step pulse of duration 0.245ns, 0.1V amplitude. (a) voltage (b) current

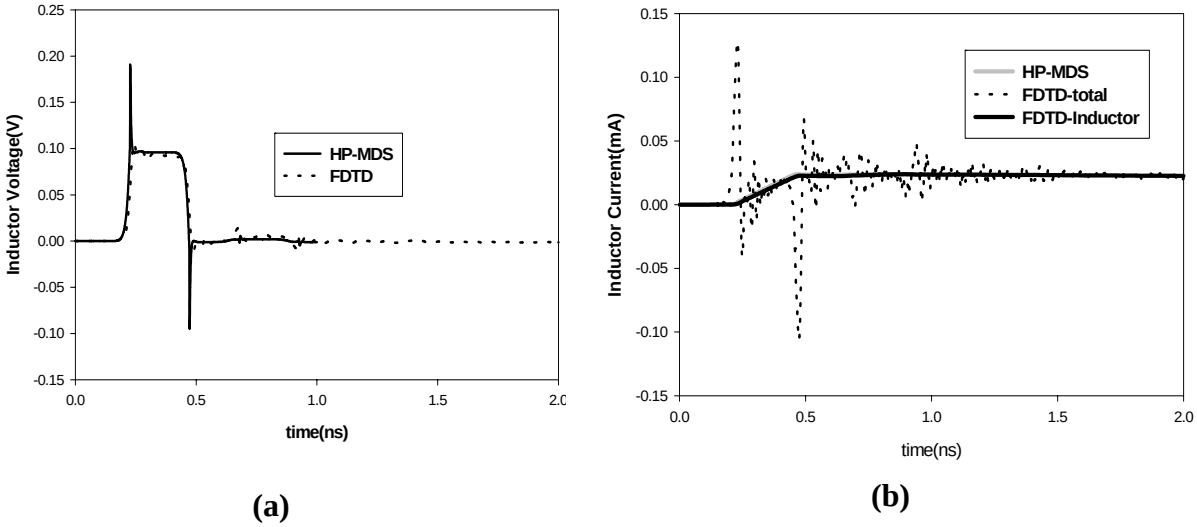

Figure 5.20 Transient response of an inductor L=1μH to a step pulse of 0.1V amplitude and duration time of 0.245 ns. (a) voltage (b) current

5.4 Modelling of Detector diodes (nonlinear resistor)

Detector diodes (Schottky diodes) are in effect nonlinear resistors whose I-V characteristic is described by:

$$I_L = I_o \cdot \left[exp\left(\frac{qV_z}{kT} \right) - 1 \right] \tag{5-15}$$

To create FDTD expressions one has to derive the discrete form of (5-15):

$$I_L^{n+\frac{1}{2}} = I_O \left[exp\left(\frac{qV_Z^{n+\frac{1}{2}}}{kT} \right) - 1 \right] = I_O \left[exp\left(\frac{q(E_z^{n+1} + E_z^n) \cdot \Delta z}{2kT} \right) - 1 \right] \tag{5-16}$$

Substitution of (5-16) to (3-36) gives the update equation for the electric field in the diode cell:

$$E_z^{n+1} = E_z^n + \frac{\Delta t}{\varepsilon} (\nabla \times \overline{H})_z^{n+1/2} - \frac{\Delta t}{\varepsilon \cdot \Delta x \cdot \Delta y} I_o \left[exp\left(\frac{q(E_z^{n+1} + E_z^n) \cdot \Delta z}{2kT} \right) - 1 \right] \tag{5-17}$$

A Newton-Raphson iteration scheme (Press et al. 1986) is used to solve nonlinear equations of this type. Unless a significant reduction in time step occurs, expression (5-17) is divergent in the FDTD context. Similar findings were reported by Ciampolini et al (1997) in the FDTD analysis of a mixer incorporating a diode. Such instabilities are not unique to FDTD simulations. Reduction in time step size was also required to produce convergent results in the case of a circuit-based time-domain analysis of transmission lines terminated with nonlinear loads (Yun and Ra 1995).

A qualitative explanation for the necessity to use small time steps is attempted here based on signal processing arguments. It is known that given a time function, it can be sampled at a rate f_s which corresponds to a Nyquist frequency $f_s/2$. A function which is bandlimited for frequencies greater than f_s, can be reconstructed accurately when it is sampled with the

Nyquist frequency $f_N = 2 f_s$. The sampling frequency corresponds to a time resolution $\Delta t = 1/f_N$ and can be completely reconstructed. If the time resolution is not enough to have the Nyquist limit then errors occur due to aliasing in frequency domain . Aliasing can cause instabilities in the case of FDTD. In linear cases the bandwidth is known beforehand and it can be easy to obey the Nyquist limit. This is what essentially is achieved when using the Gaussian pulse with parameters that control the spectrum. However in nonlinear problems, frequency generation can give significant spectral components out of a given frequency band thus leading to failure to meet Nyquist rate. It is therefore necessary to decrease Δt so no spectral components of significant magnitude will contaminate the solution due to aliasing.

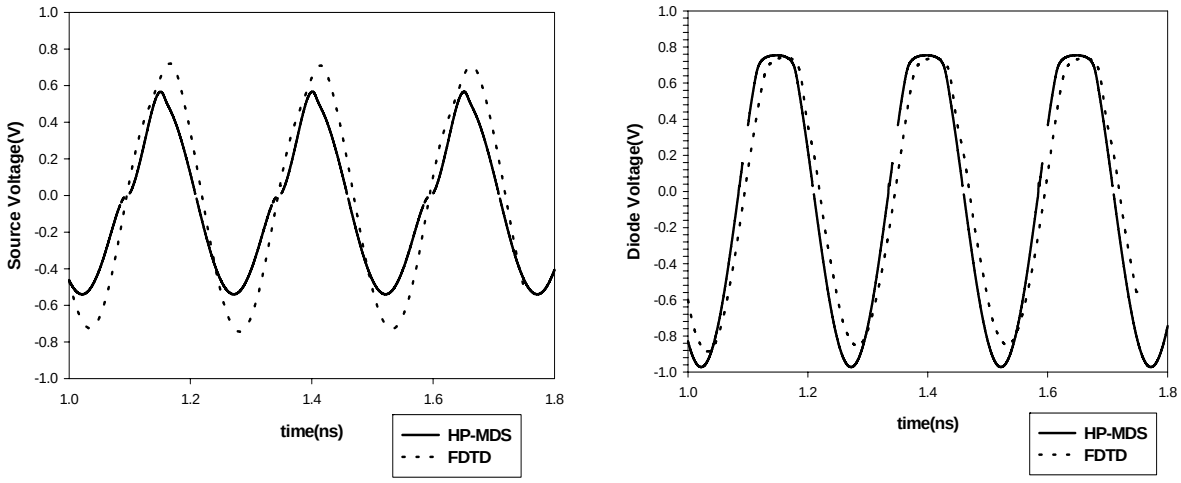

(a) **(b)**

Figure 5.21 Voltage response versus time for ramp sine input voltage f=4GHz (a) source (b) diode

Transients in a microstrip line terminated with a nonlinear resistor were investigated by Gu et al.(1992). However in their approach they used FDTD to obtain only the S-parameter matrix of the line. Piket-May et al.(1994) considered the same problem but their approach

was concurrent modelling and the one that is followed here. The test structure is a microstrip line terminated with a diode. The excitation is a sine wave of amplitude 1.0V, f=4GHz. The HP-MDS schematic which was used for the validation is shown in Figure E.4, Appendix E. Voltage clipping to 0.7 V is expected at the diode position (Figure 5.20.b). For the FDTD results an up to ten times smaller time step was used to avoid divergence. There is a slight discrepancy between the results from FDTD and HP-MDS (Figure 5.21, 5.22). These are attributed to modelling of the metal pins as it was shown in the case of the capacitive termination.

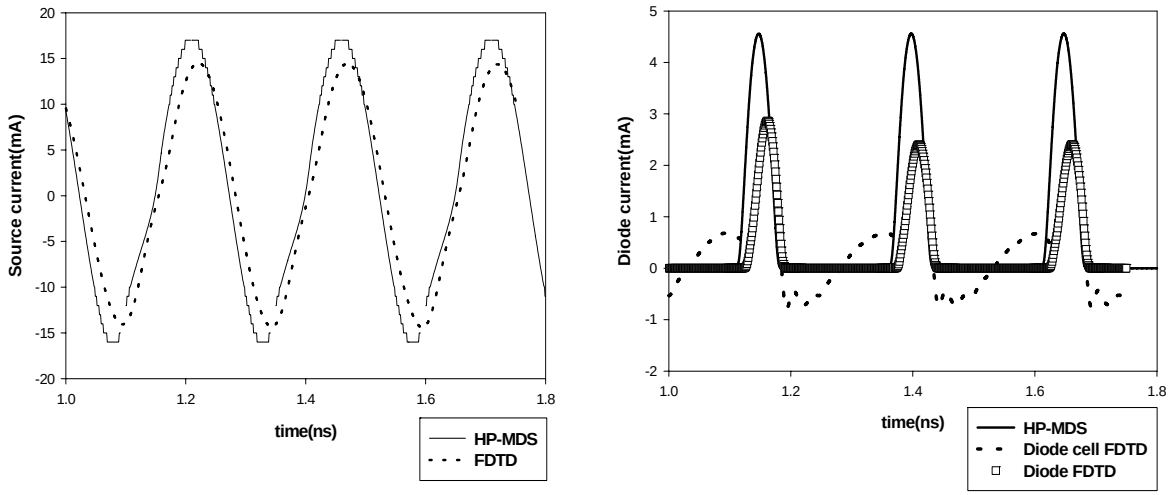

Figure 5.22 Current response for ramp sine input voltage with frequency f=4GHz (a) source (b) diode

5.6 Summary

This chapter presented applications of FDTD to antennas and circuits. A dipole was analysed to ensure proper modelling of metal pins. Original results were presented for small antennas suitable for MMIC applications. For the lumped components, the validity of circuit source,

resistor, capacitor and inductor modelling was demonstrated. Instabilities which lead to unbounded solutions may arise when incorporating nonlinear circuit elements in the FDTD context. This was found in the case of an exponential nonlinearity. Instabilities can be avoided by oversampling. An original qualitative explanation on the instability problem was presented.

CHAPTER 6
INTEGRATED ACTIVE CIRCULATOR ANTENNAS

In this chapter novel results are presented from the analysis of integrated active circulator antennas. The effect of coupling on the performance of these antennas is examined. A gain block formulation for the extended FDTD method is also presented.

6.1 Circulators

Circulators are three port networks that allow signal flow (Figure 6.1) from one port to another but not the other way. In general, any three port network is characterised by the matching at its ports, reciprocity of power flow and loss. A circulator is a device that is non-reciprocal. It can be lossless and matched at all ports (Pozar 1990).

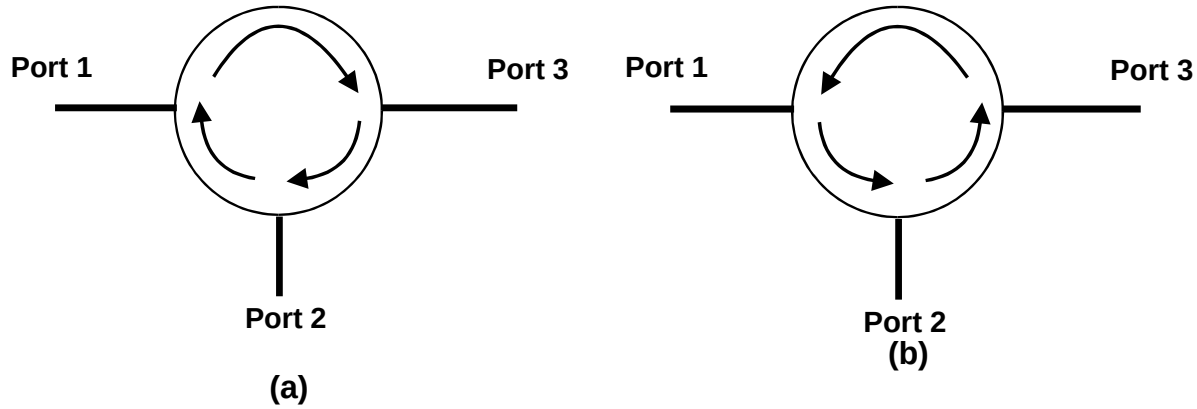

Figure 6.1 Power flow in an ideal circulator (a) Clockwise (b) Counter-clockwise

The general form of the S-parameter matrix of a three port network is,

$$S = \begin{bmatrix} S_{11} & S_{12} & S_{13} \\ S_{21} & S_{22} & S_{23} \\ S_{31} & S_{32} & S_{33} \end{bmatrix} \qquad (6\text{-}1)$$

For an ideal circulator with clockwise power flow (Figure 6.1.a) the [S] matrix is

$$S = \begin{bmatrix} 0 & 1 & 0 \\ 0 & 0 & 1 \\ 1 & 0 & 0 \end{bmatrix} \qquad (6\text{-}2)$$

For an ideal circulator with counter-clockwise power flow (Figure 6.1.b) the [S] matrix is

$$S = \begin{bmatrix} 0 & 0 & 1 \\ 1 & 0 & 0 \\ 0 & 1 & 0 \end{bmatrix} \qquad (6\text{-}3)$$

Observe that there is only one 1 in every line of the [S] matrices (6-2) and (6-3) which is the consequence of the fact that every port accepts power from only one of the other two ports.

The quasi circulator (Robertson 1995) is a type of circulator that allows power flow between two out of three ports (Figure 6.2)

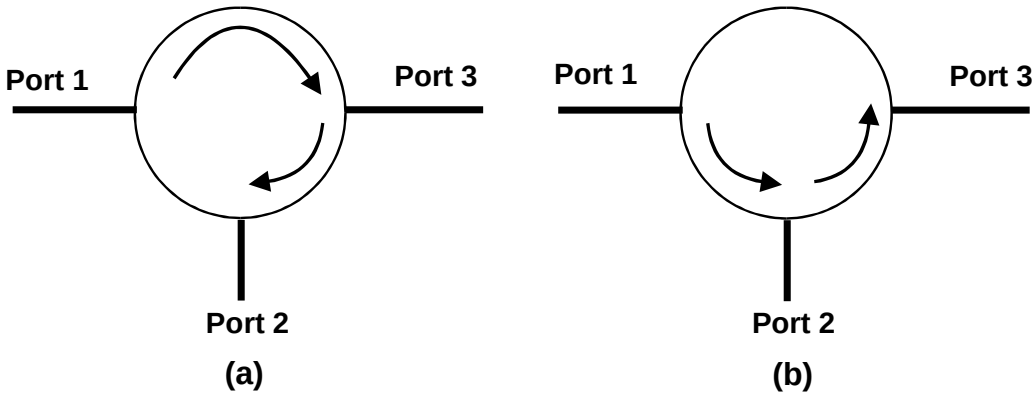

Figure 6.2 Ideal quasi circulators with (a) Clockwise (b) Counter-clockwise power flow

The [S] matrix for the quasi circulator with clockwise flow (Figure 6.2.b) becomes

$$S = \begin{bmatrix} 0 & 0 & 0 \\ 0 & 0 & 1 \\ 1 & 0 & 0 \end{bmatrix} \qquad (6\text{-}4)$$

For an ideal quasi-circulator with counter-clockwise power flow (Figure 6.2.b) the [S] matrix is

$$S = \begin{bmatrix} 0 & 0 & 0 \\ 1 & 0 & 0 \\ 0 & 1 & 0 \end{bmatrix} \qquad (6\text{-}5)$$

6.1.1 Implementation

Practical realisations of circulators must include non-reciprocal junctions to provide the isolation required. The first realisation was achieved using magnetised ferrites to exploit the Faraday effect. The other possible realisation is with transistors . Transistor devices apart from the amplification operation have the ability to isolate their input and output ports. Tanaka et al(1964) were the first to realise such a structure at a few MHz using bipolar transistor technology.

The advantages of using active circulators are size and compatibility with monolithic technology (Dougherty 1989). Several implementations have appeared on MMIC technology. Katzin et al. (1989) reported a 6-18 GHz active circulator. Kother et al.(1995) have reported devices up to 50 GHz. An additional advantage is the capability to compensate for losses by adjusting the gains of the amplifiers. In this work, active quasi-circulators are used.

6.2 Modelling of Matched Gain blocks

Modelling of active circulators or any configuration that is based on them requires modelling of gain blocks. There are two considerations arising when someone is trying to describe

them via equivalent circuits in the FDTD context. First the dependent sources and secondly the unilateral nature of the devices. Transistors are used in gain blocks with additional circuitry to provide the necessary matching. In situations like that one can neglect the inner details of a transistor and focus on the function of the block. This is equivalent to a system approach of having a block with voltage gain A. A simple structure of a linear gain block can be seen in Figure 6.3. The input and output resistors are used to match the amplifier with internal gain A, to the external structure. For the FDTD modelling, one cell can be reserved for the input stage, one cell for the output stage and a number of cells in between to create the gap. The number of gap cells is chosen such that in effect it represents the size of a chip gain block.

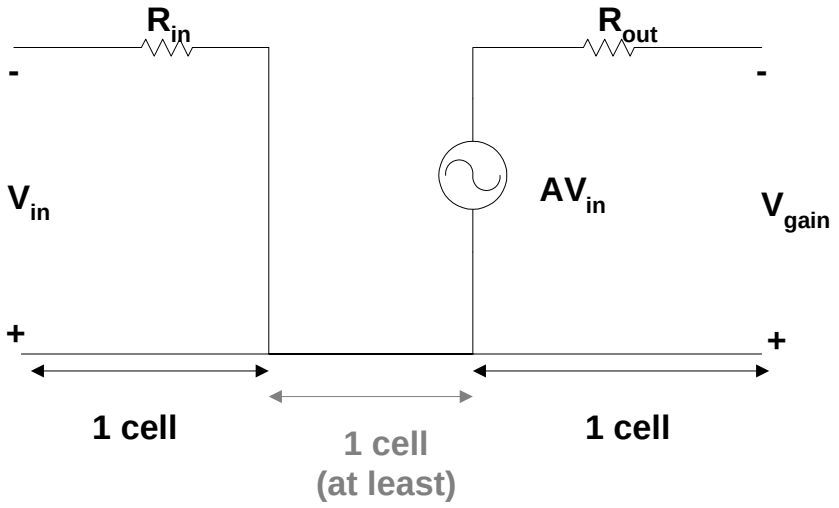

Figure 6.3 The proposed structure of a gain block for implementation in FDTD

In the cell containing the dependent voltage source the current will be:

$$I_L^{n+\frac{1}{2}} = \frac{A \cdot \Delta z \cdot E_{in}^n}{R_{out}} + \frac{(E_z^{n+1} + E_z^n)\Delta z}{2R_{out}} \qquad (6\text{-}6)$$

Substituting (6-10) to (3-36):

$$E_z^{n+1} = \frac{1 - \dfrac{\Delta t \cdot \Delta z}{2R_S \cdot \varepsilon \cdot \Delta x \cdot \Delta y}}{1 + \dfrac{\Delta t \cdot \Delta z}{2R_S \cdot \varepsilon \cdot \Delta x \cdot \Delta y}} E_z^n + \frac{\Delta t}{\varepsilon + \dfrac{\Delta t \cdot \Delta z}{2R_S \cdot \Delta x \cdot \Delta y}} (\nabla \times \overline{H})_z^{n+1/2} - \frac{\Delta t}{\varepsilon + \dfrac{\Delta t \cdot \Delta z}{2R_S \cdot \Delta x \cdot \Delta y}} \frac{A \Delta z E_{in}^{n+1}}{R_S \cdot \Delta x \cdot \Delta y} \tag{6-7}$$

The input stage field E_{in}^n comes from a resistor which is modelled using the expression (5-3) given in chapter 5.

6.2.1 A 50Ω gain block on a microstrip line

As a validation test, a 50Ω gain block was placed on a 50Ω microstrip line excited with a matched circuit source and terminated with a load of 50Ω (Figure 6.4). As a benchmark, the same structure was simulated in time and frequency domain using HP-MDS (Figure E.6 and Figure E.7 in Appendix E)

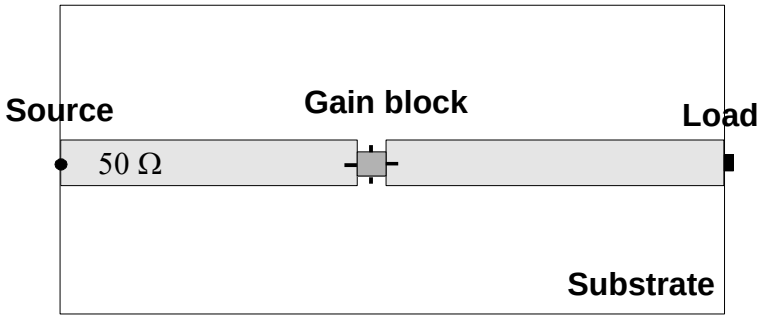

Figure 6.4 Gain block validation structure: a 50Ω gain block on a 50Ω microstrip line

From Figure 6.3 and Figure 6.4, it can be deduced that for the connected matched gain block:

$$V_{gain} = \frac{R_{out}}{R_{out} + Z_o} A \cdot V_{in} = \frac{1}{2} A \cdot V_{in} \tag{6-8}$$

since the load and the output resistance act as a voltage divider.

The time domain test uses a sinusoid excitation at 4GHz, amplitude 0.1 V. The input and output of the gain block responses were monitored and the agreement with HP-MDS is very good. The output of the gain block lags 180^{o} with respect to the input and provides the amplification required (Figure 6.5).

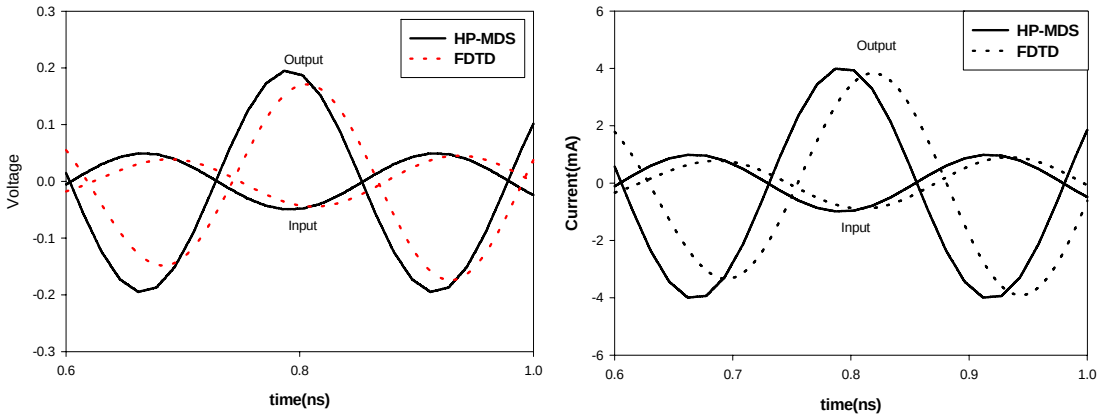

Figure 6.5 Simulated response of a 50Ω gain block on a 50Ω microstrip line for a sinusoid excitation of .1V at 4GHz.

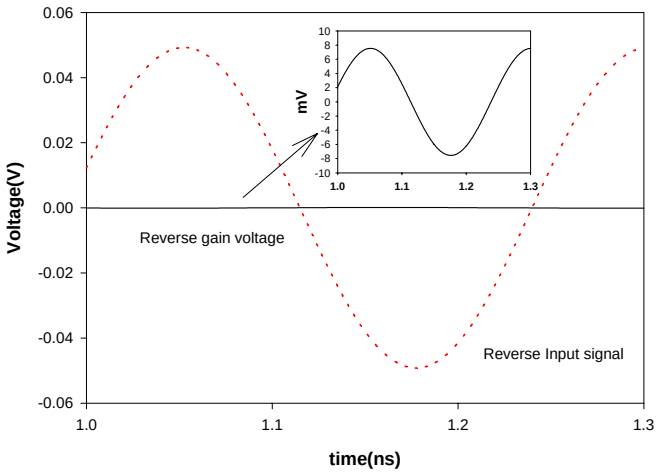

Figure 6.6 Simulation to check the isolation of the input and output of the gain block in time domain

For a properly functional gain block, it is essential to ensure isolation between input and output ports. If the position of the source with the load is interchanged (Figure 6.4) the gain block should provide the isolation. This is illustrated in Figure 6.6 where an input signal is very well isolated by the output. In an ideal gain block like the one used in HP-MDS, the isolation is perfect.

In the frequency domain, S-parameters are calculated over a band up to 10GHz to examine better the small differences in time domain. In can be seen that there is a difference in S_{11}(Figure 6.8) and S_{21}(Figure 6.9) and S_{12} for the ideal gain block is $-\infty$ (in dB). The cause of this discrepancy is that in FDTD, the gain block is placed on a physical gap which affects the isolation.

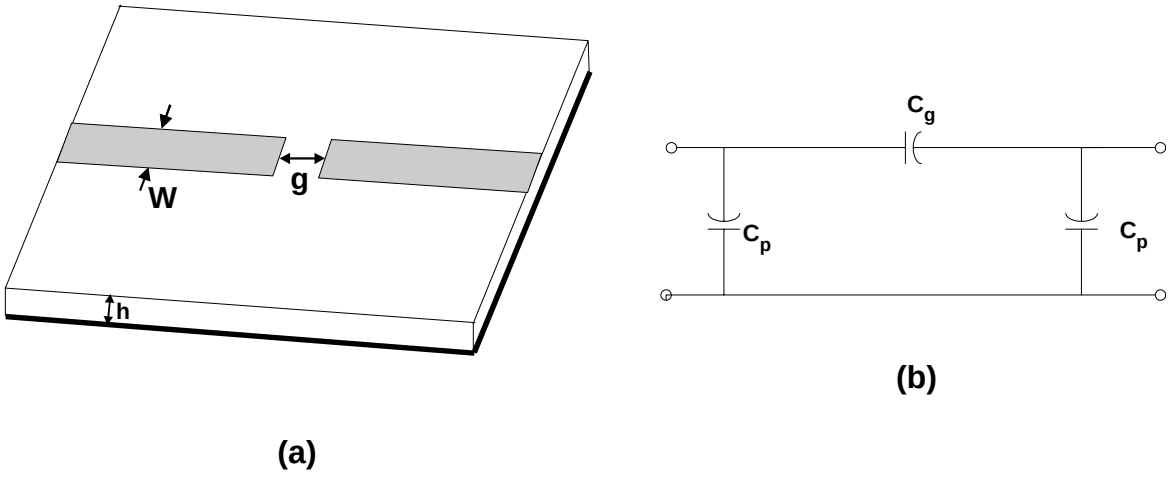

Figure 6.7 Equivalent circuit(b) for a gap discontinuity on a microstrip line(a)

For this reason another HP-MDS simulation was performed with the ideal gain block but with gap compensation. To include a gap for frequencies less than 10 GHz an equivalent network of capacitances can be used (Figure 6.7). The values of capacitances can be determined by equations based on quasi-static analysis (Edwards 1992). For the validation

structure the values are C_g=0.025pF and C_p=0.001314pF (see Appendix F). These values are only an approximation and serve as a means to explain the differences between the HP-MDS ideal gain block simulation and the FDTD modelling.

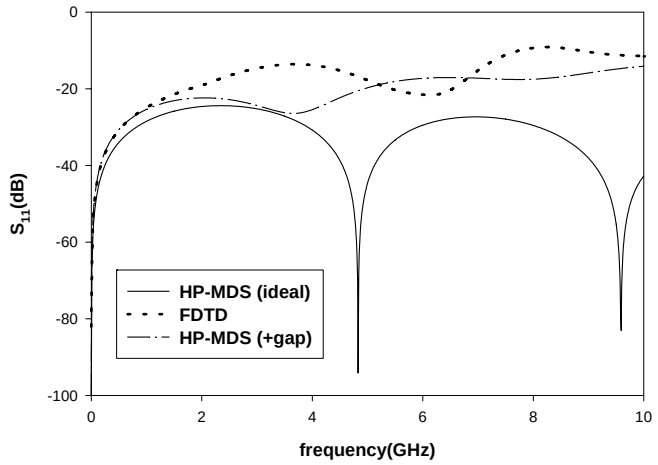

(a)

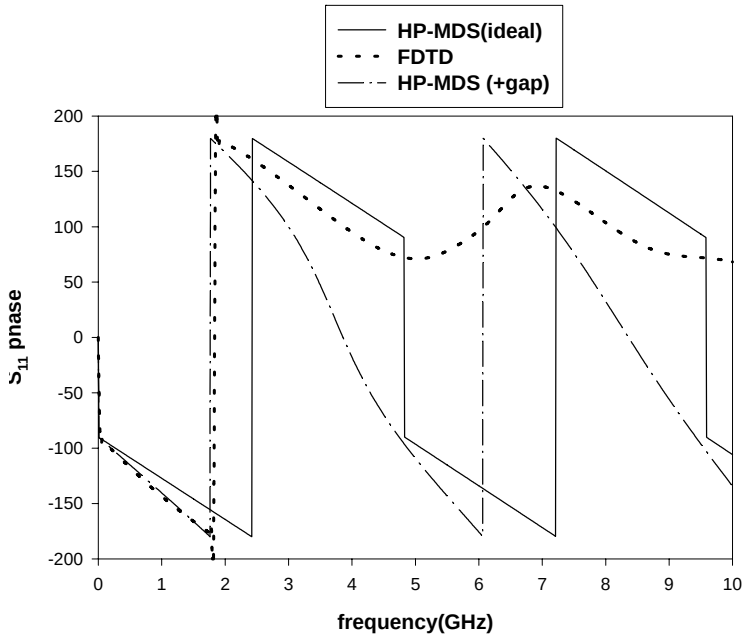

(b)

Figure 6.8 Magnitude(a) and phase(b) of the S_{11} parameter for the test structure

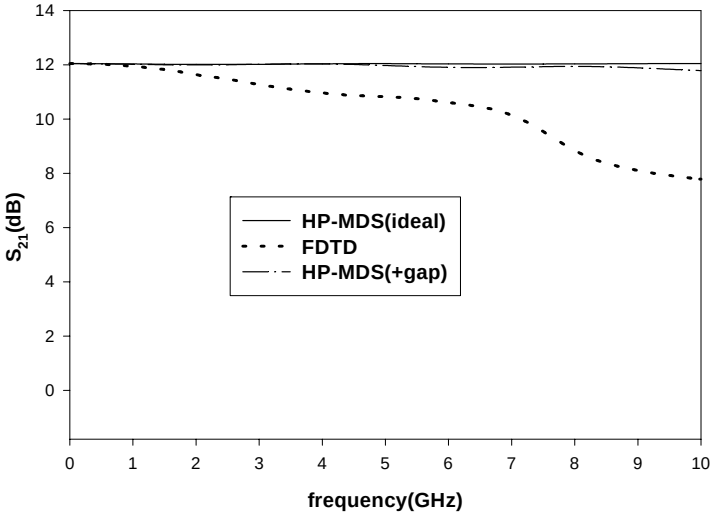

(a)

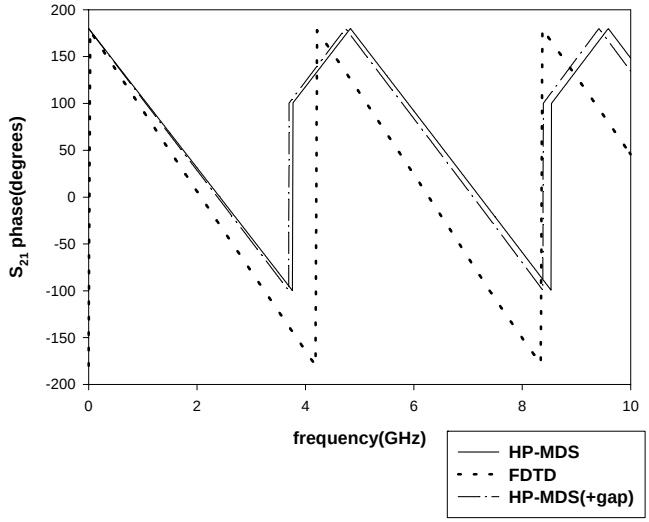

(b)

Figure 6.9 Magnitude(a) and phase(b) of the S_{21} parameter for the test structure

Observe that now in incorporating gap compensation, the agreement improves considerably (Figure 6.8, Figure 6.10). Most notably isolation (Figure 6.10) will not be infinite any more

since the gap capacitance provides a feedback mechanism which leads to a finite isolation. In effect, embedding the gain block on the FDTD space results in modelling a priori accurately the device environment with no need for a posteriori corrections as in a simulator.

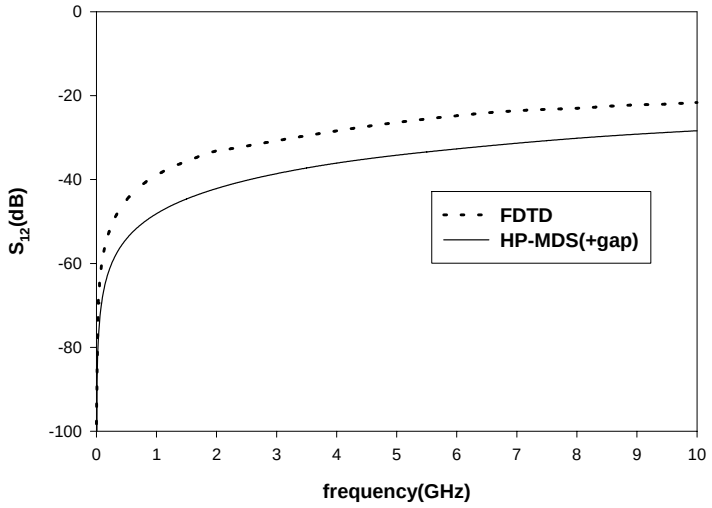

Figure 6.10 Isolation of the gain block given by $S_{12.}$

6.3 The active circulator structure

Circulators are used to separate transmit and receive paths in communication systems or radars. A hybrid active circulator implementation was used to separate transmit-receive signals for an antenna by Cryan and Hall(1997) . This active circulator utilises three gain blocks connected in a ring arrangement (Figure 6.11).

The choice of the impedance for gain blocks dictates the matching requirements accepting the fact that input lines are 50Ω. Cryan and Hall(1997) realised this circulator as a hybrid microwave integrated circuit with only 50Ω gain blocks which were readily available. The use of 50Ω introduced additional requirements for matching. The matching requirements

resulted in many different line widths. The memory and computer time requirements from FDTD simulations in microstrip structures are dictated mainly by the fine details of the circuit. If 100Ω gain blocks are used then matching difficulties are avoided and the layout is simpler. Choosing to model the 100Ω circulator results in significant memory savings without resorting to variable meshing scheme. This is done without compromising the merits of the configuration. 100Ω gain blocks can be implemented in MMIC technology which is an attractive feature of active circulators.

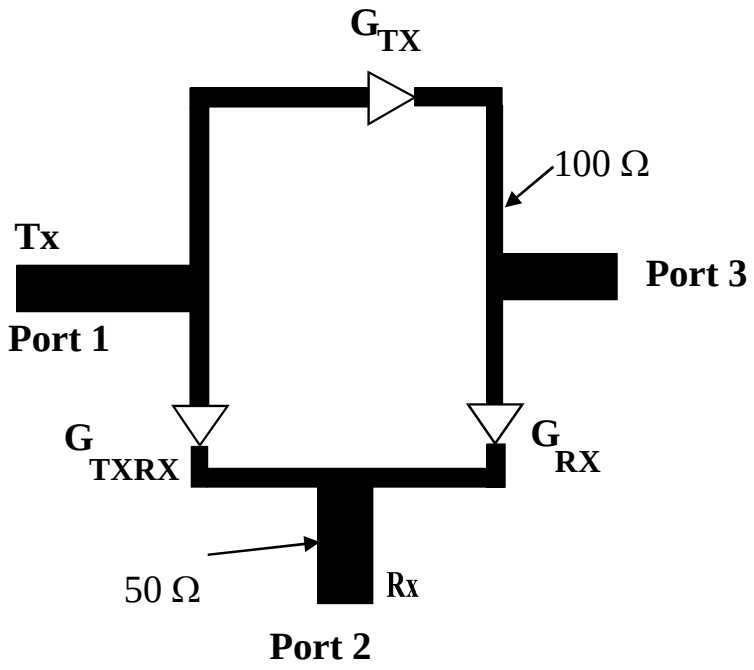

Figure 6.11 The active quasi-circulator structure

The structure allows power flow from port 1 to port 3 and from port 3 to port 2 thus operating as a quasi-circulator with clockwise flow (Figure 6.2b). Consequently there are two signal paths from the transmitter (port 1) to the receiver (port 2), one via port 3 and a direct path. By adjusting the phase lengths of these paths and the gains, phase cancellation occurs at the receiver. In other words, the condition for cancellation is that the power coming at the

receiver from the two possible paths should be of equal magnitude and the phase difference of the two paths 180^o. The circuit dimensions were determined using the Hewlett Packard Microwave Design System (HP-MDS) software. This allowed for optimisation of the amplifier gains and the lengths of the transmission lines in order to obtain the desired isolation (Figure E.9, Appendix E).

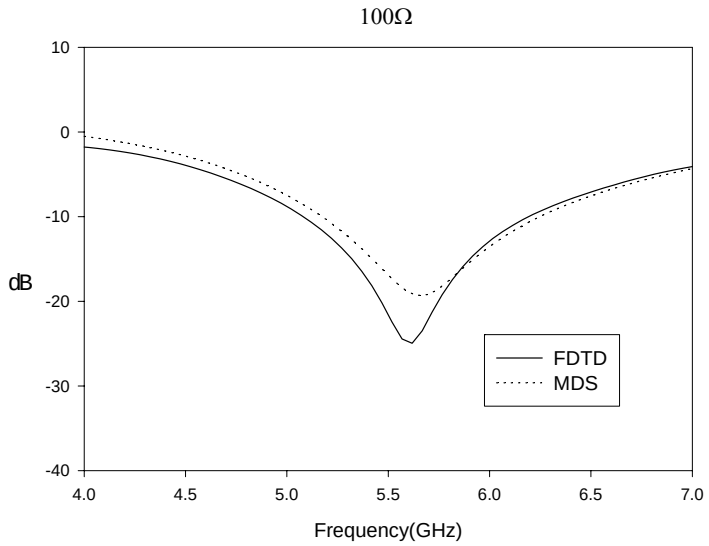

Figure 6.12 Transmit-receive isolation for the active circulator

The 100Ω circulator was simulated with FDTD. In order to simulate the circuit, gain blocks must be incorporated in FDTD. In the code used in this work, the three gain blocks were realised as described in the previous section. The distance between the input and output port was dictated by the size of a physical gain block (2mm in linear dimensions). The dimensions of the 100Ω hybrid circuit (dielectric constant ε_r=2.2, thickness h=1.1mm) are 12x19.1 mm, with the 50Ω and 100Ω lines having widths 3.3 mm and 0.9mm respectively. The gains are G_{TXRX}=1, G_{TX}=1, G_{RX}=1.8(linear units). The structure was then simulated using the

extended 3D FDTD program by using 151x151x51 cells with Δx=0.3mm, Δy=0.3mm, Δz=0.37mm. It was found by experience that at least three cells for microstrip line width and substrate are required to get accurate results. Wideband information can be retrieved from FDTD using a Gaussian pulse as excitation and performing Fourier transforms of the transients. Mur absorbing conditions were used to truncate the computational domain.

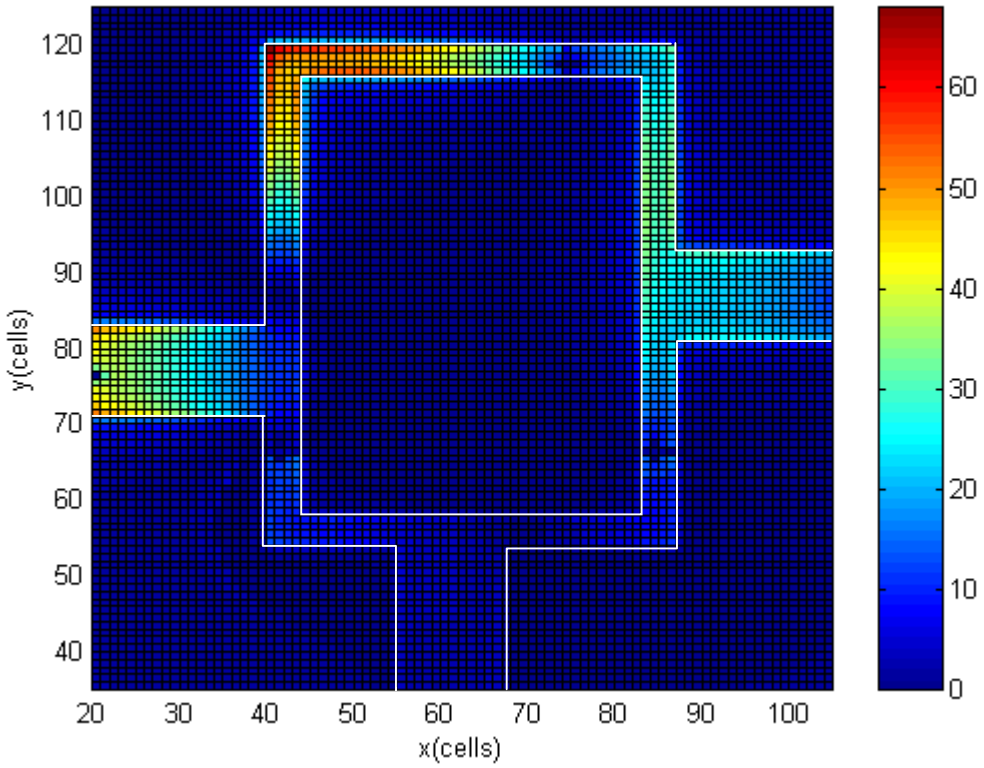

Figure 6.13 Distribution of the electric field normal to the surface for the active circulator at the maximum isolation frequency (calculated using FDTD)

The circulator exhibits good isolation between transmit-receive which is in good agreement with HP-MDS (Figure 6.12). The difference is attributed to frequency independent gain blocks used in the MDS design. FDTD can also provide valuable information on the physics

of the circuit. The spatial distribution of the electric field just underneath the metal layout at the maximum isolation frequency reveals where the phase cancellation occurs (Figure 6.13). The isolation of this class of active circulators is quite narrow band as expected for a phase cancellation technique. The use of constant phase shift networks could possibly offer broader band isolation if needed.

6.4 Integrated Active Circulator Antennas

The active circulator can be integrated with a microstrip antenna to form a module with transmit-receive operation at the same frequency and polarisation. The antenna is connected to port 3. The transmitted signal is assigned to port 1 and the received signal is assigned to port 2 (Figure 6.14).

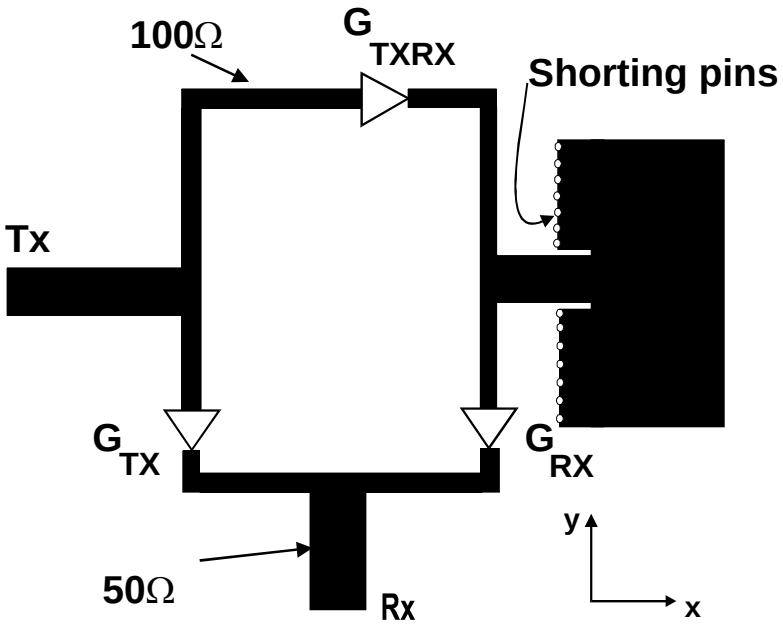

Figure 6.14 Active Circulator integrated with a microstrip antenna

Space considerations are very important. The first step to optimise space is to use a quarter wavelength short circuited, inset fed microstrip antenna. The small dimensions of this antenna permits positioning in the centre of the ring (Figure 6.15). This optimises circuit area and would allow arrays of these elements to be formed. Cryan and Hall(1997) used a geometry similar to Figure 6.15. It is anticipated that all the features should be similar for the two structures. Transmit-receive operation is possible by taking advantage of the isolation introduced by the circulator. Transmit power is amplified by gain block G_{TX} and coupled to the antenna port by a length of 50Ω microstrip line. Receive power is coupled into the circulator via the same line and passes through G_{RX} since the reverse isolation of G_{TX} prevents power coupling back into the transmitter. The transceiver is linearly polarised with the same polarisation for transmit and receive.

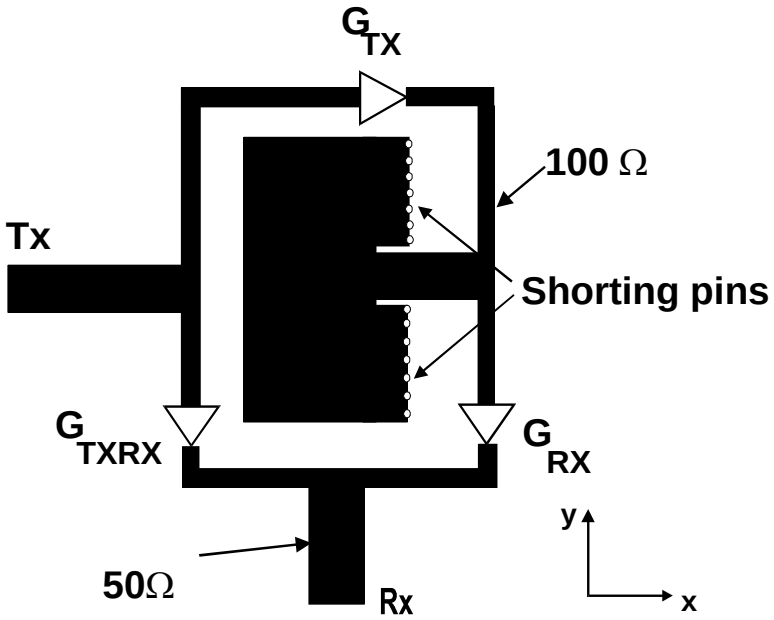

Figure 6.15 Active Circulator integrated with a microstrip antenna optimising the available ring space.

Having validated the FDTD code, it is now used to model the integrated configurations (Figure 6.14, Figure 6.15). The transmit port return loss is seen to be reasonable. The receive

port is less good but with further modifications to the matching circuits this could be improved. Comparing the results with the experimental findings, the same features are observed.

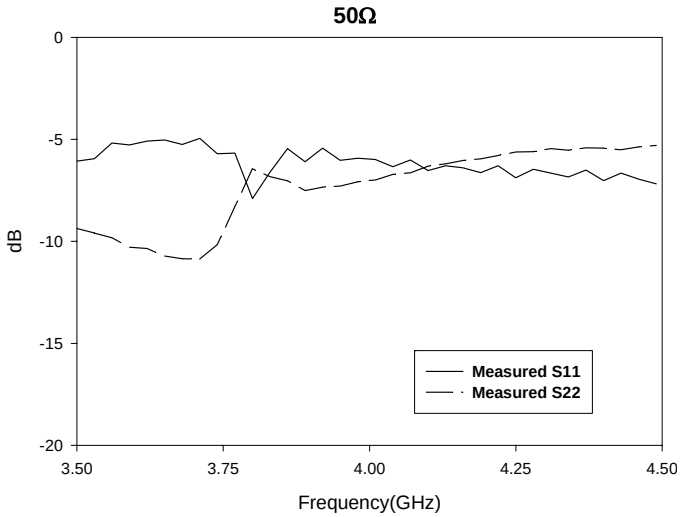

(a)

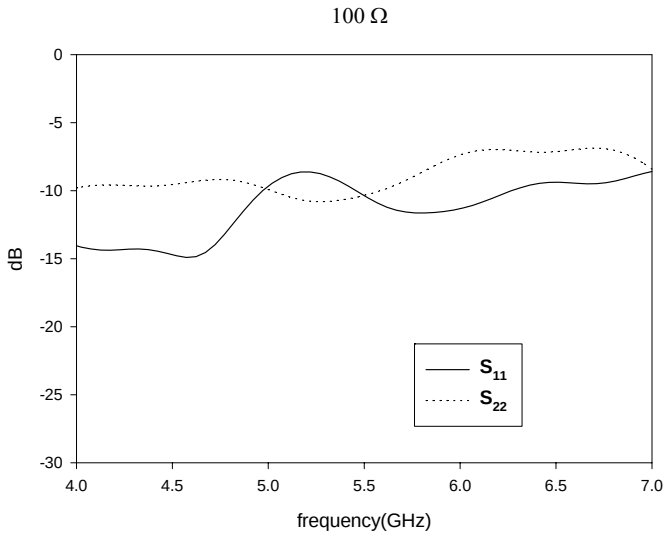

(b)

Figure 6.16 Input and output S-parameters for active circulator antenna

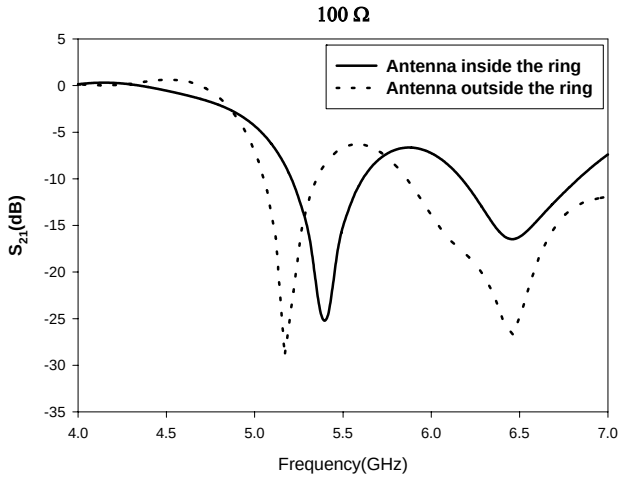

(a)

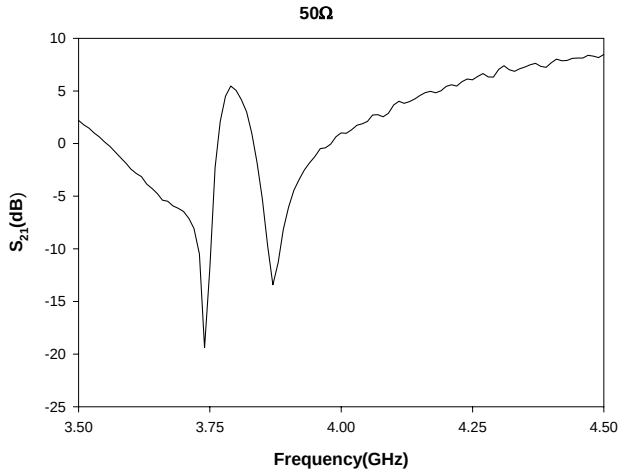

(b)

Figure 6.17 Transmit and receive parameters S-parameters for an active circulator antenna. (a) 50 Ω structure (Measured) (b) 100 Ω structure(FDTD)

Figure 6.17 shows transmit-receive isolation. There is a noticeable difference between the transmit-receive isolation of the integrated structure and that of the non-integrated circuit(Figure 6.11). Instead of one dip, a double hump appears because of the interaction of the active circulator with the antenna. The introduction of the antenna which is a resonant element causes a small additional phase shift close to resonance. That means the condition of

180^{o} phase difference can be fulfilled at another frequency, causing the second dip. However this is not the operating frequency but could be engineered to produce a more wideband configuration. Using FDTD it is possible to examine what happens when the antenna is positioned inside (Figure 6.15) and outside of the ring structure(Figure 6.14). This allows investigation of the effects of coupling, by comparing the isolation with the antenna inside and outside the ring.

The distributions of the fields when the antenna is outside(Figure 6.19) and inside(Figure 6.18) the ring reveal clearly the cause of difference in the isolation. In the case where the antenna is inside the field is disrupted considerably due to field maxima in the upper left part of the circulator. The capability of examining effects of the antenna position relative to the circuit is a unique feature of the extended FDTD method.

The transmit patterns for the 50Ω structure were measured (Figure 6.20.a). by Cryan and Hall (Figure 6.20.a). The radiation patterns for the 100Ω active integrated antenna were also calculated for the transmit case with the FDTD code. Near to far field transformation (Luebbers et al. 1991) was used to produce the radiation patterns(Figure 6.20.b). Observe that both the figures have essentially the same features. The cross-polar isolation was typically better than -10dB at boresight as expected by the inherently poor cross-polar isolation of a short circuited patch. A significant characteristic of the radiation patterns is the off-axis dip of the H-plane cross-polar radiation pattern. In the case of a short circuited patch the dip is expected very close to boresight. In order to explain the translation of the dip it is important to study Figure 6.18. The skewness in the field distribution of the patch, introduced by the coupling, results in a shift in the cross polar radiation pattern null.

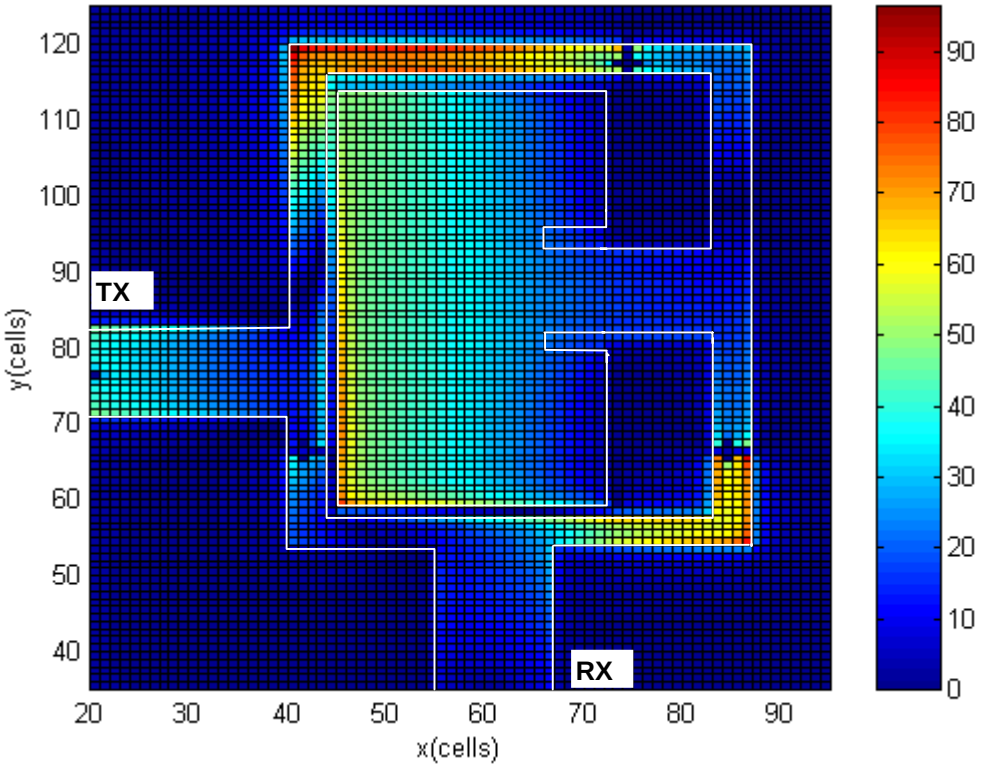

Figure 6.18 Field distribution for the active circulator antenna when the antenna is placed inside the ring

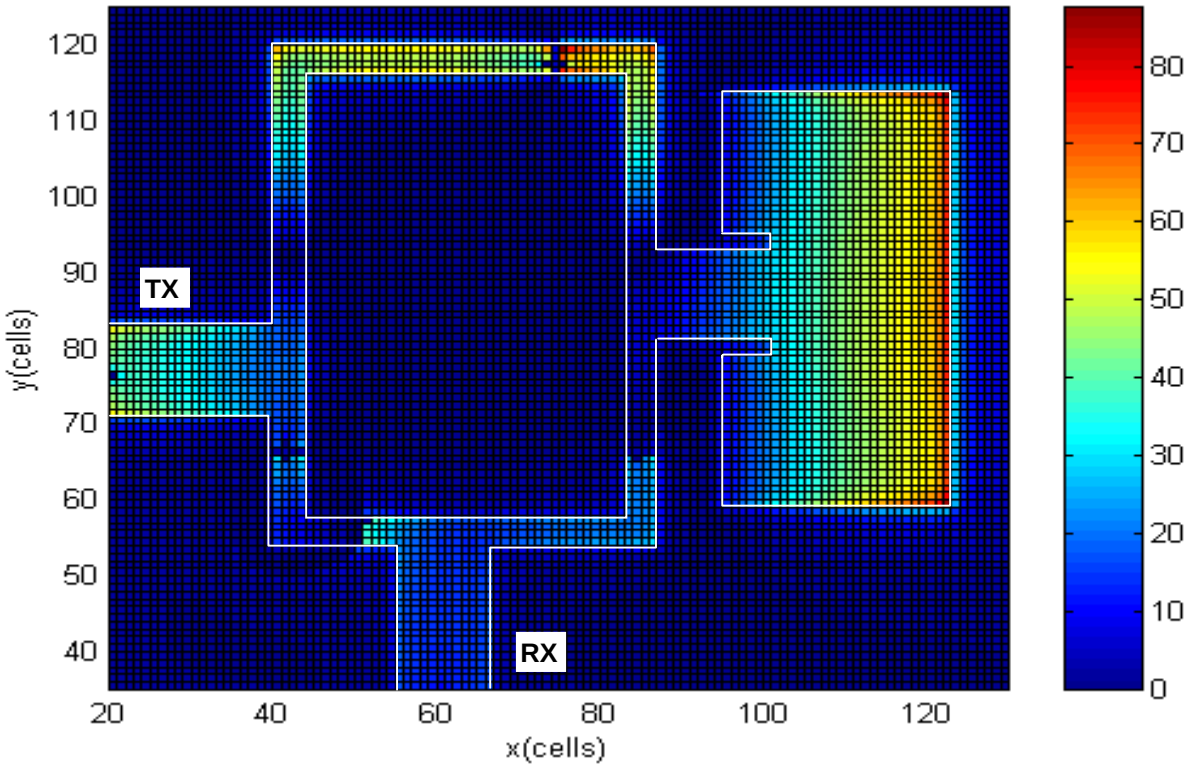

Figure 6.19 Field distribution for the active circulator antenna when the antenna is placed outside the ring

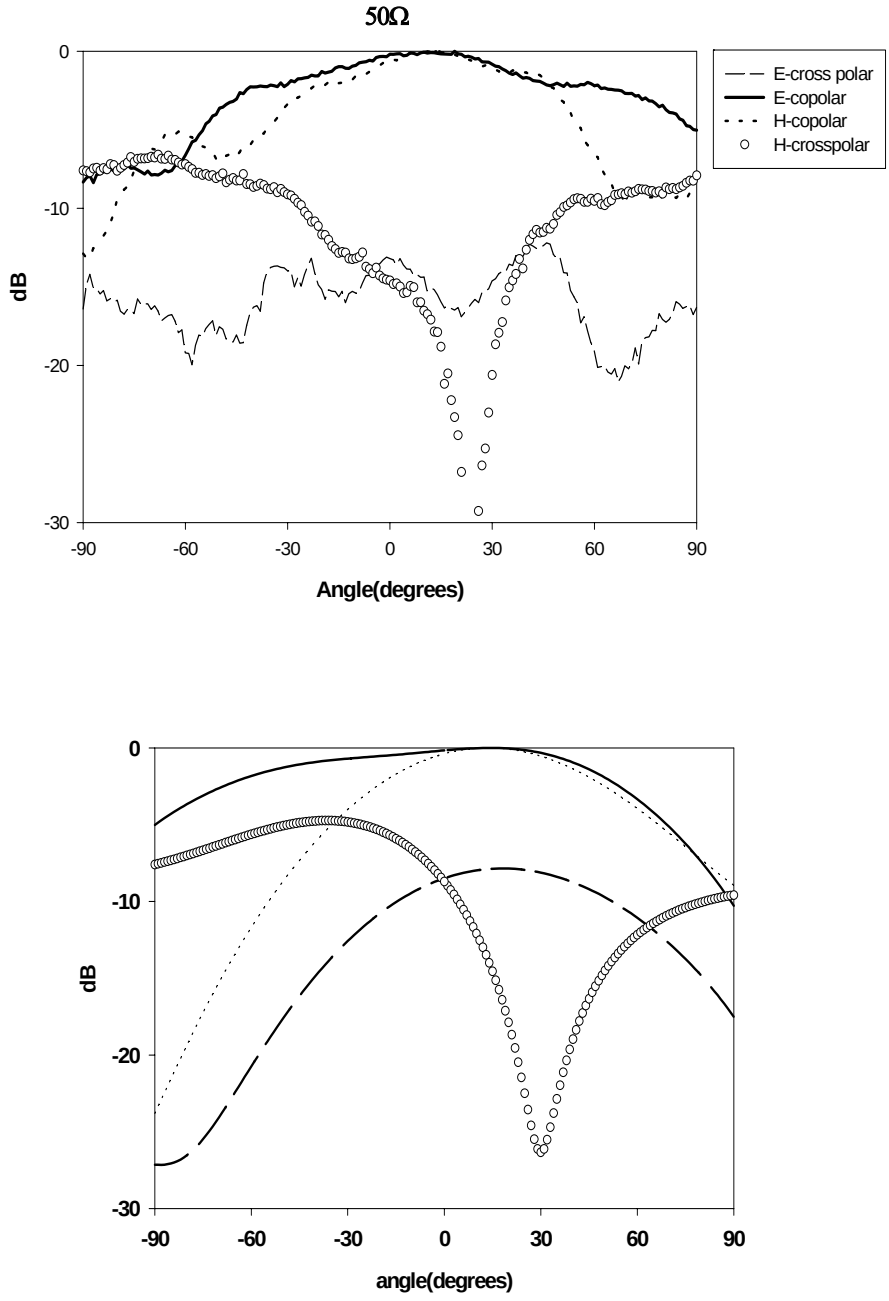

Figure 6.20 Transmit radiation patterns for an active circulator antenna(a) 50Ω structure(Measured)(Cryan and Hall 1997) (b)100Ω (FDTD)

Other antennas with less physical size could replace the radiating element in the case where size constraints are important. The additional gain introduced by the gain block could

compensate for the gain degradation of the small antenna. However, use of small antennas in conjuction with active gain compensation will inevitably degrade the Signal-to-Noise ratio. It is however feasible to optimise the noise figure of an active circulator (Gasmi et al 1997); then depending on the application the optimal antenna size can be determined for a given link budget.

6.4.1 Design considerations for optimal isolation

From the previous section it is clear that the placement of the antenna inside the ring results in a compact module but the performance(isolation, radiation patterns) is affected by the coupling. The coupling is controlled by the position of the antenna relative to the circuit. To investigate possible design solutions, two parameters were varied in order to establish trends in the design of such modules. The first parameter used is the size of the antenna. As explained in the previous section the circuit dip might be shifted because of the antenna resonant behaviour. The resonant behaviour of small microstrip antennas is achieved by using short-circuit pins. Sanad(1994) has demonstrated that the kind and number of shorting posts could affect the resonant frequency by 2 to 3%. Thus parametric investigations were performed by varying slightly the antenna length in order to optimise the isolation. Furthermore in the present case, the presence of parasitic coupling makes things very difficult to predict.

Figure 6.21 shows the effect of the antenna size where isolation is plotted over the same frequency range for values of the length close to $\lambda_g/4$ (8.9 mm, for operation at 5.6 GHz). For some value of the length which corresponds to a resonant frequency closer to the

circulator dip, improved isolation can be achieved. Another degree of freedom is the width of the antenna. By reducing the antenna width coupling can be further reduced. The second parameter chosen is the inset gap of the antenna that controls its input impedance. For the optimised geometry of Figure 6.21 (7.8mm) , FDTD simulations were performed with different values of insets. From Figure 6.22 it can be deduced that the frequency position of the dips is not strongly affected but the isolation can be improved by a few dBs as the matching of the antenna changes. Therefore using the FDTD method, the following trends can be established, enabling compactness to be achieved with predictable coupling:

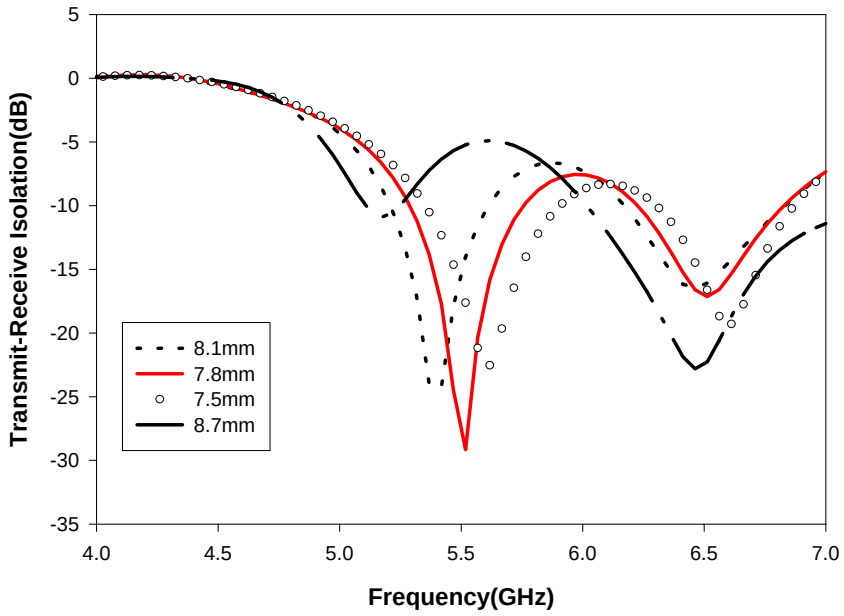

Figure 6.21 Variation of transmit-receive isolation with small variation of antenna length

- Antenna matching does not affect the frequency where the dips occur but can affect the isolation magnitude. Optimised matching can be obtained.
- The best isolation can be achieved by producing an antenna that radiates at a slightly higher frequency than that at which the circuit alone provides.

- Increased isolation can be further achieved by reduction of the antenna width.

None of the above conclusions are possible by the use of a circuit based simulator like HP-MDS.

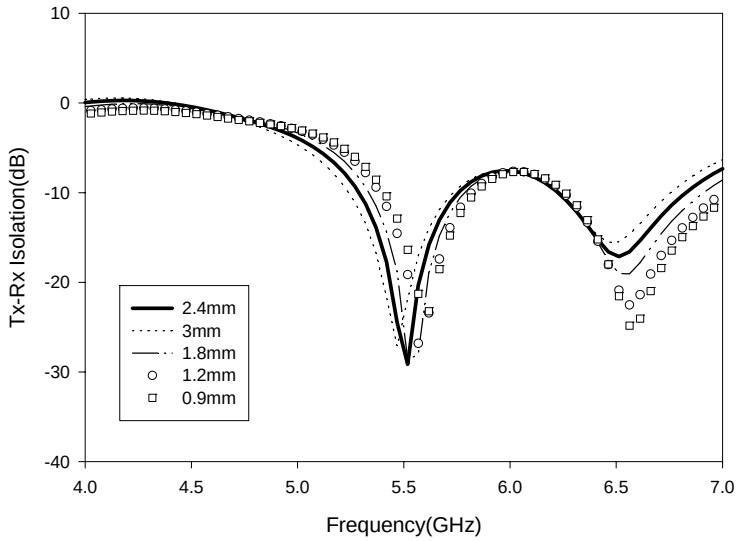

Figure 6.22 Transmit-receive isolation with variation of inset for optimum matching

6.5 Summary

A simple and effective model of a gain block was presented that takes into account gap effects. Results presented show that a hybrid active circulator can be modelled in agreement with experimental findings. Integration with antennas has been investigated and there was agreement with experimental findings. The effect of parasitic coupling was established and ways to reduce it have been suggested. The operation of an integrated active circulator antenna was discussed based on experimental results and results obtained from the application of the extended FDTD method. Arrays of these elements could overcome the

power handling problems that limit the performance of single elements. Parasitic electromagnetic coupling in integrated antenna-circuit modules is to be avoided. If it is inevitable then it should be known before hand. By using FDTD it was demonstrated how the coupling affects the operation, providing explanations on observed experimental findings. Parametric calculations were also performed to establish design trends. By adjusting the size of the antenna and its input impedance, the isolation between transmit-receive can be controlled. Design criteria like the above are crucial to reduce costly prototype fabrication cycles.

CHAPTER 7

MICROSTRIP ANTENNA-VARACTOR MODULES

In this chapter results are presented from the analysis and experiment on microstrip antenna-varactor modules. Emphasis is given on the study of harmonic radiation generated by the module due to the varactor nonlinearities. Frequency tuning is also investigated. Results are given for rectangular half wavelength and quarter wavelength microstrip antennas. Description of the varactor models in the FDTD code and their validation is included.

7.1 Introduction

In system applications, bandwidth can be distinguished as instantaneous and effective. Instantaneous bandwidth is the available bandwidth at a given time instant. Effective bandwidth is the frequency range where the system can operate. In order to clarify these concepts, let us take the case where a multichannel operation is desired. An antenna can be used with bandwidth equal to the frequency spectrum that all the channels occupy. Alternatively an antenna with narrow bandwidth equal to one or few channels can be used. What it will be required in that case is that the antenna must be able to switch channels across the required multichannel bandwidth. Then it can be said that both antennas have the same effective bandwidth but not the same instantaneous bandwidth. The DECT (Digital Enhanced Cordless Telecommunications) is an example of a system where base stations are multichannel (10 channels) but they transmit one channel per time slot.

Microstrip antennas are resonant antennas with inherently narrow instantaneous bandwidth. Separate attempts have been made to increase the instantaneous bandwidth and the effective bandwidth. In simple terms, increase of the instantaneous bandwidth requires lowering the high Q of the microstrip structure. In the case of the effective bandwidth, the instantaneous bandwidth is the same but by changing the reactive part of the antenna impedance, it is possible to force the antenna to resonate at different frequencies. The most direct way is to load the antenna with reactive elements. Varactors are variable capacitors. Their capacitance can be controlled electronically with change of their bias voltage. The possibility of integrating microstrip patches with varactor diodes was first demonstrated by Bartia and Bahl (1982). The varactors when placed on the patch appear as a parallel capacitance to the open end capacitance and alter the resonant frequency.

Applications of this effect are numerous where frequency tuning and agility are required. For example switching between transmit and receive bands for compact antennas on handsets has been suggested by Sabatier(1995). Another application is for frequency tuning of integrated active oscillator antennas (Haskins et al. 1991). In addition to the resonant frequency change, polarisation control has been reported by Haskins and Dahele(1994) and independent control of input impedance by individually biased varactor diodes also by Haskins and Dahele(1996).

Adaptive tuning systems are needed to compensate for environmental effects on the resonant frequency of resonant type antennas like microstrips. Rostbakken et al. (1996) have

demonstrated such a system. Hall et al.(1997) have suggested an integrated structure that avoids the use of the coupler.

Varactors are nonlinear elements and therefore harmonic generation is a problem that must be addressed. Hall et al.(1997) have addressed the problem of harmonics but their findings about the radiated levels were inconclusive.

Analysis of such structures has been reported using the transmission line model (Bartia and Bahl 1982) and full wave domain methods in the frequency domain. Waterhouse and Shulley(1994) have analysed probe-fed microstrip antennas and Dauguet et al.(1997) have analysed a line fed patch loaded with two diodes. No full wave model has addressed the problem of harmonic generation and its control. Furthermore no investigation of tuneable quarter wavelength antennas has been presented.

7.2 Varactor diode modelling in FDTD

An ideal varactor can be treated as a nonlinear capacitor with the charging current given by

$$I_L = C(V)\frac{dV}{dt} \qquad (7\text{-}1)$$

where the capacitance C(V) follows a static C-V characteristic of the form

$$C(V) = \frac{C_O}{\left(1-\frac{V}{\Phi}\right)^{\gamma}} \qquad (7\text{-}2)$$

with C_0 the capacitance at 0 V bias and Φ is the built-in voltage of the junction. The exponent γ determines the junction profile with values ranging from 0.4-1.25. Although the RF characteristics should be required for accurate modelling, such modelling requires specialised equipment and it is considered that the use of static characteristic gives acceptable results (Navarro and Chang 1997).

The varactor is essentially modelled as a nonlinear capacitor. The FDTD expression requires the lumped element current. In order to obtain it, the varactor voltage is split into a DC term (negative bias voltage) and a time dependent term which is the microwave signal

$$V = V_{DC} + V(t) \tag{7-3}$$

and substituted in (7-2)

$$I_L = \frac{C_O}{\left(1 - \frac{V_{DC} + V(t)}{\Phi}\right)^{\gamma}} \frac{dV}{dt} \tag{7-4}$$

A discretised version of (7-4) is required. The time derivatives are calculated at $n + \frac{1}{2}$. The quantity $V^{n+\frac{1}{2}}$ is treated as a temporal average between time steps *n*, *n+1*.

$$I_L^{n+1/2} = \frac{C_O}{\left(1 - \frac{2V_{DC} + V_Z^{n+1} + V_Z^n}{2\Phi}\right)^{\gamma}} \frac{V_Z^{n+1} - V_Z^n}{\Delta t} \tag{7-5}$$

Substitution of (7-5) into (3-36) yields

$$E_z^{n+1} = \frac{1-\frac{\sigma\cdot\Delta t}{2\varepsilon}}{1+\frac{\sigma\cdot\Delta t}{2\varepsilon}} E_z^n + \frac{\Delta t}{\varepsilon(1+\frac{\sigma\cdot\Delta t}{2\varepsilon})}(\nabla\times\overline{H})_z^{n+1/2} - \frac{\Delta t}{\varepsilon(1+\frac{\sigma\cdot\Delta t}{2\varepsilon})}\frac{E_Z^{n+1}-E_Z^n}{\Delta x\cdot\Delta y}\frac{C_O}{\left(1-\frac{V_{DC}}{\Phi}-\frac{\Delta z}{2\Phi}(E_Z^{n+1}+E_Z^n)\right)^{\gamma}} \quad (7\text{-}6)$$

The equation (7-6) is a nonlinear equation. It is solved using the iterative Newton-Raphson technique (Press et al 1989).

7.2.1 Validation

In order to validate the varactor model, a 50Ω microstrip line has been terminated with a varactor. The geometry of the structure is the same as in Figure 5.12. An HP-MDS design shown in Figure E.5 (Appendix E) was created and used to run a transient simulation. The excitation is a square pulse of duration 0.245 ns. The varactor modelled has a static capacitance C_o=2.0 pF and made of silicon (built-in potential Φ=0.7V), γ=0.5.

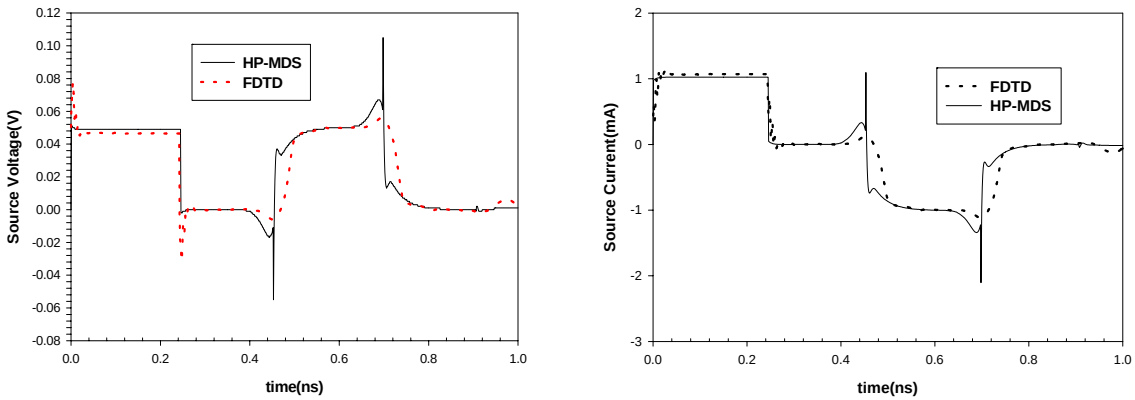

(a) **(b)**

Figure 7.1 Transient response at the source (a) voltage (b) current

At the source position (Figure 7.1), two pulses can be seen. The first is the signal launched by the source which travels towards the varactor. Then this is reflected back to the source but is

not retransmitted since the source is matched. At the varactor position (Figure 7.2), the capacitor is charged quickly because of the small time constant. Then it is discharged and reflects the formed waveform back to the source. The spikes in the HP-MDS simulation are due to the fact that the connections were assumed ideal. The spikes can be eliminated by using a parasitic inductance as was discussed in chapter 5.

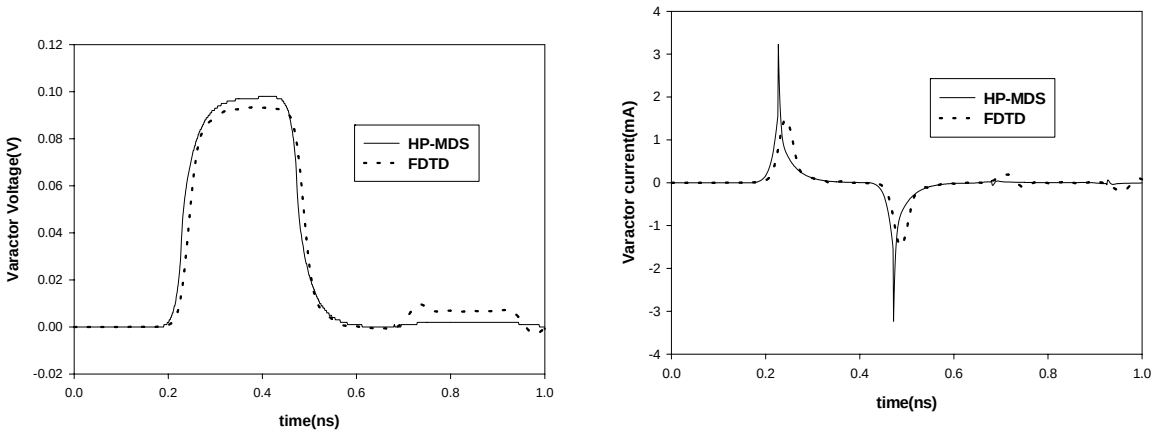

(a) **(b)**

Figure 7.2 Transient response at the nonlinear capacitor position (a) voltage (b) current

7.3 Frequency tuning

7.3.1 Half wavelength antenna-varactor module

A GaAs varactor MAH46072 was mounted on one of the radiating edges of a half wavelength patch (Figure 7.3). The C-V from the data sheet was fitted to a function of the form (7-2). Parameters used are static capacitance Co=8.25pF, built-in potential Φ=0.82, γ=0.55.

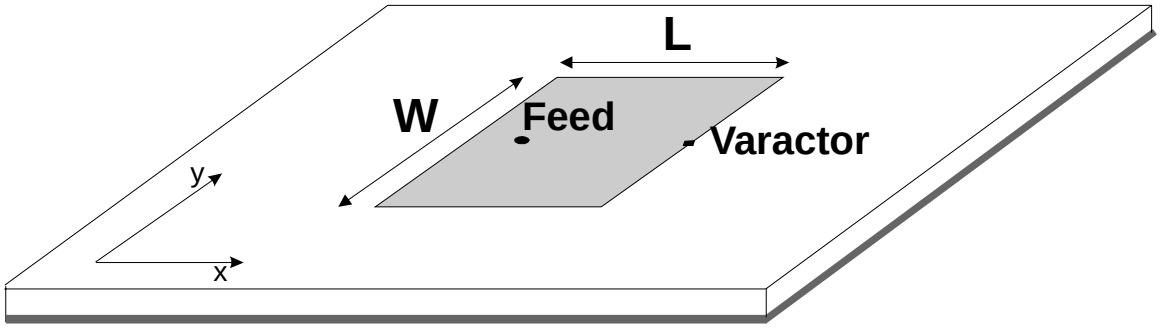

Figure 7.3 A half wavelength microstrip antenna-varactor module.

The diode was positioned at the edge by drilling a hole on the substrate and soldering one terminal to the ground and the other on the patch. The bias voltage was applied on the patch by having a wire coming from the middle of the patch and through a ferrite inductor to the DC source.

The antenna dimensions were first determined using a transmission line model from the literature (Bartia et al. 1991). The transmission line model provides closed form expression for the resonant frequency (Appendix H). The dimensions of the antenna are L=56mm, W=45mm for a resonance of 1.78 GHz.

For different values of the bias voltage, the capacitance of the varactor changes and thus alters the resonant frequency of the patch. The frequency tuning was verified experimentally (Figure 7.4) . Several FDTD calculations for different DC bias values were performed using the model described in paragraph 7.3. The FDTD grid was 133 ×121 ×51 cells using 31×23 cells to model the patch.

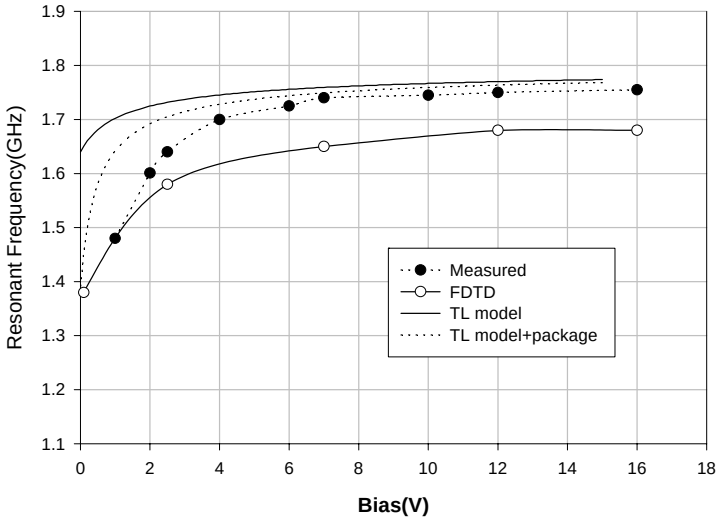

Figure 7.4 Frequency tuning of a half wavelength antenna

Observe that although the absolute values of resonant frequency have a difference from the experimental ones, the curvature of the curve is the same. The diode used in the experiment was in a plastic package, introducing package parasitics. Also a bias dependent γ can be cited as a reason for the discrepancies. In order to investigate the differences, the resonant frequency based on a transmission line model considering varactor loading was calculated. The resonant frequency is given as

$$f_r = \frac{c}{2 \cdot \pi \cdot L\sqrt{\varepsilon_{eff}}} \tan^{-1}\left[\frac{Y_o \cdot (2B + B_{ext})}{G_{rad}^2 - B^2 + 2B(B + B_{ext})}\right] \qquad (7\text{-}7)$$

where G_{rad} is the radiation conductance of the antenna, B the fringing field susceptance, B_{ext} the susceptance introduced by the varactor , Y_o the admittance of the patch. The proof of (7-7) is given in Appendix H. Observe the two different curves produced by the transmission line model. It is obvious that package parasitics can affect the slope of the resonant frequency.

Note that for higher bias voltages where the varactor response is more linear the agreement is better. However a γ which varies with bias voltage is the main reason for the discrepancy.

7.3.2 Quarter wavelength antenna-varactor module

Quarter wavelength microstrip antennas are becoming increasingly popular choices because of their small size (Encinar et al. 1993) . The unloaded antenna was first fabricated using half the dimensions of the half wavelength one. However the short circuit pins introduce inductance and it was necessary to reduce further the length (L=27mm) in order to obtain the same resonant frequency as in the half wavelength antenna.

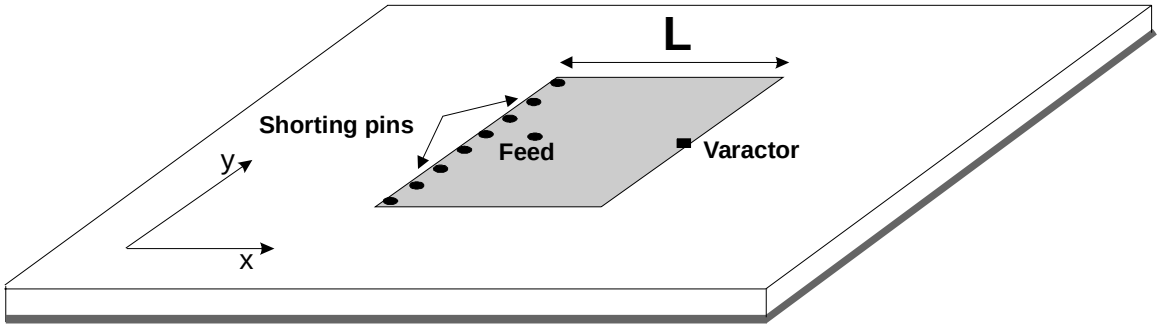

Figure 7.5 A quarter wavelength microstrip antenna-varactor module.

The same procedure as in the case of the half wavelength module was followed. The frequency tuning was verified experimentally (Figure 7.6) and by FDTD after performing calculations for several DC bias values. Observe very good agreement for high values of the voltage. There the change of the capacitance is not so abrupt and therefore the static C-V characteristic is a good representation of the varactor. For smaller bias voltages the curve changes slope which is followed again by FDTD but there is an offset for the frequency values.

The transmission line model is used to establish that the differences are partly due to packaging parasitics and partly due to variable γ. The resonant frequency of the quarter wavelength module considering the inductance of the pins is determined by

$$f_r = \frac{c}{2 \cdot \pi \cdot L\sqrt{\varepsilon_{eff}}} \tan^{-1}\left\{\frac{Y_o \cdot \left[1-(B+B_{ext})L_{sc} \cdot \omega\right]}{B+B_{ext}-Y_o \cdot L_{sc} \cdot \omega}\right\} \qquad (7\text{-}8)$$

where L_{sc} is the inductance introduced by the shorting pins and the rest of the symbols stand for the same quantities as in (7-7). A detailed proof of (7-8) is given in Appendix H. Observe how the transmission line model shows the effect of packaging parasitics in the slope of the curve (Figure 7.6) . It also proves that a variable γ is the main reason for differences between experiment and modelling.

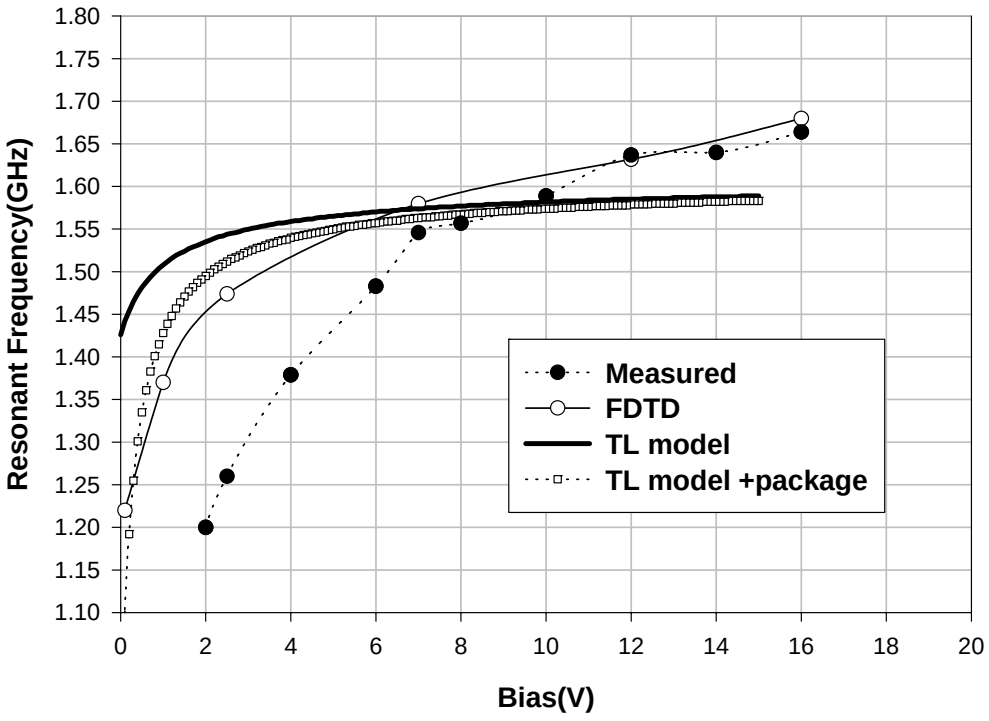

Figure 7.6 Frequency tuning of a varactor quarter wavelength antenna

7.3.3 Comparison of the tuning ranges

The tuning range can be defined as the maximum frequency shift from the resonant frequency of the unloaded patch. It can be expressed as a percentage like in the case of bandwidth. The tuning range of the quarter wavelength patch was found to be 25% experimentally (20% by FDTD). This is an interesting phenomenon that was verified experimentally and numerically. This means that for the same capacitor the quarter wavelength antennas offer greater frequency agility.

TABLE 7-1

Tuning ranges for varactor antennas

Antenna Type	FDTD prediction	Measurement
λ/4	31.8 %	32.6 %
λ/2	21.1 %	16.9 %

7.4 Fundamental resonance behaviour

7.4.1 Half wavelength module

Radiation patterns offer indispensable information for antenna systems. Radiation patterns were measured and calculated at three different bias voltages(-2.5V, -7V, -12V).

In Figure 7.7 the radiation patterns are shown for -7V. There is good agreement for the upper plane. The agreement is not as good at the lower half plane where diffraction effects are dominant. Nevertheless the shape is broadly followed. Other attempts to calculate the radiation patterns of such modules were reported in the literature (Waterhouse and Shulley

1994, Dauguet et al. 1997) but have been restricted to infinite ground planes thus giving results only for the upper half plane.

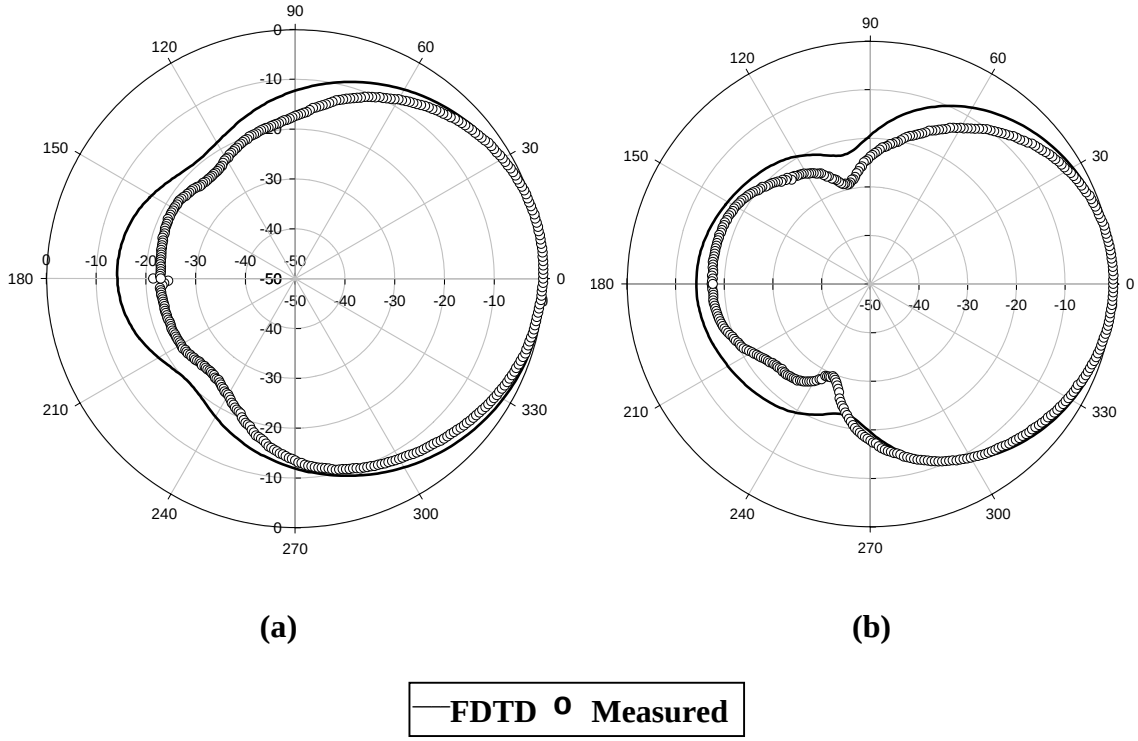

Figure 7.7 Radiation patterns for a half wavelength antenna with a varactor biased at -7V (a) E-plane (b) H-plane

The radiation patterns for the other bias voltages are found to be similar in shape to those of Figure 7.7. This is to be expected since the mode excited is the fundamental and the differences in frequency are not so great. A useful characteristic of one lobe patterns like the one coming from microstrip antennas is the 10dB beamwidth. There is a decrease as the bias voltage goes to more negative values. The variation of the 10dB beamwidth is related with the change in the electrical size of the ground plane. As the frequency goes higher with

higher bias voltage the ground plane becomes electrically larger, therefore reducing the diffraction effects. For any value of bias voltage the H-plane beamwidth remains more narrow by 20-30 degrees. All these features are predicted succesfully with FDTD. The cross polarisation levels were in general less than 20dB with a 2-3dB improvement for higher voltage, levels which were verified by FDTD. There is a cross polarisation null at zero degrees predicted accurately by FDTD. The levels are increased compared with a passive half wavelength antenna. The higher cross polarisation occurs at lower bias voltages.

The field distribution that produces the radiation patterns was calculated for the first resonance. The qualitative features are the same irrespective of the bias voltage. In Figure 7.8, observe the electric field null across the line at mid width with maxima at the radiating edges. The presence of the varactor disrupts slightly the symmetry of the maxima. This is also evident in the current density along the length of the patch (Figure 7.9) where the maximum is at the area where the electric field is zero. Minimum values occur at the radiating edges. Around the varactor, the current density is larger than at the corresponding symmetrical point at the other side of the patch. This is happening due to the fact that the varactor offers a return path for the current.

7.4.2 Quarter wavelength module

As in the case of the $\lambda/2$ radiator, radiation patterns were measured and calculated at three different bias voltages (2.5, 7, 12V) for the quarter wavelength module. Radiation patterns of such antennas have not been reported in the literature.

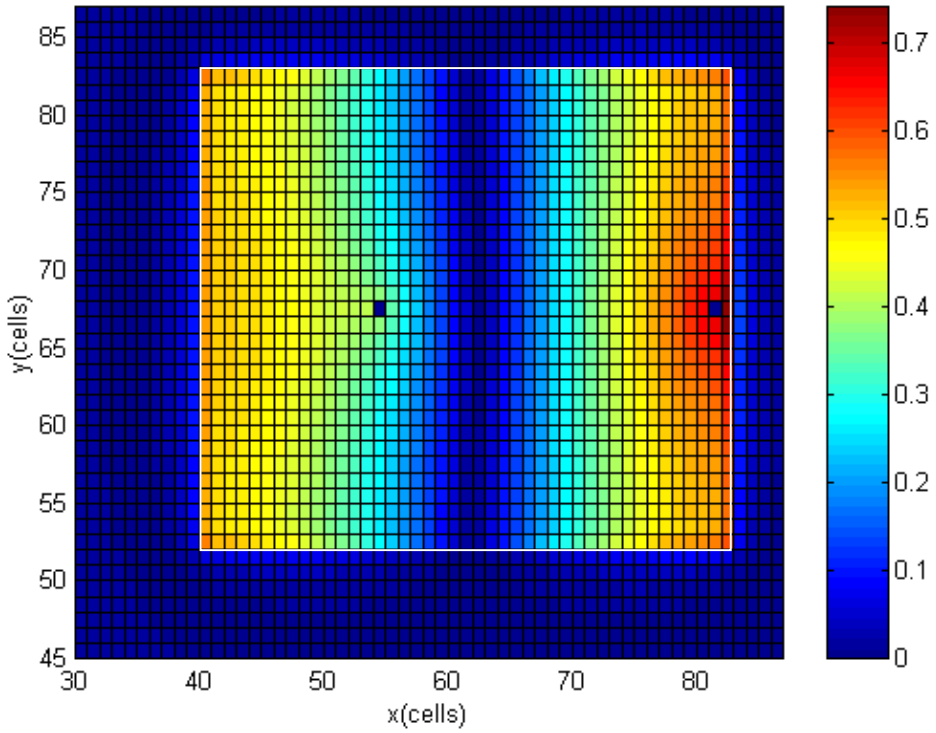

Figure 7.8 Electric Field normal to the surface of the half wavelength antenna-varactor at the first resonance (-7V)

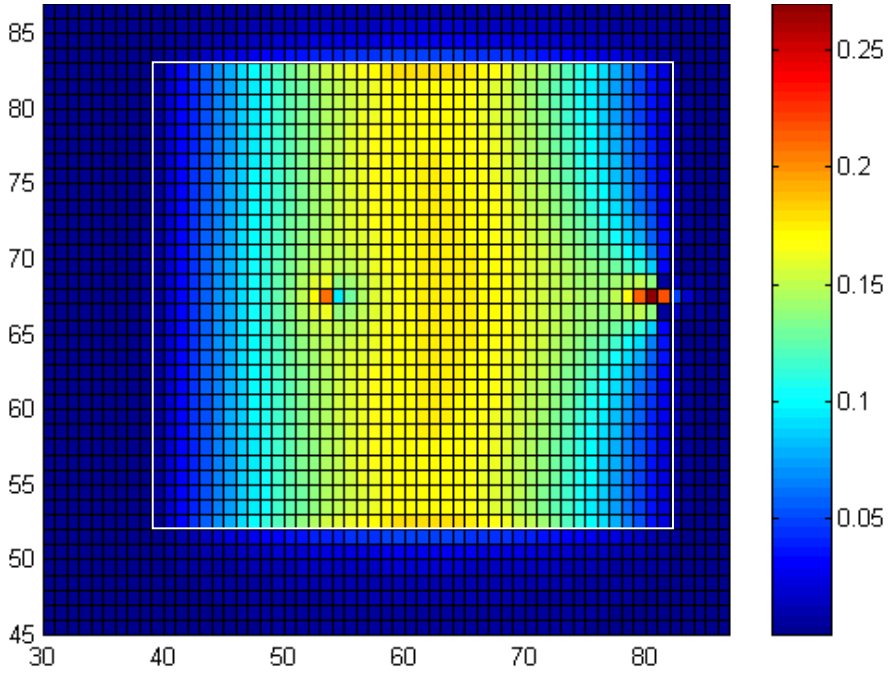

Figure 7.9 Longitudinal surface current density for the half wavelength antenna-varactor module at the first resonance (-7V bias)

In Figure 7.10 the radiation patterns show good agreement for the upper plane. As in the case of λ/2 antennas the agreement is not as good at the back plane where diffraction dominates.

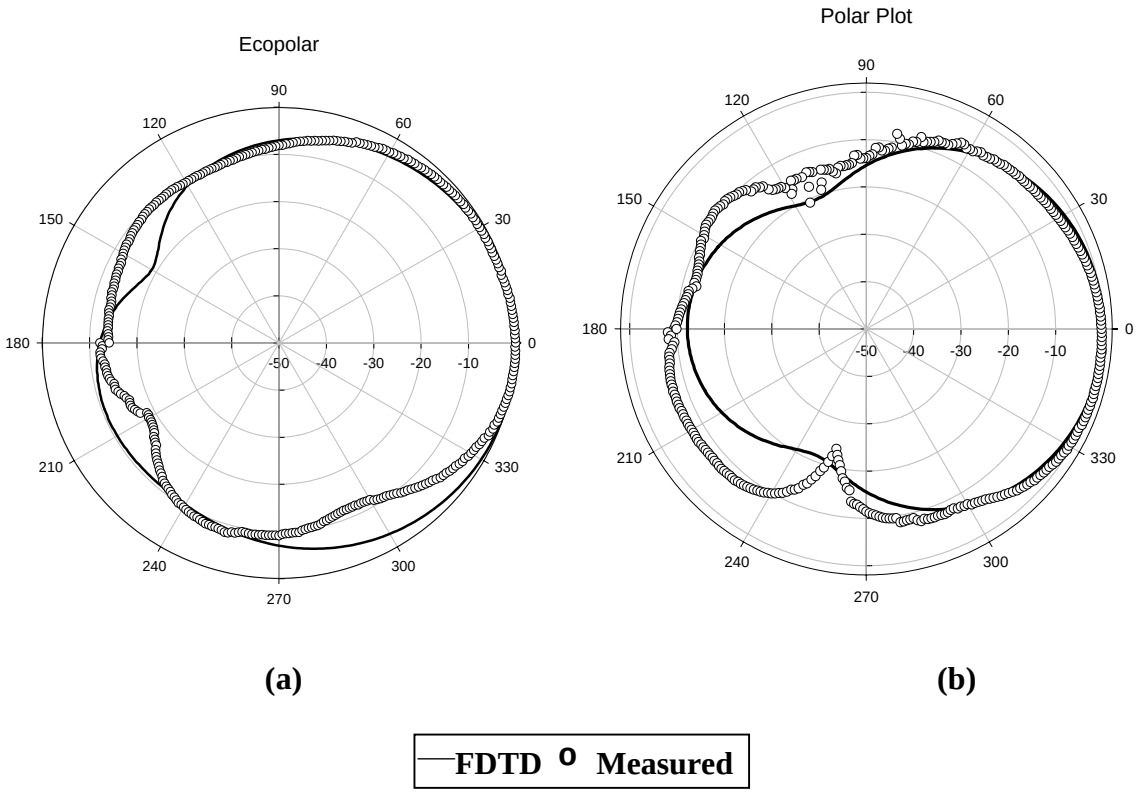

Figure 7.10 Radiation pattern for a quarter wavelength antenna-varactor module at the first resonance (-12V bias voltage) (a) E-plane (b) H-plame

The 10dB beamwidths show a variation with bias similar to the half wavelength ones. However the beamwidths are greater by 15^o-20^o. This can be explained with the increased tuning range of the λ/4 antenna. This means that for the same bias voltage, the ground plane for the quarter wavelength is electrically smaller and thus greater variation is expected. The cross polarisation levels were in general less than 20dB with 3-4 dBs improvement for higher voltage which were again verified by FDTD. There is a cross polarisation null at 0^o

degrees predicted accurately by FDTD. The crosspolarisation levels are 5-8 dBs higher than the half wavelength module. However this is expected for a quarter wave radiator.

The field distribution that produces the radiation patterns was calculated for the first resonance (Figure 7.11, Figure 7.12). The qualitative features remain the same irrespective of the bias voltage. There is an electric field null across the short circuits and a maximum at the radiating edge (Figure 7.11). Observe that the presence of the varactor disrupts the uniformity of the maximum at the radiating edge. The current density (Figure 7.12) is maximum at the short circuits but minimum at the radiating edge. The presence of the varactor disrupts the low current levels in the region acting as a current sink.

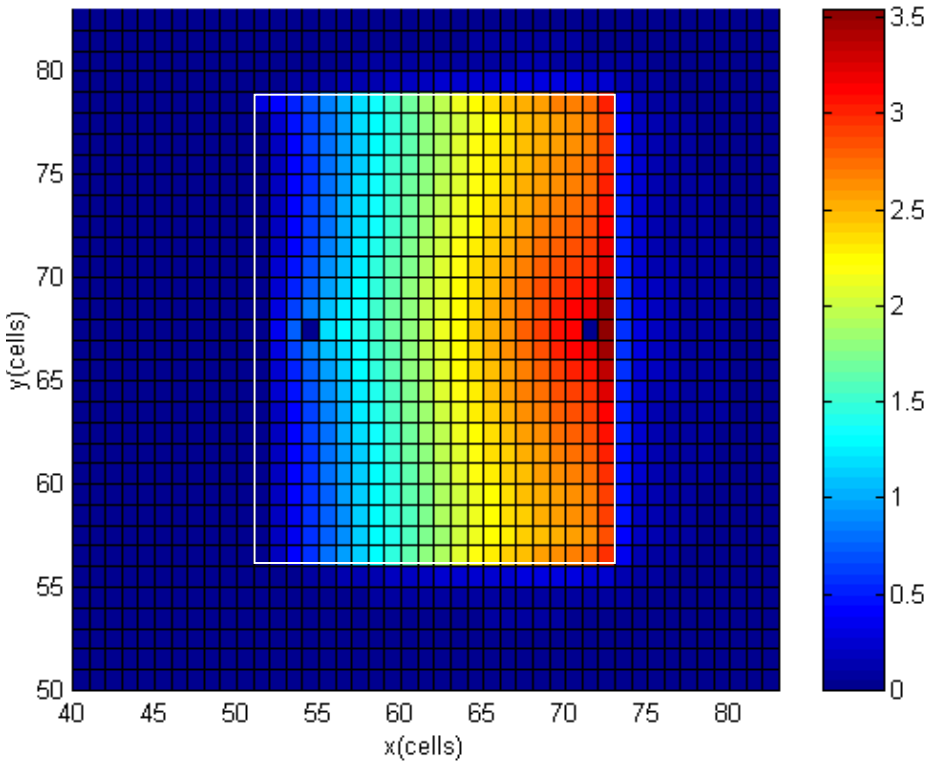

Figure 7.11 Electric Field normal to the surface for the λ/4 antenna-varactor module at the first resonance (-12V)

wavelength antenna in higher bias voltages and thus improved HIRP. Therefore a varactor loaded quarter wavelength antenna offers an attractive choice as a system component. In addition to that its small size makes it attractive for handheld applications.

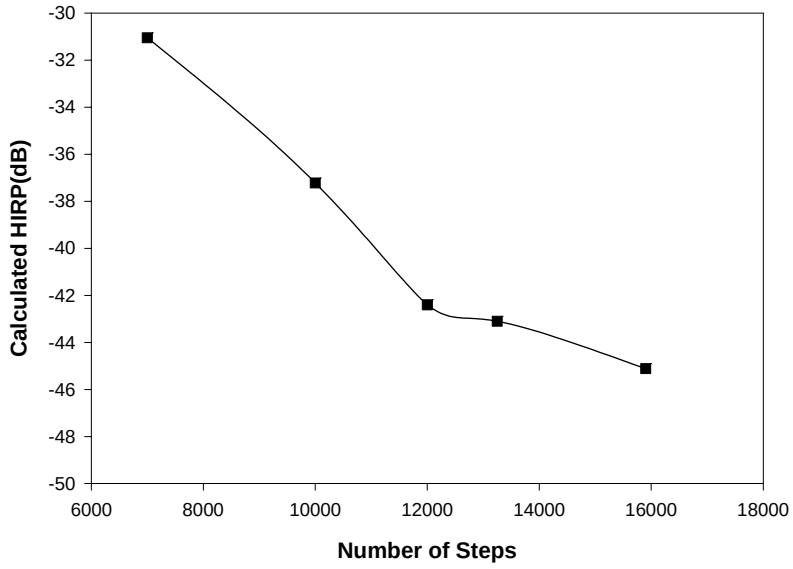

Figure 7.16 Demonstration of the effect of the number of steps on the HIRP magnitude cacluated with FDTD (Quarter Wavelength Antenna-Varactor module, bias -12V)

7.6 Harmonic Radiation and Fields

If a single channel with central frequency f_o is fed into the antenna-varactor module then radiation in channels with $2f_o$ central frequency is possible. In the previous paragraph harmonic power levels were assessed for a given orientation. In the literature the problem of harmonic radiation has not been addressed. For the first time, the radiation of an antenna-varactor module at the second harmonic has been calculated and compared with the experimental radiation patterns obtained for different bias voltages.

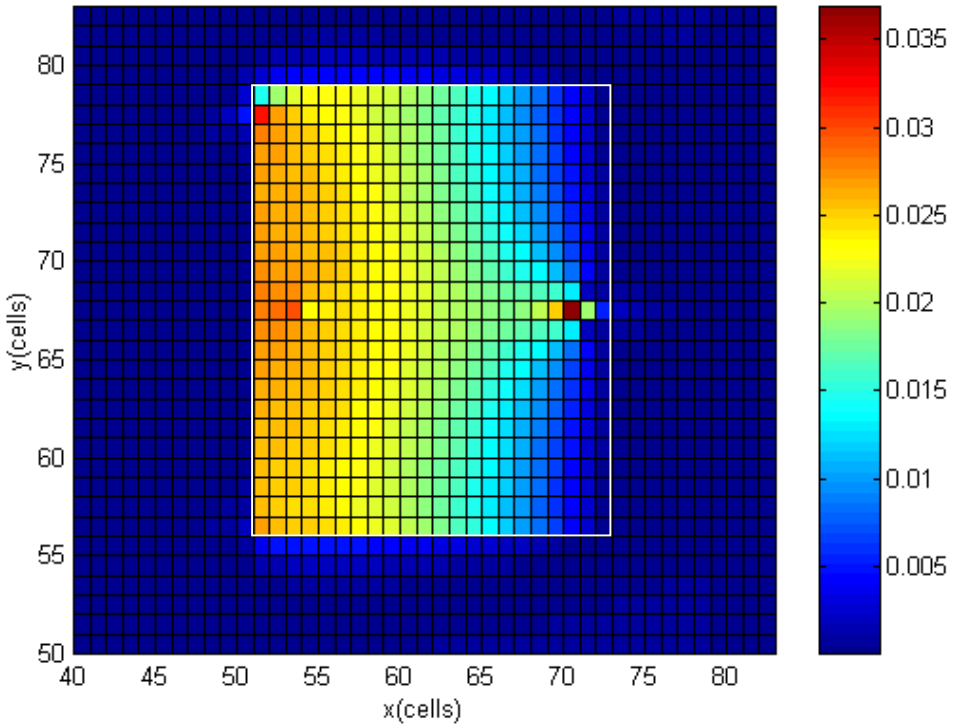

Figure 7.12 Longitudinal surface current density for -7V bias at the first resonance for the λ/4 wavelength antenna-varactor module

7.5 Radiated Harmonic Power

If a varactor antenna is a part of a wireless communications link then it is important to ensure that the harmonic power levels are low. This problem has not been addressed so far in the literature. In transmit, although a single channel signal is transmitted, the presence of nonlinearities can be the cause of harmonic generation. These cannot be cut by use of a filter since the varactor is incorporated on the antenna to form a single entity. If substantial harmonic power is radiated then it can be combined with other low power RF signals which could result in interference, obscuring the detection of the desired signal at the receiver.

It is therefore important to assess the levels of harmonics generated by antenna-circuit modules which incorporate nonlinear elements such as microstrip antenna-varactor modules.

In the absence of widely accepted figures of merit, the harmonic radiated power relative to the fundamental radiated power seems to be a good choice. In a wireless link the transmitted power will be received by an antenna. The antennas used in receivers are not of one type so in order to make the received power independent of the receiving antenna, an isotropic accepted power P_{RX}^{iso} will be used. Thus the normalised Harmonic Isotropic Radiated Power (HIRP) can be defined as the difference between the second harmonic radiated power received and the fundamental isotropic radiated power.

$$HIRP = P_{RX}^{iso}(2f_o) - P_{RX}^{iso}(f_o) \qquad (7\text{-}9)$$

The experimental arrangement for the measurement of HIRP can be seen in Figure 7.13 and it could be applied to any antenna-circuit module. The received power at a given frequency captured by an isotropic antenna can be estimated through

$$P_{RX}^{iso}(f) = P_{RX}(f) - G_{RX}(f) \qquad (7\text{-}10)$$

where P_{RX}: is the power received in dB and G_{RX} is the gain of the receiving antenna also in dB. For the measurements (Appendix G) a broadband Vivaldi antenna (Langley et al 1996) was used as the receiving antenna. The received power P_{RX} can be measured at the spectrum analyser. The HP-8563E spectrum analyser with frequency range from 9kHz-26.5GHz was used in the measurements. Therefore a measurement of HIRP as expressed in (7-9) can be readily performed .

It is useful to relate the above figure of merit to standard system concepts such as EIRP (Equivalent Isotropic Radiated Power) which is used in system budget calculations. EIRP can be defined (Roddy and Cooleen 1995) as

$$EIRP(f) = P_{TX}(f) + G_{TX}(f) \qquad (7\text{-}11)$$

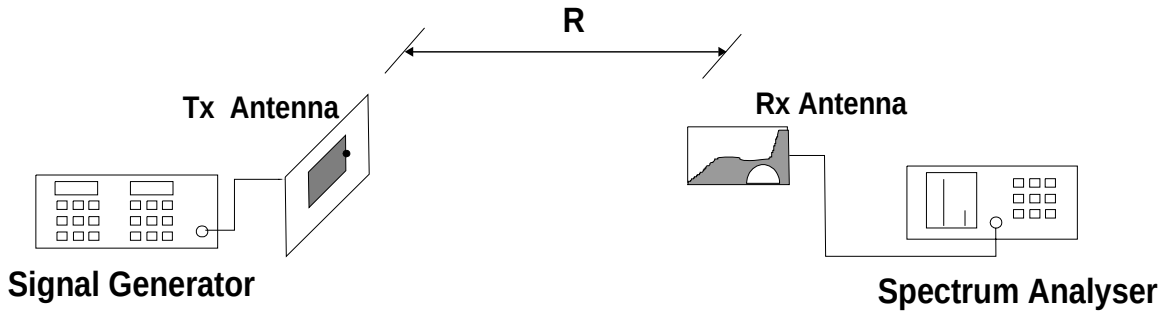

Figure 7.13 Set up for the measurement of harmonic radiated power.

The Friis transmission formula (Balanis 1996) relates transmitter and receiver parameters

$$P_{RX}(f) = G_{TX}(f) + P_{TX} + G_{RX}(f) - L_{fs}(f) \qquad (7\text{-}12)$$

where $L_{fs}(f)$ is the free space loss in dB equal to

$$L_{fs}(f_o) = 10 \cdot \log\left(\frac{4\pi \cdot R}{\lambda}\right)^2 \qquad (7\text{-}13)$$

where R is the distance between transmitter and receiver. Then taking into account (7-10), (7-11) and (7-12) EIRP can be computed using quantities measured at the receiver.

$$EIRP(f) = P_{iso}(f) + L_{fs}(f) \qquad (7\text{-}14)$$

Taking into consideration (7-14) , the normalised Harmonic Isotropic Radiated Power (HIRP) can also be expressed as

$$HIRP(dB) = EIRP(2f_o) - EIRP(f_o) - 6dB \qquad (7\text{-}15)$$

where the 6dB correction is necessary because the free space loss $L_{fs}(2f_o)$ is four times the loss $L_{fs}(f_o)$. In the case of the FDTD calculations, the far field can be calculated as explained in chapter 4. Based on the extraction of the far field quantities the radiation intensity U can be calculated . From Balanis(1996) the isotropic radiated power is given by

$$P_{RX}^{iso}(f_o) = \left(\frac{\lambda}{4\pi}\right)^2 \frac{U(f)}{R^2} \qquad (7\text{-}16)$$

Then HIRP can be found by

$$HIRP = U_{\max}(2f_o) - U_{\max}(f_o) - 6dB \qquad (7\text{-}17)$$

where the fact that the wavelength at $2f_o$ is half the wavelength at f_o was taken into account.

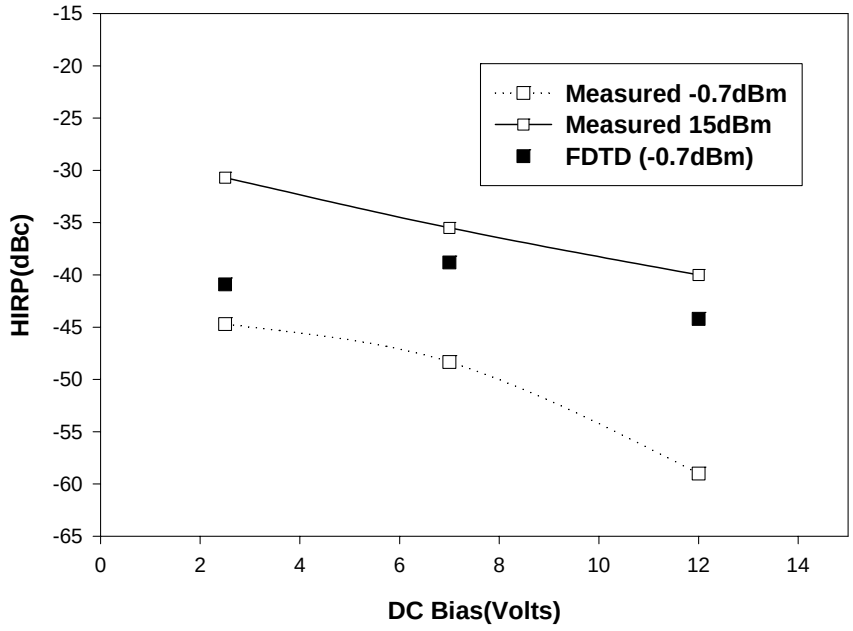

Figure 7.14 HIRP for a λ/2 antenna-varactor module as a function of bias voltage. FDTD results calculated for N=12000 steps

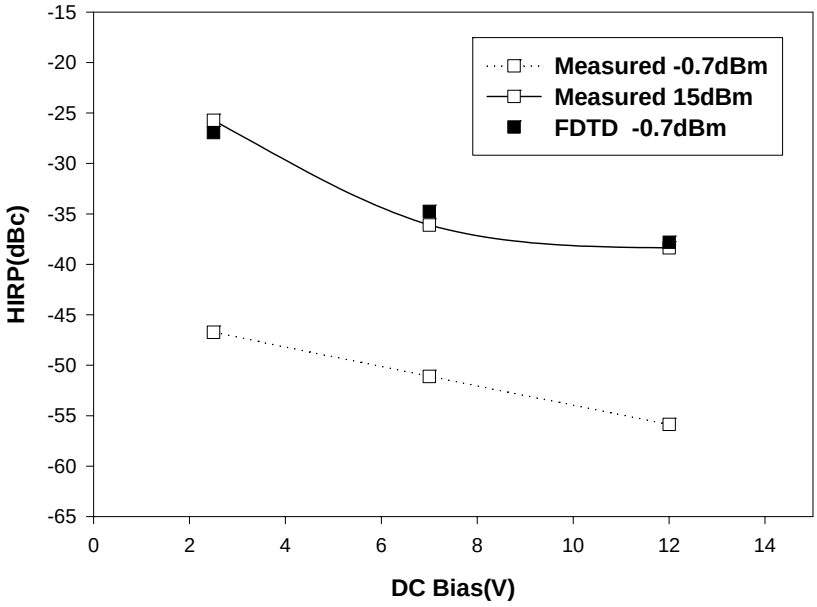

Figure 7.15 HIRP for a λ/4 antenna-varactor module as a function of bias voltage. FDTD results calculated for N=10000 steps

The HIRP for the half wavelength and quarter wavelength microstrip antenna-varactor modules are seen in Figure 7.14, Figure 7.15 respectively. A series of measurements was performed for different power levels form -0.7dBm to 15 dBm . The upper limit of input power was determined by the power handling limit of the varactor in use which was 50mW (17dBm) .

Observe that the harmonic power level depends on the input power and on the bias voltage. The lower the bias voltage, the more nonlinear is the region of operation of the varactor, making harmonic radiation stronger and the HIRP lower. Higher input power levels for a given bias voltage cause the dynamic voltage across the varactor to cover a larger portion of its characteristic and thus the behaviour is more nonlinear comparing with the lower power.

The FDTD calculated results follow the change in HIRP with bias voltage but the calculated values seem to disagree with the experimental ones. In order to understand such a discrepancy, the process of the calculation of harmonic radiation is described. A monochromatic signal excites the varactor loaded antenna for a certain and limited number of steps. Then at the three dimensional surface a DFT is performed to obtain the equivalent currents at the fundamnetal and the harmonic frequency. Then via the near-to-far field transformation (see Chapter 4 and Appendix D) the radiated power is calculated. However the DFT of the currents does not produce accurate results for any small number of time steps. Recall that DFT allows calculation of frequencies Δf apart where $\Delta f = \frac{1}{N \cdot \Delta t}$. In an FDTD simulation the time resolution is fixed and therefore the frequency resolution can be controlled only by the number of time steps N. The estimation of the spectrum peaks is susceptible to errors due to the finite Δf and the fact that the desired frequencies do not fall in integer multiples of Δf . The errors however should reduce with increasing N. DFT computations were performed of a two tone signal resulting from the application of a single sinusoid to a nonlinearity of similar nature. The results showed that the power of the fundamental relative to that of the second harmonic had a very strong dependence on N and could be up to 20dB different. For one of the cases (Figure 7.16) , FDTD computations with different number of time steps were performed to demonstrate that effect. In Figure 7.16, it can bee seen how N affects severely the HIRP level. A difference of 14 dB was noted when doubling the number of time steps.

In comparison both antennas have more or less the same harmonic performance for a given bias voltage. However the difference in the tuning range permits use of the quarter

7.6.1 Half wavelength module

Patterns were measured by exciting the antenna at its second resonance. The radiation patterns were measured for three bias voltages (2.5 ,7 ,12) and the normalisation was done for each plane separately.

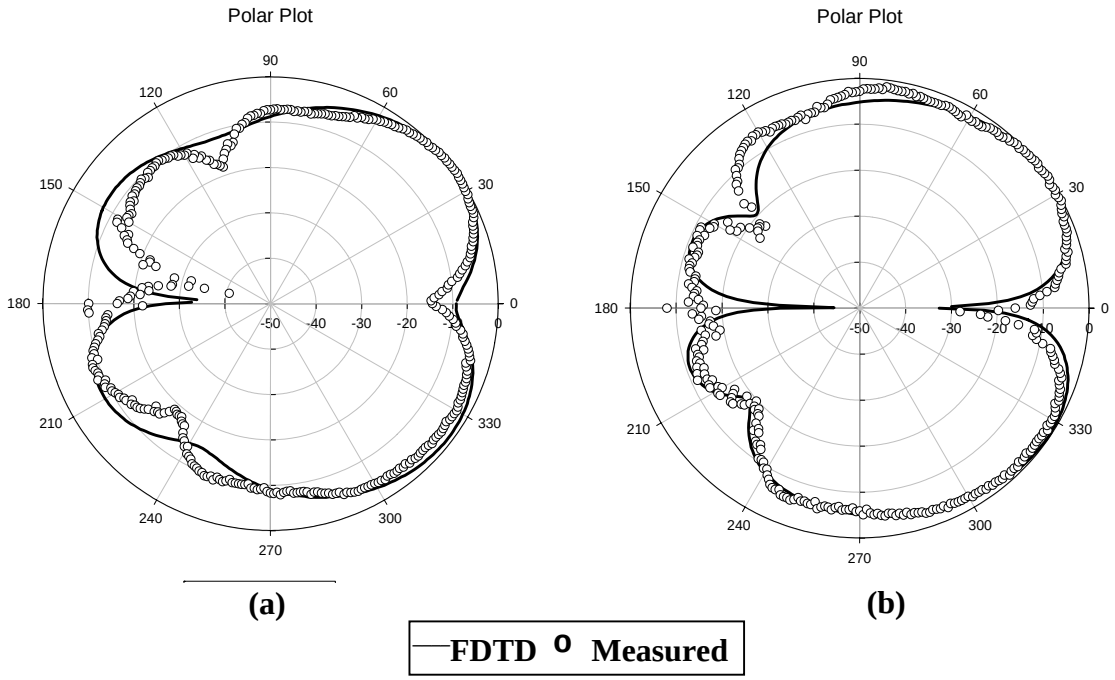

Figure 7.17 Radiation patterns for a λ/2 antenna-varactor module at the second harmonic (Bias -2.5 V) (a) E-plane (b) H-plane cross polar

The agreement is excellent for the upper plane and the lower half plane following closely the nulls (Figure 7.17). The better agreement can be explained due to increased distance from the absorbing boundaries (Rayner et al. 1994) for the higher frequency. The radiation patterns are similar for the other voltages. The radiation patterns have maximum off axis indicating the excitation of a different mode.

The electric field distribution on the surface of the module is seen in Figure 7.18. The electric field has a distribution that presents maxima at the corners of the radiating edges. Observe the markedly different distribution at the fundamental (Figure 7.8). The current density both longitudinal and transverse was also calculated (Figure 7.19). Note that at the region of the varactor there is significant transverse current flowing through its pin unlike the fundamental mode.

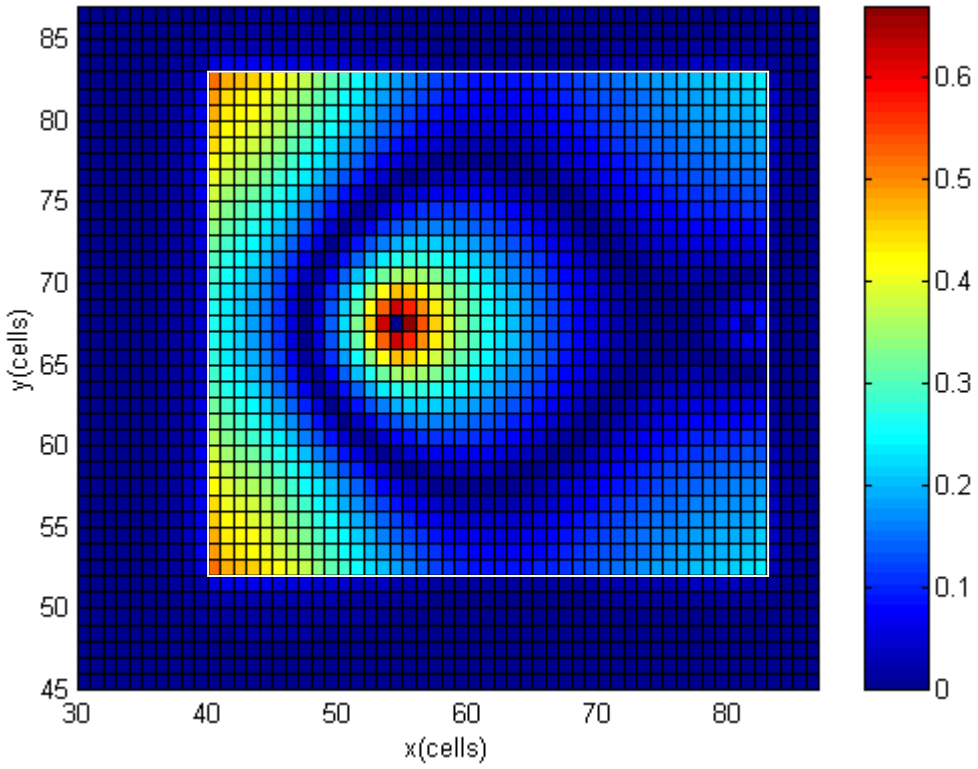

Figure 7.18 Distribution of the electric field normal to the surface of a λ/2 module at its second resonance (Bias -2.5 V)

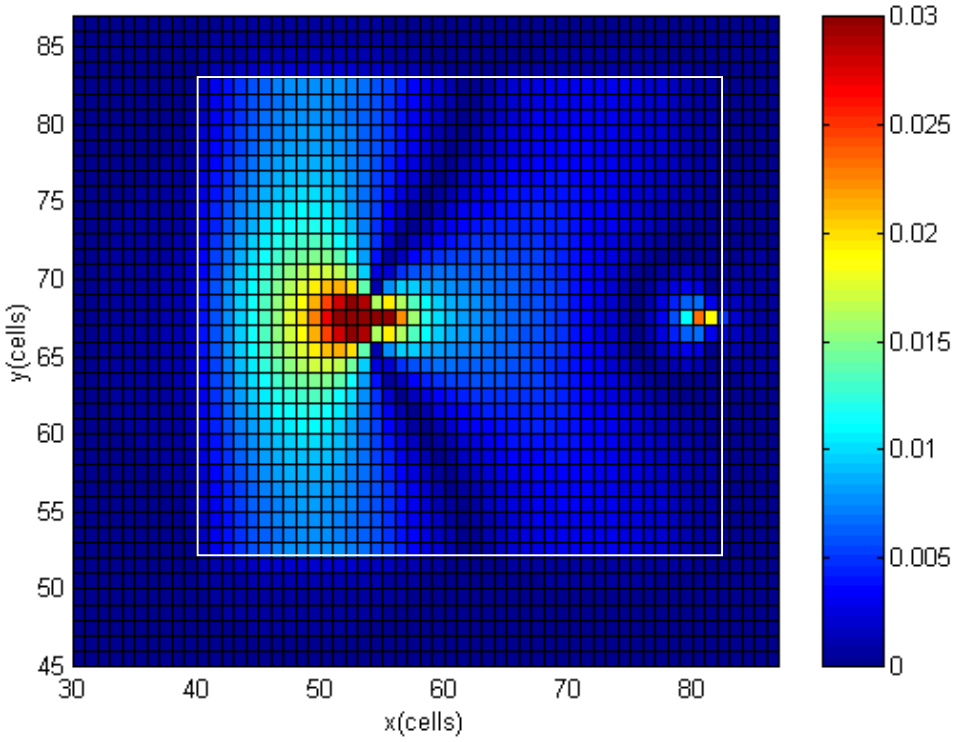

(a)

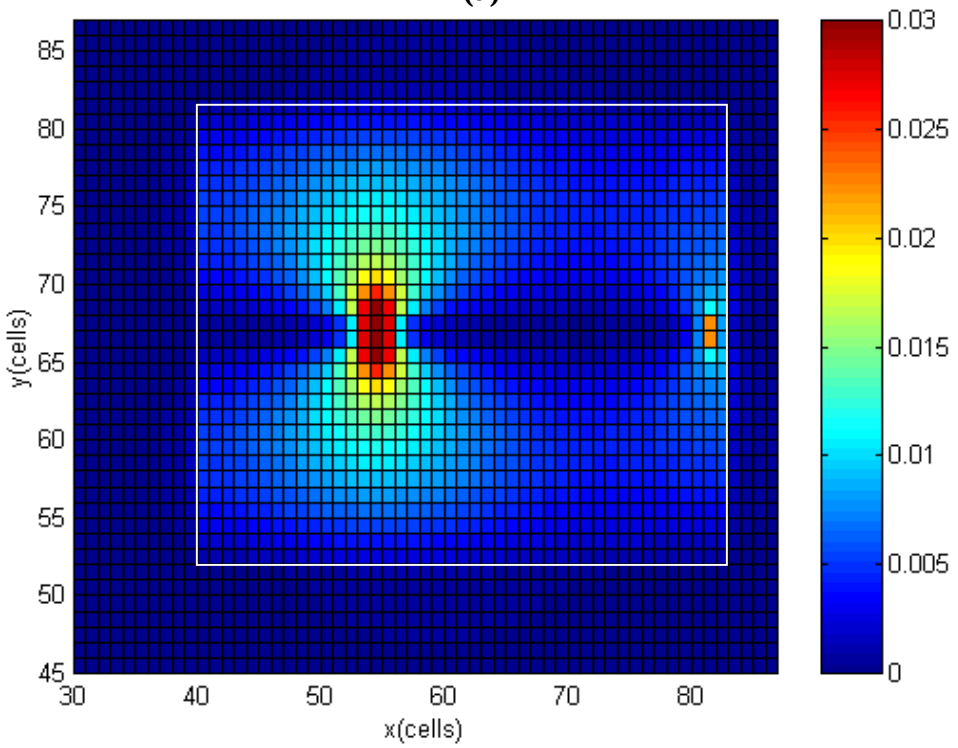

(b)

Figure 7.18 Surface current density distribution for a λ/2 module (Bias -2.5 V) (a)longitudinal (b) transverse

7.6.2 Quarter wavelength module

Although the quarter wavelength antenna does not have a second resonance however the presence of the varactor on the antenna changes its behaviour. This is consistent with the observations in the literature that the addition of any short circuiting pin changes the resonances of an antenna.

The radiation patterns were measured for three bias voltages (2.5 ,7 ,12). The levels are normalised for each plane separately. The patterns obtained with -2.5 bias voltage are presented in Figure 7.20.

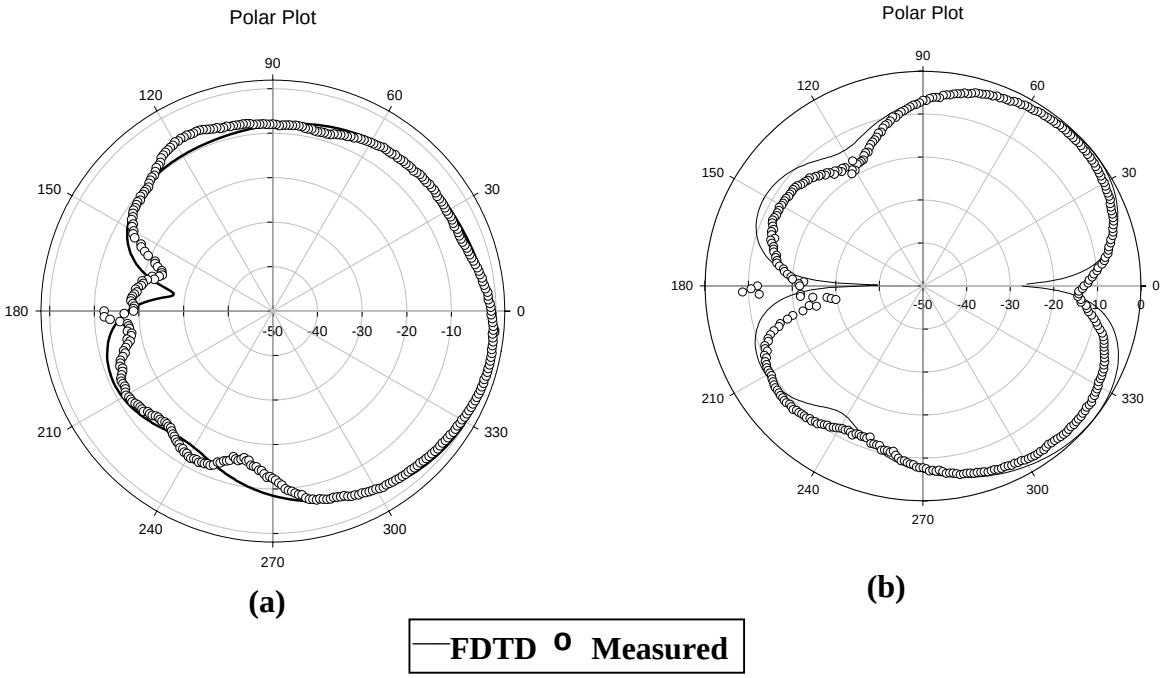

Figure 7.20 Radiation patterns for a λ/4 module at the second resonance (Bias -2.5 V)
(a) E-plane (b) H-plane cross polar

As in the λ/2 case the agreement is excellent for the upper plane and the lower half plane following closely the nulls. The radiation patterns are similar for the other voltages.

The electric field distribution is seen in Figure 7.21. The current density both longitudinal and transverse were also calculated (Figure 7.22). At the region of the varactor there is significant transverse current density. It is interesting to compare the radiation patterns in the E-plane for the two modules. This means that the mode excited in the case of the λ/4 antenna is different than in the case of the λ/2 antenna as it is shown explicitly in Figure 7.18 and Figure 7.21.

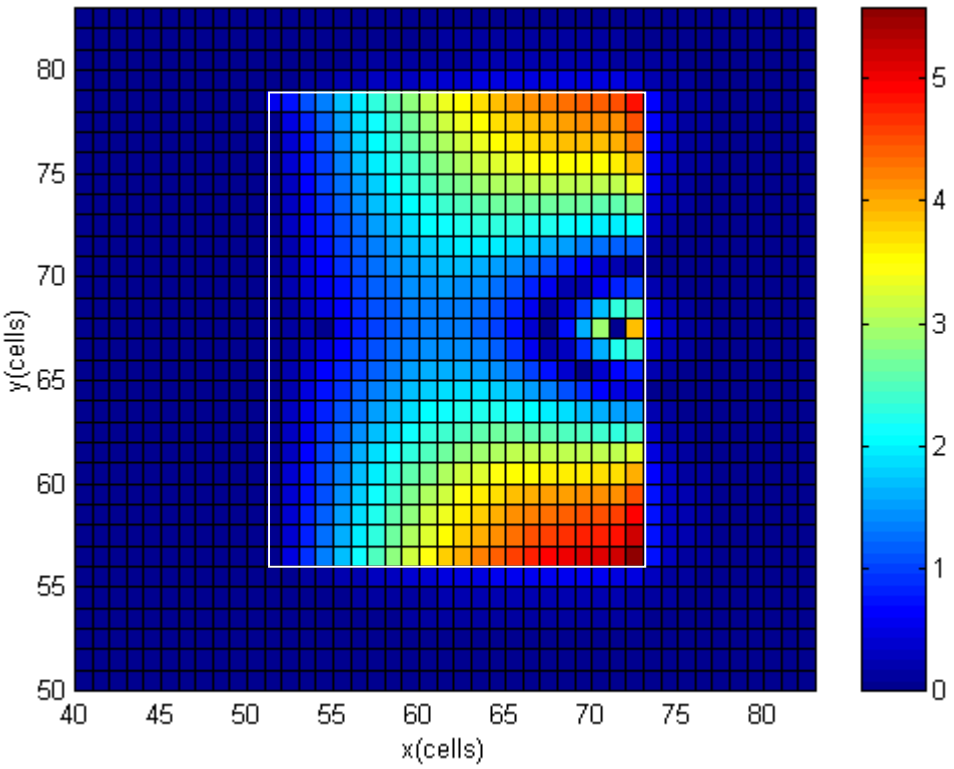

Figure 7.21 Electric field distribution normal to the surface of a λ/4 module at the second harmonic.(-2.5 V bias)

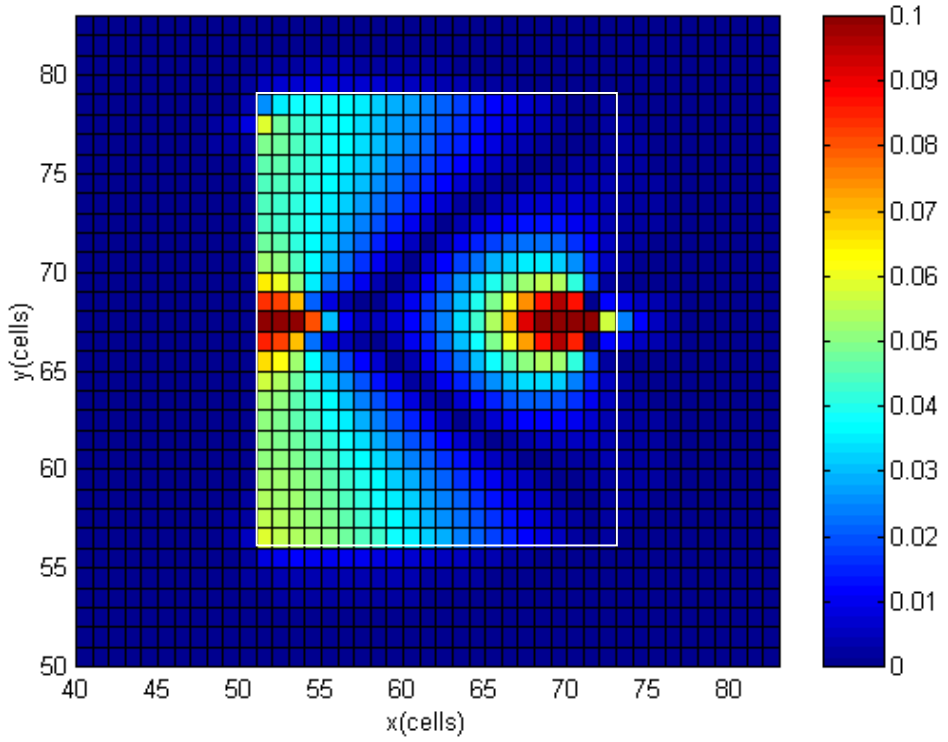

(a)

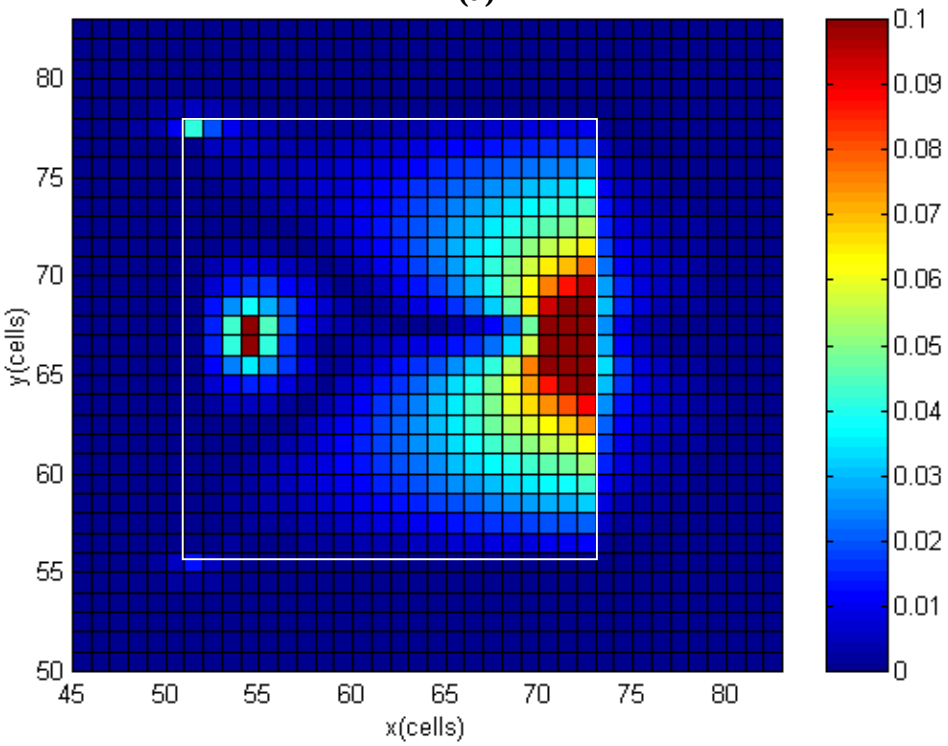

(b)

Figure 7.22 Surface current density of a λ/4 module at the second harmonic.(-2.5 V bias) (a)longitudinal (b) transverse

7.7 Summary

In this chapter a varactor model for FDTD calculations was presented. This was validated with HP-MDS. Microstrip antennas incorporating varactors were studied. Frequency tuning , radiation patterns and harmonic performance were investigated both experimentally and theoretically for the first time in the open literature. Also a double tuning range was observed in the short-circuited quarter wavelength module, a phenomenon that offers greater frequency agility and improved harmonic performance. Such a configuration could also be useful in integrated adaptive tuning systems. The increased effective band operation compared to the half wavelength module is achieved at the expense of increased cross-polarisation levels.

CHAPTER 8

MICROSTRIP ANTENNA-GUNN OSCILLATOR MODULES

In this chapter the focus is on the modelling of Gunn oscillators and how these are combined with microstrip antennas. The implementation of a large signal Gunn diode equivalent circuit in the FDTD code is described and validated using a microstrip line oscillator with an arbitrary load. Single and dual device self oscillating antennas are then studied.

8.1 FDTD Modelling of Gunn diodes

One port active elements like Gunn and IMPATT diodes exhibit negative resistance. The most common way of representing them is through equivalent circuits which always accommodate a current source F(V) and some other lumped elements. There are different equivalent circuits even for the same device. Hirota et al (1980) used an equivalent circuit like the one in Figure 8.1.a to model a microstrip line Gunn oscillator. More recently Toland et al. (1993) implemented a large signal equivalent circuit (Figure 8.1.b) and they incorporated it in their FDTD code in an attempt to model a single device waveguide oscillator. The value of the capacitor used by both researchers was C=0.2pF. The nonlinear current sourse is represented as a function of the voltage involving cubic nonlinearities:

$$F(V_S) = -G_1 \cdot V_S + G_2 \cdot V_S^{\,3} \qquad (8\text{-}1)$$

The negative conductance corresponding to the current source is

$$G(V_s) = -G_1 + 3 \cdot G_2 \cdot V_S^2 \qquad (8\text{-}2)$$

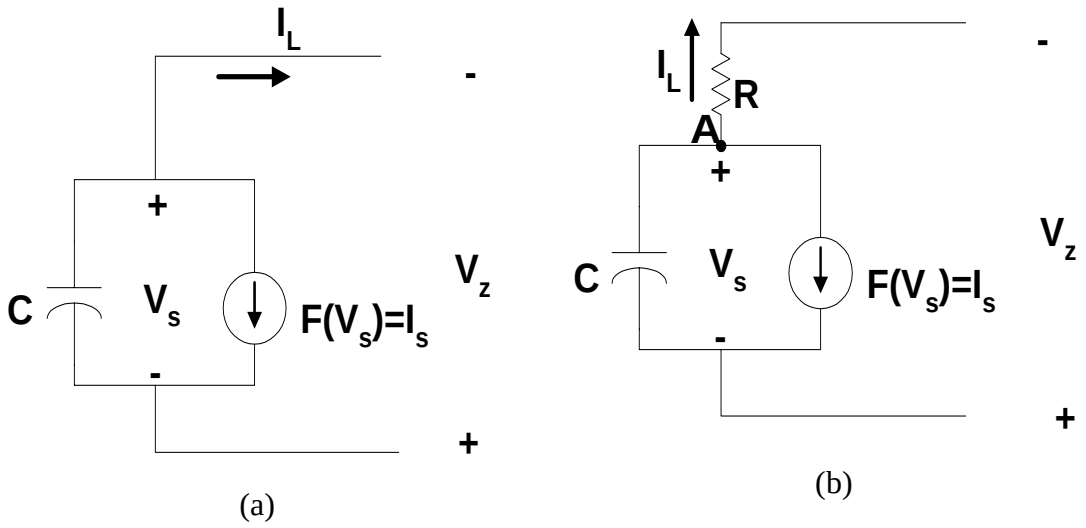

Figure 8.1 Equivalent circuits used for Gunn diodes with F(Vs) representing a nonlinear dependent current source. (a) with no series loss (b) with series loss R.

For this work the equivalent circuit of Figure 8.1.b is used. Recall that in expression (3-36) the current $I_L^{n+\frac{1}{2}}$ is required. This is computed as

$$I_L^{n+\frac{1}{2}} = \frac{V_S^{n+\frac{1}{2}} + V_Z^{n+\frac{1}{2}}}{R} \Rightarrow I_L^{n+\frac{1}{2}} = \frac{V_S^{n+1} + V_S^n + V_Z^{n+1} + V_Z^n}{2R} \qquad (8\text{-}3)$$

The objective is to obtain a discrete solution for the voltage V_S. The differential equation governing the behaviour of the circuit of Figure 8.1.b is derived by adding the currents at node A.

$$I_S + C\frac{dV_S}{dt} + I_L = 0 \qquad (8\text{-}4)$$

Taking into account that $I_L = \frac{V_S + V_Z}{R}$ and dividing by RC, transforms the differential equation (8-3) to the following expression:

$$\frac{dV_S}{dt} + \frac{F(V_S)}{C} + \frac{V_S}{RC} = -\frac{V_Z}{RC} \qquad (8\text{-}5)$$

(8-5) is solved numerically using forward time finite differences. Quantities at time $n+\frac{1}{2}$ are averaged with quantities at n and n+1 times. Thus the finite difference expression of (8-5) is of the form:

$$\frac{V_s^{n+1}-V_s^n}{\Delta t}+\frac{F(V_s^{n+1})+F(V_s^n)}{2C}+\frac{V_s^{n+1}+V_s^n}{2RC}=-\frac{V_z^{n+1}+V_z^n}{2RC} \qquad (8\text{-}6)$$

A first order Taylor approximation is used for $F(V_s^{n+1})$

$$F(V_s^{n+1})=F(V_s^{n+1})+\frac{dF(V_S)}{dV_S}\cdot(V_S^{n+1}-V_S^n) \qquad (8\text{-}7)$$

where the derivative $\dot{F}=\frac{dF(V_S)}{dV_S}$ is calculated for $V_S=V_S^n$. Grouping terms and multiplying by 2RCΔt, (8-6) yields

$$(2RC+\Delta t+R\dot{F})V_S^{n+1}+(2RC-\Delta t+R\dot{F}\Delta t)V_S^n+2R\Delta tF(V_S^n)=\Delta t(V_Z^{n+1}+V_Z^n) \qquad (8\text{-}8)$$

Expression (8-8) can be written in a more compact arrangement as

$$V_S^{n+1}=\frac{A_1}{\beta}V_S^n-\frac{A_2}{\beta}F(V_S^n)-\frac{A_3}{\beta}\Delta z(E_Z^{n+1}+E_Z^n) \qquad (8\text{-}9)$$

where: $\beta=2RC+\Delta t(1+R\dot{F})$ (8-10) $A_1=2RC-\Delta t(1-R\dot{F})$ (8-11)

$A_2=2R\Delta t$ (8-12) $A_3=\Delta t$ (8-13)

Having a solution for V_S^{n+1} means that (8-3) provides an iterative solution for $I_L^{n+\frac{1}{2}}$. Substitution of (8-3) to (3-36) taking into account (8-9) will give the update equation for the field at the device cell:

$$E_z^{n+1} = \frac{\frac{\varepsilon}{\Delta t} - \frac{\Delta z}{\Delta x \cdot \Delta y}\frac{1-A_3}{2R}}{\frac{\varepsilon}{\Delta t} + \frac{\Delta z}{\Delta x \cdot \Delta y}\frac{1-A_3}{2R}} E_z^n + \frac{1}{\frac{\varepsilon}{\Delta t} + \frac{\Delta z}{\Delta x \cdot \Delta y}\frac{1-A_3}{2R}} (\nabla \times \overline{H})_z^{n+1/2}$$

$$- \frac{(1+A_1)V_S^n - A_2 F(V_S^n)}{2R_S \cdot \Delta x \cdot \Delta y(\frac{\varepsilon}{\Delta t} + \frac{\Delta z}{\Delta x \cdot \Delta y}\frac{1-A_3}{2R})} \qquad (8\text{-}14)$$

Therefore the inclusion of the negative device in the FDTD method is a two level iterative procedure. At each time step, first calculate E_Z^{n+1} via (8-14). Then calculate V_S^{n+1} through (8-9). This value of V_S^{n+1} is used as the value of V_S^n for the next time step.

8.2 Negative Resistance Oscillators

Oscillators are essential components in any circuit providing the high frequency signal from a DC biased active device.

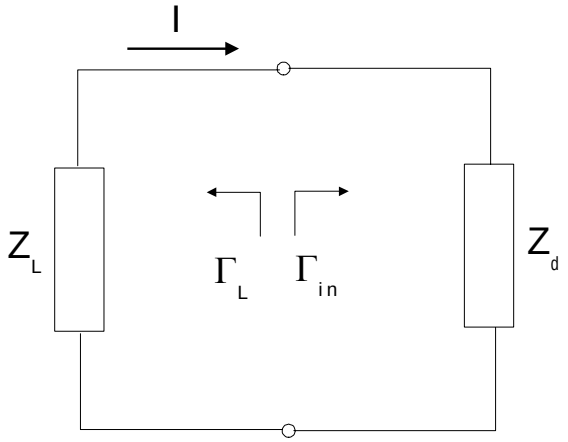

Figure 8.2 A one port negative resistance oscillator circuit

If a load $Z_L=R_L+jX_L$ is connected to an active device $Z_d=R_d+jX_d$ (Figure 8.2) then in order to have a signal flow, it is required (Pozar 1990) that

$$(Z_L + Z_d)I = 0 \qquad (8\text{-}15)$$

This is equivalent to

$$R_L + R_d \leq 0 \qquad (8\text{-}16)$$

$$X_L + X_d = 0 \qquad (8\text{-}17)$$

where in (8-16) the inequality is for the start-up and the equal sign is for the steady state. Therefore the active device (the load is passive and has positive resistance) must exhibit negative resistance. Semiconductor circuit elements either exhibit inherent negative resistance, like the Gunn diodes modelled above, or as in the case of FETs, they can be configured to have an effective negative resistance by the addition of an external circuit. Condition (8-17) determines the oscillation frequency.

The conditions for oscillation can also be expressed with the help of S-parameters (Vendelin et al 1990). In order to have a circuit start oscillating, the loop gain must be greater than one and the phase must change sign from positive to negative ensuring the clockwise rotation of the circle(1+j0) in the impedance plane (Nyquist stability criterion).

8.3 A microstrip line Gunn Oscilllator

A Gunn MIC oscillator (Figure 8.3) was chosen to validate the one-port active device expressions. The microstrip line has characteristic impedance Z_o=50Ω, (substrate height is 0.51mm, ε_r=2.2), open in the one end and terminated by a load in the other end.

The Gunn diode used is represented by an equivalent circuit of the Figure 8.1.b. The values used are G_1=0.0252 Siemens, G_2=0.0265 Siemens, series loss R=1 Ω, capacitor C=0.2pF. The conductance curve is the derivative of the current characteristic (8-1).

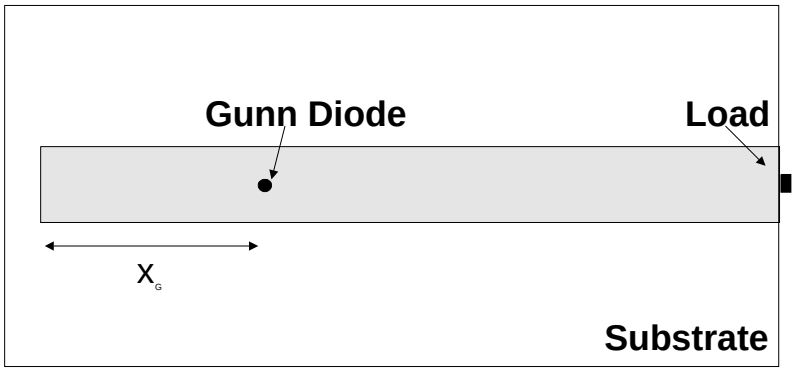

Figure 8.3 A microstrip Gunn oscillator (top view)

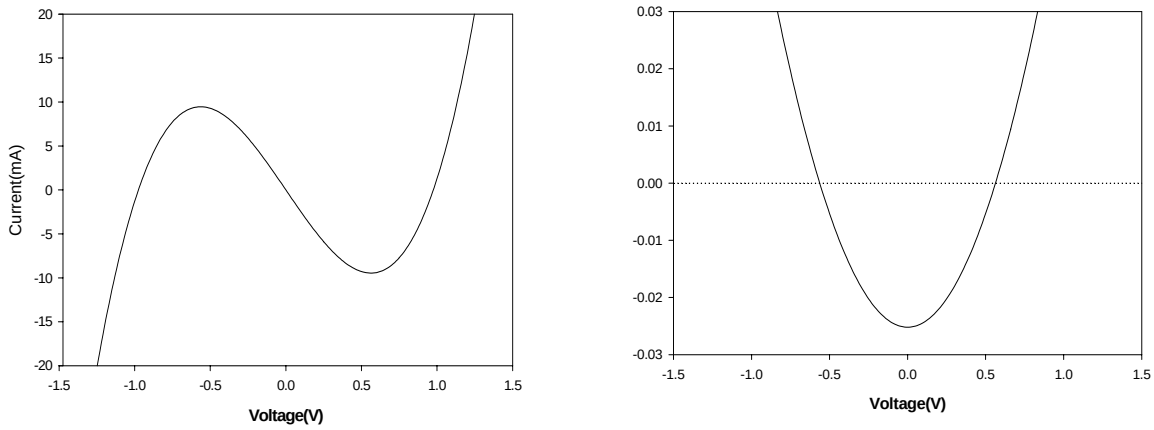

(a) **(b)**

Figure 8.4 Nonlinear Current Source Characteristics for an X-band Gunn diode (a) Current vs. voltage (b) Conductance vs. Voltage

In Figure 8.5 the FDTD simulated oscillation is observed with the onset and the steady state clearly seen. In laboratory conditions the oscillation is triggered by ambient noise. In the simulation a one time step duration voltage pulse was imposed at the Gunn diode FDTD

cell to replicate the effect of noise. Initially the oscillator is placed at the (0,0) point of the I-V characteristic (Figure 8.4.b). The introduction of the triggering voltage forces a small perturbation from the equilibrium point.

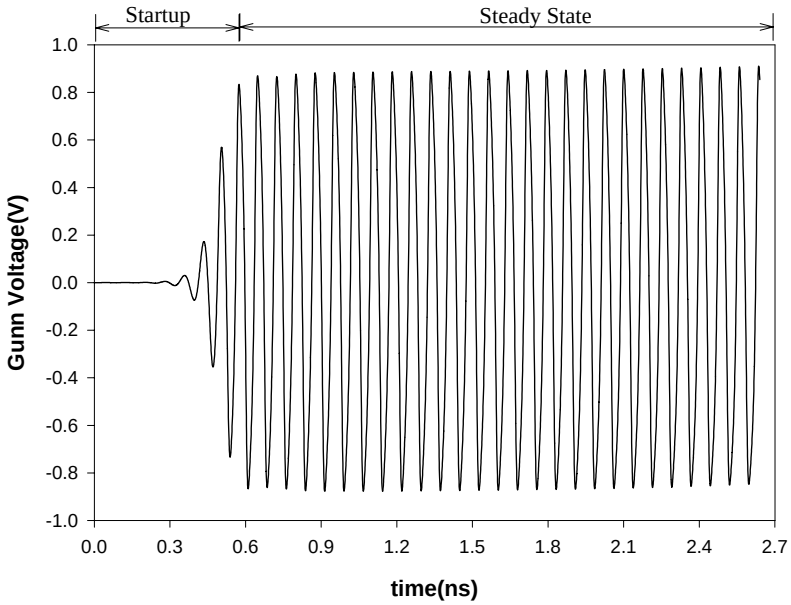

Figure 8.5 FDTD calculated voltage for a microstrip line Gunn Oscillator.

The steady state can be seen in Figure 8.6 where the presence of harmonics are manifested as a distortion of the dominant signal of 13.8 GHz. This is better seen in the spectrum of the oscillation (Figure 8.7) where the main oscillation and the harmonics are seen.

The same circuit was analysed with HP-MDS to establish the predicted frequencies by using the S-parameter design that is offered with the simulator (Appendix E, Figure E.10) The Gunn diode model was also implemented in HP-MDS using the S-parameter design technique. TABLE 8-1 gives a comparison of the predicted frequencies.

TABLE 8-1

Comparison of predicted frequencies
for HMIC Gunn oscillator for different loads

	R=50Ω	R=100Ω
HP-MDS S-parameter design	13.8	15.4
FDTD Calculated	13.1	14.4
Difference (%)	5.07	6.99

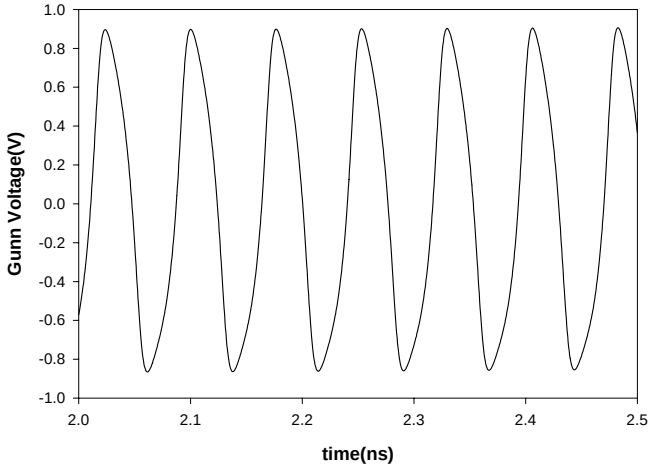

(a)

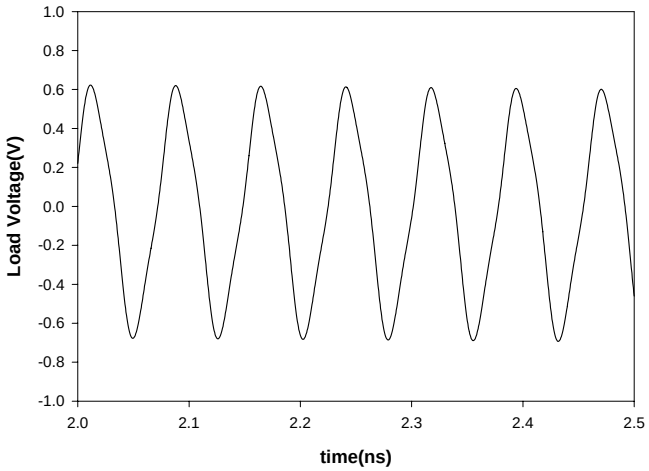

(b)

Figure 8.6 The steady state of a Gunn diode MIC oscillator terminated with a 50 Ω load

(a) Gunn diode(b) load

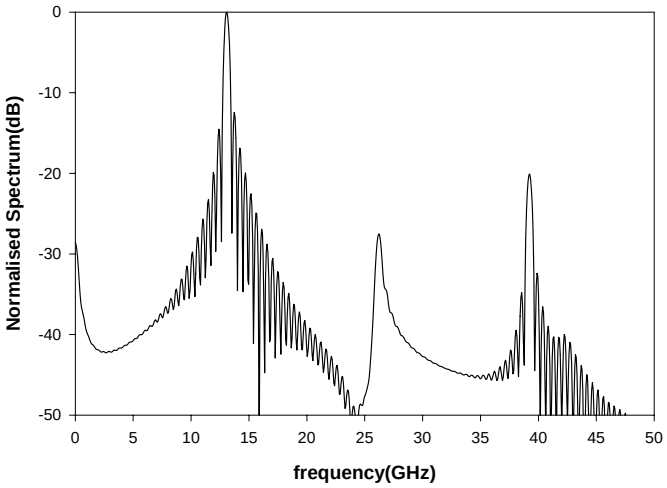

Figure 8.7 Spectrum of the voltage at the Gunn diode cell

Reasons for this discrepancy include radiation losses and inductances of the feed pin not modelled by HP-MDS. It has been also documented by Cryan(1997) that the HP-MDS simulator gives overestimated predictions of the experimental circuit oscillation by 5%.

It is interesting to see from TABLE 8-1 the manifestation of frequency pulling. This occurs because using different loads cause a change in the reflection coefficient (Maas 1988). This demonstrates the usefulness of the extended FDTD for simulating not only antennas but also conventional circuit oscillators.

8.4 Modelling of a compact Gunn Oscillator-antenna

The power combining arrays become more compact when the RF source is integrated with the antenna. In Figure 8.8 a module is shown where the Gunn diode is located on the patch. Such an arrangement avoids any interconnection losses and optimises substrate space and

subsequently minimises cost. This configuration is to be contrasted with the one analysed by Toland et al (1994) which involves a microstrip line Gunn oscillator, like the one studied in paragraph 8.3, feeding a microstrip antenna.

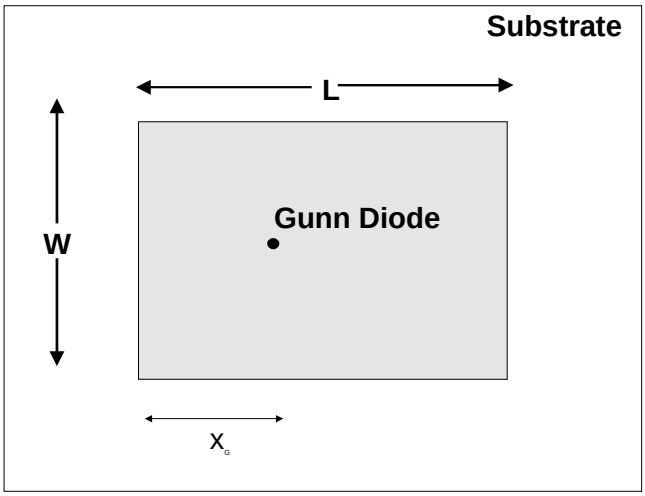

Figure 8.8 Microstrip antenna-Gunn oscillator module (top view)

The module of Figure 8.8 has been investigated only experimentally. It was first suggested by Thomas et al. (1984). The same structure was studied by Chang et al(1989) and York and Compton(1992) whose results are used for comparison . The antenna dimensions are 9.8×8.0 mm, ε_r=4.1, integrated with an X-band Gunn diode. For the Gunn diode the large signal equivalent circuit of Figure 8.1.b. is used.

The antenna acts as the load and as the resonator. Any attempt to model the structure must consider the fact that the antenna is a modal device. If the antenna is modelled as a load with one or two resonant circuits to represent one or two modes then many features cannot be addressed. These could include frequency hopping in oscillators (Chew and Itoh 1997) and out-of-band stability problems which may cause oscillation in amplifier designs.

The oscillation frequency was found close to 10GHz in agreement with experimental work by York and Compton(1992). See also the third harmonic present in the spectrum. The third harmonic is to be expected since the nonlinear characteristic (8-1) has first and third order terms.

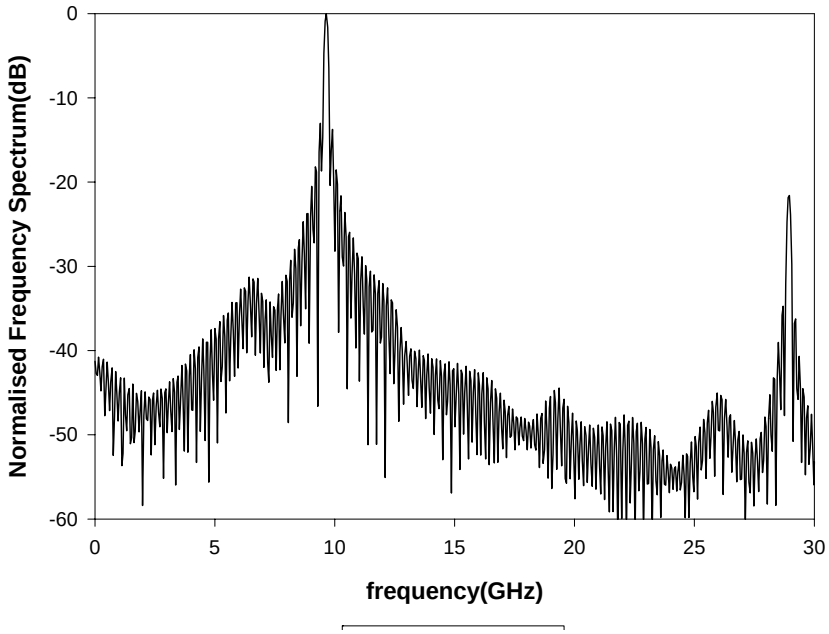

Figure 8.9 FFT of the Gunn voltage response revealing the spectrum of the single device oscillator-antenna

The radiation patterns were calculated at the fundamental for both planes (Figure 8.10,Figure 8.11). Observe the asymmetric copolar patterns. These can be explained by looking at the field distribution (Figure 8.12) where the asymmetry can be seen. Another striking feature is the high cross polarisation specially for the H-plane. For angles larger than 45^o and less than -45^o the crosspolarised radiation becomes more significant than the copolarised radiation and by 10dB. This is in agreement not only with York and Compton (1992) whose results are directly compared here but also with Thomas et al.(1984). The

high cross polarisation levels implies that a transverse mode is excited in addition to the fundamental mode. In general, the diode presents a field discontinuity and higher order modes are excited in order to accommodate its presence.

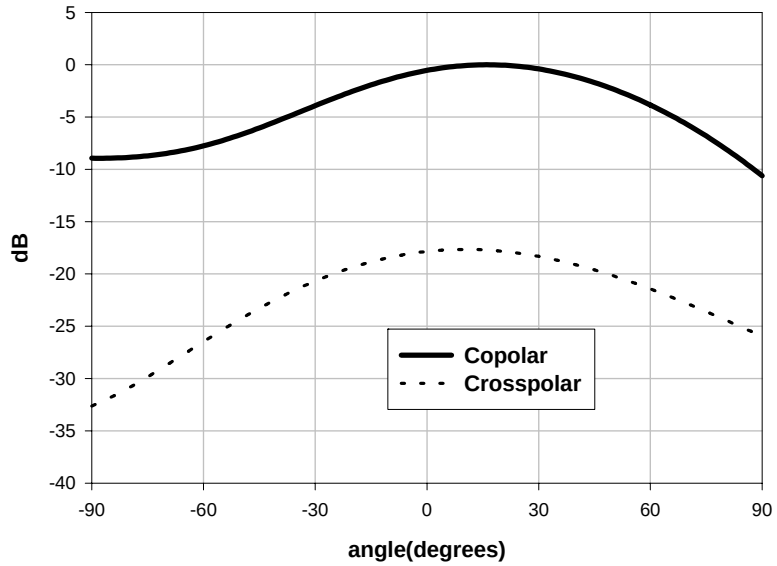

Figure 8.10 E- plane Radiation Pattern of a single device Gunn oscillator antenna

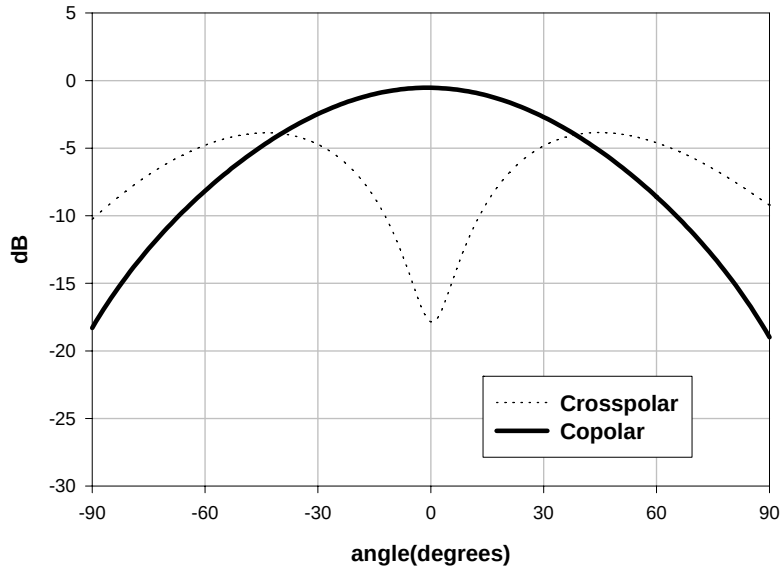

Figure 8.11 H- plane Radiation Pattern of a Gunn oscillator antenna

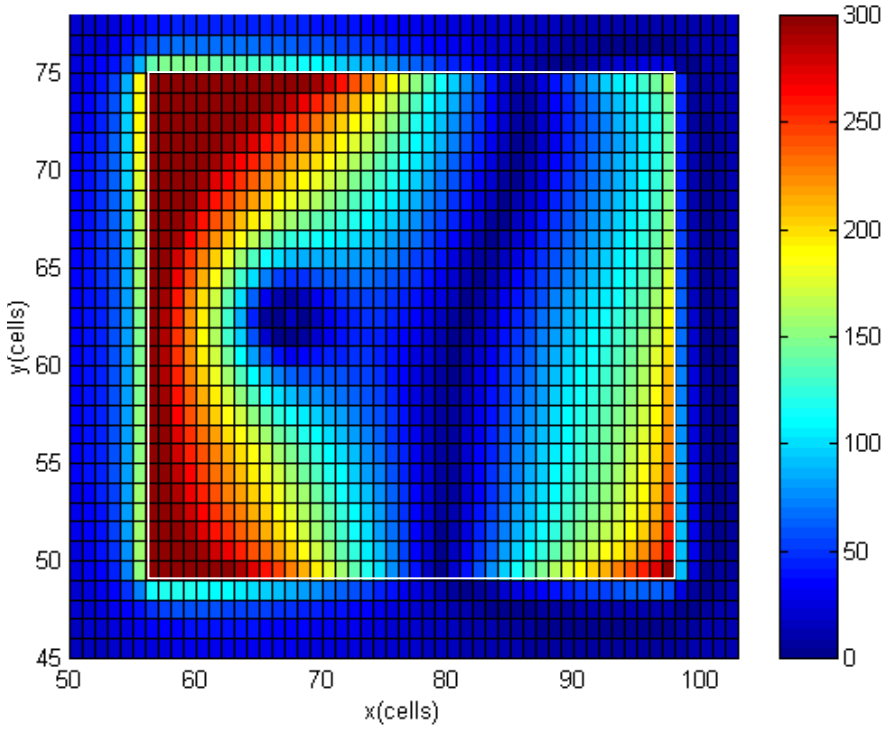

Figure 8.12 Electric field distribution at the fundamental frequency of the single device Gunn oscillator antenna

8.5 Modelling of a dual device compact Gunn Oscilllator-antenna

The very high cross polarisation of the single device Gunn has led to search of better topologies. The introduction of another device would in principle result in a more symmetrical configuration and therefore in a reduction of cross polarisation radiation levels. Wu and Chang (1995) have realised experimentally a dual FET self oscillating antenna. York and Compton(1992) have investigated experimentally a similar structure but implemented it with Gunn diodes (Figure 8.13). Another incentive of adopting such configuration is the increase in radiated power compared with the single device case.

Calculations were performed with two identical Gunn diodes located symmetrically. The frequency of oscillation is expected to change slightly because of the increase in capacitance due to the second Gunn diode. An interesting feature is the presence of a second harmonic

(Figure 8.14) not present in the spectrum of the single device (Figure 8.9). A possible explanation of this effect is that the one diode perturbs the operation of the other in such a degree that the I-V curve of the Gunn contains and second order terms. If a slight deviation δV in equilibrium from the I-V characteristic expression (8-1) due to the presence of the loss resistor is allowed then

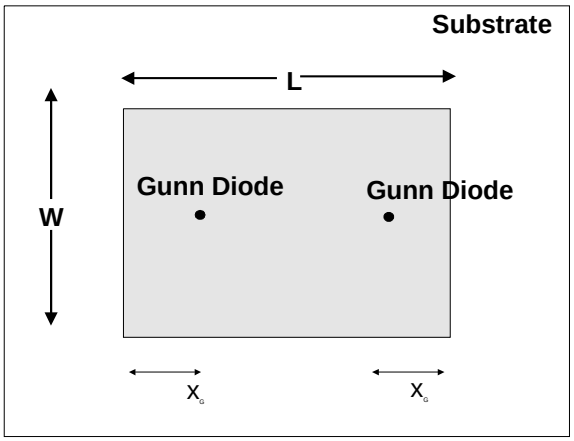

Figure 8.13 An integrated dual device Gunn Oscillator antenna

$$F(V_S + \delta V) = -G_1(V_S + \delta V) + G_2(V_S + \delta V)^3 \qquad (8\text{-}18)$$

Expanding (8-18) and neglecting terms containing δV^2, δV^3 then

$$F(V_S + \delta V) = -G_1(V_S + \delta V) + G_2 V_S^3 + 3G_2 V_S^2 \delta V \qquad (8\text{-}19)$$

Observe that in expression (8-19), there is now an additional square term which becomes more significant as the deviation δV becomes stronger. In the dual device module each diode distorts the other and the deviation δV gets significant unlike the single device module.

For the radiation patterns (Figure 8.16, Figure 8.17) observe that the main patterns are now more symmetrical which could be explained due to the more symmetrical fields produced .

For instance the electric field is shown in Figure 8.15. The striking feature is the significant reduction of the H-plane cross polar radiation, indicating that a balanced feed approach would be the solution for better power combining arrays. The cross polar at boresight is very close to -30 dB in agreement with York and Compton (1992).

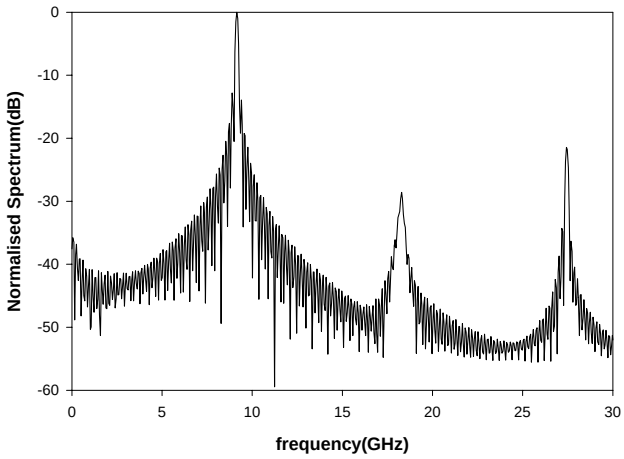

Figure 8.14 Spectrum for the dual device oscillator-antenna at the Gunn position

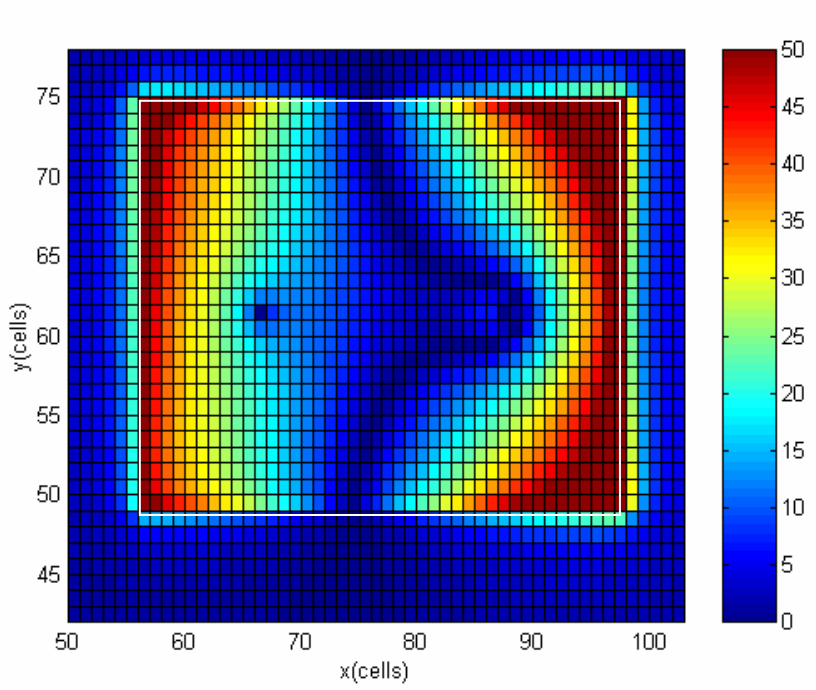

Figure 8.15 Electric field distribution for a dual device Gunn Oscillator-Antenna at the fundamental oscillating mode.

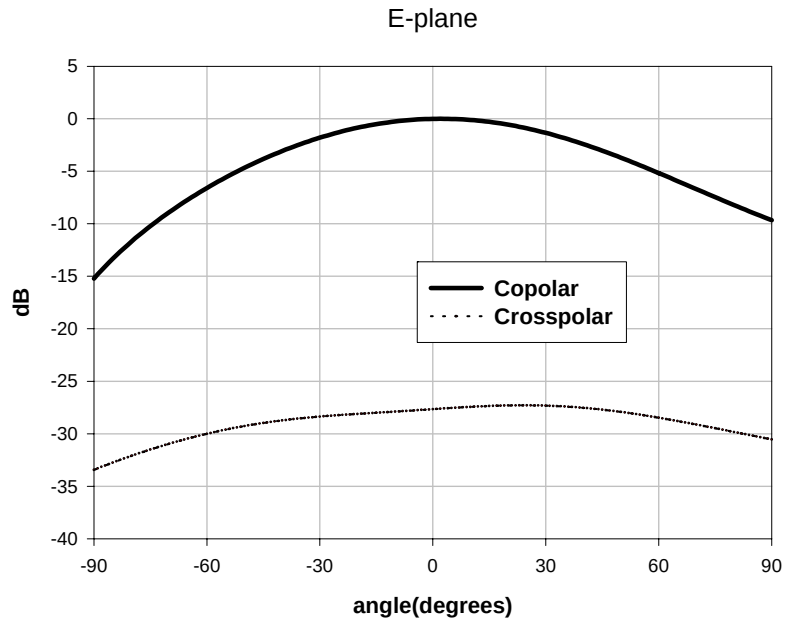

Figure 8.16 E- plane Radiation Pattern for a dual device Gunn oscillator microstrip antenna

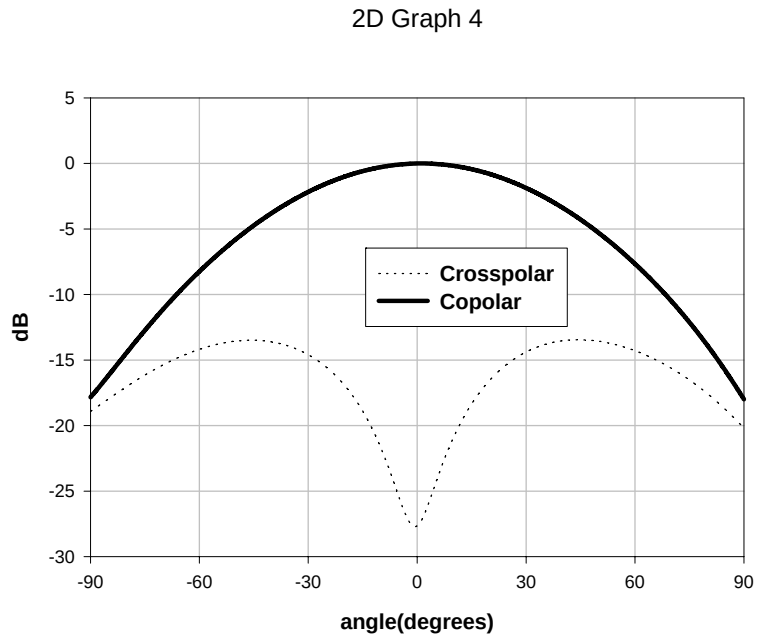

Figure 8.17 H -plane Radiation pattern for a dual device Gunn oscillator microstrip antenna

8.6 Summary

A Gunn diode model was incorporated in the code adapted from the literature presenting the full derivation. This was validated successfully by studying a microstrip line Gunn oscillator having very good agreement with the HP-MDS simulator. Compact Gunn oscillator antennas were studied with single and dual device configurations. Radiation patterns were calculated for the first time and compared favourably with published experimental results. The dual device module was proved to give reduced cross polar levels and improved radiation characteristics. However it was shown that more harmonics are generated.

CHAPTER 9
CONCLUSIONS AND FUTURE WORK

9.1 Conclusions

9.1.1 FDTD Method

The FDTD method has been gaining increasing popularity among the EM community. Its applicability has been investigated for the analysis of compact microstrip antenna-circuit modules. The main advantages from the use of the method are;

- can model arbitrary coupling
- arbitrary geometry modelling without changes in the algorithm
- can model dispersion in microstrips. For instance broadening of pulses when they propagate on microstrips.
- transient phenomena e.g. the onset of oscillations
- radiation patterns including finite size ground plane effects
- combination with circuit elements exceeding the capabilities of any other existing CAD and CAE tools
- broadband information utilising pulse excitation
- qualitative understanding of circuit operation with field plots.

Disadvantages include

- computer resources. This is a major problem of all the full wave methods.
- frequency resolution. All the frequency domain results result from Fourier transforming time domain results. This could be problematic in structures of very high Q

- considerable resources are applied to calculations in regions where the field has little or no importance e.g. the free space surrounding the structure.
- instabilities due to incorporation of nonlinear elements. Unfortunately there is no standard method to incorporate stable numerical expressions and these have to be addressed each time. Time oversampling was used in this work as a bypass to avoid the instabilities.

9.1.2 Compact Antenna-Circuit modules

Compact modules that can offer more functions are possible. The major problems for these are parasitic coupling and harmonics which are very important for electromagnetic compatibility requirements. At the present, conventional passive filtering is prohibited because of the size of the filter structures. FDTD with the extended capabilities of including circuit elements was applied successfully to representative antenna-circuit modules. Modules analysed in this work have integrated amplification, frequency tuning and oscillation functions.

Half and quarter wavelength microstrip antennas integrated with varactors have been investigated theoretically and experimentally in Chapter 7. Especially quarter wavelength antennas have been studied for the first time. An improved tuning range was observed and justified both experimentally and theoretically for the quarter wavelength modules. It has been shown that an accurate model of the device is necessary. The main adjustment that must be made is that the exponent γ is variable with bias. The varactors being nonlinear elements can be responsible for the radiation of harmonics. The radiation patterns were predicted with very good agreement with experiment . Power level harmonics have also shown that the use of antennas with no second harmonic resonance (when they are unloaded) is not a solution.

The integration of the antenna with a device creates a structure with potentially different modal behaviour than the antenna on its own. This was demonstrated more dramatically in the case of quarter wavelength modules emphasising the importance of concurrent modelling. The improved tuning range offers a way of operation with reduced level of harmonics. Its main repercussion is to enable such antennas to be used with a higher DC bias on the varactors thus operating at more linear regions of their C-V characteristics.

Compact oscillator-antennas based on Gunn diodes were also studied theoretically for the first time and compared favourably with published experimental results. Single and dual device oscillators were modelled . Using a large signal model of the Gunn diode, the radiation patterns were predicted. A comparative study between two topologies, one with a single device and another with a dual balanced arrangement was performed. The dual oscillator was seen to give reduced cross polarisation radiation but at the expense of increased second harmonic levels caused by the mutual interaction between the two nonlinear sources. The modelling of the oscillators will allow examining new modules in the design stage, reducing considerably the time for the production of prototypes.

The implementation of a novel transceiver using hybrid active circulators integrated with a small short-circuited antenna showed the effect of arbitrary coupling. Coupling mainly affected the isolation between transmit-receive and the radiation patterns. Useful design implications were derived by performing parametric calculations and trying to optimise antenna matching and length for maximum isolation.

In the process of validating the code, it was shown how FDTD can be used as a rigorous alternative for circuit simulation. In addition to that, the capability to model passive antennas was verified. The code written for this work was used to model and explain significant features and original results of a small MMIC antenna that was developed at the same time in the Communications Engineering Group (Singh et al. 1997).

9.2 Suggestions for future work

9.2.1 FDTD Methods

In principle an integrated CAD tool should be able to consider concurrently electromagnetics, circuit/device modelling and thermomechanical aspects. A first issue is how to integrate successfully all these diverse modelling methodologies. The interface between EM simulators with circuit modelling has been shown to be very promising by using the lumped element FDTD. It is envisaged that solid state based circuit simulators can be linked. Thermal modelling of devices and mechanical (e.g. moving parts, stress effects) is required so a fully global simulation can be performed. FDTD, owing to its time domain nature, is ideal to include the electromagnetics of moving parts.

The second issue in having an integrated tool is the speed and efficiency. This is necessary so realistic time scales are achievable in a commercial environment. Optimisation and synthesis requires fast solvers. Therefore one direction for future work should be directed to reduce the demand in time and computer resources. Computer time is going down as computer processors increase in speed and are available in ever decreasing prices. However, further improvements to the method could be made to make the method even faster. There are two

distinct areas of development ; firstly enhancement of FDTD methods and secondly hybrid methods involving combination of FDTD with other methods. For the former area of research, development of stable nonuniform and non orthogonal meshing techniques is required. Ideally FDTD methods must reach the maturity of finite element methods that produce conformal meshes. However these tend to reduce the accuracy of the code and require smooth transition of the cell size. Any meshing technique fixes the size of the cells for the duration of the simulation. Adaptive gridding is another idea that could be pursued by having a time dependent cell size. This could be beneficial for example in the modelling of moving parts. Alternative or modified time domain algorithms have been also recently been suggested with more prominent the application of wavelet techniques (Tentzeris et al 1998). A wavelet enhanced FDTD, coined MRTD(MultiResolution Time Domain), can provide results with the same accuracy as a conventional FDTD solution with double the resolution.

For the latter area of research, hybrid methods are based on the assertion that there is no universally optimum method for any problem. Thus a segmentation of a problem is required with a suitable method applied to each area. FDTD with the circuit extension appears to be the method of choice of antenna-circuit modules. A suitable interface is necessary. The computation of radiation as applied in FDTD methods, where a near field surface is defined as the interface with the near to far field integral transform, can be considered as an example of how other methods could be interfaced with FDTD. Diakoptiks and solution of each part with the optimum method (Righi et al. 1997) appear to be candidates for hybrid methods.

Of course also several CAD functions must provide good graphical user interface to make FDTD an easy to use tool. Also libraries of circuit elements will be indispensable in an R&D environment.

9.2.2 Integrated Antenna-Circuit modules

The hybrid active circulator studied in Chapter 6 could be implemented in MMIC technology. Other active circulators could also be investigated to be integrated with the antenna. Other small antennas like the small H shaped antenna could be considered as alternatives for integration.

The higher tuning range and thus operation at higher DC bias voltages make them attractive candidates for adaptive tuning systems. Further reduction in harmonics could be achieved by applying resistive mode damping. Energy conservation would not allow short-circuit pins to be effective dampers. Reduced harmonics could also be achieved with better (more linear) diodes or linearising topologies for diodes which could come as an integrated circuit. Also tunable antennas could form part of other modules with enhanced functionality, for instance in low phase noise tuneable oscillators (Underhill 1998)

Other Oscillator-antenna topologies using FET elements or diodes can be now analysed. The fundamental characteristic is the radiation pattern that needs to be taken into account. Strong cross polarisation may be needed to be reduced by using balanced configurations.

This work could be also expanded to investigate modulation effects on antenna-circuit modules. Kykkotis et al(1998) analysed oscillator arrays and injection locking using circuit-based techniques. Similar and even more compact configurations could be now be examined by using the FDTD tool developed here.

Another area that would be of interest for FDTD modelling is about millimeter wave circuits. Although these do not explicitly have an antenna, however the trend is to include full wave methods in CAD tools. Closely spaced active and passive devices, with many levels of transmission lines and discontinuities are amenable to full wave analysis. The high density can lead to crosstalk coming from parasitic coupling, surface waves and unwanted radiation. Since digital electronic systems use clocks and synchronisation is important, it is preferable to use a time domain simulator. Going higher in frequencies results in very small wavelengths and localised electromagnetic effects could be addressed in active devices structures.

The proximity of antennas with devices in compact configurations lead to considerations about the heat dissipation. This problem will be exacerbated when the device efficiency is decreased as it is the case for millimeter and submillimeter waves. Thermal effects can be included in equivalent circuits and therefore could be accounted for in an electromagnetic simulation. Time domain simulation also offers the possibility of monitoring the temperature rise in the circuit. Millimetric wave packaging considerations are quite significant in industry and could also be investigated using FDTD. Kuo et al (1997) have reported analysis of packaged microwave circuits using the FDTD method.

The reciprocity theorem cannot be applied to active antennas. Therefore it is interesting to examine the behaviour of these structure on the receive. Transponder structures which can be used in RFID tags could be dynamically modelled by utilising the work described in this thesis. In electromagnetic terms one antenna is a reflective systems and the other acts as a transmissive system. Similar situations are met in quasi-optical systems (York and Popovic 1997). Rectennas (antennas integrated with rectifying diodes) are used for microwave energy transmission/reception could be also modelled (Yoo and Chang 1992).

Modelling of a complete wireless front end and of a system on a chip which would include mixed signal components will be an important milestone. The FDTD method, with the extensions for circuits elements and, as shown in this work, its suitability for the prediction of radiation of tightly coupled modules, can serve as the backbone method for that formidable task.

APPENDIX A

LIST OF PUBLICATIONS

- **C.Kalialakis**, M.J.Cryan, P.S. Hall, P.Gardner ," FDTD Simulation of an Active Integrated Antenna", *Electronics Letters,* vol. 33, no.25, pp.2091-2092, 1997.

- **C.Kalialakis**, M.J.Cryan, P.S. Hall, P.Gardner, "Preliminary Results on the FDTD Analysis of Active Circulator Antennas", *Journal of Applied Electromagnetism*, vol.1, no.3, pp. 61-64,1998. (Based on a poster presentation in *NATO Advanced Study Institute on Applied Computational Electromagnetics: State of the Art and Future Trends*, Samos, Greece, 26 Jul-5 Aug 1997)

- **C.Kalialakis**, M.J.Cryan, P.S. Hall, and P.Gardner "Analysis of Integrated Active Circulator Antennas Using the Extended FDTD Method", *Proceedings of the URSI International Symposium on Electromagnetic Theory*, pp. 702-704, 25-28 May 1998, Thessaloniki, Greece.

- P.S .Hall, S.Kapoulas, R.Chauhan, **C.Kalialakis**, " Microstrip Antennas with Adaptive Integrated Tuning", *International Conference on Antennas and Propagation ICAP-97*, vol. 1, pp.501-504.

- P.S.Hall, P.Gardner, M.J.Cryan, D.Singh, **C.Kalialakis** (1997), "Novel Developments in Active Integrated antennas for microwave and millimeter wave applications", *(Invited Paper), Microwaves and RF 97 Conference Proceedings*, pp. 76-82, Oct. 1997, London, UK.

- **C.Kalialakis**, M.J.Cryan, P.S. Hall, P.Gardner, " FDTD analysis of microstrip circuits incorporating gain blocks", *IEE Colloquium on RF and Microwave Components for Communication Systems,* Digest 126/1997, pp.7.1-7.5, Bradford, 23 April 1997.

- P.S .Hall, S.Kapoulas, R.Chauhan, **C.Kalialakis**, "Adaptive Tuning of Microstrip Antennas", *IEE Colloquium on Optimal Mobile Handset Antenna Design in the Presence of Biological Tissue, Digest* , Digest 022/1997, pp.3.1-3.3, London 20th January 1997.

- **C.Kalialakis**, P.Gardner, P.S. Hall, "FDTD Analysis of Antenna-Circuit Modules", *22nd QMW Antenna Symposium Digest*, London,UK , April 1998.

Also the following papers have been submitted for publication

- D.Singh, **C. Kalialakis**, P. Gardner, and P. S. Hall, "Small H-Shaped Antennas for MMIC Applications", submitted to *IEEE Transactions on Antennas and Propagation*

- **C.Kalialakis**, M.J.Cryan, P.S. Hall, P.Gardner, " Analysis and Design of Integrated Active Circulator Antennas" , submitted to *IEEE Transactions on Microwave Theory and Techniques*

- **C.Kalialakis**, P.S. Hall, P.Gardner, " Investigations on the Performance of Varactor Loaded Microstrip Antennas" , to be submitted to *IEEE Transactions on Antennas and Propagation*

- **C.Kalialakis**, P.S. Hall, P.Gardner, " Harmonic Performance of Single and Dual Device Gunn-Oscillator Microstrip Antennas using the LE/FDTD Method" to be submitted to *Microwave and Optical Technology Letters*.

APPENDIX B

THE FDTD SOFTWARE

B.1 The structure

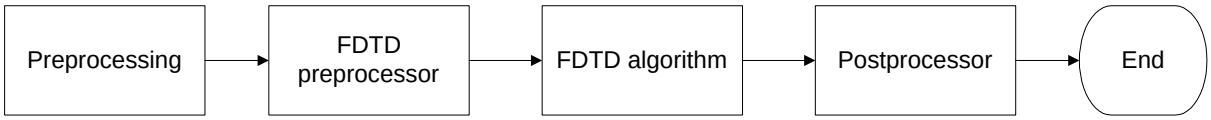

Figure B.1 The flowchart showing the overall structure of the FDTD software tool

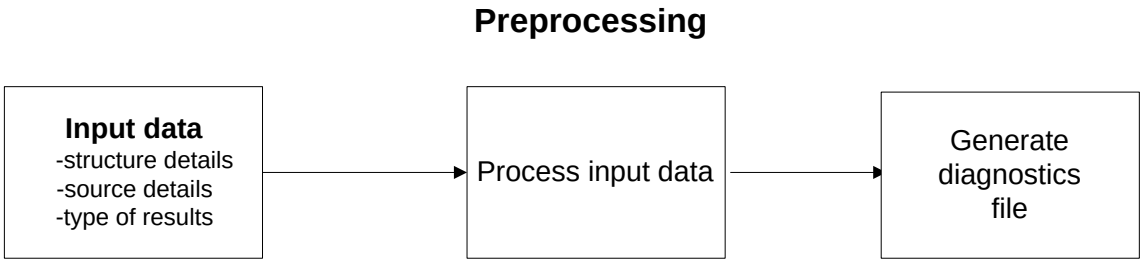

Figure B.2 Flowchart showing the preprocessing procedures

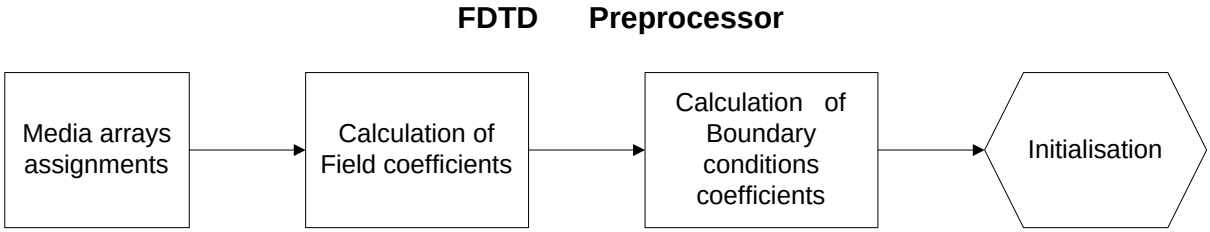

Figure B.3 Flowchart showing the FDTD preprocessor structure.

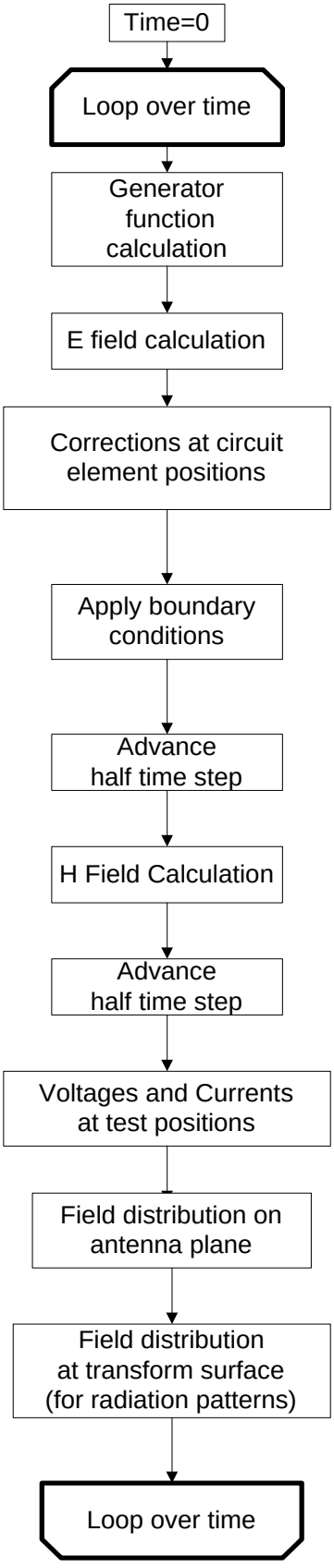

Figure B-4 Flowchart showing the FDTD algorithm structure**.**

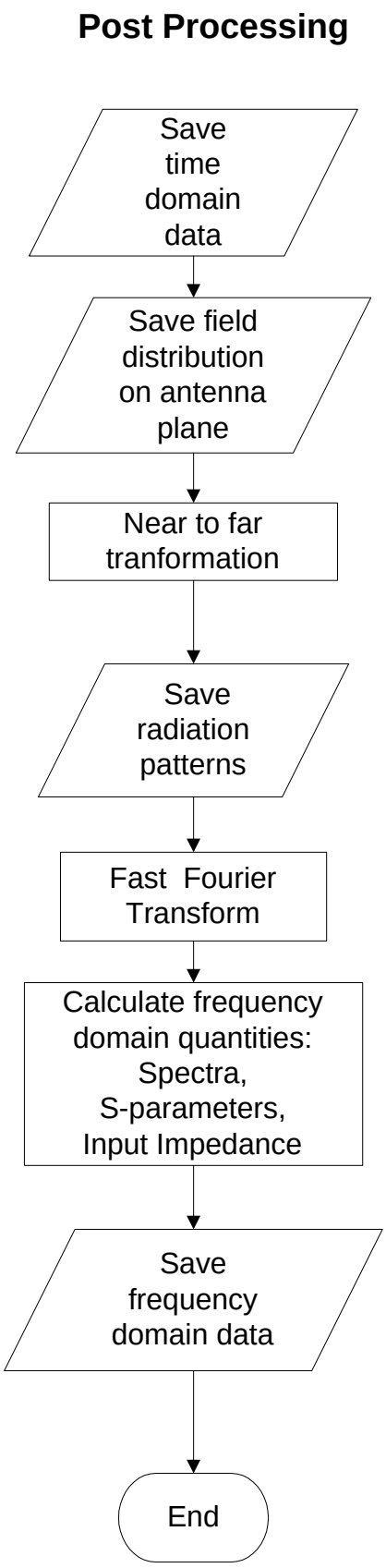

Figure B.4 Flowchart showing the postprocessor structure

B.2 COMPUTER RESOURCES REQUIREMENT FOR FDTD SOFTWARE

An estimation of the FDTD resource requirements is necessary in order to provide an estimation of the order of the problem that can be simulated on a given machine. Kunz and Luebbers(1993) have provided a rough guideline of the resources needed for the FDTD algorithm.

$$FDTD\ Memory = N\ cells \times (6\ components \times 4\ bytes + 3\ media\ arrays \times 1\ byte) =$$

$$= 27N\ bytes \qquad \text{(B-1)}$$

The required CPU time required can be found by calculating the Floating Point Operations needed for the algorithm.

$$Operations = N\ cells \times (6\ field\ components \times 10\ operations) \times T \qquad \text{(B-2)}$$

The number of time steps is on the order of ten times the number of cells on one side of the problem space.

$$T = 10 \times N^{1/3} \qquad \text{(B-3)}$$

Therefore the number of operations for the FDTD algorithm is

$$FDTD\ Operations = 600 \times N^{4/3} \qquad \text{(B-4)}$$

For a size of $N=10^6$ cells, then memory of roughly 27 MB of memory is needed a size that is quite easily attainable in modern computing suites. The operations required amount to 60 Gflop. Let us estimate the processor time needed for some average computing platforms that can be found easily in academic and company environments. A figure that is widely used to indicate the processing power is usually Mflops i.e Millions flop per second. A typical estimation for a 50 MHz workstation (Sun SPARCStation 10) is around 20Mflops which

would lead to a 50 min CPU time. A PC Pentium (100MHz) has about 10 Mflops processing power that would result to 100 mins.

However in realistic problems, boundary conditions are required and impose additional load on computer resources. The boundary conditions are applied on the six faces of the computational region. In the case of Mur conditions the following estimates are provided

$$Memory = N^{2/3}\ cells \times 6\ faces \times 4 \text{ cells depth} \times (4\ components \times 4\ bytes) =$$

$$= 384 \times N^{2/3}\ Bytes \qquad \text{(B-5)}$$

The operations can be calculated according to the following estimation:

$$Operations = N^{2/3}\ cells \times 6\ faces \times 4\ field\ components \times 10\ operations) \times T \qquad \text{(B-6)}$$

Taking into account the time step estimation (B-3), the required operations are given by:

$$Mur\ Operations = 2400N \qquad \text{(B-7)}$$

For a problem of $N=10^6$ cells size, the memory required is 3.7 MB. The operations needed amount to 2.4 Gflop. In a typical 50 MHz workstation (Sun SPARCStation 10) is around 20Mflops which would lead to an additional 2min time. A PC Pentium (100MHz) has about 10 Mflops processing power that would result to 4 mins.

APPENDIX C

FINITE DIFFERENCE EXPESSIONS OF MUR BOUNDARY CONDITIONS

C.1 Derivation of fist order conditions

The finite difference expressions for the boundary conditions of the E_z component will be derived. The one way wave equation at x=0, under approximation (4-27) yields

$$\frac{\partial E_z}{\partial x} = \frac{1}{c}\frac{\partial E_z}{\partial t} \Rightarrow \frac{\Delta E_z}{\Delta x} = \frac{1}{c}\frac{\Delta E_z}{\Delta t} \qquad \text{(C-1)}$$

Time derivatives will be calculated at time step $n+\frac{1}{2}$. This implies that the spatial derivative will be also be calculated at the same time step. However, in the FDTD algorithm as we have discussed in chapter 3, electric field is calculated at time step *n*. A temporal average is therefore required:

$$\frac{\Delta E_z^{\,n+\frac{1}{2}}}{\Delta x} = \frac{1}{2}\left(\frac{\Delta E_z^{\,n+1}}{\Delta x} + \frac{\Delta E_z^{\,n+1}}{\Delta x}\right) \qquad \text{(C-2)}$$

Spatial derivative is calculated around x=0.5, implying that the temporal derivative is calculated at the same point. Therefore spatial average is required for the time derivative

$$\frac{\Delta E_z}{\Delta t} = \left[\frac{\Delta E_z(1,j,k)}{\Delta t} + \frac{\Delta E_z(0,j,k)}{\Delta t}\right] \qquad \text{(C-3)}$$

Taking into account (C-2) and (C-3), the left hand side of (C-1) reads

$$LHS = \frac{E_z^n(1,j,k+0.5)}{2\cdot\Delta x} - \frac{E_z^n(0,j,k+0.5)}{2\cdot\Delta x} + \frac{E_z^{n+1}(1,j,k+0.5)}{2\cdot\Delta x} - \frac{E_z^{n+1}(0,j,k+0.5)}{2\cdot\Delta x}$$

(C-4)

and the right hand side of (C-1) reads

$$RHS = \frac{E_z^{n+1}(1,j,k+0.5) - E_z^n(1,j,k+0.5)}{2\cdot c\cdot\Delta t} - \frac{E_z^{n+1}(0,j,k+0.5) - E_z^n(0,j,k+0.5)}{2\cdot c\cdot\Delta t}$$

(C-5)

After equating (C-4) and (C-5), multiplication with $c\cdot\Delta t\cdot\Delta x$ and solving for $E_z^{n+1}(0,j,k+0.5)$ yields,

$$E_z^{n+1}(0,j,k+0.5) = E_z^n(0,j,k+0.5) + \frac{c\cdot\Delta t - \Delta x}{c\cdot\Delta t + \Delta x}\left[E_z^{n+1}(1,j,k+0.5) - E_z^n(1,j,k+0.5)\right]$$

(C-6)

C.2 Derivation of second order conditions

The one way wave equation for a second order approximation, using (4-29) and multiplying by D_t/c to avoid operators in the denominators, reads

$$\frac{1}{c}\frac{\partial^2 E_z}{\partial x\partial t} - \frac{1}{c^2}\frac{\partial^2 E_z}{\partial t^2} + \frac{1}{2}\left(\frac{\partial^2 E_z}{\partial z^2} + \frac{\partial^2 E_z}{\partial y^2}\right) = 0 \qquad \text{(C-7)}$$

The objective is to solve for $E_z^{n+1}(0,j,k+0.5)$. The derivatives that produce these terms are the ones that involve time and partial derivatives with respect to x variable.

Approximating derivatives

$$\frac{\partial^2 E_z}{\partial x \partial t} = \frac{1}{2 \cdot \Delta t}\left(\frac{\Delta E_z^{n+1}}{\Delta x} - \frac{\Delta E_z^{n-1}}{\Delta x} \right) \tag{C-8}$$

with

$$\frac{\Delta E_z^{n+1}}{\Delta x} = \frac{1}{2 \cdot \Delta t \cdot \Delta x}\left[E_z^{n+1}(1,j,k) - E_z^{n+1}(0,j,k) \right] \tag{C-9}$$

and

$$\frac{\Delta E_z^{n-1}}{\Delta x} = \frac{1}{2 \cdot \Delta t \cdot \Delta x}\left[E_z^{n-1}(1,j,k) - E_z^{n-1}(0,j,k) \right] \tag{C-10}$$

The second time derivative is spatially averaged

$$\frac{\partial^2 E_z}{\partial t^2} = \frac{1}{2}\left[\frac{\Delta}{\Delta t}\left(\frac{\Delta E_z(1,j,k)}{\Delta t} \right) + \frac{\Delta}{\Delta t}\left(\frac{\Delta E_z(0,j,k)}{\Delta t} \right) \right] \tag{C-11}$$

with

$$\frac{\Delta}{\Delta t}\left(\frac{\Delta E_z(1,j,k)}{\Delta t} \right) = \frac{1}{\Delta t^2}\left[E_z^{n+1}(1,j,k) - 2 \cdot E_z^{n}(1,j,k) + E_z^{n-1}(1,j,k) \right] \tag{C-12}$$

and

$$\frac{\Delta}{\Delta t}\left(\frac{\Delta E_z(0,j,k)}{\Delta t} \right) = \frac{1}{\Delta t^2}\left[E_z^{n+1}(0,j,k) - 2 \cdot E_z^{n}(0,j,k) + E_z^{n-1}(0,j,k) \right] \tag{C-13}$$

Substitute (C-8) and (C-9) into (C-7) taking into account (C-9), (C-10) and (C-12), (C-13).

Multiplication by $2c^2 \cdot \Delta t^2 \cdot \Delta x$ and solving for $E_z^{n+1}(0,j,k+0.5)$ yields

$$E_z^{n+1}(0,j,k+0.5) = -E_z^{n-1}(1,j,k+0.5) + \frac{c \cdot \Delta t - \Delta x}{c \cdot \Delta t + \Delta x}\left[E_z^{n+1}(1,j,k+0.5) + E_z^{n-1}(1,j,k+0.5) \right]$$
$$\frac{2 \cdot \Delta x}{c \cdot \Delta t + \Delta x}\left[E_z^{n}(1,j,k+0.5) + E_z^{n}(0,j,k+0.5) \right] + \frac{c^2 \Delta t^2 \Delta x}{c \cdot \Delta t + \Delta x}\left(\frac{\partial^2 E}{\partial y^2} + \frac{\partial^2 E}{\partial y^2} \right) \tag{C-14}$$

where

$$\frac{\partial^2 E}{\partial y^2} = \frac{1}{2}\left[\begin{array}{l} E_z^{n}(,j,k+0.5) - 2E_z^{n}(,j,k+0.5) + E_z^{n}(1,j,k+0.5) + \\ E_z^{n}(,j,k+0.5) - 2E_z^{n}(,j,k+0.5) + E_z^{n}(1,j,k+0.5) \end{array} \right] \tag{C-15}$$

$$\frac{\partial^2 E_z}{\partial z^2} = \frac{1}{2}\left[\begin{array}{l} E_z^n(,j,k+0.5) - 2E_z^n(,j,k+0.5) + E_z^n(1,j,k+0.5) + \\ E_z^n(,j,k+0.5) - 2E_z^n(,j,k+0.5) + E_z^n(1,j,k+0.5) \end{array}\right] \quad \text{(C-16)}$$

Same procedure can be applied for the other boundaries. The corresponding one way wave equations are for the $x=N_x$ boundary

$$\frac{1}{c^2}\frac{\partial^2 E}{\partial x \partial t} + \frac{1}{c^2}\frac{\partial^2 E_z}{\partial t^2} - \frac{1}{2}\left(\frac{\partial^2 E_z}{\partial z^2} + \frac{\partial^2 E_z}{\partial y^2}\right) = 0 \quad \text{(C-17)}$$

for the boundary y=0,

$$\frac{1}{c^2}\frac{\partial^2 E_z}{\partial y \partial t} - \frac{1}{c^2}\frac{\partial^2 E_z}{\partial t^2} + \frac{1}{2}\left(\frac{\partial^2 E_z}{\partial z^2} + \frac{\partial^2 E_z}{\partial x^2}\right) = 0 \quad \text{(C-18)}$$

for the boundary $y=N_y$,

$$\frac{1}{c^2}\frac{\partial^2 E_z}{\partial y \partial t} + \frac{1}{c^2}\frac{\partial^2 E_z}{\partial t^2} - \frac{1}{2}\left(\frac{\partial^2 E_z}{\partial z^2} + \frac{\partial^2 E_z}{\partial x^2}\right) = 0 \quad \text{(C-19)}$$

for the boundary z=0,

$$\frac{1}{c^2}\frac{\partial^2 E_z}{\partial z \partial t} - \frac{1}{c^2}\frac{\partial^2 E_z}{\partial t^2} + \frac{1}{2}\left(\frac{\partial^2 E_z}{\partial x^2} + \frac{\partial^2 E_z}{\partial y^2}\right) = 0 \quad \text{(C-20)}$$

for boundary $z=N_z$,

$$\frac{1}{c^2}\frac{\partial^2 E_{x,y}}{\partial z \partial t} + \frac{1}{c^2}\frac{\partial^2 E_{x,y}}{\partial t^2} - \frac{1}{2}\left(\frac{\partial^2 E_z}{\partial x^2} + \frac{\partial^2 E_z}{\partial y^2}\right) = 0 \quad \text{(C-21)}$$

APPENDIX D

NEAR TO FAR FIELD TRANSFORMATION IN FREQUENCY DOMAIN

D.1 Derivation

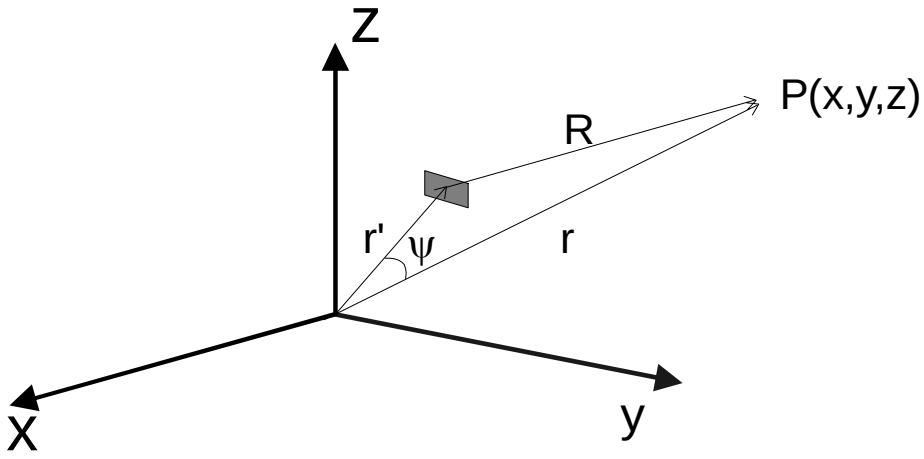

Figure D.1 For the derivation of the near to far field transform.

Consider a source with given electric and magnetic current densities $\bar{J}_S(r')$, $\bar{M}_S(r')$ respectively . Then the resultant magnetic vector potential is

$$\bar{A}(\bar{r}) = \frac{\mu}{4\pi}\int_S \bar{J}_S(r')\frac{e^{-jkR}}{R}ds' \qquad \textbf{(D-1)}$$

and its dual quantity, the electric vector potential,

$$\bar{F} = \frac{\varepsilon}{4\pi}\int_S \bar{M}_S(r')\frac{e^{-jkR}}{R}ds' \qquad \textbf{(D-2)}$$

where $k = \frac{2\pi}{\lambda}$ is the wavenumber, R,r,r' distances defined in Figure D.1.

When the two potentials $\overline{F}$ and $\overline{A}$ are known then the electric and magnetic fields can be calculated (Balanis 1989) as

$$\overline{E} = \overline{E}_A + \overline{E}_F \qquad \text{(D-3)}$$

$$\overline{H} = \overline{H}_A + \overline{H}_F \qquad \text{(D-4)}$$

where

$$\overline{E}_A = -j\omega\overline{A} - \frac{j\omega}{k^2}\nabla\cdot(\nabla\cdot\overline{A}) \quad \text{(D-5)}$$

$$\overline{H}_F = -j\omega\overline{F} - \frac{j\omega}{k^2}\nabla\cdot(\nabla\cdot\overline{F}) \quad \text{(D-6)}$$

In far field the gradient contribution of the potentials vanishes leading to

$$E_A \cong -j\omega A \quad \text{(D-7)} \qquad H_F \cong -j\omega F \quad \text{(D-8)}$$

In spherical coordinates (r,θ,φ) (D-7) and (D-8) can be separated into components

$$(E_A)_\theta \cong -j\omega A_\vartheta \,\text{(D-9)} \qquad (H_F)_\theta \cong -j\omega F_\theta \,\text{(D-10)}$$

$$(E_A)_\varphi \cong -j\omega A_\phi \,\text{(D-11)} \qquad (H_F)_\phi \cong -j\omega F_\phi \quad \text{(D-12)}$$

where the r component has been suppressed. In the far field E_F and H_F are expected to be orthogonal (plane waves). That means they are related with free space impedance Z_o (something that is always valid only for TEM waves). Taking into account (D-9) to (D-12) and put into (D-3) we get

$$E_\theta = (E_A)_\theta + Z_o(H_F)_\phi = -j\omega A_\theta - j\omega Z_o F_\phi \qquad \text{(D-13)}$$

$$E_\phi = (E_A)_\phi + Z_o(H_F)_\theta - j\omega A_{\phi\theta} - j\omega Z_o F_\vartheta \qquad \text{(D-14)}$$

The next step is to find the expressions for far field potentials. The distance R can be found by applying the cosine law for the triangle OSP(Figure D.1)

$$R = \sqrt{r^2 + (r')^2 - 2rr'\cos\psi} \qquad \text{(D-15)}$$

In far field it is r>>r'. Then distance R can be approximated as

$$R \cong \sqrt{r^2 - 2rr'\cos\psi} = r\sqrt{1 - 2\frac{r'}{r}\cos\psi} \qquad \text{(D-16)}$$

First order binomial approximation $(1-x)^n \cong 1-nx$ is used for phase variations,

$$R \cong r(1 - 2\frac{1}{2}\frac{r'}{r}\cos\psi) = r - r'\cos\psi \qquad \text{(D-17)}$$

but for amplitude variations $R \cong r$. Taking these approximations into account the potential can be expressed as

$$\overline{A} = \frac{\mu}{4\pi}\int_S \overline{J}_S(r')\frac{e^{-jk(r-r'\cos\psi)}}{r}ds' \qquad \text{(D-18)}$$

and having constant terms out of the integral reads

$$\overline{A} = \frac{\mu}{4\pi}\frac{e^{-jkr}}{r}\int_S \overline{J}_S(r')\frac{e^{jkr'\cos\psi}}{r}ds' \qquad \text{(D-19)}$$

Similarly :

$$\overline{F} = \frac{\varepsilon}{4\pi}\frac{e^{-jkr}}{r}\int_S \overline{M}_S(r')\frac{e^{jkr'\cos\psi}}{r}ds' \qquad \text{(D-20)}$$

We define the integral quantities in (D-19) and (D-20) radiation vectors (Balanis 1989, Ramo et al. 1993)

$$\bar{N} = \int_S \bar{J}_S(r') \frac{e^{jkr'\cos\psi}}{r} ds' \qquad \text{(D-21)}$$

$$\bar{L} = \int_S \bar{M}_S(r') \frac{e^{jkr'\cos\psi}}{r} ds' \qquad \text{(D-22)}$$

Then using the radiation vectors components (D-13) and (D-14) are transformed to

$$E_\theta = -j \frac{e^{-jkr}}{r} (kZ_o N_\vartheta + L_\phi) \quad \text{(D-23)}$$

$$E_\phi = -j \frac{e^{-jkr}}{4\pi r r} (Z_o N_\phi - L_\theta) \quad \text{(D-24)}$$

What is now required is to find the expressions for the components of the radiation vectors in terms of the cartesian components of the electric and magnetic current densities which are the only known quantities.

In matrix form the electric current density can be expressed as:

$$\bar{J} = \begin{bmatrix} J_x & J_y & J_z \end{bmatrix} \begin{bmatrix} \hat{x} \\ \hat{y} \\ \hat{z} \end{bmatrix} = \begin{bmatrix} J_r & J_\vartheta & J_\phi \end{bmatrix} \begin{bmatrix} \hat{r} \\ \hat{\theta} \\ \hat{\phi} \end{bmatrix} \qquad \text{(D-25)}$$

The cartesian and spherical coordinate systems are related by a rotation matrix

$$\begin{bmatrix} \hat{x} \\ \hat{y} \\ \hat{z} \end{bmatrix} = \begin{bmatrix} \sin\theta\cos\phi & \cos\theta\cos\phi & -\sin\phi \\ \sin\theta\sin\phi & \sin\theta\cos\phi & \cos\phi \\ \cos\theta & -\sin\theta & 0 \end{bmatrix} \begin{bmatrix} \hat{r} \\ \hat{\theta} \\ \hat{\phi} \end{bmatrix} \qquad \text{(D-26)}$$

Using (D-26) in the (D-25) yields

$$\begin{bmatrix} J_r & J_\theta & J_\phi \end{bmatrix} = \begin{bmatrix} J_x & J_y & J_z \end{bmatrix} \begin{bmatrix} \sin\theta\cos\phi & \cos\theta\cos\phi & -\sin\phi \\ \sin\theta\sin\phi & \sin\theta\cos\phi & \cos\phi \\ \cos\theta & -\sin\theta & 0 \end{bmatrix} \qquad \text{(D-27)}$$

or

$$J_r = J_x \sin\vartheta\cos\varphi r + J_y \sin\vartheta\cos\varphi - J_z \sin\phi \quad \text{(D-28)}$$

$$J_\theta = J_x \sin\vartheta\cos\varphi r + J_y \sin\vartheta\cos\varphi - J_z \sin\phi \quad \text{(D-29)}$$

$$J_\phi = J_x \hat{r} \sin\vartheta + J_z \sin\varphi \quad \text{(D-30)}$$

Therefore radiation vector N components can be expressed as

$$N_\theta = \int_S J_\theta(r')\frac{e^{jkr'\cos\psi}}{r}ds' = \int_S (J_x \cos\theta\cos\phi + J_y \sin\phi\cos\theta - J_z \sin\theta)\frac{e^{jkr'\cos\psi}}{r}ds' \quad \text{(D-31)}$$

$$N_\phi = \int_S J_\theta(r')\frac{e^{jkr'\cos\psi}}{r}ds' = \int_S (-J_x \sin\phi + J_y \sin\phi)\frac{e^{jkr'\cos\psi}}{r}ds' \quad \text{(D-32)}$$

Its dual quantity L comes from changing J to M

$$L_\theta = \int_S M_\theta(r')\frac{e^{jkr'\cos\psi}}{r}ds' = \int_S (M_x \cos\theta\cos\phi + M_y \sin\phi\cos\theta - M_z \sin\theta)\frac{e^{jkr'\cos\psi}}{r}ds' \quad \text{(D-33)}$$

$$L_\phi = \int_S M_\theta(r')\frac{e^{jkr'\cos\psi}}{r}ds' = \int_S (-M_x \sin\phi + M_y \sin\phi)\frac{e^{jkr'\cos\psi}}{r}ds' \quad \text{(D-34)}$$

APPENDIX E

HP-MDS DESIGNS

E.1 Loaded Microstrip Line

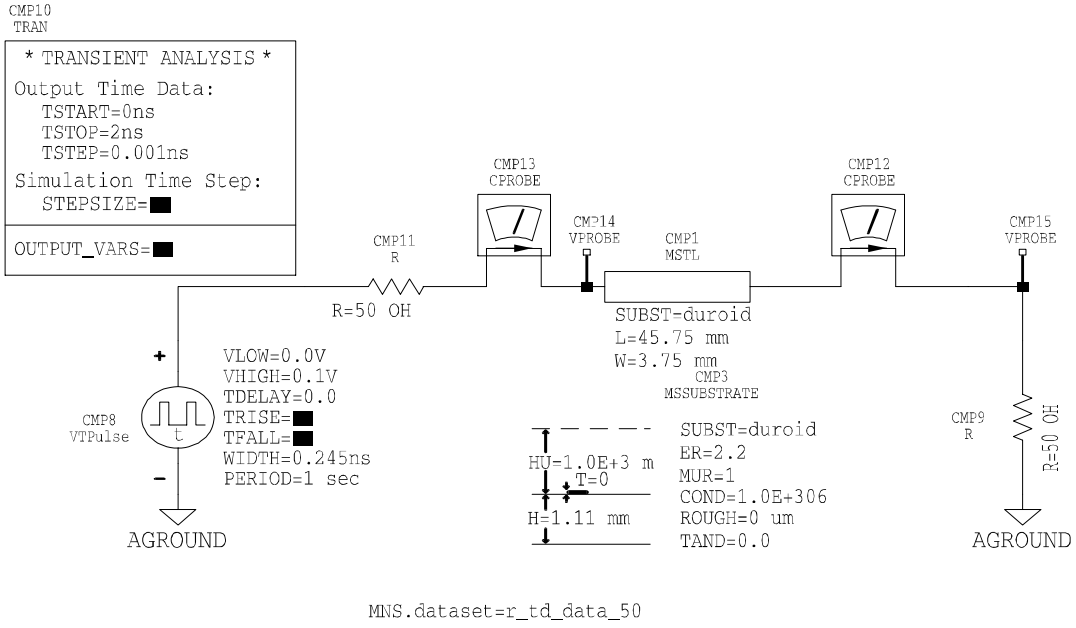

Figure E.1 Schematic for a resistor terminating a microstrip line-Time domain

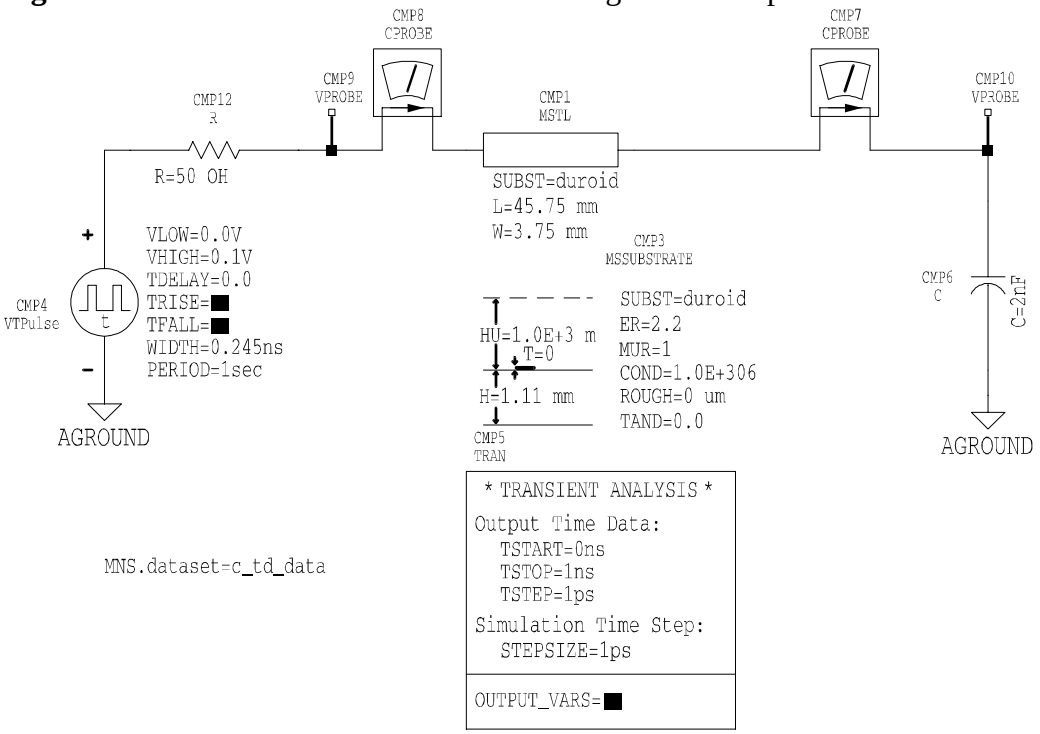

Figure E.2 Schematic for a capacitor terminating a microstrip line

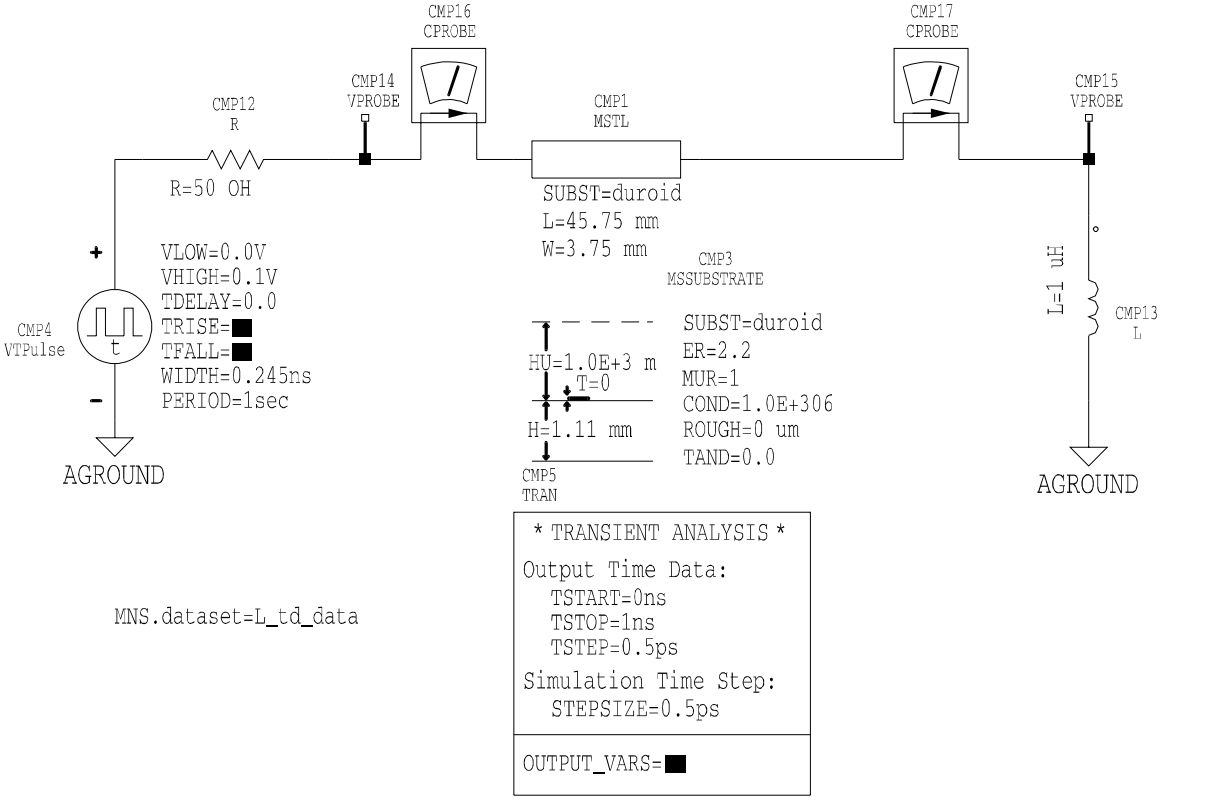

Figure E.3 Schematic for an inductor terminating a microstrip line

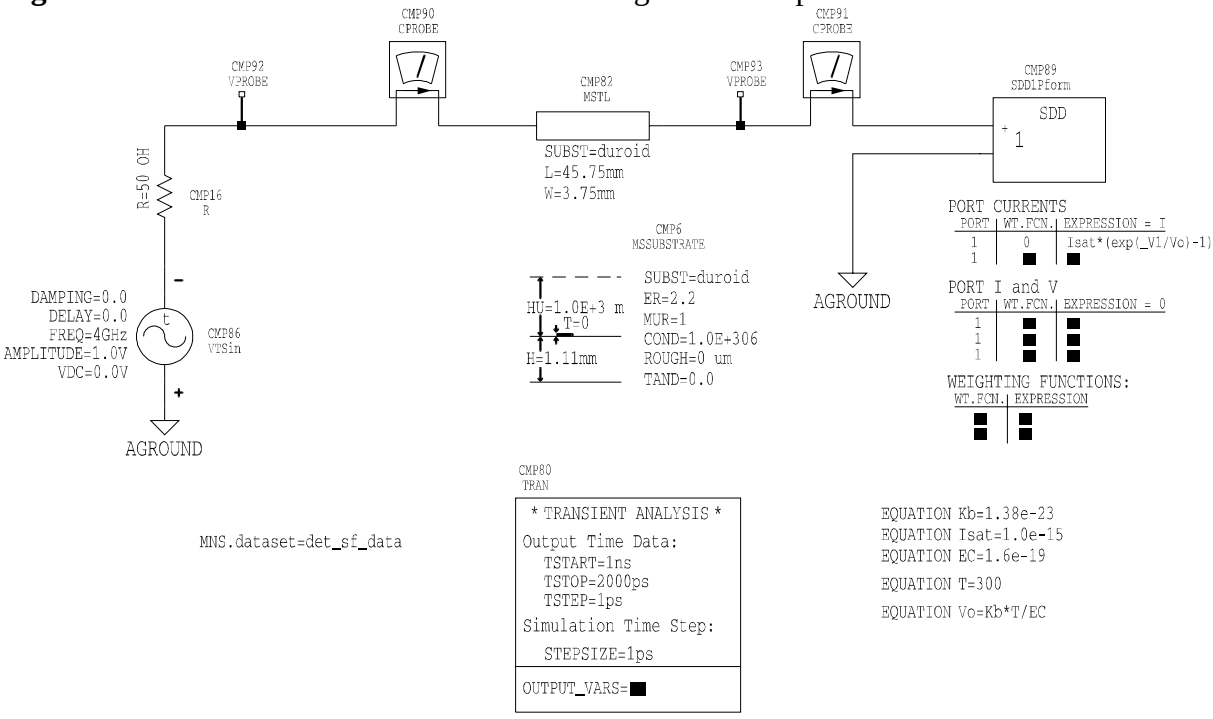

Figure E.4 Schematic for a diode terminating a microstrip line. The diode is incorporated in MDS by an one port Symbolic Defined Device.

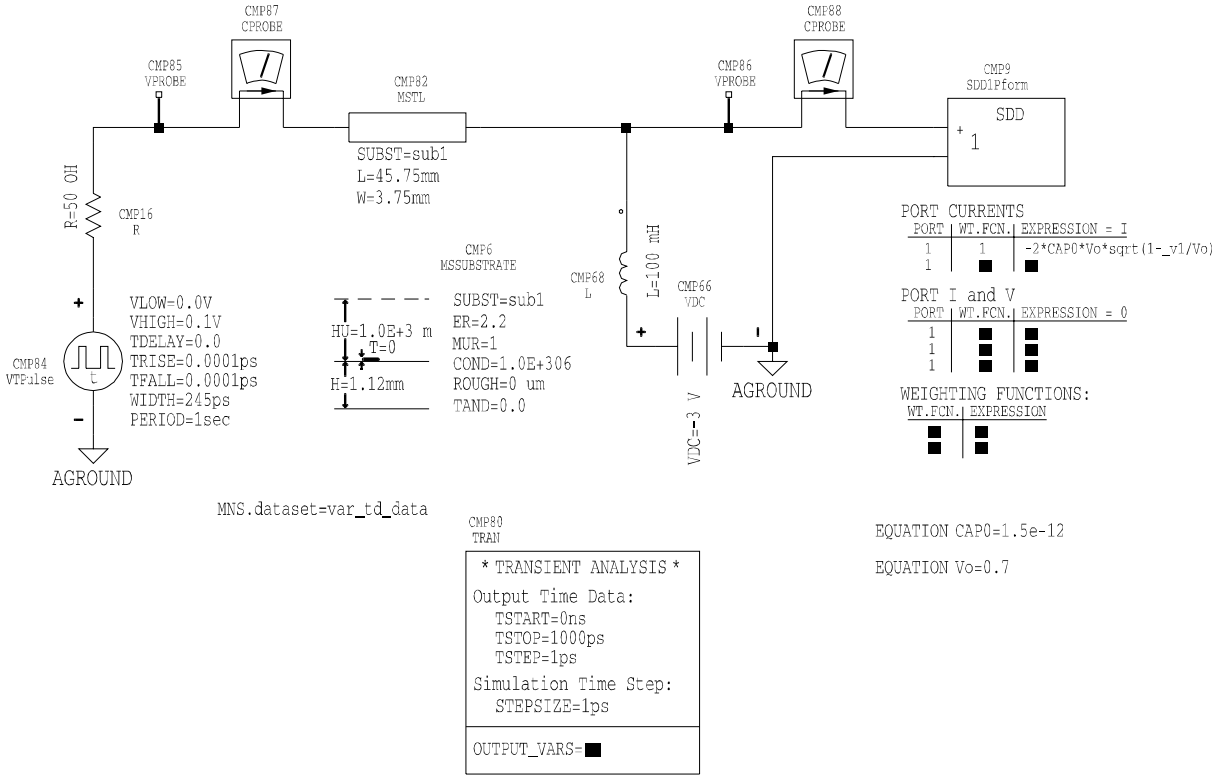

Figure E.5 Schematic for a varactor terminating a microstrip line. The diode is incorporated in MDS by an one port Symbolic Defined Device.

E.2 Gain block

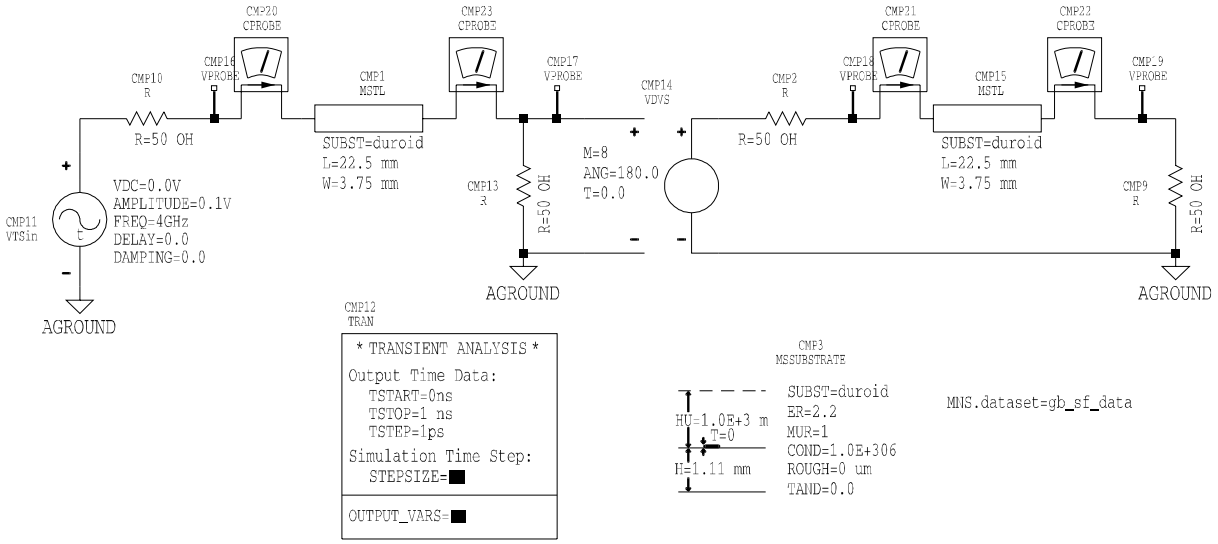

Figure E.6 Schematic of a gain block on a microstrip line-time domain

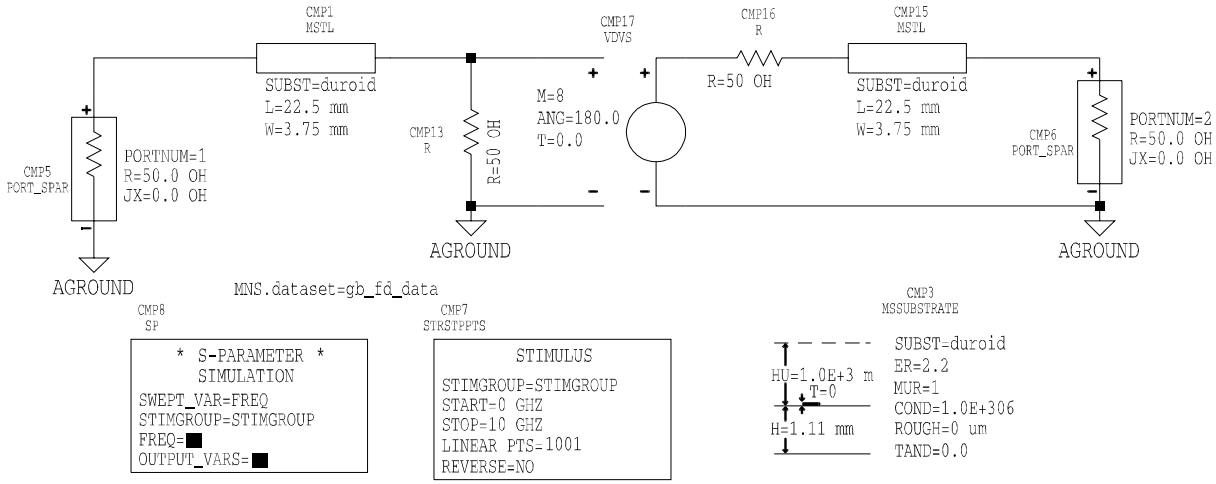

Figure E.7 Schematic of an ideal gain block on a microstrip line-frequency domain

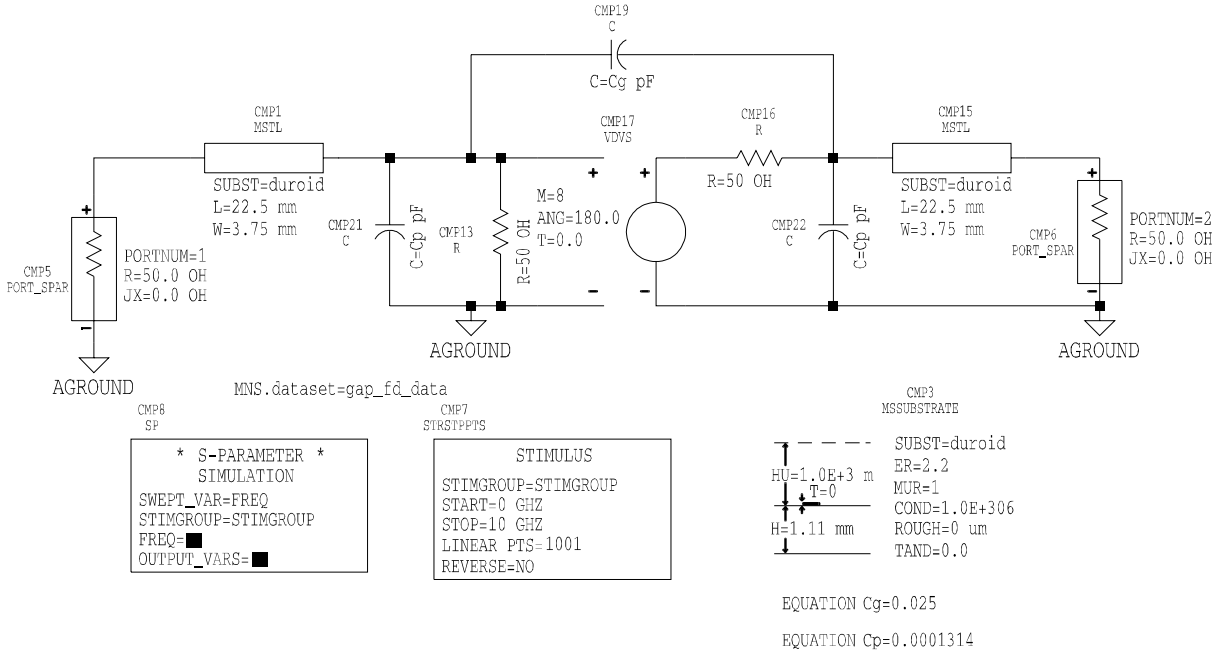

Figure E.8 Schematic of an ideal gain block on a microstrip line with gap compensation using equivalent circuit-frequency domain

E.3 Active Circulator

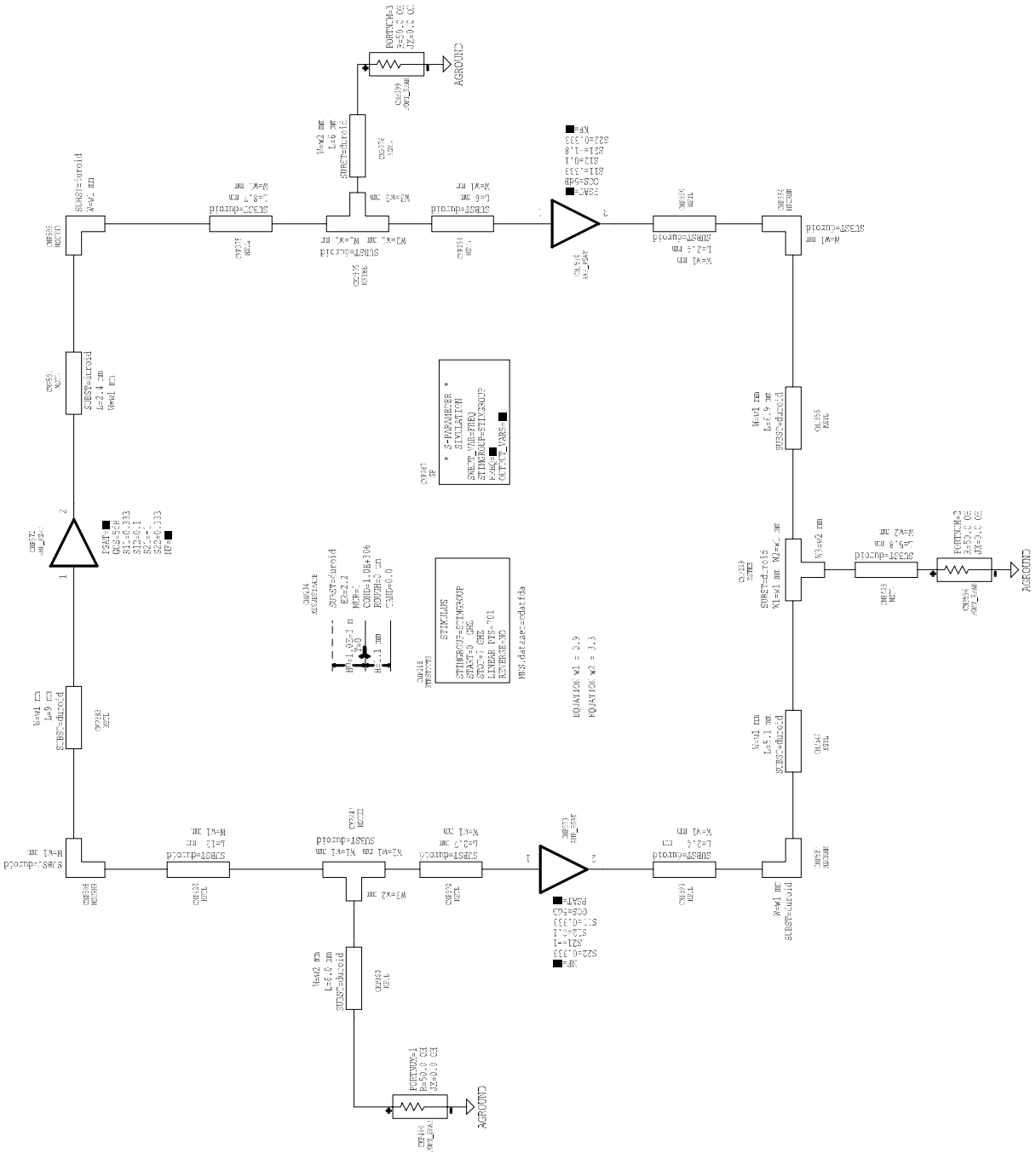

Figure E.9 Schematic of an microstrip active circulator using three gain blocks set for frequency domain simulation

E.4 Oscillator

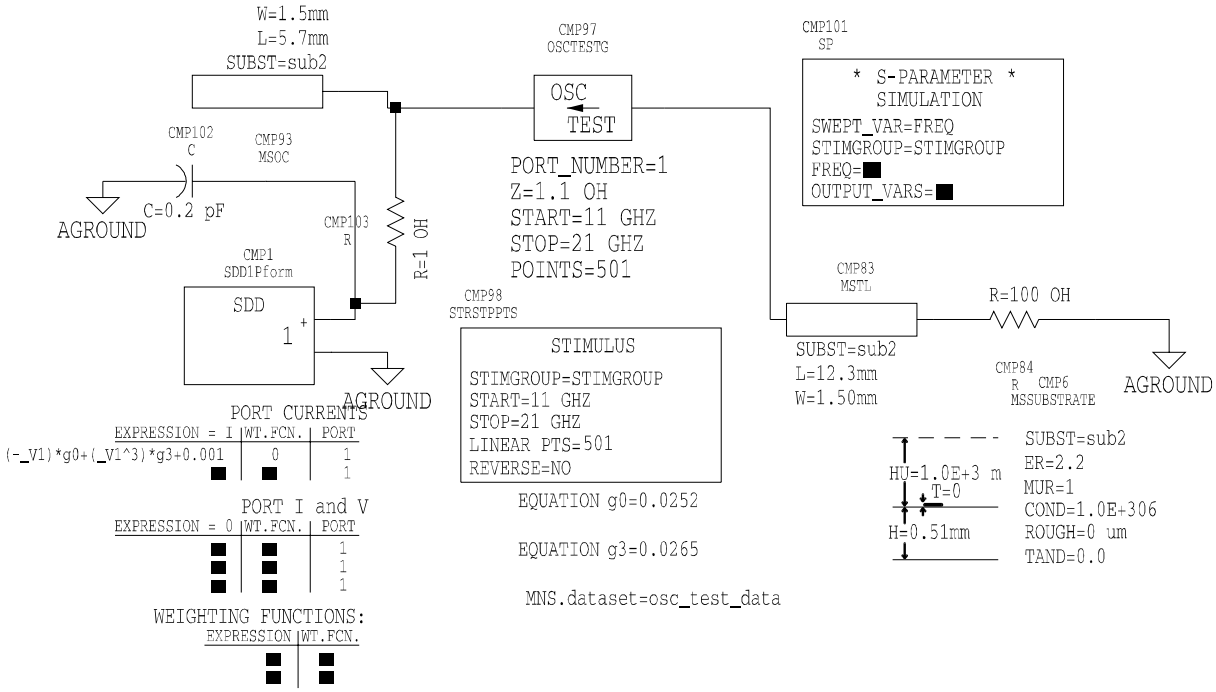

Figure E.10 Schematic of an microstrip oscillator using a Gunn diode equivalent circuit for determination of the oscillation frequency.

APPENDIX F

MICROSTRIP GAP EQUIVALENT CIRCUIT USING MathCAD™

MICROSTRIP SERIES GAP EQUIVALENT CIRCUIT

Based on Edwards(1992)

Substrate thickness $h := 1.1 \cdot 10^{-3}$

Dielectric Constant $\varepsilon r := 2.2$

Line Width $w := 3.75 \cdot 10^{-3}$

Gap dimension $go := 0.75 \cdot 10^{-3}$

Normalised quantities

$wn := \frac{w}{h}$ $wn = 3.409$

$gn := \frac{go}{w}$ $gn = 0.2$

Equivalent Circuit Capacitance

$mo := wn \cdot (0.619 \log(wn) - 0.3853)$ $mo = -0.19$

$ko := 4.26 - 1.453 \log(wn)$ $ko = 3.486$

$Co := w \cdot e^{ko} \cdot (gn)^{mo}$ $Co = 0.166$

$$me := \begin{cases} \left[\frac{1.565}{(wn)^{0.16}} - 1 \right] & \text{if } 0.3 \le gn \le 1.0 \\ 0.8675 & \text{if } 0.1 \le gn \le 0.3 \end{cases}$$

$$ke := \begin{cases} \left(1.97 - \frac{0.03}{wn} \right) & \text{if } 0.3 \le gn \le 1.0 \\ \left(2.043 \cdot wn^{0.12} \right) & \text{if } 0.1 \le gn \le 0.3 \end{cases}$$

$Ce := w \cdot e^{ke} \cdot (gn)^{me}$

Scaling

$Co := Co \cdot \left(\frac{\varepsilon r}{9.6} \right)^{0.8}$

$Ce := Ce \cdot \left(\frac{\varepsilon r}{9.6} \right)^{0.9}$

Capacitance values

$C1 := \frac{Ce}{2.0}$ $C1 = 1.314$

$Cg := \frac{Co - C1}{2.0}$ $Cg = 0.025$

APPENDIX G

ANTENNA MEASUREMENTS

The antenna radiation patterns were measured at the facilities of the Communications Engineering Group, using the automated antenna measurement system shown in Figure G.1.

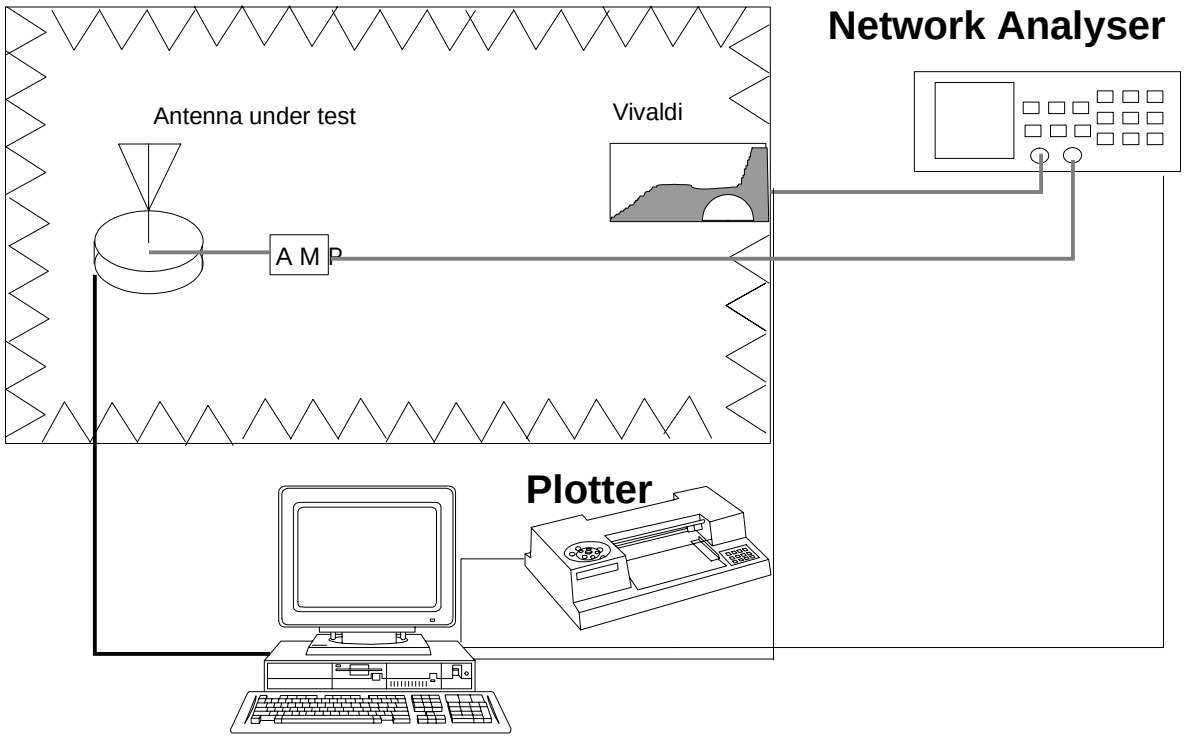

Figure G.1 The antenna measurement system

As a reference antenna an antipodal Vivaldi antenna was used. This is a broadband antenna (Langley et al. 1996). The antenna can be positioned in two orthogonal positions allowing measurements of copolar and crosspolar radiation patterns. The gain of the Vivaldi is shown in Figure G.2.

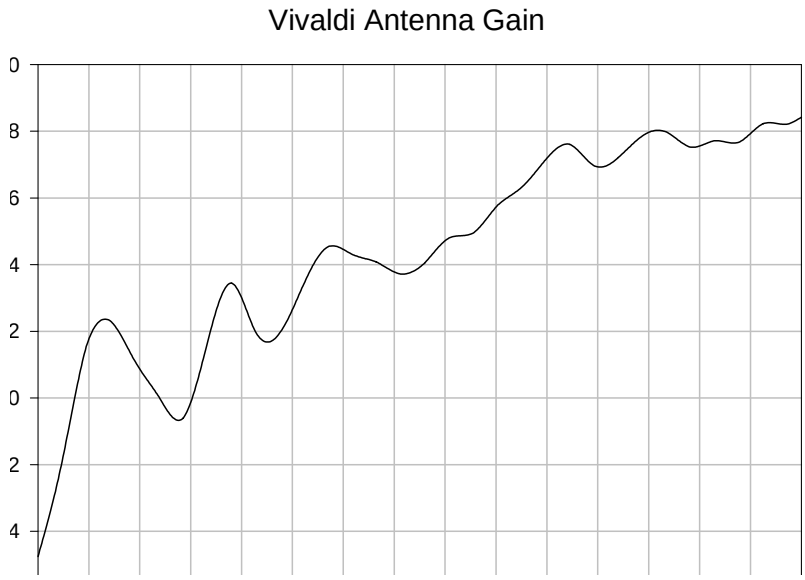

Figure G.2 Measured Vivaldi antenna gain

APPENDIX H

TRANSMISSION LINE MODELLING FOR VARACTOR LOADED MICROSTRIP ANTENNAS

H.1 Transmission line model basics

The characteristic impedance Zo of the patch treated as a line of width W is given by

$$Z_o = \frac{42.4}{\sqrt{\varepsilon e_r + 1}} \ln\left\{1 + \frac{4h}{W}\left[\frac{14+\frac{8}{\varepsilon_r}}{11}\frac{4h}{W} + \sqrt{\left(\frac{14+\frac{8}{\varepsilon_r}}{11}\right)^2\left(\frac{4h}{W}\right)^2 + \frac{\pi^2}{2}\left(1+\frac{1}{\varepsilon_r}\right)}\right]\right\} \quad \text{(H-1)}$$

The line extension to account for fringing field effects is given by

$$\Delta l = 0.412 \cdot h \frac{\left(\varepsilon_{eff} + 0.3\right)\left(\frac{W}{h} + 0.264\right)}{\left(\varepsilon_{eff} - 0.258\right)\left(\frac{W}{h} + 0.813\right)} \quad \text{(H-2)}$$

where the effective dielectric constant is given by

$$\varepsilon_{eff} = \frac{\varepsilon_r + 1}{2} + \frac{\varepsilon_r - 1}{2}\left(1 + \frac{10h}{W}\right)^{-\frac{1}{2}} \quad \text{(H-3)}$$

The radiation conductance is given by

$$G_{rad} = \frac{I_1^2}{120\pi^2} \quad \text{(H-4)}$$

where I_1

$$I_1 = \int_0^{\pi} \sin^2\left(\frac{\pi W \cos\theta}{\lambda}\right) \tan^2\theta \sin\theta \; d\theta \qquad \text{(H-5)}$$

The above equations are found in Bartia et al (1991).

Susceptance due to open end (Bahl and Bartia 1982) is equal

$$B = \frac{\beta \Delta l}{Z_o} \qquad \text{(H-6)}$$

H.2 Half Wavelength Antenna

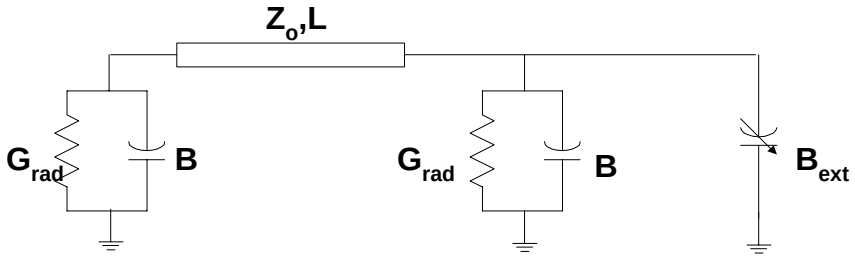

Figure H.1 Equivalent circuit for transmission line modelling of a half wavelength antenna loaded with a varactor represented by variable susceptance B_{ext}.

The determination of the resonant frequency for the circuit of Figure H.1 requires the total admittance which equals to

$$Y_{tot} = G_{rad} + j(B + Bext) + Y_A \qquad \text{(H-7)}$$

The admittance for a transmission line terminated by a load Y_L is

$$Y_A = \frac{Y_L + jY_o \tan\beta L}{Y_o + jY_L \tan\beta L} \qquad \text{(H-8)}$$

Inserting load admittance $Y_L = G_{rad} + jB$ in (H-2) leads to

$$Y_A = \frac{G_{rad} + jB + jY_o \tan\beta L}{Y_o + j(G_{rad} + jB)\tan\beta L} = \frac{G_{rad} + j\left(B + Y_o \tan\beta L\right)}{Y_o - B\tan\beta L + jG_{rad} \tan\beta L} \qquad \text{(H-9)}$$

Multiplication of (H-3) by the conjugate of the denominator and keeping only terms with tanβL yields

$$Y_A = \frac{G_{rad}Y_o - jB^2\tan\beta + jBYo + jY_o^2\tan\beta - jG_{rad}^2\tan\beta}{Y_o - 2BY_o\tan(\beta L)} \quad \text{(H-10)}$$

The resonance frequency is determined by the following condition

$$Imag(Y_{tot})=0 \quad \text{(H-11)}$$

Condition (H-5) leads to

$$\left(Y_o - 2BY_o\tan(\beta L)\right)G_{rad}Y_o - jB^2\tan\beta + jBYo + jY_o^2\tan\beta - jG_{rad}^2\tan\beta = 0 \quad \text{(H-12)}$$

Solving for tanβL gives

$$\tan(\beta L) = \frac{BYo}{B^2 + Y_o^2 - G_{rad}^2} \quad \text{(H-13)}$$

Taking into account that

$$\beta = \frac{2\pi}{\lambda}\sqrt{\varepsilon_{eff}} = \frac{2\pi c_o}{\lambda}\sqrt{\varepsilon_{eff}} \quad \text{(H-14)}$$

The resonant frequency f_r is determined by the following formula

$$f_r = \frac{c}{2\cdot\pi\cdot L\sqrt{\varepsilon_{eff}}}\tan^{-1}\left[\frac{Y_o\cdot(2B + B_{ext})}{G_{rad}^2 - B^2 + 2B(B + B_{ext})}\right] \quad \text{(H-15)}$$

H.3 Short Circuited Quarter Wave Antenna

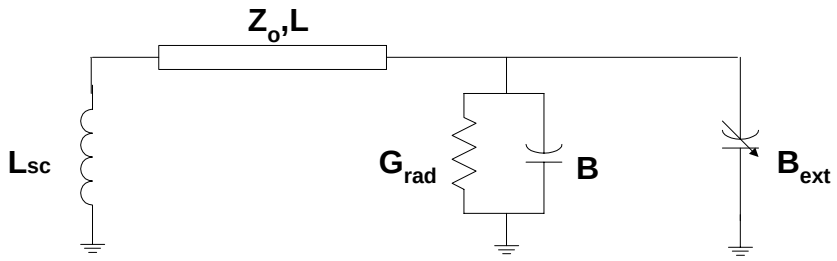

Figure H.2 Equivalent circuit for transmission line modelling of a microstrip antenna short circuited at one radiating edge, loaded with a varactor represented by variable susceptance B_{ext}.

Total admittance for the equivalent circuit of Figure H.2 is given by

$$Y_{tot} = G_{rad} + j(B + Bext) + Y_A \qquad \text{(H-16)}$$

Inserting load admitance $Y_L = \dfrac{1}{jL_{sc}\omega}$ in (H-10)

$$Y_A = \frac{\dfrac{1}{jL_{SC}\omega} + jY_o \tan(\beta L)}{Y_o + j\dfrac{1}{jL_{SC}\omega}\tan(\beta L)} \qquad \text{(H-17)}$$

which becomes

$$Y_A = -j\frac{Y_o - Y_o^2 L_{SC}\omega}{Y_o L_{SC}\omega + \tan(\beta L)} = -jB_{SC} \qquad \text{(H-18)}$$

Total admittance is

$$Y_{tot} = G_{rad} + j(B + Bext) - jB_{sc} \qquad \text{(H-19)}$$

Then by virtue of the condition (H-5),

$$\frac{Y_o - Y_o^2 \omega L_{SC}}{Y_o L_{SC} \omega + \tan(\beta L)} = B + B_{ext} \qquad \text{(H-20)}$$

Solving (H-20) for tanβL gives

$$\tan \beta L = \frac{Y_o \cdot \left[1 - (B + B_{ext}) L_{sc} \cdot \omega\right]}{B + B_{ext} - Y_o \cdot L_{sc} \cdot \omega} \qquad \text{(H-21)}$$

Taking into account (H-8), (H-14) yields the resonant frequency as

$$f_r = \frac{c}{2 \cdot \pi \cdot L \sqrt{\varepsilon_{eff}}} \tan^{-1} \left\{ \frac{Y_o \cdot \left[1 - (B + B_{ext}) L_{sc} \cdot \omega\right]}{B + B_{ext} - Y_o \cdot L_{sc} \cdot \omega} \right\} \qquad \text{(H-22)}$$

For ideal shorting pins L_{sc} is set to zero.

H.4 Calculation of Varactor Susceptance B_{ext}

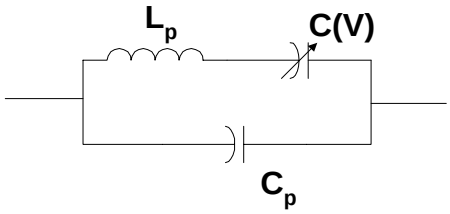

Figure H.3 Equivalent circuit of a packaged varactor diode

$$Y_1 = \frac{1}{Z_1} = \frac{1}{j\omega Lp + \frac{1}{j\omega C(V)}} = \frac{j\omega L_p}{1 - j\omega^2 L_p C(V)} \qquad \text{(H-23)}$$

$$Y = \frac{j\omega C}{1 - j\omega^2 L_p C(V)} + j\omega C_p = j\left[\frac{j\omega C}{1 - j\omega^2 L_p C(V)} + j\omega C_p\right] \quad \text{(H-24)}$$

$$B_{ext} = \omega\left[\frac{C_V}{1 - \omega^2 L_p C(V)} + C_p\right] \quad \text{(H-25)}$$

In the case of an ideal nonlinear capacitor (H-25) leads to

$$B_{ext} = \omega C_V \quad \text{(H-26)}$$

REFERENCES

ABARBANEL S. and GOTTLIEB D.(1997), "Mathematical Analysis of the PML Method", *Journal of Computational Physics*, vol. 134, pp. 357-363.

AN H., NAUWELAERS B., and VAN DE CAPELLE A. (1993), "Measurement Technique for Active Microstrip Antennas", *Electronics Letters*, vol.29, No. 18, pp.127-129.

AN H. , DIERICKS G., BAMPS E. , NAUWELAERS B., and VAN DE CAPELLE A.(1993), "Active Microstrip Antenna Design With the Simplified Real Frequency Technique", *Proceedings of the International Conference on Antennas and Propagation,* Pt. 1, pp. 299-302, Edinburgh, UK.

AYASLI Y.(1989), "Field Effect Transistor Circulators", *IEEE Trans. on Magnetics*, Vol. 25, No.5, pp.3242-3247.

BARTIA P. and BAHL I.J.(1982), "Frequency Agile Microstrip Antennas", *Microwave Journal*, vol.37, pp.67-70

BARTIA P., RAO K.V.S. , and TOMAR R.S. (1991) , *Millimeter-Wave Microstrip and Printed Circuit Antennas,* Artech House.

BALANIS C.A.(1997), *Antenna Theory: Analysis and Design*, John Wiley.

BALANIS C.A.(1989), *Advanced Engineering Electromagnetics,* John Wiley.

BECKER W., S.CHEBOLU and R.MITTRA (1995), "Finite Difference Time Domain Modelling of High Speed Electronic Packages", *Microwave Journal*, pp.62-74.

BERENGER J.-P.(1994), "A Perfectly Matched Layer for the Absorption of Electromagnetic Waves", *Journal of Computational Physics*, vol.114, 1994, pp.185-200.

BIRKELAND and ITOH T.(1989),"FET-based Planar Circuits for Quasi-Optical Sources and Transceivers", *IEEE Transactions on Microwave Theory and Techniques*, vol.37, pp.1452-1459.

BUECHLER D.N., ROPER D., DURNEY C.H., and CHRISTENSEN D.A.(1995),"Modeling Sources in the FDTD formulation and their use in Quantifying Source and Boundary Condition Errors", *IEEE Transactions on Microwave Theory and Techniques*, vol.43, pp.810-814.

CAMIADE M., SERRU V., BRANDEAU J.P., and PARISOT M. (1996), "New Generation of Low Cost GaAs MMICs for 5.8 GHz Short Range Communications", *M+RF 96 Conference Proceedings*, pp.276-280, London, UK.

CHANG K. and NAVARRO J.(1995) , "Design of Integrated Notch and Inverted Stripline Patch Antenna Modules", *Design Approaches for Integrated Circuit-Antenna Modules Workshop*, Orlando, Florida, USA.

CHANG K., HUMMER K.A., and KLEIN J.L.(1989) , “Experiments on Injection Locking of Active Antenna Elements for Active Phased Arrays and Spatial Power Combiners”, *IEEE Transactions on Microwave Theory and Techniques*, vol.37,no.7, pp.1078-1084.

CHEBOLU S., MITTRA R., and BECKER W.(1996), "The Analysis of Microwave Antennas Using the FDTD Method", *Microwave Journal*, pp.134-150.

CHEN Q. and FUSCO V.F. (1996) , “ Time-domain Diakoptics Active Slot Ring Antenna Analysis Using FDTD”,*26th European Microwave Conference Proceedings*, pp.440-443, Prague, Czech Republic.

CIAMPOLINI P., MEZANOTTE P., ROSELLI L.,SORRENTINO R. (1996), “Accurate and Efficient Circuit Simulation with Lumped Element FDTD Technique”, *IEEE Transactions on Microwave Theory and Techniques*, vol.44,no.12, pp.2207-2215.

CIAMPOLINI P., ROSELLI L. and STOPONI G.(1996), “ Integrated FDTD and Solid-State Device Simulation “,*IEEE Microwave and Guided Wave Letters*, vol.6,No.11, pp.419-421.

CRYAN M.J.(1997), “Small and Large Signal Design of Microstrip Patch Oscillators Using Hewlett Packard Microwave Design Systems”, Communications Engineering Research Group, The University of Birmingham.

CRYAN M.J. and HALL P.S. (1997), “Integrated active circulator antenna”, *IEEE Microwave and Guided Wave Letters*, Vol.7, No.7, pp.190-191.

CRYAN M.J., HALL P.S., TSANG K.S.H., and SHA J.(1997) “Integrated active antenna with full duplex operation”, *IEEE Transactions on Microwave Theory and Techniques*, Vol.45, No.10 pt 1, pp.1742-1748.

DARNBROUGH J.(1998), “Market Aspects of UMTS”, *IEE Colloquium on Personal Communications in the 21st Century(I*), Digest 1998/214, pp.4/1-4/18, London.

DAUGUET S., GILLARD R. , CITERNE J., and PITON G.(1997),” Global Electromagnetic Analysis of Microstrip Agile Antenna”, *Electronics Letters*, vol.33, no. 13, pp.1111-1112.

DOUGHERTY R.(1989), “Circulate Signals With Active Devices on Monolithic Chips”, *Microwaves and RF*, pp.85-89.

EDWARDS T.C.(1992), *Foundations for Microstrip Circuit Design*, John Wiley.

ENCINAR J.A., PEREZ J.J., and BADENES J.(1993), ”Quarter Wavelength Microstrip Antenna for the Handset of DECT System”, *8th International Conference on Antennas and Propagation Proceedings*, vol. 1, pp.245-248.

ERTURK V.B., ROJAS R.G, and ROBLIN P.(1996)," Design/Analysis of an Active Integrated Antenna", *IEEE Antennas and Propagation Society Symposium Digest*, pp. 1322-1325, Baltimore, USA.

FANG J. and XEU D.(1995) "Numerical Errors in the Computation of Impedances by FDTD Method and Ways to Eliminate Them", *IEEE Microwave and Guided Wave Letters*, vol.5, pp6-8.

FURSE C.M, and GANDHI O.P.(1995) " Why the DFT is Faster than the FFT for FDTD Time-to-Frequency Domain Conversions", *IEEE Microwave and Guided Wave Letters*, vol.6,pp326-328.

FUSCO V.F.(1992), "Series Feedback Integrated Active Microstrip Antenna Synthesis and Characterisation", *Electronics Letters*, vol.28, No.1 , pp.89-91.

GASMI A., HUYART B., BERGEUALT E., and JALLET L.(1997), " Noise and Power Optimisation of a MMIC Quasi Circulator", *IEEE Transactions on Microwave Theory and Techniques*, vol.45, No.9, pp.1572-1577.

GILLARD R., LEGAY H., FLOC'H J.M., and CITERNE J. (1991), " Rigorous Modelling of Receiving Active Microstrip Antenna *Electronics Letters*, vol.27, No.25 , pp.2357-2359.

GU Q., SHEEN D.M., and ALI S.M. (1992), "Analysis of Transients in Frequency-Dependent Interconnections and Planar Circuits With Nonlinear Loads", *IEE Proceedings-Part H: Microwaves, Antennas and Propagation*, vol. 139, no.1, pp.38-44.

GUPTA K.C (1994), "CAD of Active Microstrip Antennas and Microstrip Arrays", *Asia-Pacific Microwave Conference Proceedings*, vol.3, pp.891-895.

GUPTA K.C(1995) , "Network Modeling of Integrated Microstrip Circuit-Antenna Modules", *Design Approaches for Integrated Circuit-Antenna Modules Workshop*, Orlando, Florida.

HALL P.S.(1996)," Advances in quasi-optic active antennas", *Microwaves and RF 96 Conference Proceedings*, pp.208-213, London, UK.

HALL P. S. and MORROW I.L.(1994) "Analysis of Radiation from Active Microstrip Antennas", *IEE Proceedings Microw. Antennas Propag, vol. 141, No. 5*, pp. 359-365

HALL P. S. and FUSCO V.(1995) , "Design of Active Antenna Elements and Arrays", *Design Approaches for Integrated Circuit-Antenna Modules Workshop*, Orlando, Florida.

HALL P.S., KAPOULAS S.,CHAUHAN R. and KALIALAKIS C. (1997), " Microstrip Antennas with Adaptive Integrated Tuning", *International Conference on Antennas and Propagation ICAP-97*, vol. 1, pp.501-504.

HASKINS P.M., HALL P.S, and DAHELE J.S.(1991)," Active Patch Antenna Element with Diode Tuning", *Electronics Letters*, vol.30, No. 13, pp.1074-1076.

HASKINS P.M. and DAHELE J.S.(1994), ” Varactor-diode Loaded Passive Polarisation Agile Patch Antenna”, *Electronics Letters,* vol.27,No. 20, pp.1846-1848.

HIROTA T., NAKAJIMA M., and IKENOUE J.-I(1980), “ A Simple Equivalent Circuit of Microstrip Oscillator Allowing for Nonlinearity”, *International Journal of Electronics,* vol.48, no.5, pp.427-434.

HOCKANSON D. M., DREWNIAK J.L., HUBING T.H, and VAN DOREN T.P(1995), “FDTD Modeling of Thin wires for Simulating Common-Mode Radiation from Structures with Attached Cables”, *IEEE Conference Proceedings on Electromagnetic Compatibility*, pp. 168-173.

IEEE Workshop(1995), *Design Approaches for Integrated Circuit-Antenna Modules*, Orlando, Florida.

ITOH T.(ed.)(1989), *Numerical Techniques for Microwave and Millimeter-Wave Passive Structures*, John Wiley..

JAMES J.R. and HALL P.S(eds.)(1989), *Handbook of Microstrip Antennas*, Peter Peregrinus.

KALIALAKIS C. , CRYAN M.J. , HALL P.S., GARDNER P. (1997),“ FDTD Simulation of an Active Integrated Antenna”, *Electronics Letters,* vol. 33, no.25, pp.2091-2092.

KATZ D.S, THIELE E.T., and TAFLOVE A.(1994) , “Validation and Extension to Three Dimensions of the Berenger PML Absorbing Boundary Condition for FDTD Meshes*”, IEEE Microwave and Guided Wave Letters*, vol.4, pp.268-270.

KATZIN P., AYASLI Y. , REYNOLDS L., and B. BEDARD B. (1992), “6 to 18 GHz MMIC Circulators”, *Microwave Journal*, no.5, pp. 248-256.

KERR A.R., SIEGEL P.H., and MATTAUCH R.J.(1977), “A Simple Quasi-Optical Mixer for 100-120 GHz”, *IEEE MTT-S Symposium Digest*, pp. 96-98.

KIM I.S. and HOEFER W.J.R.(1991) “The Numerical Energy Conservation of the TDFD Method”, *IEEE Transactions on Magnetics*, vol. 27, No.5,pp. 4056-4060.

KOTHER D., HOPF B., SPORKSMANN T., WOLFF I.,and KOBLOWSKI S. (1995), “ New Types of MMIC Cicrulators”, *IEEE MTT-S International Microwave Symposium Digest*, pp.887-880.

KUNZ K. S. and LUEBBERS R.J.(1993), *The Finite Difference Time Domain Method for Electromagnetics*, CRC Press.

KUO C.-N., HOUSMAND B., and ITOH T. (1997), “Full-Wave Analysis of Packaged Microwave Integrated Circuits with Active and Nonlinear Devices: An FDTD Approach”, *IEEE Transactions on Microwave Theory and Techniques*, vol.45, no.5, pp.819-826.

KYKKOTIS C., HALL P. S, and GHAFOURI-SHIRAZ H. (1998)**, “** Performance of active antenna oscillator arrays under modulation for communication systems”, *IEE Proceedings: Microwaves, Antennas and Propagation,* Vol.145, No.4, pp313-320.

LANGLEY J.D.S., HALL P.S., and NEWHAM P. (1996), " Balanced Antipodal Vivaldi Antenna for Wide Bandwidth Phased Arrays", *IEE Proceedings: Microwaves, Antennas and Propagation*, Vol.143, No.2, pp.97-102.

LECKEY J.G., PATTERSON A.D. , and STEWART J.A.C. (1995), "A Vector Corrected Waveform and Load Line Measurement System for Large Signal Transistor Characterisation", *IEEE MTT-S Symposium Digest*, pp.1243-1245.

LIN J. and ITOH T.(1993), "Analysis of Device Failures in a Power Combining Array", *23rd European Microwave Conference Proceedings*, pp. 912-913, Madrid, Spain.

LIN J. and ITOH T.(1994), "Active Integrated Antennas", *IEEE Transactions on Microwave Theory and Techniques*, vol.42, No.12, pp.2186-2194.

LIU Y.(1996) , "Fourier Analysis of Maxwell Equations", *Journal of Computational Physics*, vol. 124, pp. 396-416.

LUEBBERS R.J. and BEGGS J.(1992), "FDTD Calculation of WideBand Antenna Gain and Efficiency", *IEEE Transactions on Antennas and Propagation*, Vol. AP-40, No.11, pp.1403-1407.

LUEBBERS R.J., KUNZ K. S., SCHNEIDER M., and HUNSBERGER F., (1991)"A Finite Difference Time Domain Near-Zone to Far-Zone Transformation", *IEEE Transactions on Antennas and Propagation*, Vol. AP-39, pp.429-433.

LUEBBERS R.J. and LANGDON H.S.(1996), "A Simple Feed Model that Reduces Time Steps Needed for FDTD Antenna and Microstrip Calculations", *IEEE Transactions on Antennas and Propagation*, Vol. AP-44, No.7, pp.1000-1005.

MAAS A. S. (1988), *Nonlinear Microwave Circuits*, Artech House

MARTENS L., DE MOERLOSSE J., DE JUTTER D., DE POORTER J., DE WAGTER C.(1995), "Calculation of the Electromagnetic Fields Induced in the Head of an Operator of a Cordless Telephone", *Radio Science*, Vol. 30, No. 1, pp. 283-290.

McDOWALL D.S. and FUSCO V.F.(1995)"Concurrent Large Signal Simulation of an Active Microstrip Antenna", *International Journal of Numerical Modelling: Electronic Networks, Devices and Fields, v*ol.8, No.1, pp.3-12.

MINK J.W.(1986), "Quasi-optical Power Combining of Solid State Millimeter-Wave Sources", *IEEE Transactions on Microwave Theory and Techniques*, vol. 34, No.2, pp.273-279.

MITCHELL, A. R. and GRIFFITHS (1980), *The Finite Difference Method In Partial Differential Equations*, John Wiley.

MUR G. (1981), "Absorbing Boundary Conditions for the Finite Difference Approximation of the Time Domain Electromagnetic Field Equations", *IEEE Transactions on Electromagnetic Compatibility*, vol.23 , pp.377-382

NAM S., UWANO T, and ITOH T. (1987), "Microstrip-fed planar frequency-multiplying space combiner", *IEEE Transactions on Microwave Theory and Techniques*, vol.35, pp.1271-1276

NAVARRO J.A., HUMMER K.A., and CHANG K. (1991), "Active Integrated Antenna Elements", *Microwave Journal*, pp.115-126.

NAVARRO J.A and CHANG K (1996), *Integrated Active Antennas and Spatial Power Combining*, John Wiley.

PALANISAMY V. and GARG R.(1985), "Rectangular ring and H-shaped microstrip antennas-alternatives to rectangular patch antenna", *Electronics Letters*, vol. 21, No. 19, pp. 874-876.

PARFITT A.J.(1996) , "Feedback Design of a Coupled Patch-Oscillator Array", *IEEE Antennas and Propagation Society Symposium Digest*, pp. 1330-1333, Baltimore, USA

PEKONEN O.P.M., XU J., and NIKOSKINEN K.I.(1996),"Rigorous Analysis of Circuit Parameter Extraction from an FDTD Simulation Excited with a Resistive Voltage Source, *Microwave and Optical Technology Letters*, Vol.12, No.4, pp.205-210.

PETROPOULOS P.G.(1994) "Phase Error Control for FD-TD methods of Second and Fourth Order Accuracy", *IEEE Transactions on Antennas and Propagation*, Vol. AP-42, pp.859-862.

PIKET-MAY M., TAFLOVE A., and BARON J.(1994), "FDTD Modelling of Digital Signal Propagation in 3D Circuits with Passive and Active Loads", *IEEE Transactions on Microwave Theory and Techniques*, vol.42, No.8, pp.1514-1523.

POBANZ C.W. and ITOH T.(1994),"A Microwave Non-Contact Identification Transponder Using Subharmonic Interrogation", *IEEE Microwave Theory and Techniques Society Symposium Digest*, pp. 883-886.

POTTER D.(1973), *Computational Physics*, John Wiley.

POZAR D.M.(1990), *Microwave Engineering*, Addison-Wesley.

PRESS W., FLANNERY B.P., TEUKOLSKY S.A., and VETTERLING W. T. (1986), *Numerical Recipes: The Art of Scientific Computing (Fortran Edition)* , Cambridge University Press.

RAMO S., WHINNERY J.R., and VAN DOUZER T. (1994) , *Fields and Waves in Communication Electronics*, John Wiley.

RAYNER M., OLVER A. D., and MONK A.D.(1996) , "Proximity Effects of Absorbing Boundary Conditions on Antenna Radiation Patterns" , *Radio Science*, vol. 31, no.6, pp. 1845-1852.

REINEIX A. and JECKO J.(1989),"Analysis of Microstrip Patch Antennas Using Finite Difference Time Domain Method", *IEEE Transactions on Antennas and Propagation*, Vol. AP-37, pp.1361-1369.

RIGHI M., TARDIOLI G., CASCIO L., HOEFER W.J.R. (1997), "Time-domain characterization of packaging effects via segmentation technique", *IEEE Transactions on Microwave Theory and Techniques*, Vol.45, No.10 pt 2, pp.1905-1910

ROBERT B., RAZDAN T., and PAPIERNIK A.(1992), "Compact Amplifier Integration in Square Patch Antenna", *Electronics Letters*, vol.28, No.19, pp.1808-1810.

ROBERTSON I.D.(ed.) (1995), *MMIC Design*, IEE Press.
RODDY D. and COOLEEN J. (1995), *Electronic Communications*, 4th edition, Prentice-Hall.

ROPER D.H. and BAIRD J.M.(1992), "Analysis of Overmoded Waveguides Using the Finite Difference Time Domain Method", *IEEE Microwave Theory and Techniques Society Symposium Digest*, pp. 401-404.

ROSTBAKKEN O., HILTON G.S. and RAILTON C. J. (1995), "Adaptive Feedback Frequency Tuning for Microstrip Patch Antennas", *Proceedings of the International Conference on Antennas and Propagation*, pp. 166-170.

SABATIER C.(1995), "2GHz Compact Antennas on Handsets", *IEEE Antennas and Propagation Society Symposium Digest*, pp.1136-1139, Newport Beach, USA.

SADIKU M.N.O. , AGBO S.O., and BEMMEL V.(1990), "Stability Criterion for Finite Difference Time Domain Algortihms", *Proceedings of IEEE SouthEastcon*, pp.48-50

SAFAVI-NAEINI S., CHOW Y.L., KEYNFAVAR M., NIKNESHAN S., FAYYAZ N, and HODJAT N.(1996), "A Simple Two-Port model for Active Printed Board Antenna Element", *IEEE Antennas and Propagation Society Symposium Digest*, pp. 530-533, Baltimore, USA.

SANAD M.(1994), "Effect of Shorting Posts on Short Circuit Microstrip Antennas," *IEEE Antenna and Propagation Society Symposium Digest*, pp. 794-797.

SHEEN D.M., ALI S.M., ABOUZAHRA M.D., and KONG J.A.(1990)," Application of the 3D FDTD Method to the Analysis of Planar Microstrip Circuits", *IEEE Transactions on Microwave Theory and Techniques*, vol.38, No.7, pp. 849-857.

SINGH D., GARDNER P., and HALL P.S.(1997), "Miniaturised Antenna for MMIC Applications", *Electronics Letters*, vol.33,No. 22, pp.1830-1831.

SINGH D., GARDNER P., and HALL P.S.(1997), "Integrated Push-Push Frequency Doubling Active Microstrip Transponder", *Electronics Letters*, vol.33,No. 6, pp.505-506.

SINGH D. (1999), "Monolithic Millimeter and Microwave Active Antennas, Ph.D Thesis(submitted), University of Birmingham.

SMITH G.D. (1978), *Numerical Solution of Partial Differential Equations: Finite Difference Methods*, Oxford University Press.

STEPHAN K.D. and ITOH T. (1984), "A Planar Quasi-Optical Subharmonically Pumped Mixer Characterised by Isotropic Conversion Loss", *IEEE Transactions on Microwave Theory and Techniques*, vol. 32, No.1, pp.97-102.

SUI W., CHRISTENSEN D. and DURNEY C.H. (1992), "Extending the 2-D FDTD Method to Hybrid Electromagnetic Systems with Active and Passive Lumped Elements", *IEEE Transactions on Microwave Theory and Techniques*, vol.40,no. 4,pp.724-730.

TAFLOVE A.(1995), *Computational Electrodynamics: The Finite Difference Time Domain Method*, Artech House.

TANAKA S., SHIMOMURA N. and OHTAKE K. (1965), "Active Circulators-The Realisation of Circulators Using Transistors", *Proceedings of the IEEE*, Vol. 53, No. 3, pp. 260-267.

TENTZERIS E.M., ROBERTSON R.L., KATEHI L.P.B., CANGELLARIS A. (1997),"Space- and time-adaptive gridding using MRTD technique", *IEEE MTT-S International Microwave Symposium Digest*, Vol.1, pp.337-340

THOMAS H.J., FUDGE D.L., and MORRIS G.(1984), "Gunn Source Integrated With Microstrip Patch", *Military Microwaves Conference Proceedings*, pp.245-249.

THOMAS V.A., LING K.-M., JONES M.E., TOLAND B., LIN J., ITOH T.(1994), "FDTD Analysis of an Active Antenna", *IEEE Microwave and Guided Wave Letters*, vol.4, no.9, pp.296-298.

TOLAND B., LIN J., HOUSMAND B., and T. ITOH.(1994), " Electromagnetic Simulation of Mode Control of a Two Element Active Antenna", *IEEE Microwave Theory and Techniques Society Symposium Digest*, pp. 883-886.

TOLAND B., HOUSMAND B., and ITOH T.(1993), "Modelling of Non-Linear Active Regions with the FDTD Method", *IEEE Microwave and Guided Wave Letters*, vol.3, No.9, pp. 333-335.

TRUEMAN C.W., LUEBBERS R.J, AND MISHRA S.R. (1993), "FDTD computation of the RCS of high permittivity cubes", IEEE Antennas and Propagation Society International Symposium Digest), pp.846-849

UNDERHILL M.J (1998), " The Need for Better Varactor Diodes in Low Phase Noise Tunable Oscillators" , *IEE Colloquium on Microwave & Millimetre- Wave Oscillators and Mixers*, Digest 480/1998, pp.5/1,5/6.

VENDELIN G.D. , PAVIO , ROHDE U.(1990), *Microwave Circuit Design Using Linear and Nonlinear Techniques*, John Wiley

YEE, K.S (1966) “Numerical Solution of Initial Boundary Value Problems Involving Maxwell’s Equations in Isotropic Media”, *IEEE Transactions on Antennas and Propagation*, Vol. AP-14, pp.302-307,.

YOGUCHI Y., OHTANI M., MARIKO K., and MATSUMOTO F. (1998), “Crosstalk of Microstrip lines with Capacitor Loads”, *International Journal of Electronics*, vol.85, no.3, pp.327-336.

YORK R.A. and COMPTON R.C. (1992), “Dual-Device Active Patch Antenna With Improved Radiation Characteristics”, *Electronics Letters*, vol.28, No. 11, pp.1019-1021.

YORK R. and POPOVICH Z.B. (eds) (1997), *Active and Quasi-optical Arrays for Solid State Power Combining*, John Wiley.

YOO T.W., CHANG K.(1992), **“**Theoretical and experimental development of 10 and 35 GHz rectennas”, *IEEE Transactions on Microwave Theory and Techniques*, Vol.40, No.6, pp.1259-1266

YUN C.-.E and RA J.-W. (1995), “Time-Domain Analysis of Transmission Lines With Arbitrary Nonlinear Loads”, *Microwave and Optical Technology Letters*, vol.8, no.5, pp.264-268.

ZHANG J., WANG Y., and WANG X.(1996), “Combination of Piecewise Harmonic Balance Technique and Neural Networks for Analysing Active Antenna”, *IEEE Antennas and Propagation Society Symposium*, pp. 514-517, Baltimore, USA.

WATERHOUSE R.B. and SHULLEY N.V.(1994) , “Full Characterisation of Varactor Loaded , Probe-fed, Rectangular, Microstrip Patch Antennas, *IEE Proceedings Microw. Antennas Propag*, vol. 141, No. 5, pp. 367-373.

WU X.D. and CHANG K. (1995), “Dual FET Active Patch Elements for Spatial Power Combiners”, *IEEE Transactions on Microwave Theory and Techniques*, vol. 43, no.1, pp.26-30.